AD-A010 516

ARPA/NRL X-RAY LASER PROGRAM - SEMIANNUAL TECHNICAL REPORT TO DEFENSE ADVANCED RESEARCH PROJECTS AGENCY

Naval Research Laboratory

Prepared for:

Defense Advanced Research Projects Agency

May 1975

NRL Memorandum Report 3057

ARPA/NRL X-RAY LASER PROGRAM
Semiannual Technical Report
to
Defense Advanced Research Projects Agency
1 July 1974 - 31 December 1974
ARPA Order 2694

Interaction Physics Branch
Optical Sciences Division

May 1975

NAVAL RESEARCH LABORATORY
Washington, D.C.

SECURITY CLASSIFICATION OF THIS PAGE *(When Data Entered)*

REPORT DOCUMENTATION PAGE		READ INSTRUCTIONS BEFORE COMPLETING FORM
1. REPORT NUMBER NRL Memorandum Report 3057	2. GOVT ACCESSION NO.	3. RECIPIENT'S CATALOG NUMBER
4. TITLE *(and Subtitle)* ARPA/NRL X-RAY LASER PROGRAM — SEMIANNUAL TECHNICAL REPORT TO DEFENSE ADVANCED RESEARCH PROJECTS AGENCY — 1 JULY 1974 — 31 DECEMBER 1974		5. TYPE OF REPORT & PERIOD COVERED Semiannual technical report; work continuing. 6. PERFORMING ORG. REPORT NUMBER
7. AUTHOR(s) Interaction Physics Branch Optical Sciences Division		8. CONTRACT OR GRANT NUMBER(s)
9. PERFORMING ORGANIZATION NAME AND ADDRESS Naval Research Laboratory Washington, D.C. 20375		10. PROGRAM ELEMENT, PROJECT, TASK AREA & WORK UNIT NUMBERS NRL Problems N01-43, N01-33 ARPA Order 2694, Program Code 4D10
11. CONTROLLING OFFICE NAME AND ADDRESS Defense Advanced Research Projects Agency Washington, D.C. 20301		12. REPORT DATE May 1975 13. NUMBER OF PAGES 187
14. MONITORING AGENCY NAME & ADDRESS *(If different from Controlling Office)*		15. SECURITY CLASS. *(of this report)* Unclassified 15a. DECLASSIFICATION/DOWNGRADING SCHEDULE

16. DISTRIBUTION STATEMENT *(of this Report)*

Approved for public release; distribution unlimited.

17. DISTRIBUTION STATEMENT *(of the abstract entered in Block 20, if different from Report)*

18. SUPPLEMENTARY NOTES

19. KEY WORDS *(Continue on reverse side if necessary and identify by block number)*

X-ray lasers
Lasers
Ultraviolet lasers
Laser-plasma interactions

20. ABSTRACT *(Continue on reverse side if necessary and identify by block number)*

The ARPA/NRL x-ray laser program is concerned with demonstrating gain in the soft x-ray region. The program is jointly supported by ARPA and NRL. The approaches include electron-collisional pumping in picosecond laser pumped plasma, resonant charge transfer pumping, optical parametric mixing to short wavelengths, traveling wave e-beam pumping, and analysis and numerical modeling. This report covers the progress made during the first half of FY-75.

DD FORM 1 JAN 73 1473 EDITION OF 1 NOV 65 IS OBSOLETE
S/N 0102-014-6601

SECURITY CLASSIFICATION OF THIS PAGE *(When Data Entered)*

The Interaction Physics Branch of the Optical Sciences Division, Naval Research Laboratory, Washington, D.C. prepared this semiannual report on work sponsored jointly by the Defense Advanced Research Projects Agency, DARPA Order 2694, and the Naval Research Laboratory. Co-authors of the report were R. A. Andrews, R. C. Elton, J. Reintjes, R. C. Eckardt, R. H. Lehmberg, R. Waynant, T. N. Lee, and L. J. Palumbo.

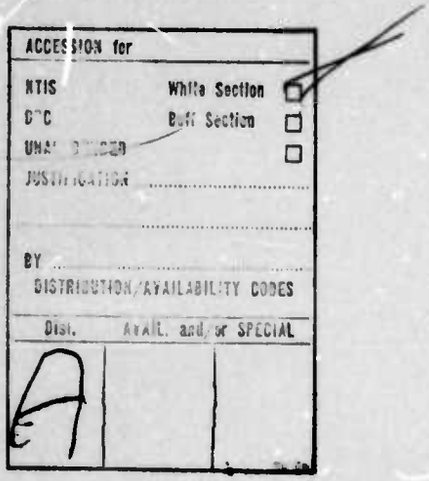

CONTENTS

SEMIANNUAL TECHNICAL REPORT

Reporting Period

1 July 1974 - 31 December 1974

1.	DAPPA Order	2694
2.	Program Code No.	4D10
3.	Name of Contractor	Naval Research Laboratory Optical Sciences Division
4.	Effective Date of Contract	1 January 1974
5.	Contract Expiration Date	Continuing
6.	Amount of Contract	$250K (FY 75)
7.	Contract No.	N/A
8.	Principal Investigator	Dr. R. A. Andrews
9.	Telephone No.	202-767-3528
10.	Scientific Officer	Dr. C. M. Stickley, ARPA
11.	Title of Work	X-Ray Lasers

Sponsored by

Defense Advance Research Projects Agency

ARPA ORDER 2694

ARPA/NRL X-RAY LASER PROGRAM
Semiannual Technical Report to Defense Advanced Research Projects Agency
1 July 1974 – 31 December 1974

I. INTRODUCTION

This is the second semiannual technical report for the ARPA/NRL X-ray Laser Program. An attempt was made in the first report (NRL Memo Report 2910) to provide background for each of the approaches being pursued. Hence, no attempt will be made to duplicate that information in this report. Every attempt is made, however, to cover the experimental details, changes in direction, and results of analysis which occured during this reporting period.

The individual activities in the program have remained the same, i.e.,

(1) Electron collisional pumping using picosecond laser heating of a cold plasma,
(2) Traveling wave (TW) high energy electron beam pumping,
(3) Nonlinear optical mixing starting with intense 1600 Å radiation,
(4) Resonant charge transfer pumping using a laser plasma expanding into a neutral gas background, and
(5) Theory, analysis, and numerical modeling in support of the above and other approaches.

Each of these activities is in a different stage of development. The e-collisional pumping and nonlinear mixing experiments depend on the NRL short pulse laser facility. This reporting period has seen major improvements in this laser systems to improve the quality of the laser ouput and improve the reliability of several components. This work has been extensive and as a consequence the time available for laser interaction studies has been reduced.

In the nonlinear mixing activity, the nonlinear components, ovens, etc., that were designed and ordered during the last reporting period were received and tested as individual components during this period. The TW electron beam device has undergone several engineering changes based on the first series of evaluation tests performed during the last reporting period. The resonant charge transfer experiment has been assembled and the first series of experiments is underway at this time. Examples of the early data are included in this report. Finally, analysis has been continuing. Work has been done on e-collisional pumping to understand the electron heating and several new candidates for short wavelength lasers using this pumping technique have been identified. More work has been done to identify possible lasers using resonant charge transfer. Significant progress has been made in developing a code to model the $3p \rightarrow 3s$ quasi-cw

Note: Manuscript submitted May 7, 1975.

laser scheme (e-collisional pump) discussed in the last report.

The following sections of this report describe the details of progress made in each of these areas during the last six months. A summary of the important points is included in the last section. In some instances the work has been prepared for publication or has been published. In these cases the reprint has been included as an appendix and only brief mention of the work is made in the main body of the report. Each section also contains a few sentences about where the work is going and plans for the next reporting period.

II. E-COLLISIONAL PUMPING VIA PICOSECOND LASER PUMPING OF PLASMAS

II. A. LASER/PLASMA EXPERIMENT

The basic idea[1] for generating a soft x-ray laser using the $3p \rightarrow 3s$ transition scheme is to produce an elongated plasma from a line focus of a laser beam (pre-pulse) and then subsequently inject another short-pulse laser beam (main pulse) onto the plasma axially to heat the plasma within a very short period of time. This collision dominated, unequilibrated plasma will hopefully achieve a preferential population inversion. It is therefore important to know whether a laser produced plasma can be heated rapidly with the main laser beam and also what other physical processes take place when the short pulse laser beam interacts with the plasma.

An experiment has been performed[2] using a mode-locked Nd:YAG laser beam with energies up to 100 mJ in a 25 ps pulse. The laser beam is focused onto a slab target of Plexiglass ($C_5O_2H_8$) at power densities up to 8×10^{13} W/cm^2. The pre-pulse is obtained from the main laser beam using a beam splitter and is then focused collinearly onto the same spot as the main focus within $\pm$ 10 μm. The focal spot size as well as the pulse length of the laser beam is monitored for each laser shot using a diode array and an picosecond resolution streak (image converter) camera, respectively. The spot size varies between 40 and 55 μm in diameter and the pulse length varies between 25 and 35 ps. Three identical x-ray detectors are used in order to determine the electron temperature as well as approximate bremsstrahlung profile. Each x-ray detector consists of a 1.3 mm thick NE 102 plastic scintillator and photomultiplier. Each scintillator has a different absorber (beryllium foil) and they are placed approximately the same distance from the target focal spot in the target vacuum chamber. The scintillations are collected and led outside the chamber to the photomultipliers by means of fiber optics. The detectors are calibrated with respect to one another by using the same thickness absorbers. The thinnest absorber is chosen so that is prevents any possible line radiation (hydrogen-like oxygen lines, $\sim$ 15 Å) from being transmitted.

Figure 1 shows relative x-ray intensities measured through three different absorbers (19 mg/cm^2, 28.5 mg/cm^2, and 38 mg/cm^2) in which the pre-pulse in addition to the main pulse is focused onto the target.

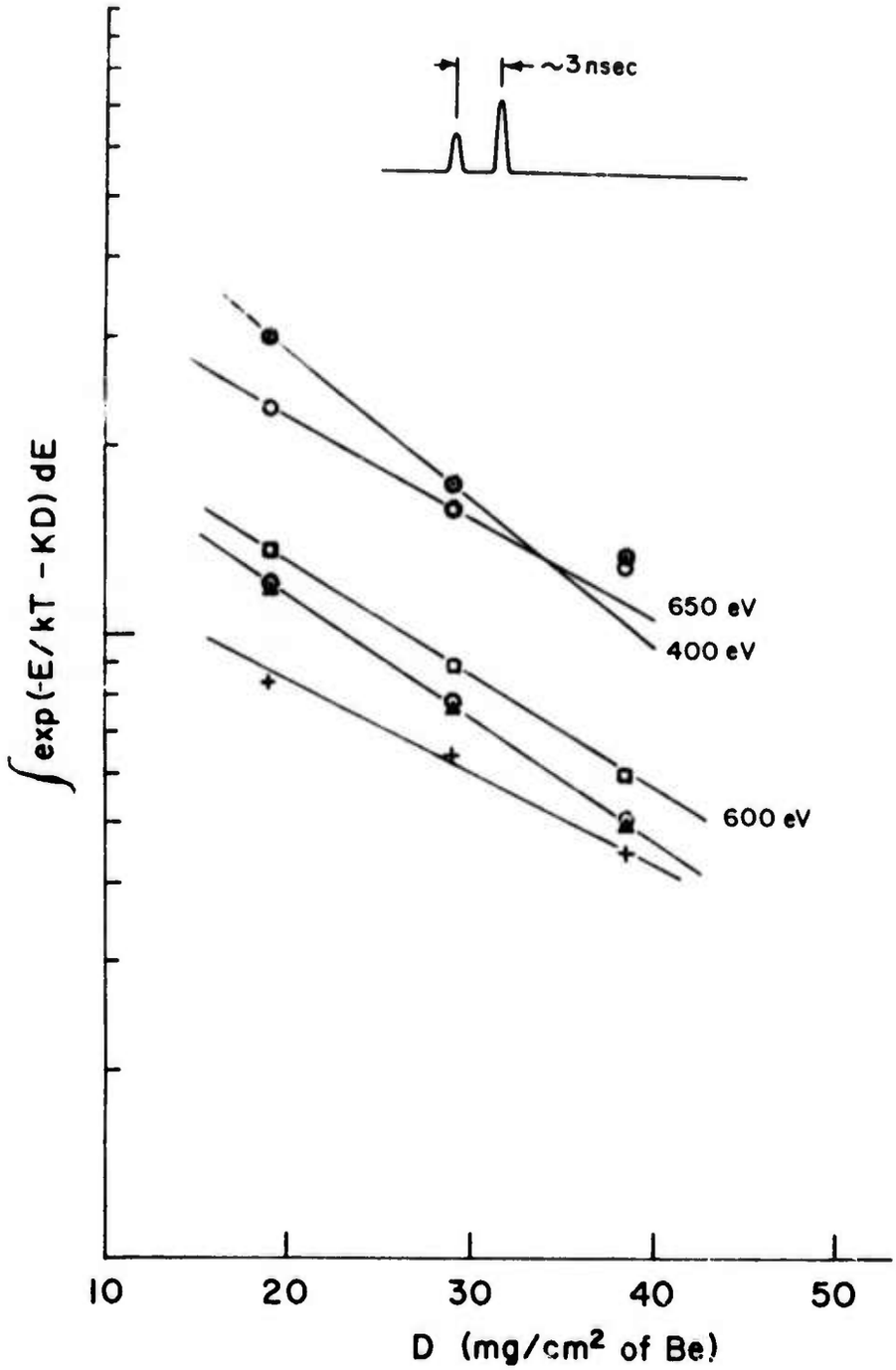

Fig. 1 — Relative x-ray intensities as a function of absorber thickness for 5 different laser shots

The pre-pulse has intensities varying 10 to 30% of the main pulse and the time delay between the pre-pulse and the main pulse is typically 3 to 6 ns. As can be seen in the figure, the measured values for each shot approximately fall onto straight lines (in a semi-logarithmic plot) which indicate that the bremsstrahlung profiles in this x-ray energy range are thermal. However, when the level of bremsstrahlung is high, the profile tends to deviate from that of thermal as can be seen in the upper two curves. The electron temperatures deduced from this graph vary from one shot to another in the range from 500 to 800 eV. The temperature fluctuation is mainly due to the shot-to-shot variation in the laser power density on the target but also the possibility can not be ruled out that extremely small laser pulses (non-reproducible for shot-to-shot) due to an imperfect selection of a single pulse from the mode-locked wave train contribute as pre-pulses in addition to the applied pre-pulse. The importance of these laser pre-pulses in the front of the main laser pulse in the laser-matter interaction has been pointed out recently[3] in the literature. In order to investigate the bremsstrahlung in the even higher x-ray photon energies (with the pre-pulse), a set of thicker beryllium absorbers (48 mg/cm^2 and 72 mg/cm^2) are used and the result is shown in Fig. 2. Since only three x-ray detectors are available currently, a detailed spectra can not be deduced from the data but the graph clearly suggests that the deviation from the thermal bremsstrahlung is even greater in all cases at the higher photon energies. It is also very likely that the laser-produced plasma consists of two temperature components, i.e., a low and a high temperature component. The low temperature component is in approximate agreement with the one expected from the normal (classical) absorption process in a simple hydrodynamic model[4]. The high temperature component, on the other hand, cannot be explained from the classical absorption but may be understood from the anomalous absorption near the cut-off density region due to the parametric instability. The parametric instability has a threshold[5] laser power density ($\sim 3 \times 10^{14}$ W/cm^2) above which the anomalous absorption increases.

The electron temperature and the bremsstrahlung profile between the cases with and without pre-pulse in addition to the main laser pulse can be compared. Figure 3 shows the result when the relative x-ray intensities are plotted in a logarithmic scale as a function of thickness of the absorber. As can be seen, with the pre-pulse the level of the bremsstrahlung x-ray emission is greatly enhanced by an order of magnitude (even with the lower power density than the other case) compared to the case where only the main pulse is present. One other difference between the two cases is that there is a distinct and enhanced low temperature component with the pre-pulse whereas without the pre-pulse the low temperature compone' seems to be osbscured by the high temperature component. The latter case is likely due to the fact that the level of the low temperature component is lower or comparable to the high temperature component as is indicated in Fig. 4. The effect of the pre-pulse may be explained in the following way: without the pre-pulse, the volume of the plasma

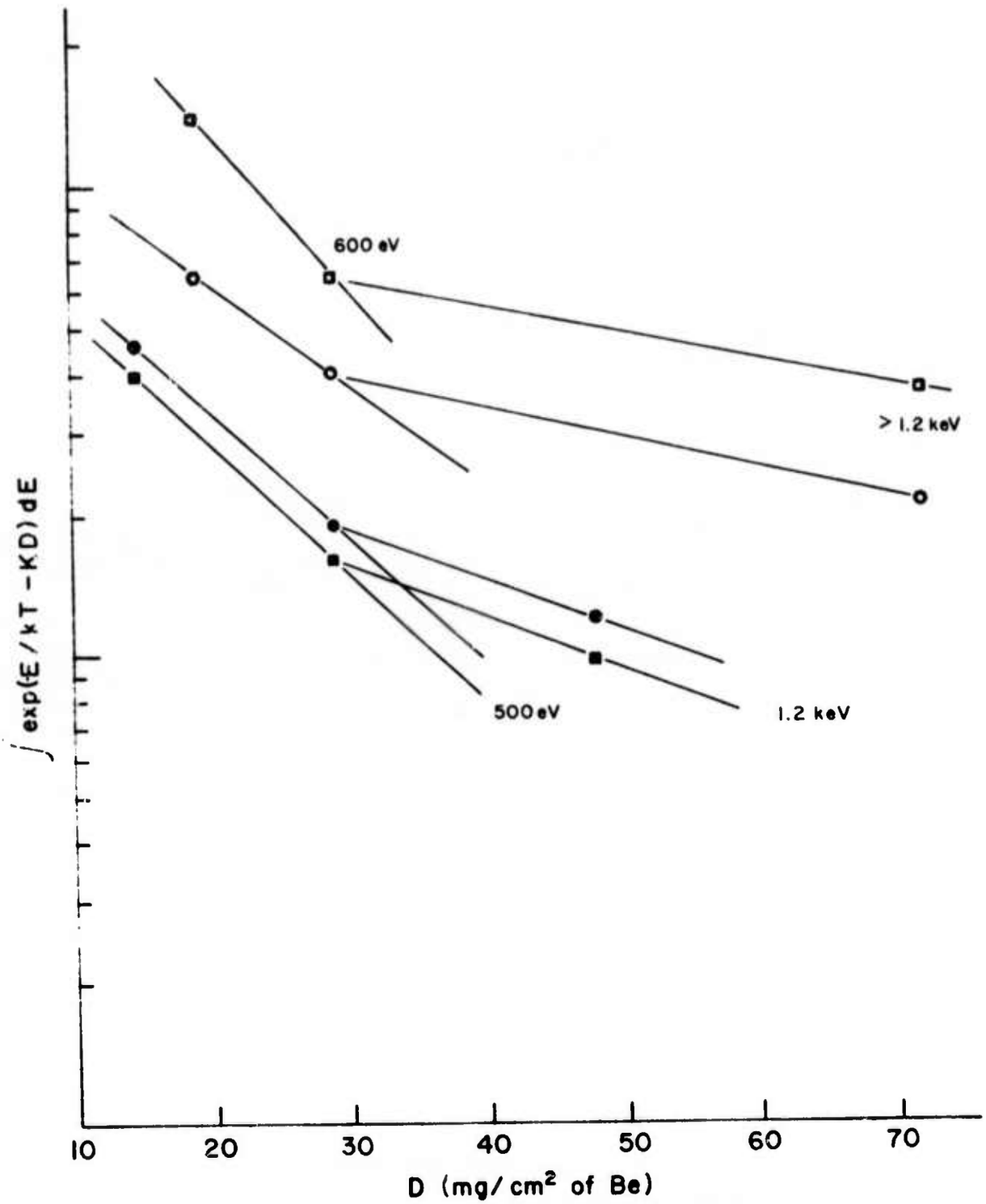

Fig. 2 — Relative x-ray intensities measured through different set of absorbers showing two temperature plasma component

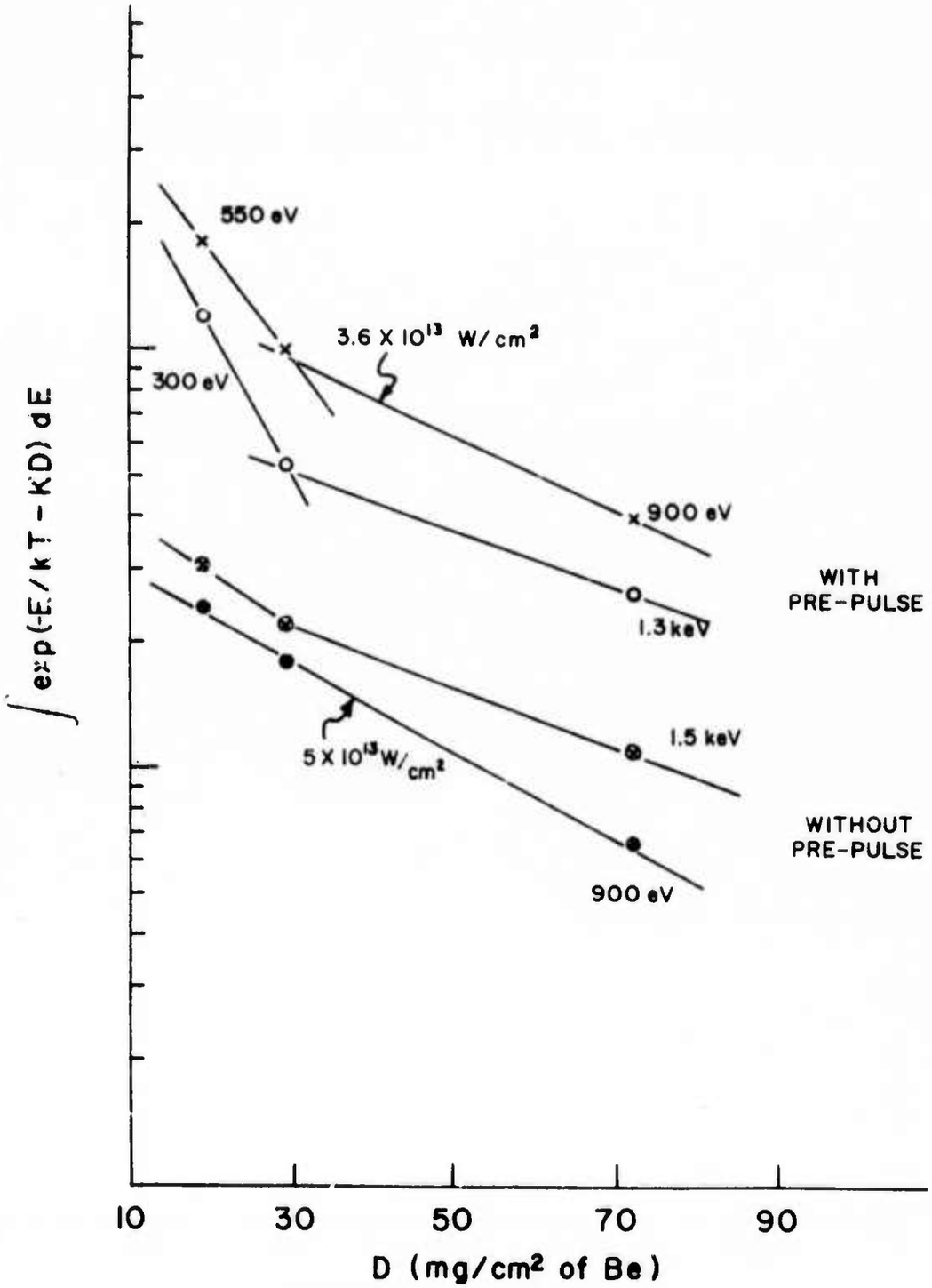

Fig. 3 — Relative x-ray intensities measured through different set of absorber showing the difference between shots with and without pre-pulse

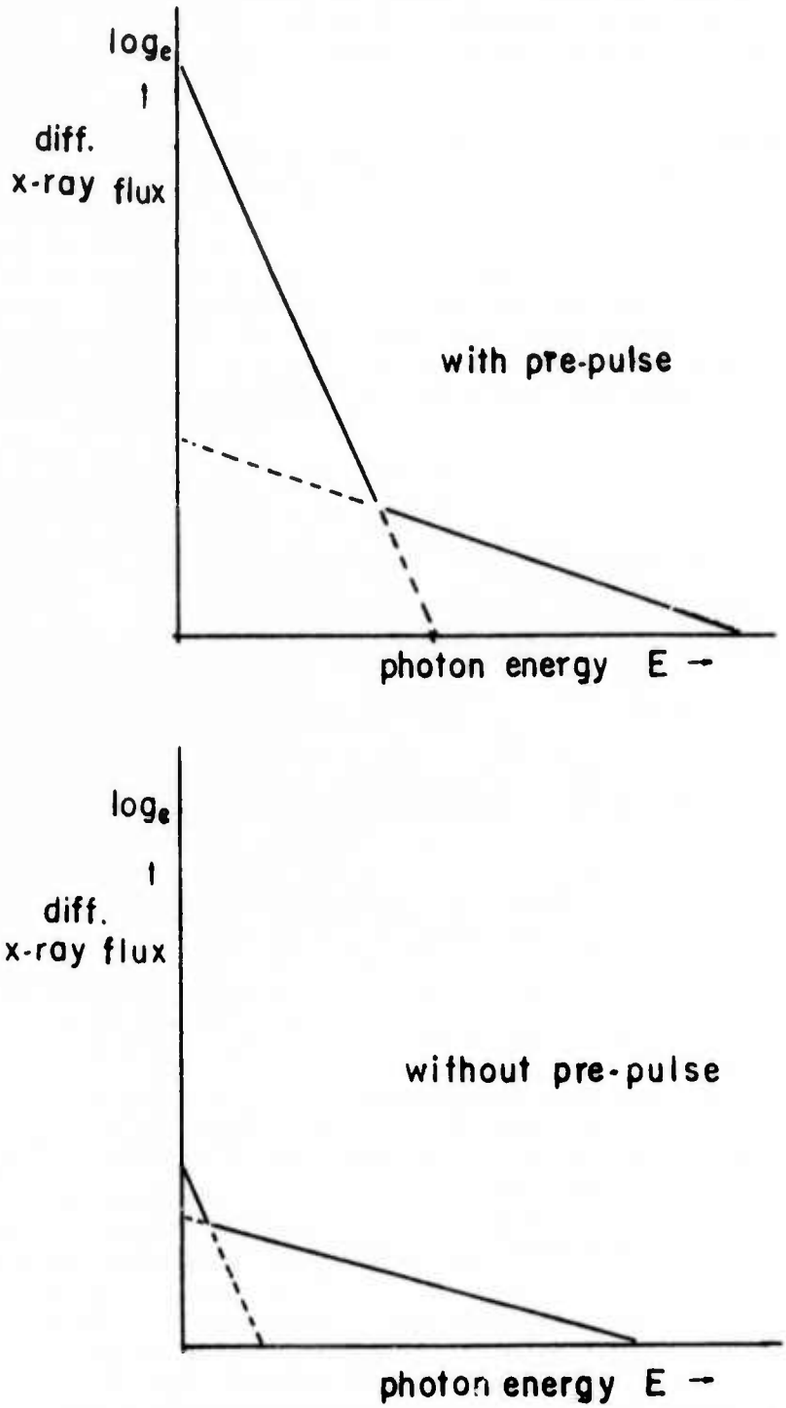

Fig. 4 – Deduced two component bremsstrahlungs as a function of photon energy for the cases with and without the pre-pulse

where normal absorption can take place is extremely small since the beam energy in the 25 ps laser is only about 100 mJ and therefore the laser mainly interacts with small area of the cut-off region through anomalous absorption. With the pre-pulse, on the other hand, the subcritical region increases its volume and also the area of the cut-off region to produce enhanced bremsstrahlung due to both plasma components.

In summary, the laser produced plasma obtained by focusing the 25 ps, 0.1 J Nd:YAG laser onto the Plexiglass target consists of two thermal components with electron temperature ranging from 500 to 1500 eV. With the presence of the pre-pulse, the level of the bremsstrahlung from both components increases by an order of magnitude over the case without the pre-pulse. No electron temperature increase is seen with the pre-pulse. The situation may be somewhat different when the present pre-pulse (25 ps, 10 - 30 mJ) is replaced by one of much longer duration and energy (2 ns, 5J glass laser). Further study will be extended for this case.

REFERENCES

1. R. C. Elton, Appl. Optics 14, 97 (1975).

2. J. F. Reintjes, T. N. Lee, R. C. Eckardt, J. L. DeRosa, R. A. Andrews, and R. C. Elton, Bul. Am. Phys. Soc. 19 885 (1974).

3. J. F. Holzrichter, R. Speck, and J. Swain, Bul. Am. Phys. Soc. 19 855 (1974).

4. T. P. Donaldson, R. J. Hutcheon, and M. H. Key, J. Phys. B 6 1525 (1973).

5. C. Yamanaka, T. Yamanaka, T. Sasaki, J. Mizui, and H. B. Kang, Phys. Rev. Lett. 32 1038 (1974).

II. B. SHORT PULSE LASER FACILITY

This section describes the picosecond laser facility used in the X-Ray Laser Program. Although this is the primary application, the lasers discussed here are versatile research tools with broad areas of potential use. In addition to studies of laser generated plasmas, it is also being used for such nonlinear optical effects as parametric generation of coherent x-rays and studies of resonantly enhanced self defocusing. The long range goal of the X-ray Laser Program is to generate population inversions at x-ray wavelengths in laser produced and laser pumped plasmas with ultimate application to an x-ray laser. For this application, a unique state-of-the-art laser is required which necessitates in-house development. This development is continuing with major portions of the facility now operational.

Controlled studies of interactions between laser pulses and laser generated plasma requires a laser system with unique characteristics. In particular, several synchronized pulses with durations on different time scales are required for purposes of prepulsing, plasma heating, and plasma diagnosis. Also, reliable operation in terms of reproducibility of pulse energy, duration, and profile, and of interpulse synchronization are important for systematic study of appropriate interactions. Good beam quality is required for efficient use of optical power; and short pulse durations at extremely high intensity are required for plasma heating. Finally, diagnostics for quantitative measurements of all these properties are necessary for meaningful comparison of the experiments with theoretical models.

Such a laser system which is tailored to the needs of these experimental studies has been developed and its fundamental characteristics were described in the last technical report. A schematic diagram of the system is shown in Fig. 5. The laser system produces multiple syncrhonized pulses on both nanosecond and picosecond time scales simultaneously. The picosecond pulses are generated in a mode-locked Nd:YAG laser that provides two 200 mJ output pulses of 30 psec duration with a time delay between them variable between 0 and 10 nsec. The nanosecond pulse is generated in a Q-switched laser and is variable in duration between 0.5 nsec and about 30 nsec with energy in the 1 to 10 J range. The two lasers are synchronized with a versatile switching technique which overcomes the jitter inherent in the production of either of the pulses separately and provides jitter times in the subnanosecond range. With this system plasmas can be generated with either the Q-switched pulse or one of the mode-locked pulses. The two output pulses of the mode-locked laser can be used for both pumping of existing plasmas and plasma diagnositics.

At the time of the last technical report the mode locked laser was fully operational with two output pulses of about 200 mJ, and preliminary work had begun on both the Q-switched laser and the synchronizing process. During the present reporting period, the major emphasis has been placed on design of the Q-switched oscillator and its synchronization with the mode locked laser. Development of the Q-switched laser amplifiershas also been proceeding and they have also been completed. Work on the mode locked laser has been in the following areas: a) completion of diagnostic measurements of the output with the determination of beam divergence and spectral width, b) improvement of long term performance by adding an isolation Pockels cell after the third amplifier, c) elimination of low level prepulsing which affects both the target experiments and the synchronization accuracy by addition of a flowing dye cell after the first amplifier and d) formulation of plans to extend the energy capability of the mode-locked laser to the 2 J range by adding a Nd:glass amplifier in one of the output arms.

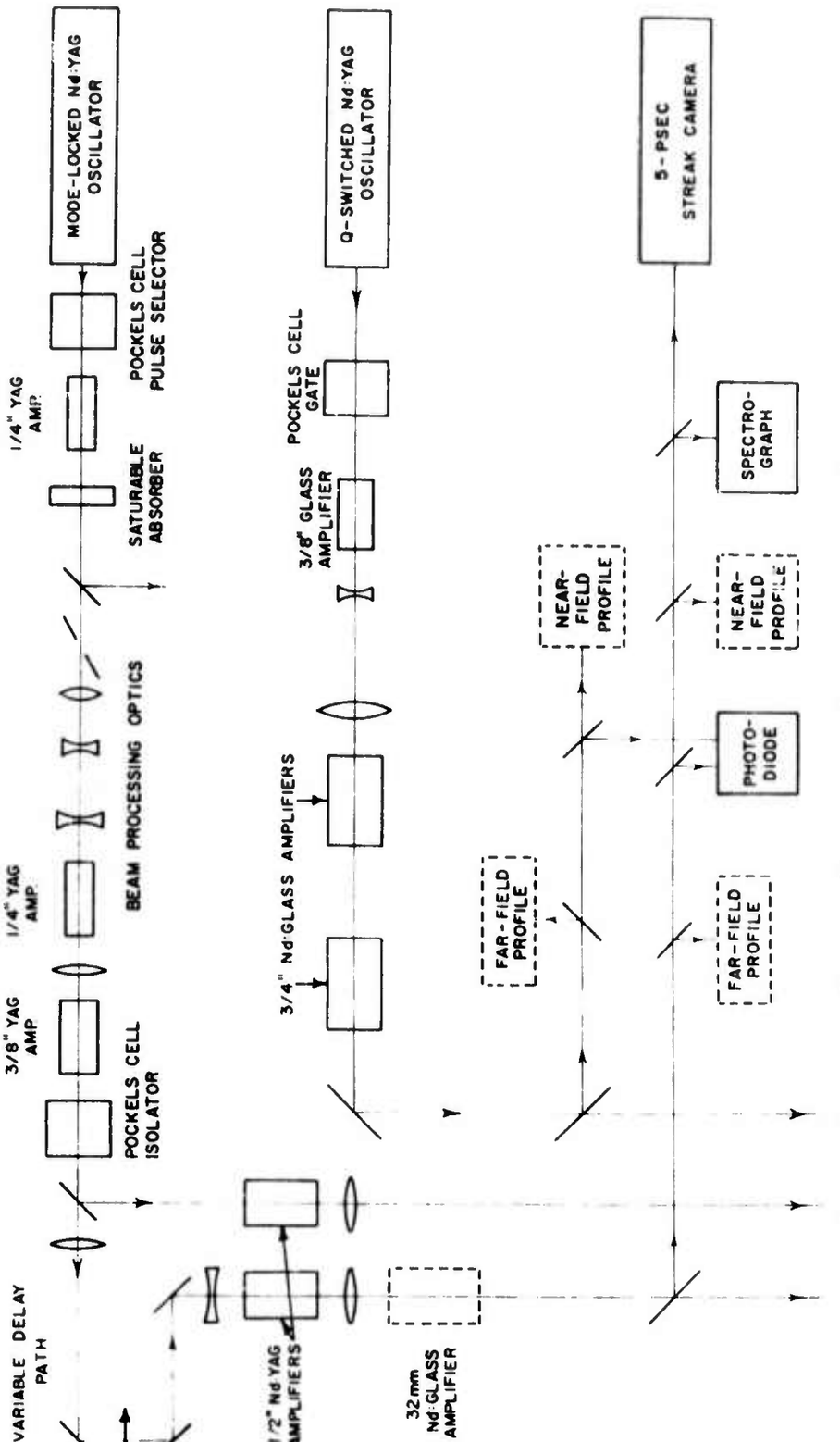

Fig. 5 — Schematic diagram of laser system showing synchronized mode-locked and Q-switched lasers and diagnostic equipment

II. B. 1. MODE LOCKED LASER

Laser Diagnostics

Diagnostics of the mode locked laser output have been completed in this period with measurements of the beam divergence and the spectral width. The beam divergence was measured by focusing the laser output onto a silicon diode array with a 400 cm, f/400 lens. Although this method of analyzing beam quality is not very sensitive to small aberrations, it does give a direct measure of focal spot size which is of primary interest in target experiments. The results of this measurement, shown in Fig. 6, show a smoothly varying angular distribution with a width (FWHM) of 120 μrad. For comparison, a beam which fills the last amplifier rod has a corresponding theoretical divergence angle of 108 μrad, indicating that the beam is about 10% above the diffraction limit. Some of this excess divergence is due to linear distortion in the 3/8" YAG amplifier rods and a small amount is due to the nonlinear distortion of self focusing.

The spectral width of the pulses was measured with a 1 m grating spectrograph, with typical results shown in Fig. 7. The spectral width varied from .7 to 2 cm^{-1}. The Nd:YAG oscillator produces bandwidth limited pulses of about .7 cm^{-1} spectral width. The amplified pulses show a small amount of spectral broadening due to self phase modulation which is consistent with our original estimates of a 1 cm^{-1} increase in spectral width in propagating through the amplifier chain.

Pockels Cell Isolation

During the course of operation, damage to the pulse selecting pockels cell was observed when the laser was used in target experiments. It was decided that this damage was caused by radiation reflected backwards from the target and amplified in the early undepleted stages of the amplifier chain. Reflection ratios of only a few percent are adequate to produce damaging intensities at the location of the pulse selector. To overcome this problem, a second Pockels cell was added after the third amplifier as shown in Fig. 5 which is timed to be transmitting for only a short period of time around the passage of the laser pulse and to block radiation reflected from the target. It also serves to help prevent earlier pulses in the train from reaching the target which could give rise to spurious prepulse effects. In order to eliminate any intensity fluctuations due to jitter in timing between the two Pockels cells, it is desirable to use the same electrical pulse to drive both switches. In the geometry shown, however, the Pockels cells cannot be operated in series because of the slow propagation speed of the electrical pulse. Furthermore, space did not permit the needed folding of the beam to make this mode of operation feasible. Therefore it was decided to operate the two Pockels cells with a doubly connected laser triggered spark gap which is shown in Fig. 8. Two cables are connected to the output electrode, each bringing a signal

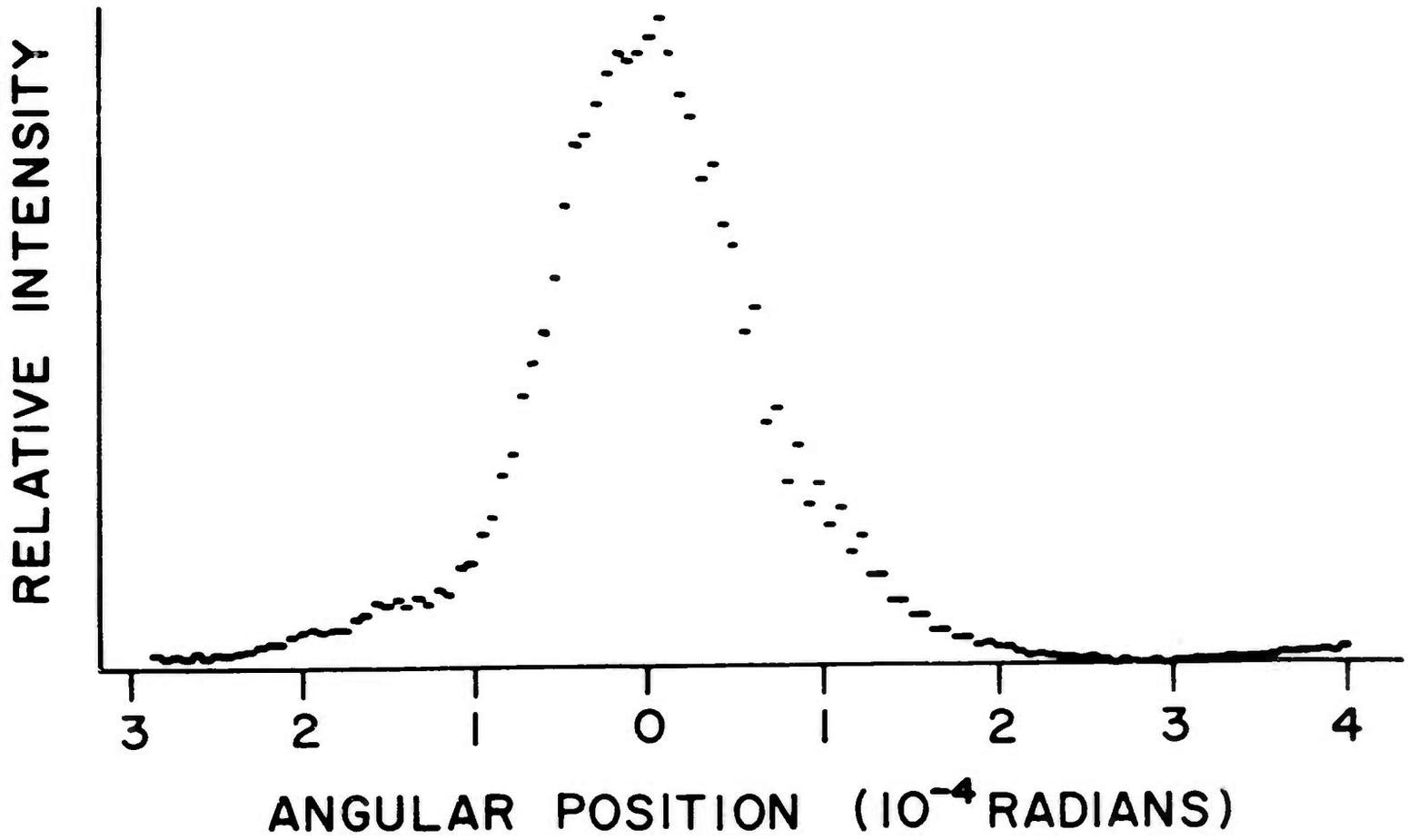

Fig. 6 — Spatial intensity profile of a single, amplified, mode-locked pulse

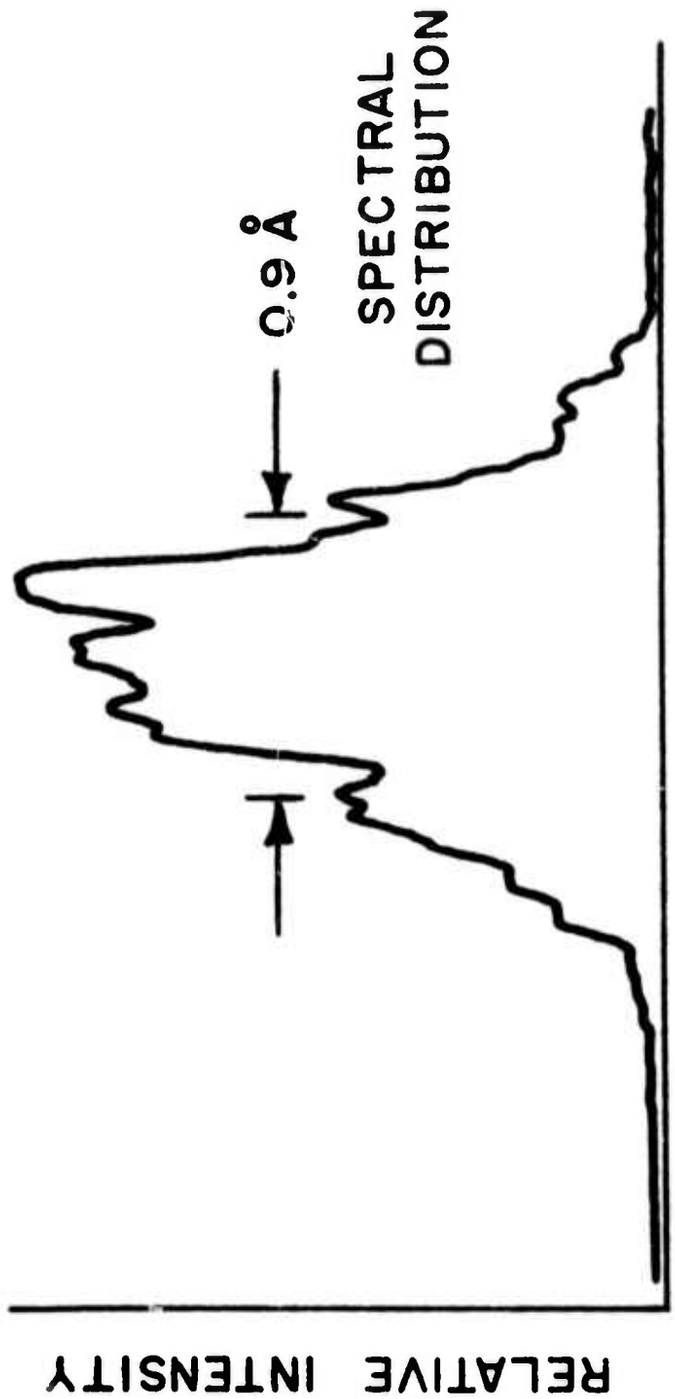

Fig. 7 — Spectral distribution of a single, amplified, mode-locked pulse

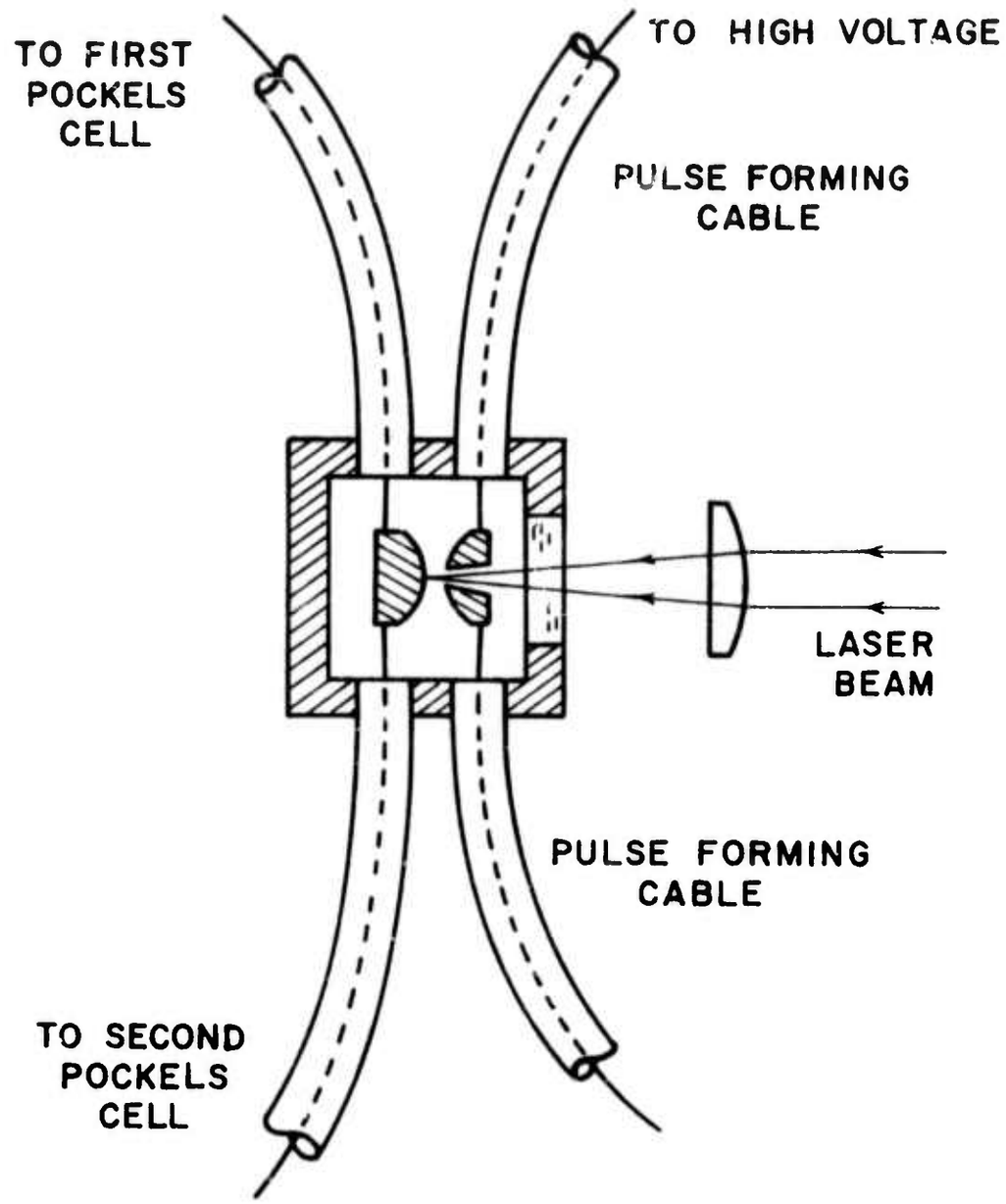

Fig. 8 — Schematic representation of doubly connected laser triggered spark gap. Two identical lengths of cable connected in parallel are used as the pulse forming network.

pulse to one of the Pockels cells. Two charging cables are used to match the impedences of the pulse forming network and the load. The difference in electrical length of the load cables is made equal to the optical path length between the two pockels cells.

The switching characteristics of the doubly connected spark gap were investigated and found to be equivalent to those of the conventional single cable gap. The transmission of the isolating Pockels cell was studied by comparing the transmitted fraction of a mode locked pulse with a voltage pulse applied to that without voltage, but with a 90° rotator placed between the polarizers. The transmission obtained with the Pockels cell switched is slightly greater than that obtained with the 90° rotator, indicating full switching of the Pockels cell. Overall insertion loss of the isolator due to surface reflections is about 30%.

External Dye Cell

A flowing dye cell was added to the laser just after the first amplifier as is indicated in Fig. 5, to attenuate low level pulses prior to the selected one which leak through the pulse selector as well as any secondary pulses which are transmitted due to imperfect pulse selection. It works in conjunction with the Pockels cell isolator to prevent any spurious prepulses from reaching the target, and also greatly improves the stability of the synchronization with the Q-switched laser. A dye concentration was chosen to give a low level transmission of 1% and a high level transmission of about 60%. In order to compensate for the additional losses of the dye cell and isolator the third amplifier was changed to $\frac{1}{4}$", increasing the amplification of this stage by a factor of 3 and bringing the net gain of the amplifier chain back to its original value.

Glass Amplifier

As was indicated in the last report, the output level of 200 mJ is the maximum that can be achieved with $\frac{1}{2}$" YAG rods. Since at this level, about 40% of the stored energy is being extracted from the last amplifier stages, further increases in stored energy are limited by parasitic oscillations in the rod, and further increases in beam intensity are accompanied by distortion due to self focusing. Therefore plans have been made to add a 32 mm diameter glass rod to the delayed output arms. This amplifier should provide a gain of 10 to give output energies near 2J without depletion. The larger diameter of the glass rod means that the intensity is not increased and therefore severe distortion due to self focusing will not occur. Table I indicates the performance of the mode-locked laser at various stage with the glass amplifier included.

TABLE I

MEASURED PARAMETERS OF PICOSECOND LASER SYSTEM

STAGE	PULSE ENERGY (mJ)	PULSE DURATION (PSEC)	POWER (W)	BEAM PROFILE	INTENSITY (W/CM^2)	AMPLIFIER GAIN	
OSCILLATOR	.20	25	8×10^6	1 mm (Circular Gaussian)	10^9		
AMPLIFIER							
1st STAGE	4.8	25	1.9×10^8	2 mm	6×10^9	30	(30)
2nd STAGE	13.2	25	5×10^8	.6 X .3 CM (Elliptical Airy Disc)	3.5×10^9	10.6	(12)
3rd STAGE	114.0	30	4×10^9	.5 X .9 CM	1.1×10^{10}	9.4	(12)
4th STAGE	210	30	7×10^9	.5 X 1.2 CM	1.25×10^{10}	4.1	(7)
TARGET	190	30	6.3×10^9	$30\mu \times 60\mu$	5×10^{14}		
AMPLIFIER*	2	30	6×10^{10}	32 mm (Circular)	8×10^9	10	
TARGET	2	30	6×10^{10}	$40\mu \times 40\mu$	6×10^{15}		

NOTE: The parameters of the picosecond laser system are tabulated at various stages. Large signal gain under actual operating conditions is given in the last column with small signal gain in parentheses. Total gain is reduced from the product of individual gains by power loss at the apertures and reflections.

*Values of glass amplifier are projected.

II. B. 2. Q-SWITCHED LASER

The primary application of the Q-switched laser system is to provide a pulse for generating a plasma which can subsequently be heated or pumped with a short pulse generated by the mode-locked laser. To meet this need we are developing a neodymium YAG and glass laser oscillator-amplifier system. Good spatial beam quality is again important to provide high brightness on target and to avoid self focusing in the amplifier chain. Single longitudinal mode operation of the oscillator is desired to provide reproducible pulses with no mode beating for reproducible plasma generation. High frequency beating of widely separated modes must also be surpressed to avoid self-phase modulation during amplification. Adjustable pulse duration in the $\frac{1}{2}$ nsec to 30 nsec range with energies between 1 and 10 J will allow control of the properties of the plasma.

Neodymium:YAG is used as the active material in the Q-switched oscillator because its narrow bandwidth of 7 Å makes single longitudinal mode operation easier to obtain. Fundamental transverse mode operation is obtained by placing an aperture in the resonant cavity. A Pockels cell is used as the Q-switching device and provides the rapid build up times required for synchronization with the mode-locked pulse train generated by the first laser. Build up times typically 110 nsec $\pm$ 5 nsec are observed from triggering of the Pockels cell to the peak of the Q-switched pulse. A second Pockels cell placed external to the oscillator is used to select a portion of the Q-switched pulse of variable length. A folded delay path is used to bring this pulse into synchronization with the single mode-locked pulse. The Q-switched pulse is then expanded and passes through three stages of amplification. Neodymium:glass is used in the amplifier stages because of improved energy storage. The first stage is 3/8 inch by 6 inches long and the second and third are $\frac{3}{4}$ inch diameter by 12 inches long.

The required short build up time of the Q-switched oscillation makes it difficult to operate this laser in a single longitudinal mode. The small number of round trip transits between Q-switching and the peak of the Q-switched laser oscillation, approximately 30, requires good discrimination between the primary or "single" lonitudinal mode and other longitudinal modes. For example, if the intensity of the second strongest mode is required to be less than 10^{-4} that of the peak mode, the amplitude will be approximately 10^{-2} of the amplitude of the peak mode resulting in a 4% intensity ripple. If the oscillations build up from more or less equal intensities of random noise in each mode before Q-switching, and the strongest longitudinal mode is required to be 10^4 more intense than any other at the peak of the Q-switched output, then the net gain for all other modes must be down at least $(10^{-4})^{1/30} = .736$ per cavity round trip transit. Of course, Q-switching will not be perfect and there will always be some feed back in the cavity. The initial fields in the modes will not be random noise, and the above number is for the worst case.

A resonant reflector consisting of 3 flat parallel saphire elements was used for frequency selection as reported in the last technical report. That resonant reflector appeared to give satisfacory mode-selection when the laser output was monitored with a .5 nsec risetime photodiode-oscilloscope combination. Observation with a high resolution Fabray Perot interferometer, however, showed what appeared to be a single mode was actually two modes spaced by .6 cm^{-1} as shown in Fig. 9. The beating frequency of these two modes was 18 GHz, too fast to be seen on the oscilloscope.

It is now planned to use a birefringent filter in combination with a resonant reflector (Fig. 10) to obtain better frequency selection. A calcite slab will be used as a high order retardation plate. Retardation will be adjusted by angular orientation of the crystal. In this way retardation at the center of the fluorescence spectrum can be set to a whole number of wavelengths to provide maximum transmission through the polarizer. Slightly different wavelengths will have noninteger values of retardation and not be completely transmitted through the polarizer. Transmission through the filter is given by the expression

$$I_{out}/I_{in} = \cos^2(\phi/2)$$

where ϕ is the angular retardation. Using a 2 cm calcite slab as planned, there will be only .26 cm^{-1} range to either side of the fluorescence peak where mode discrimination is less than 10^4 in 30 round trip transits. Recall that with fluorescence alone the range was .83 cm^{-1} to either side of the peak. With the addition of the birefringent filter, selection of a single longitudinal mode will be greatly facilitated.

The build up time of the Q-switched oscillation must be kept short to ensure minimum jitter. Q-switching is triggered on the early part of the mode-locked pulse train, and the peak of the Q-switched oscillation must overlap the peak of the mode-locked pulse train. Delay times from Q-switching to peak output of typically 110 nsec with jitters of $\pm$ 5 nsec have been obtained as shown in Fig. 11. As was indicated in the section on synchronization these times are satisfactory for synchronizing the two lasers. Operation of the external Pockels cell shutter for selection of the $\frac{1}{2}$ nsec to 30 nsec pulse segment is also discussed in the synchronization section.

Energy output of the Q-switched oscillator is typically 20 mJ. The Nd:glass amplifiers amplify the energy of a segment of this pulse to a final value to 1 to 10 J depending on the length of the gated segment. The 3/8 X 6 inch amplifier has a maximum low level gain of 10 and the two $\frac{3}{4}$ X 12 inch amplifiers each have maximum gain of 20 (Fig. 12). Total gain of the amplifier system is 4000. Energy stored in the final $\frac{3}{4}$ X 12 inch rod when at a gain of 20 is 53 J.

(a)

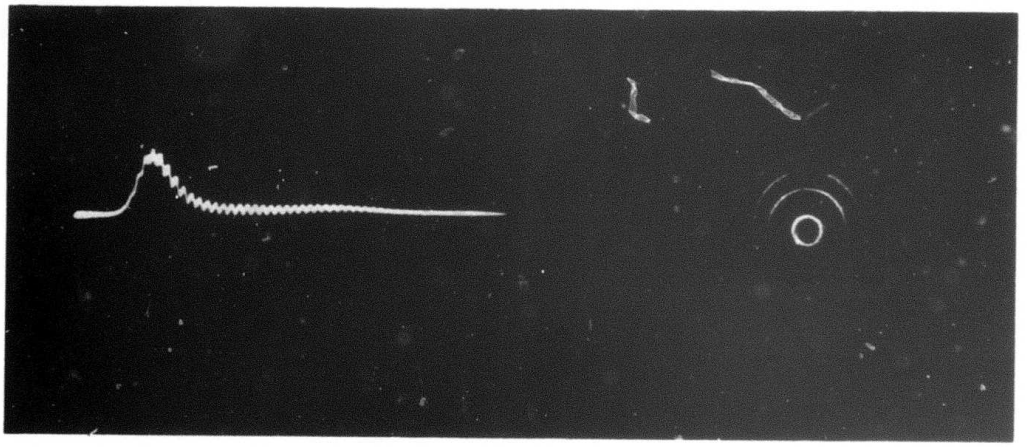

(b)

Fig. 9 — Oscillograms and Fabray Perot interferograms of two pulses generated by the Q-switched oscillator. The pulse display in (a) appears smooth on the oscillogram but actually consists of two modes of nearly equal intensity but widely spaced in frequency as shown on the interferogram. No widely spaced components are shown in the interferogram of (b); some adjacent mode heating, however, is seen in the oscillogram.

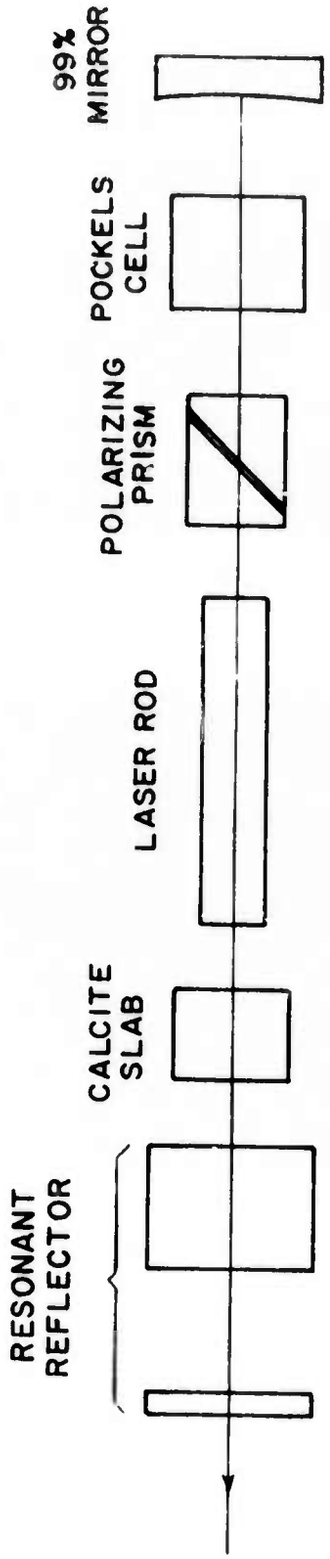

Fig. 10 — Q-switched oscillator cavity showing position of the calcite slab. The calcite slab, used as a high-order waveplate, and the polarizing prism form a birefringent filter that improves frequency selection.

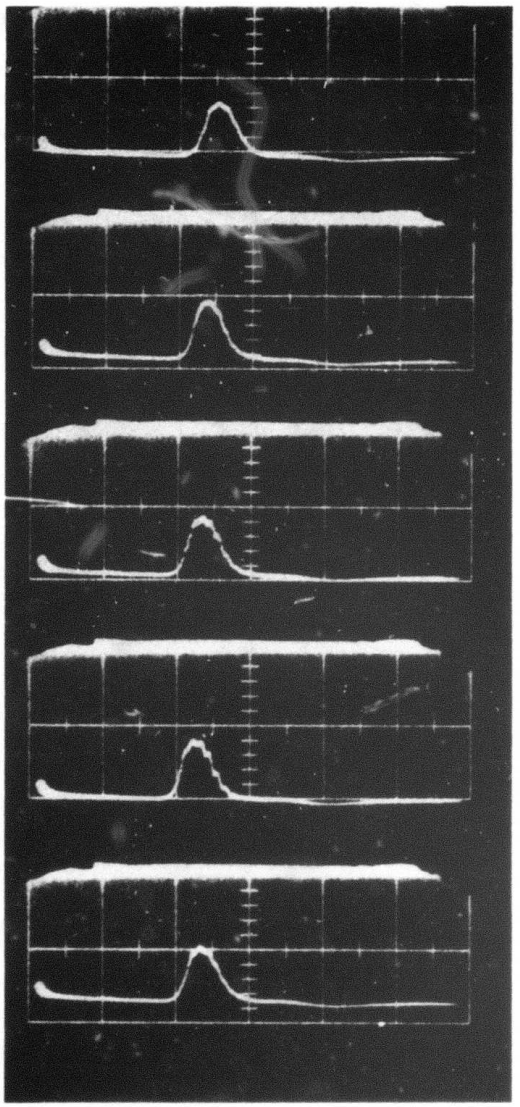

Fig. 11 -- Oscillograms showing buildup time and jitter of the Q-switched pulse. The oscilloscope was triggered with the voltage applied to the Pockels cell Q-switch. Sweep speed is 50 nsec per division. Five successive oscillograms indicate reproducibility.

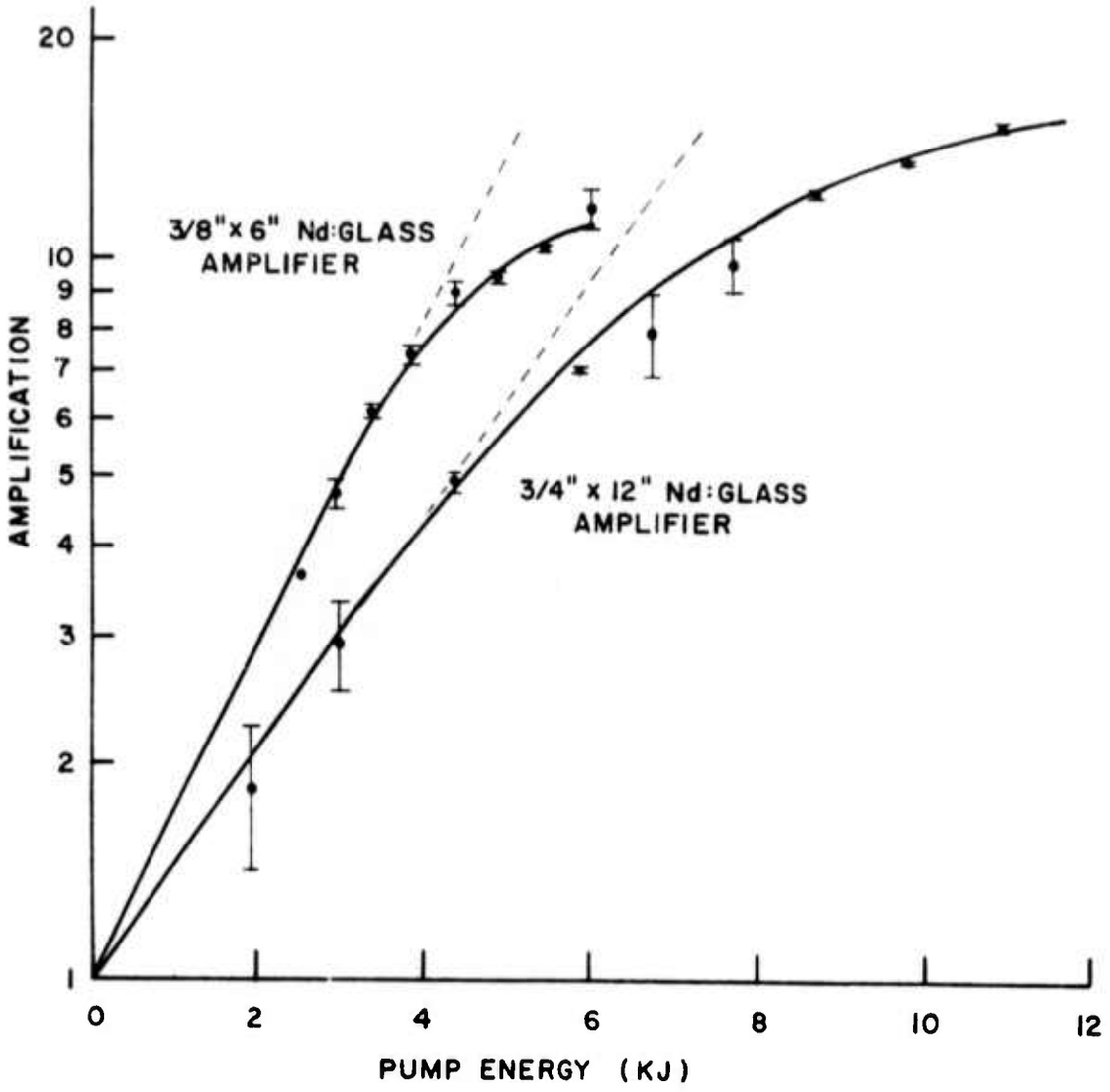

Fig. 12 — Amplifier pumping curves show low intensity amplification as a function of pump energy

Therefore gain saturation will be a small problem in the proposed output range. The amplifier pumping curves show that gain is limiting because of amplified stimulated emission. It would be of little advantage to increase the level of pumping. If more gain is desired it could be obtained by suppressing parasitic oscillations by the technique of index matching with the cooling solution.

II. B. 3. SYNCHRONIZATION

A major effort during this period was devoted to stabilizing the synchronization between the two oscillators. The synchronizing scheme was described in detail in the last report and is outlined briefly here. The technique involves a three step switching process as indicated in Fig. 13. The synchronization process starts with the appearance of the mode-locked pulse train with a jitter of about $\pm$ 10 μsec relative to the flash lamp pulse. A PIN silicon photodiode is used to detect the pulse train and trigger an electronically switched spark gap that removes the voltage from the Pockels cell Q-switch in the second laser. The Pockels cell is switched on an early pulse in the mode-locked pulse train to allow for the 35 nsec delay of the spark gap and build up time of the Q-switched oscillation. The peak of the Q-switch pulse is synchronized to the peak of the mode-locked train with a jitter of $\pm$ 25 nsec. A laser triggered spark gap is then switched on the leading edge of the Q-switched pulse and a voltage pulse is applied to another Pockels cell which switches out a single pulse from the mode-locked train. The jitter in timing of the selected pulse is limited by the 6-7 nsec pulse spacing in the train. The selected mode-locked pulse is then used to shutter out a portion of the Q-switched pulse near its peak. This last switching event can be accomplished by using a greatly overdriven spark gap, which can provide ultimate synchronization accuracy in the subnanosecond range.

At the time of the last report the first step in the process had been accomplished using a glass Q-switched oscillator and a Krytron switch for the Q-switching Pockels cell instead of a spark gap. In this period complete synchronization has been achieved and considerable effort has been spent in optimizing important parameters at every stage. In the first stage the Q-switched pulse is synchronized with the mode locked pulse train (Fig. 14) with a jitter of $\pm$ 25 nsec. The electronically triggered spark gap represents a major improvement over the Krytron switch in reducing the overall delay in appearance of the Q-switched pulse. The shorter delay allows the Q-switched pulse to be reliably overlapped with the peak of the mode locked train. In Fig. 15, the selection of a single mode locked pulse by the Q-switched pulse is shown. In (a) the electrical pulse which drives the pulse selecting Pockels cell is shown relative to the Q-switched pulse. In (b) the rejected pulse train is shown, indicating selection of a mode locked pulse near the peak of the train. Finally in (c), the selected mode locked pulse is shown along with the Q-switched pulse. In all three pictures the delays between the two signals have been adjusted so that the pictures show the relative timing of the two

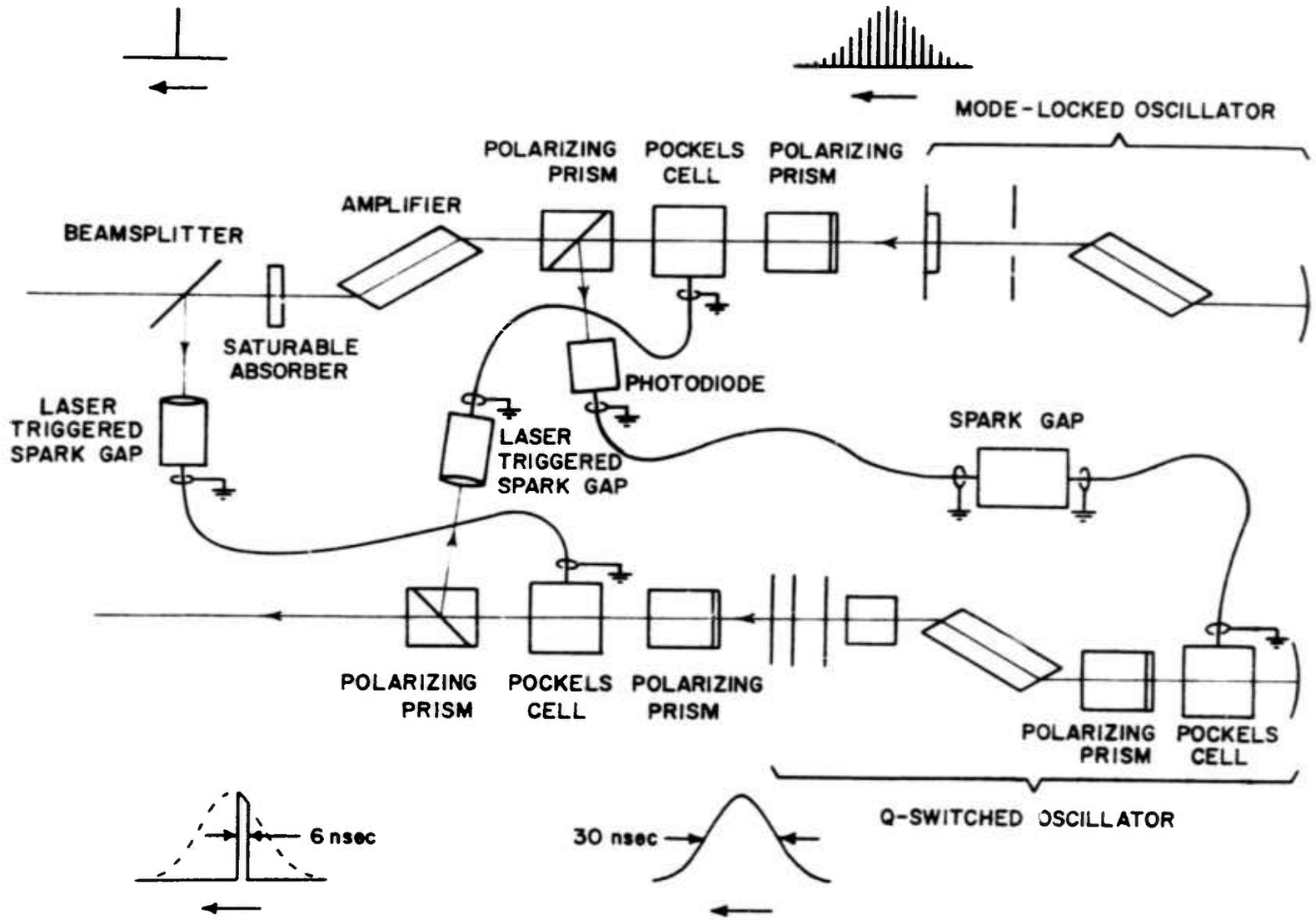

Fig. 13 — Synchronization scheme of pulsed laser oscillators

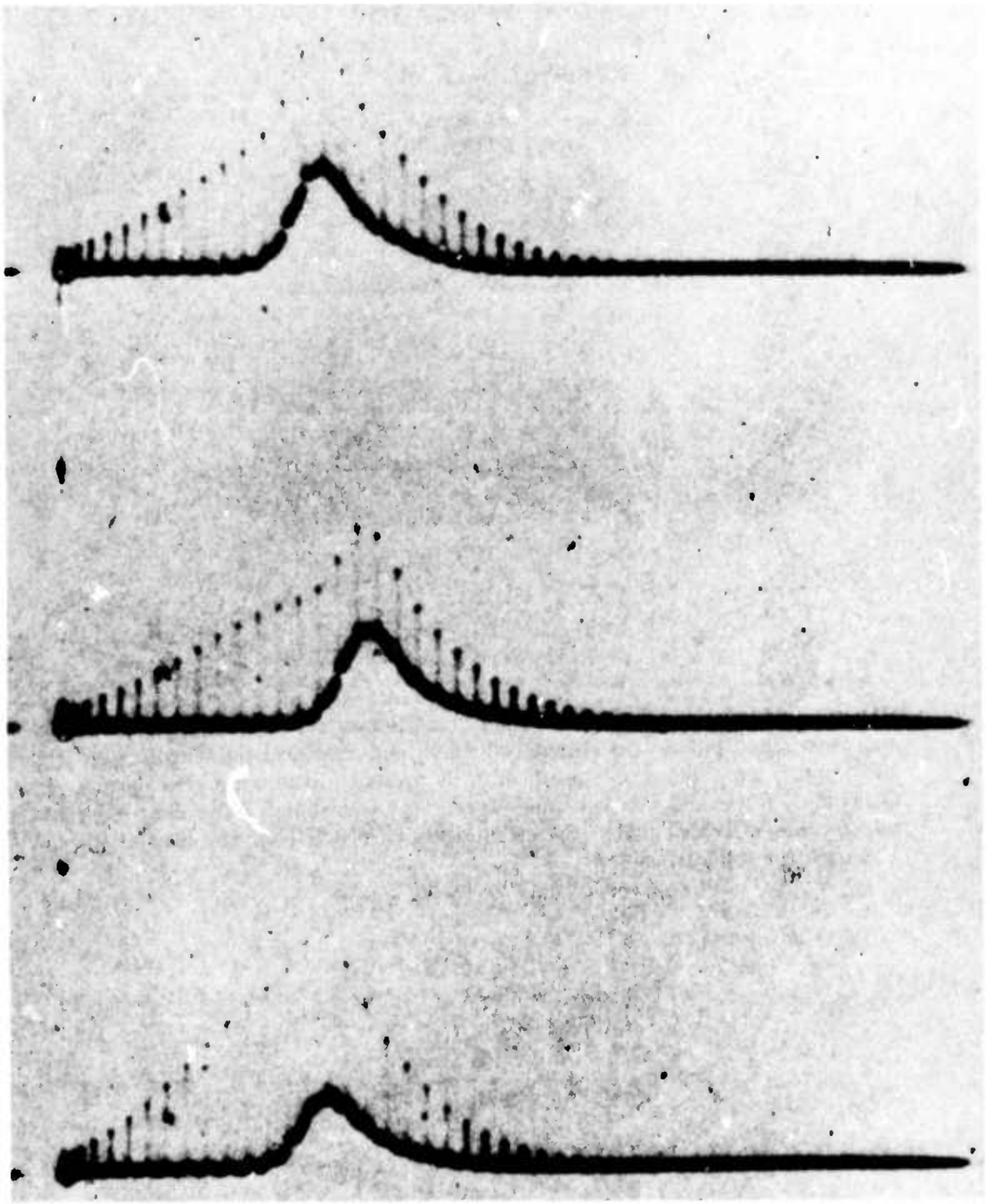

Fig. 14 — Oscillograms displaying both synchronized mode-locked pulse train and Q-switched laser pulse. Both laser beams were incident on the same photodiode. Sweep duration is 300 nsec. Three successive oscillograms are shown.

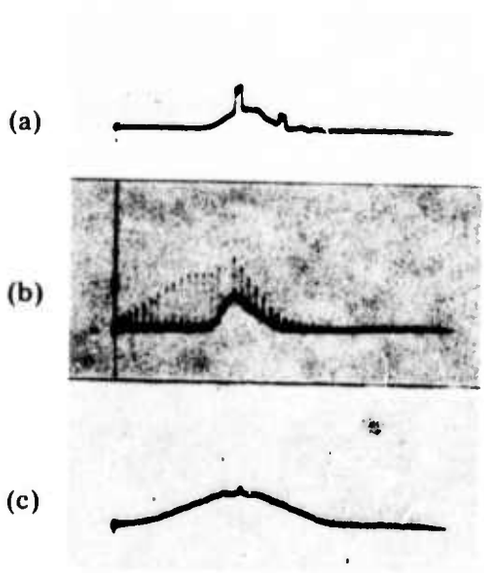

Fig. 15 — Oscillograms showing synchronization of selected mode-locked pulse and Q-switched pulse. (a) Q-switched pulse and electrical pulse from laser triggered spark gap. Some cable reflection is present in the combined signals. (b) Q-switched pulse and rejected pulse train. (c) Q-switched pulse laser pulse and selected mode-locked pulse. Sweep durations are 300 nsec for (a) and (b) and 120 nsec for (c).

pulses at the position of the Q-switching gate.

The complete synchronization is shown in Fig. 16 with a single mode locked pulse superimposed on a 6ns gated Q-switched pulse. Again three successive oscillograms are shown, indicating the degree of reproducibility of the timing. The delay between the two pulses can be varied by changing their relative optical path. For example, the mode locked pulse can be placed after the Q-switched pulse (Fig. 17).

The standard deviation of 200 psec in the delay between the two pulses is adequate for our target experiments. However, an absolute delay of 18 nsec was required to bring the pulses into concidence. Since space does not permit the reliable use of such an unwieldy optical path a study was made of the characteristics of a laser triggered spark gap when fired by a single mode locked pulse. The delay in spark gap firing was measured as a firing function of voltage on the spark gap at a constant laser pulse energy of 11 μJ. The results show that as the voltage approaches the spontaneous breakover value, the delay time decreases, with the jitter somewhat larger near the maximum voltage than at lower voltages. It is clear from these results that for minimum delay the spark gap should be operated as near to the spontaneous breakover point as possible. The delay time was also measured as a function of laser pulse energy with the voltage held constant at 93% of its spontaneous breakover value (Fig. 18). At low laser pulse energies, the delay is on the order of 15 ns, which is comparable to that observed in measurements of the synchronized laser pulses. For pulse energies on the order of 1 μJ, the jitter is less than 1 nsec, also consistent with the previous measurements. As the laser energy is increased, the delay decreases, while the jitter first increases and then levels off at a value higher than that obtained at lower energies. Such behavior has been attributed to the effects of low level leakage pulses which appear prior to the selected pulse. At low laser energies, the level of these pulses is too small to fire the gap and the triggering is primarily determined by the single selected pulse. When the laser energy is increased by three orders of magnitude from threshold, however, the leakage pulses can be effective in pretriggering the gap causing an increase in jitter. In order to test this hypothesis, an external dye cell was added to the mode locked laser to eliminate these low level leakage pulses and the measurements were repeated. In the course of this second set of measurements it was observed that precise focusing of the pulse onto the electrodes is very important and changes of the order of ½ mm in focusing distance result in very large perturbations of timing stability. Results of measurements at two laser powers with the set up at optimium focus are indicated in Fig. 19. Here it is seen that at the high level laser energy, the delay is comparable too that obtained without the dye cell, but the jitter has been decreased by a factor of 5 to a value of .12 nsec. At lower laser power, both the delay and jitter increase, as is expected. Hence, this set up is capable of providing very precise timing of the mode locked and Q-switched pulses with a delay sufficiently short to make

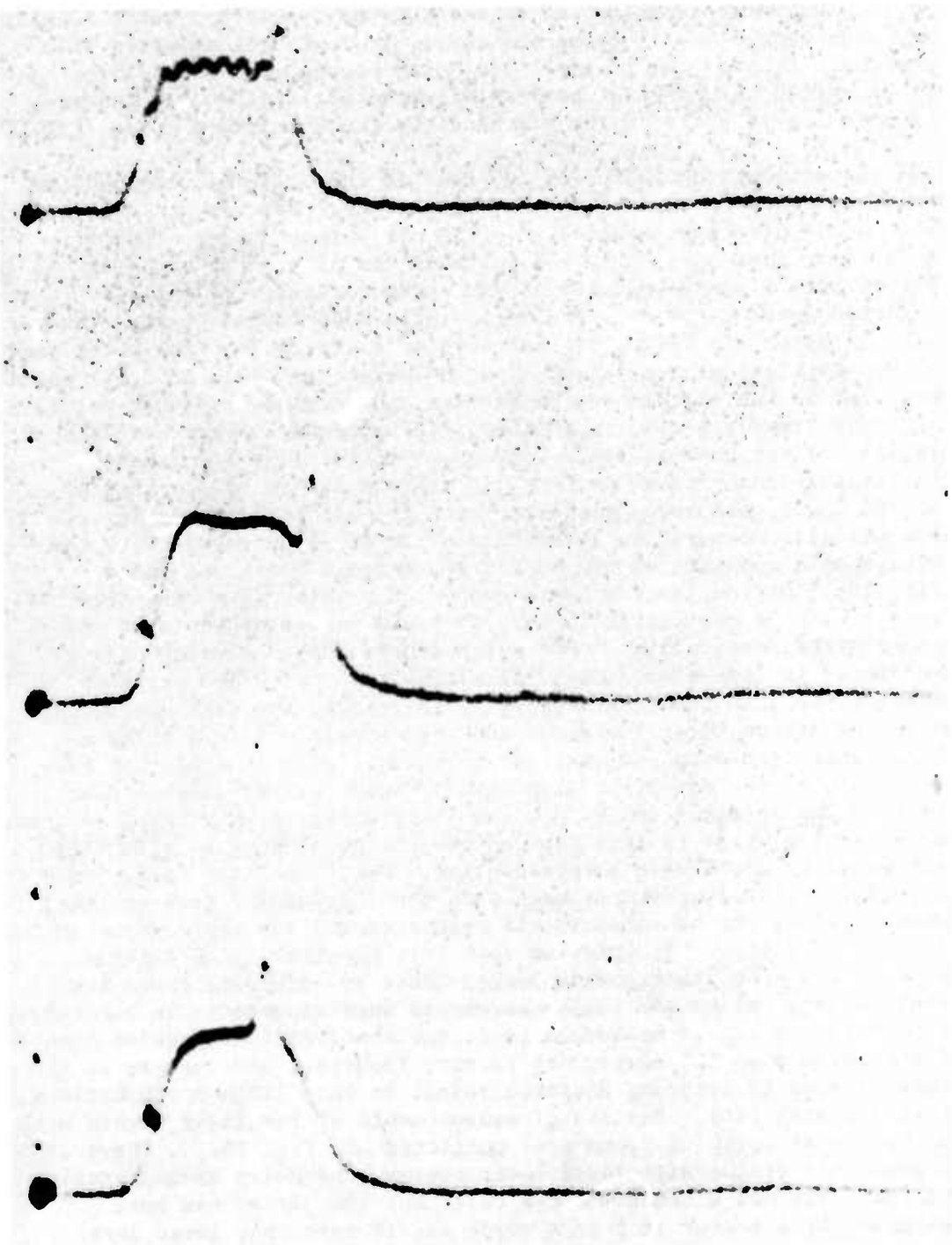

Fig. 16 — Oscillograms of synchronized switched out mode-locked pulse and 6 nsec shuttered portion of Q-switched pulse. Both pulses were incident on the same photodiode. Sweep duration is 30 nsec. Successive oscillograms are shown.

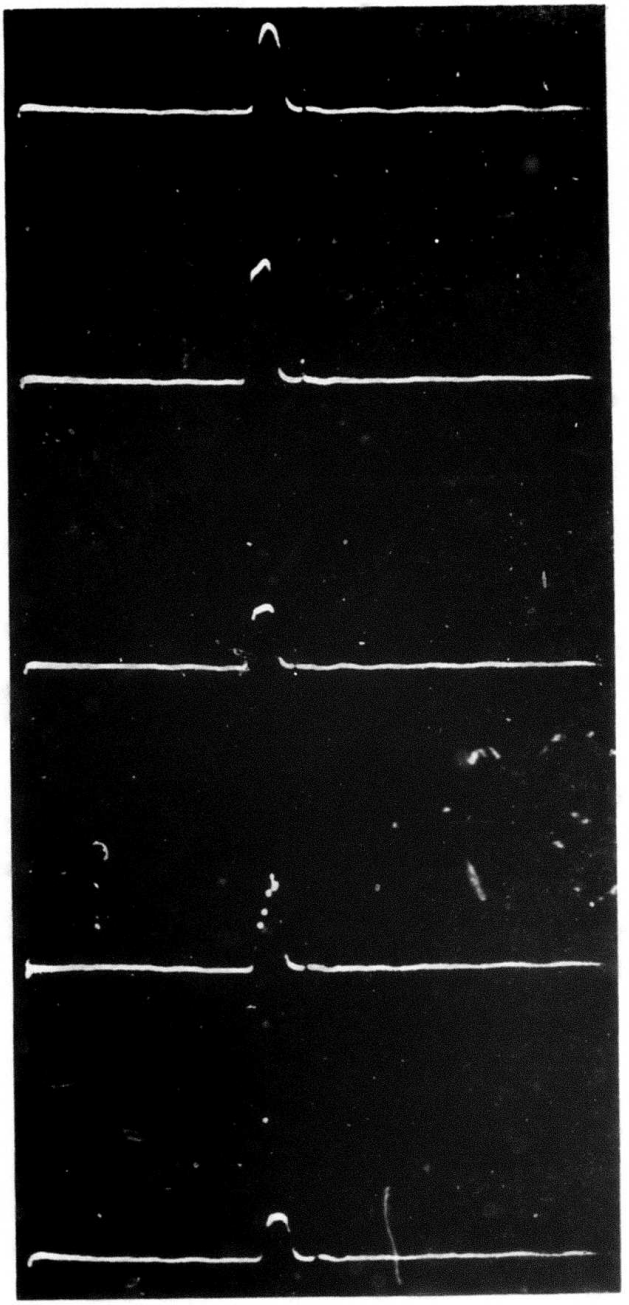

Fig. 17 — Oscillograms of synchronized pulses with mode-locked pulse delayed and placed after the Q-switched pulse segment. Five successive oscillograms indicate reproducibility. Sweep duration is 60 nsec.

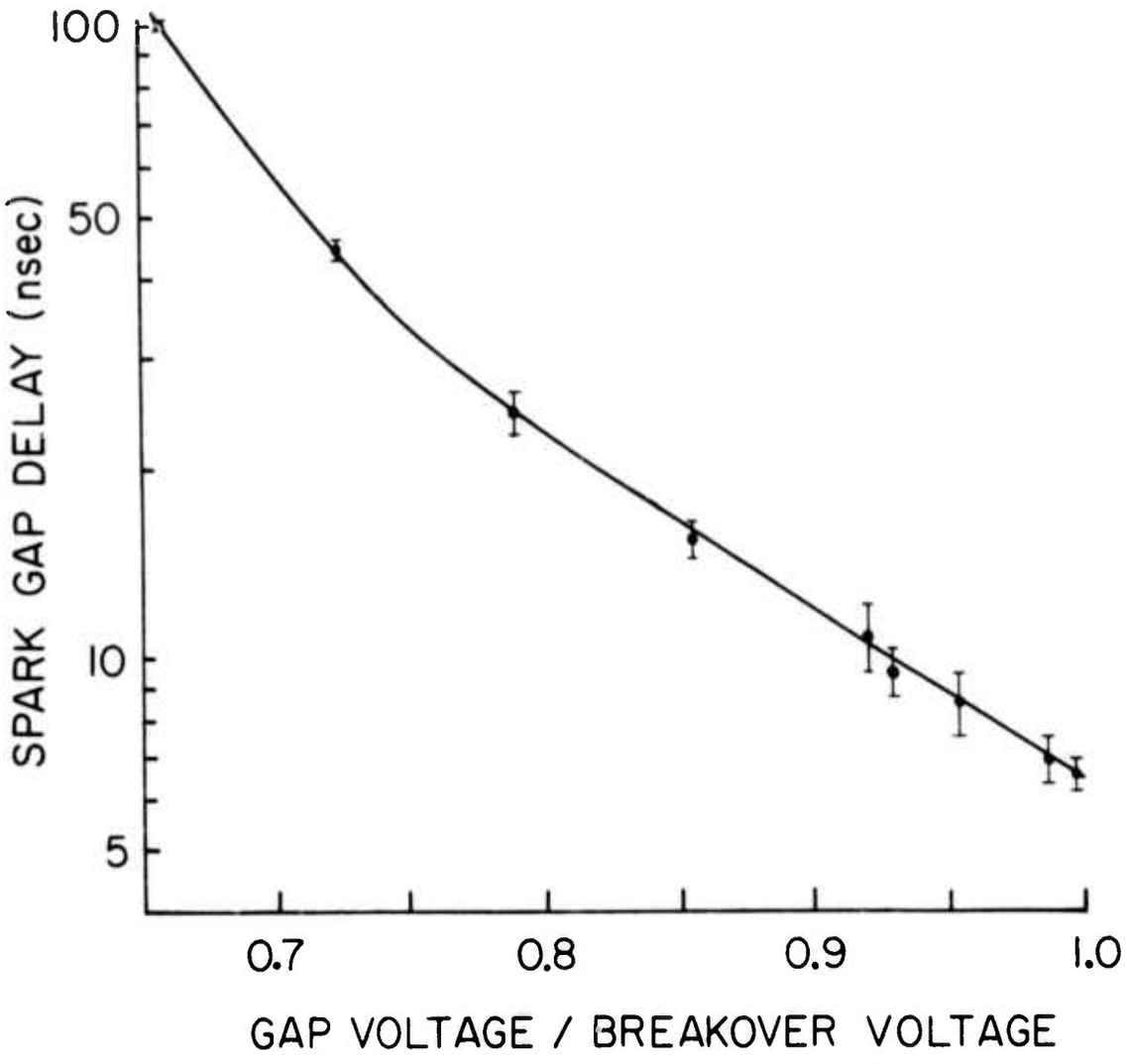

Fig. 18 — Laser triggered spark gap delay as a function of voltage applied to the gap

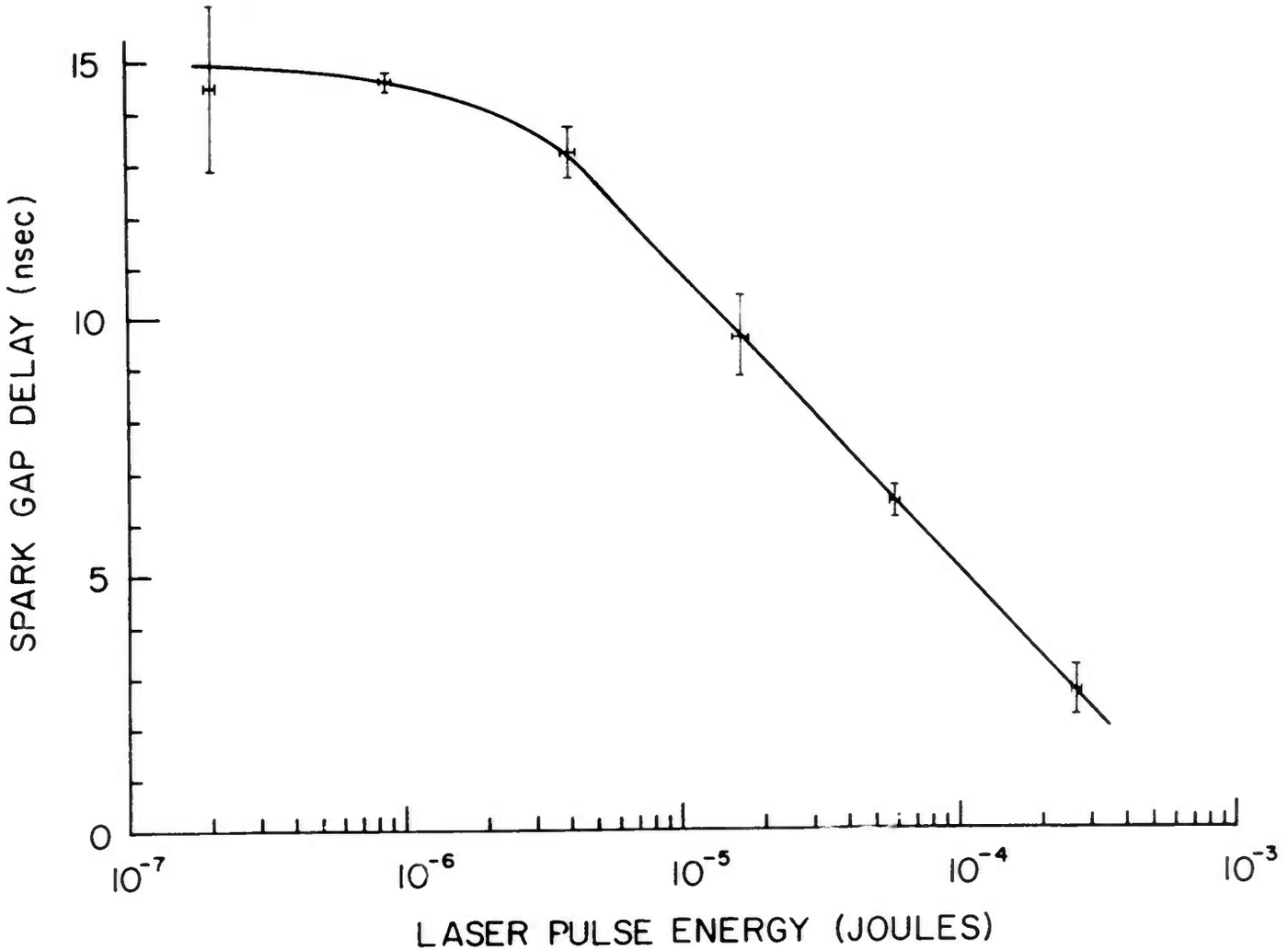

Fig. 19 — Delay in firing of a laser triggered spark gap as a function energy of the 25 psec laser pulse

beam handling more practical.

III. RESONANT CHARGE TRANSFER PUMPING

III. A. ANALYSIS

In the last semiannual report, the motivation for achieving preferential level population by resonance charge transfer in carbon-ion/atom collisions was discussed at some length, and evidence for the large cross section involved was presented. Since that time, the classical Landau-Zener formulation has been extended to lighter elements in a search for resonant transitions populating 3s levels in hydrogenic or helium-like ionic species[1]. The hope is to achieve a quasi-cw population inversion between 3s and 2p levels similar to that which was extrapolated for 3p→3s transitions from the near-UV (See Section VI.B.) but resulting in shorter wavelength lasing. (Direct 1s→3s pumping is inefficient; hence a search for an energy-resonant transition.) The scheme is diagrammed in Fig. 20, where ΔE_{exo} indicates the energy defect in an exothermic reaction. The velocity dependence of the cross section resonances are reproduced[2] in Fig. 21 for various energy defects, where approximate ion thermal velocities for hydrogenic and helium-like species are also indicated. Inversion of these data produces the resonance peaks as a function of ΔE shown in Fig. 22 for various degrees of ionization. Here also are shown the various ion/atom combinations leading to resonant transitions into excited quantum states, n^*, indicated numerically; thus the preferred $n^*=3$ state transitions shown in Fig. 20.

Further parameters for some of the possible transitions are included in Table II, where transitions to the ground state are intentionally omitted since inversion of such seem most unlikely possibilities, at least at present. In this table are given the laser wavelengths, the "maximum" electron densities above which collisional depopulation seriously competes with radiative decay, the maximum background-atom pressure P_A permitted for transmission of the radiation over a 3 cm length. (P_A could be increased up to about 100 Torr before laser breakdown effects become troublesome, should significant photoionization of the background gas occur; for hydrogen the protons produced by photoionization do not absorb). Also shown are the spontaneous lifetimes t_u of the upper laser level, of use for self-terminating transitions (not for the 3s→2p scheme). Finally the gain coefficient α is given.

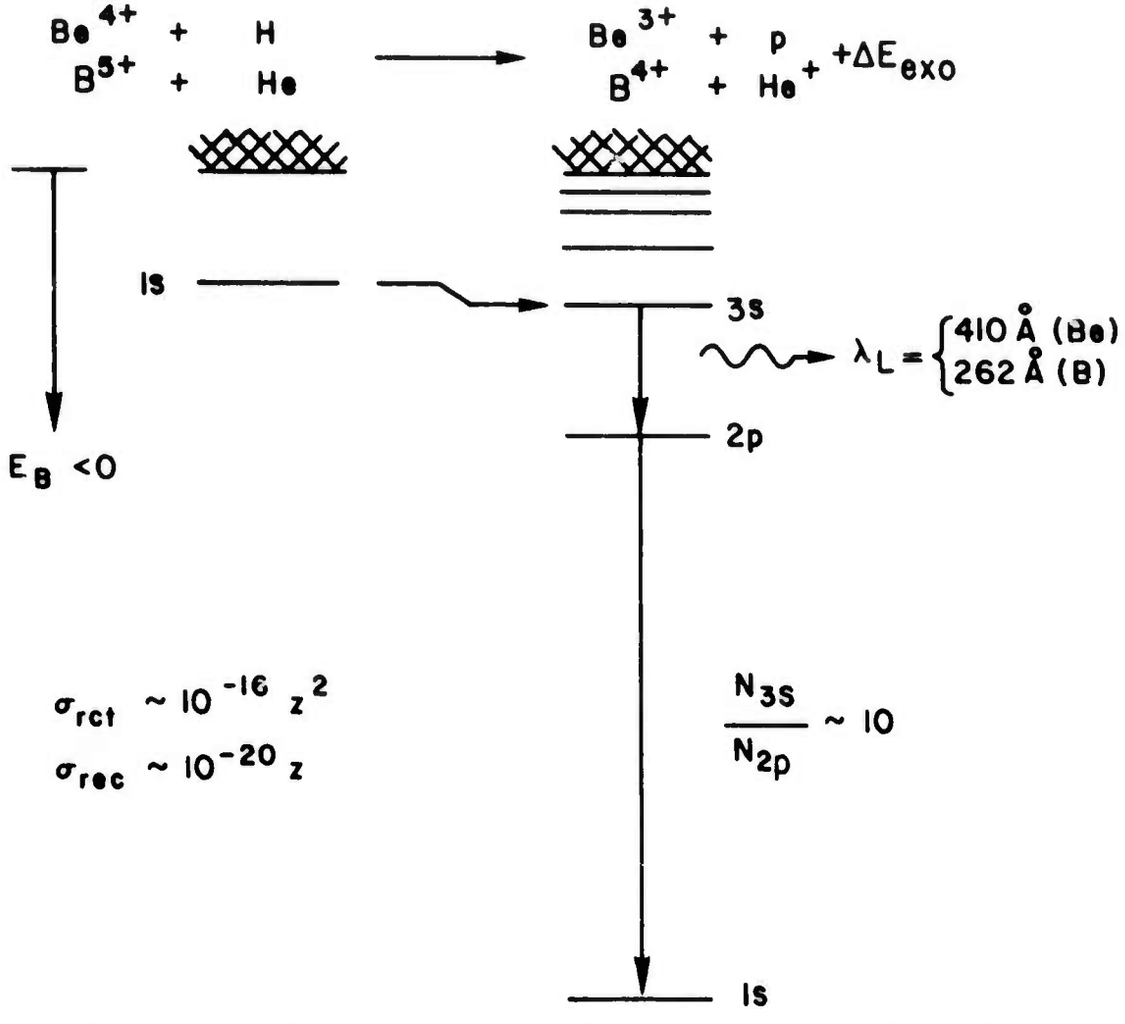

Fig. 20 — Schematic diagram of exothermic s-s resonance charge transfer reaction leading to a quasistationary population inversion between 3s and 2p levels in certain helium-like or hydrogenic ions. Refer to Fig. 8 for other possible ion/atom combinations. E_B is the binding energy; σ_{rct} and σ_{rec} show the cross section scalings for resonance charge transfer and radiative recombination, respectively.

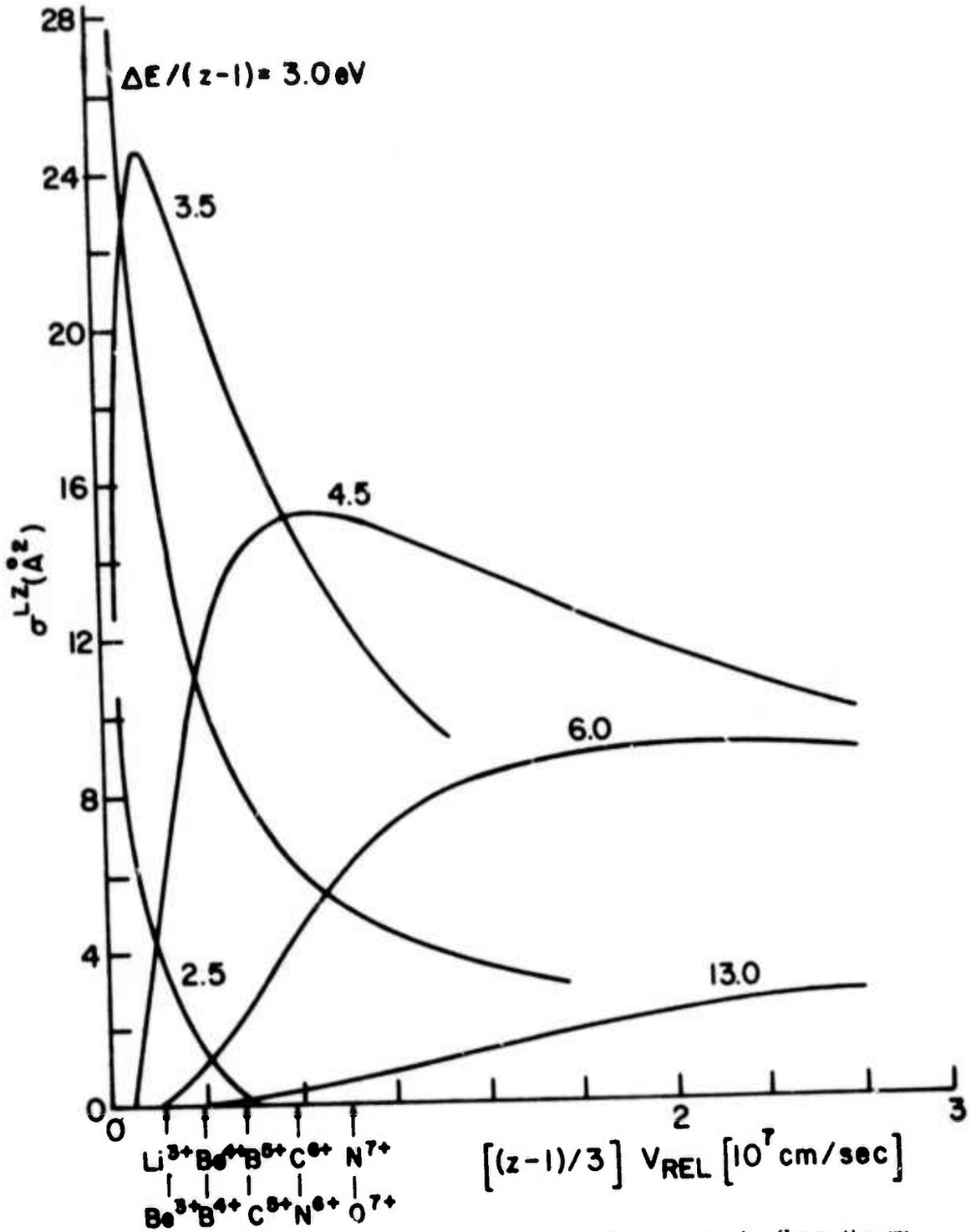

Fig. 2: — Resonance charge transfer cross section from s-s Landau-Zener theory versus scaled relative velocity for the atom-ion combination. (Data adapted from Ref. 12). ΔE represents the energy defect in eV for the exothermic reaction, z the effective charge of the ion. Velocities for ions designated are assumed thermal, with the kinetic temperature chosen as I.P./4 for creating the ion.

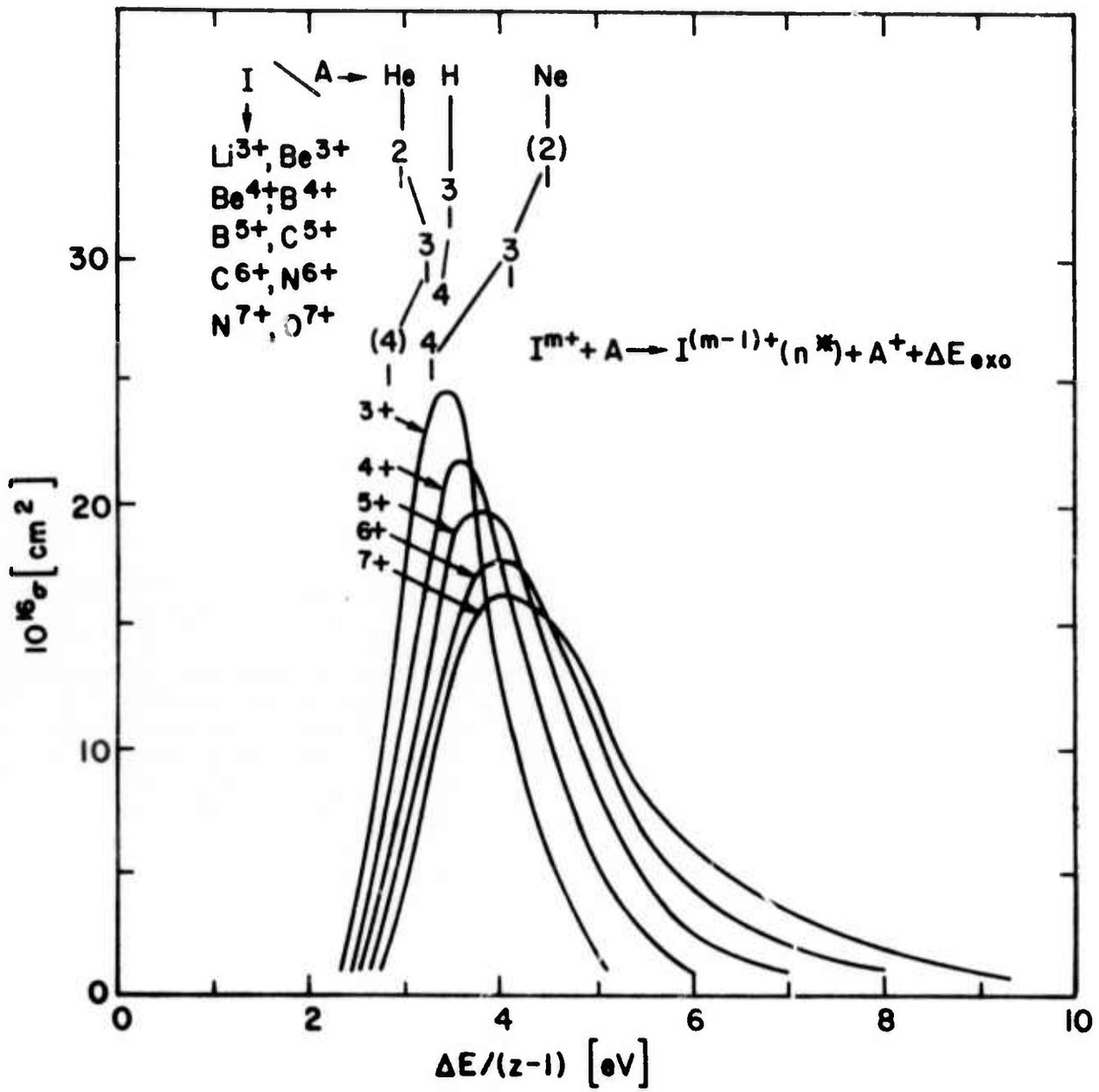

Fig. 22 — Resonance charge transfer cross section obtained by inversion of Fig. 7 data. Final quantum states of high capture probability for each ion I^{m+} and atom A combination are indicated by numerals, with parentheses to indicate less probable transitions. ΔE is the exothermic energy defect and z the effective ion charge.

TABLE II. RESONANCE CHARGE TRANSFER LASER PUMPING PARAMETERS

	Δ_n	λ (Å)	$10^{-18} N_e$ (cm^{-3})	P_A (Torr)	$10^{12} t_u$ (sec)	α (cm^{-1})
$(Be, B)^{4+}$ + H	3-2	400	1	0.7	75	20
$(B, C)^{5+}$ + (He, Ne)	3-2	250	6	1	60	30
$(C, N)^{6+}$ + H	4-3	520	2	0.3	80	50
	4-2	130	2	20	90	40
$(N,O)^{7+}$ + (He, Ne)	4-3	380	6	0.3	45	30
	4-2	95	6	20	50	30

III. B. EXPERIMENT

An experiment intended to test this method of pumping has been constructed and is shown schematically in Fig. 23 and is illustrated in Figs. 24 and 25. A high power glass laser beam will be focused in a line image onto various target materials placed on a rotatable disc in front of the entrance slit of a grazing incidence vacuum spectrograph. The plasma formed expands into a background gas in an upward direction, parallel to the slit, and in a confined slab configuration by the use of a solenoidal magnetic field (not shown). Rotation of the focusing lens permits both axial and transverse observations for indications of amplification. Spatial resolution along the direction of expansion is provided by a slot placed between the entrance slit and the grating as indicated. Experiments to verify anomalous populations under optically-thin conditions will be carried out at lower densities further from the target by a simple displacement of the target and lens assembly.

At present, the vacuum chamber housing the lens and target assembly has been assembled and mounted to the grazing incidence spectrograph along with a manifold to puff the background gas into the chamber at the desired pressure before the laser is triggered. For initial experiments, a 350 megawatt, 20 nanosecond high repetition rate ruby laser has been mounted and aligned through a focusing lens onto a carbon target. This laser focused to a point segment of the eventual line image, along with a wide spectrograph slit (100 μm), have greatly increased the initial data acquisition efficiency. The results from these present experiments should be applicable to the high power

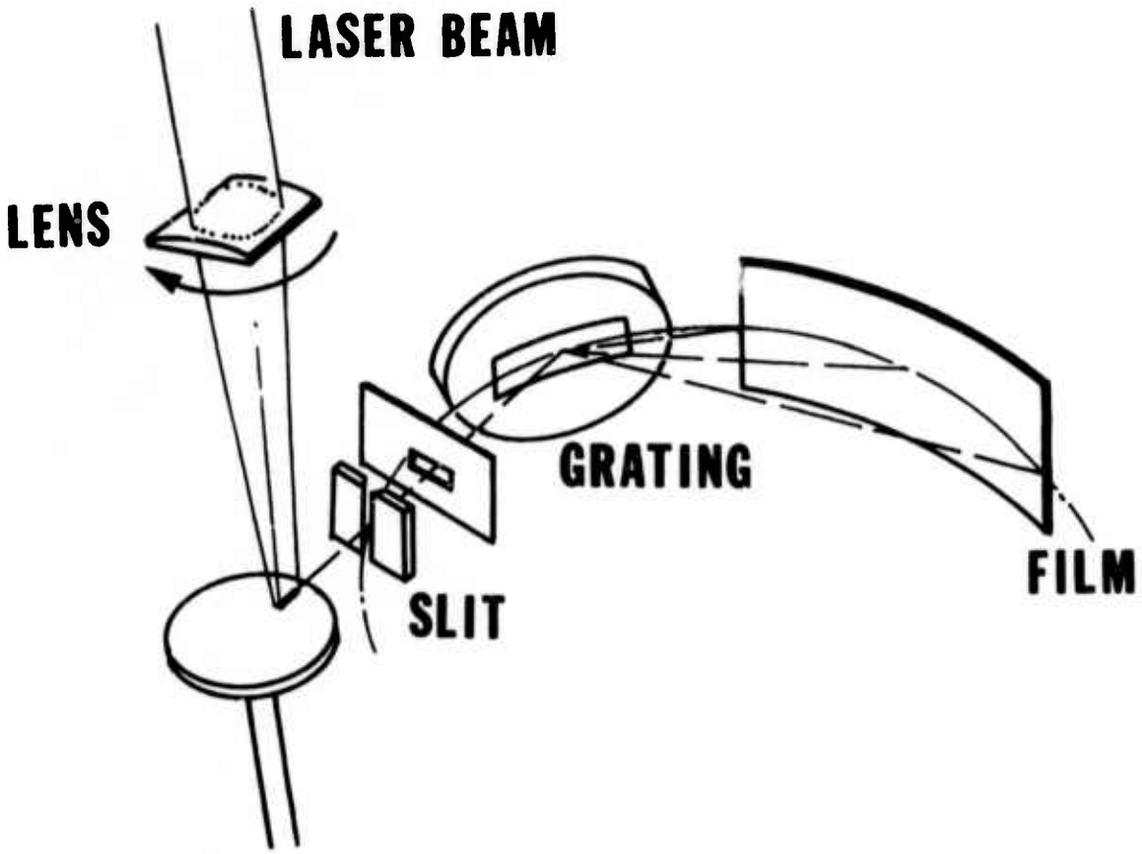

Fig. 23 — Schematic diagram of the NRL resonance charge transfer experiment, including the grazing incidence vacuum spectrograph. The horizontal slot provides spatial resolution along the direction of plasma expansion from the target surface. Rotation of the lens permits both axial and radial viewing. The background (atomic) gas is not indicated, nor is a planned guiding magnetic field.

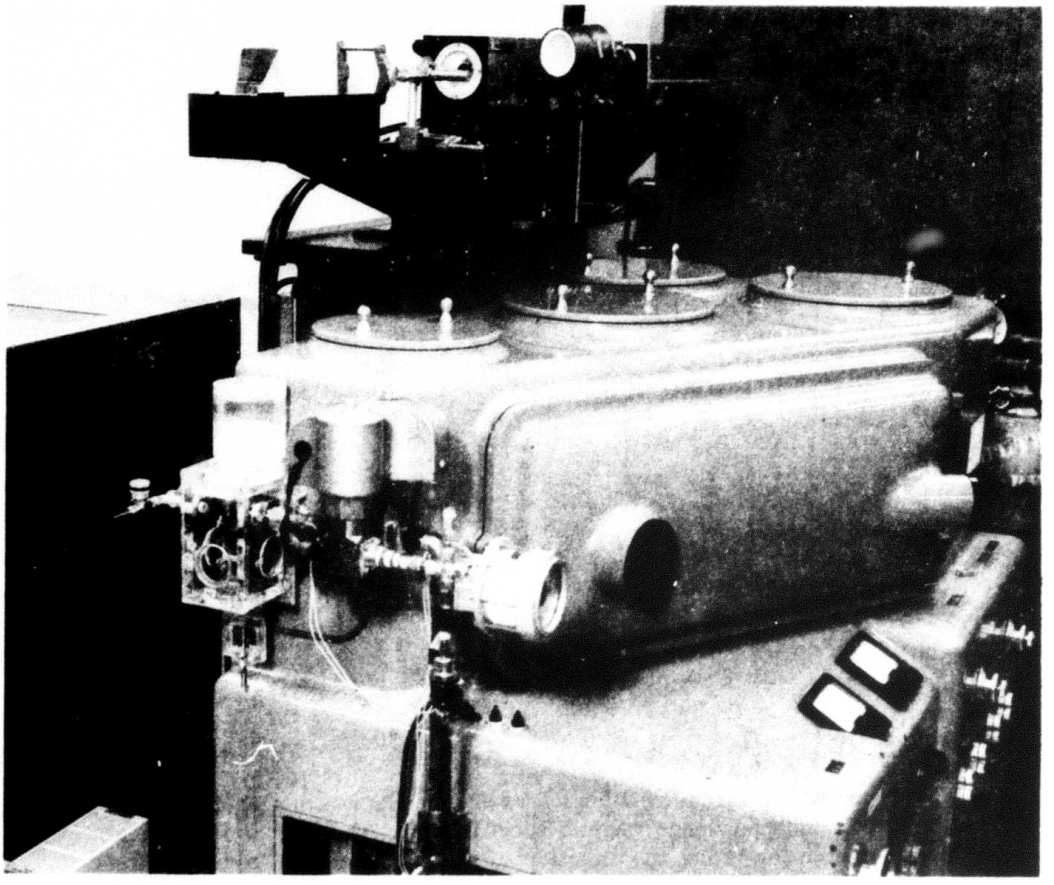

Fig. 24 — Overall view of the resonant charge transfer experiment showing the grazing incidence spectrograph, experimental chamber, gas handling system, and ruby laser

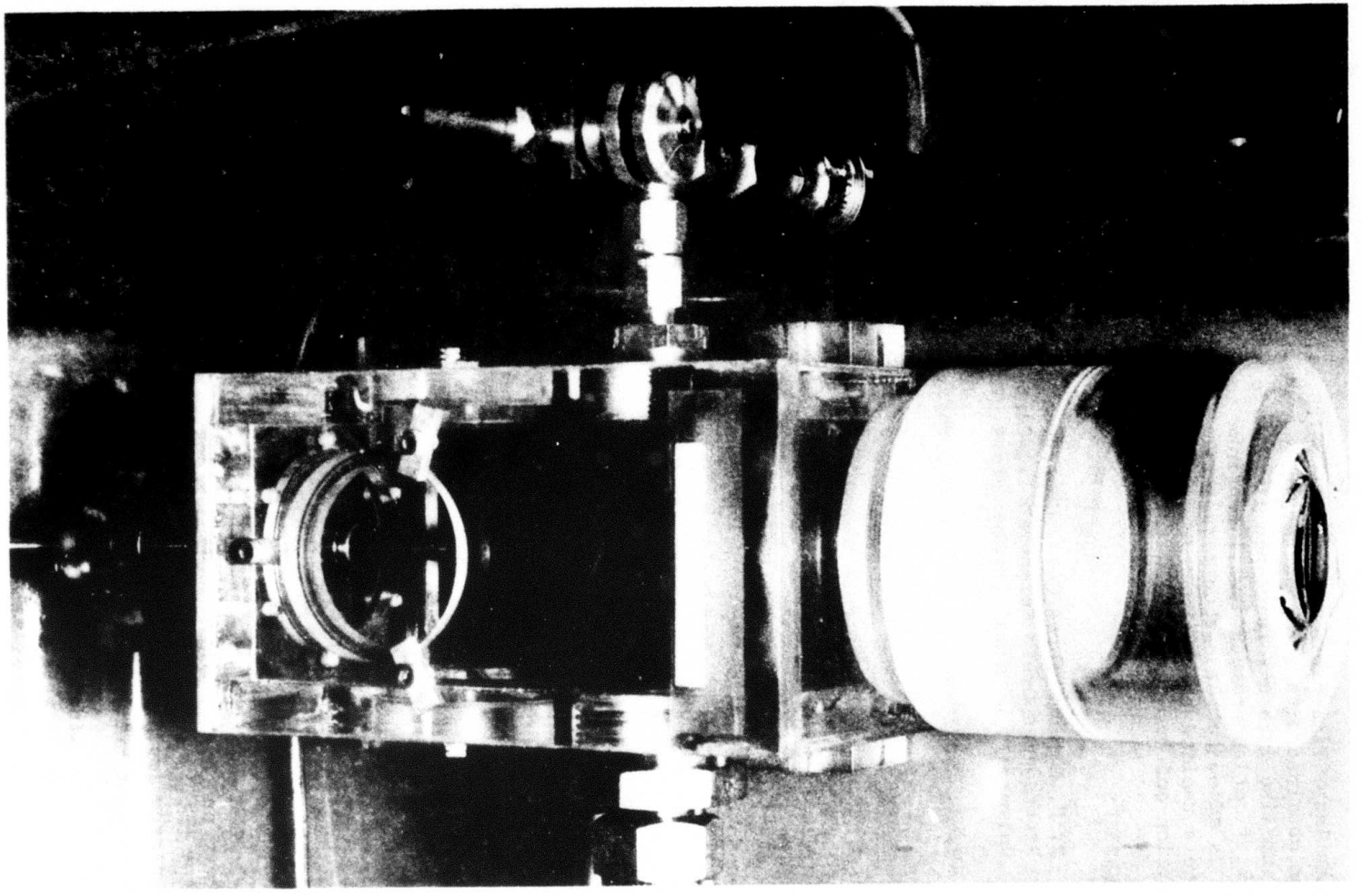

Fig. 25 — Closeup view of the experimental chamber for the resonant charge transfer experiment showing the focusing optics and rotatable carbon target

glass laser line focus experiments which will follow. Spectra has been obtained with a carbon target in vacuum (See Fig. 26), and helium-like carbon V resonance lines have been identified. The line identification procedure will continue to other series as background gas is added to the carbon target experiment and as Boron and Lithium targets replace the carbon target. Spatial resolution, varying target position and eventually higher power line focus experiments are planned.

REFERENCES

1. R. C. Elton, "Three Quasi-CW Approaches to Short Wavelength Lasers", Proccedings Orbis Scientiae 11, Center for Theoretical Studies, University of Miami (Plenum Press, to be published, 1975).

2. H. J. Zwally and D. W. Koopman, Phys. Rev. A 2, 1851 (1970).

IV. GENERATION OF COHERENT VUV/SOFT X-RAY PULSES BY NONLINEAR MIXING

IV. A. BACKGROUND

The generation of short wavelength coherent radiation through harmonic generation and nonlinear mixing of laser pulses has been shown to be effective in producing light to wavelengths down to 1000 Å[1]. Extension of these techniques to shorter wavelengths is an attractive method of producing coherent soft x-radiation because the generated radiation maintains the spatial and temporal coherence of the pumping radiation. With the conversion efficiencies reported to date, however, pulses generated in the VUV range as harmonics of a Nd:YAG laser at 1.06μ are too weak to use as sources for driving higher order nonlinear interactions.

There have also become available molecular lasers operating in the spectral range between 1100 and 1800 Å (e.g., H_2, Xe, CO). When operated as travelling wave oscillators, these lasers produce powers in the range of 10^6 W, which is again too low to serve as a source for pumping high order nonlinear processes. However, when used as an amplifier for picosecond pulses generated externally in the VUV range, they hold promise for providing the needed additional energy for driving the higher order nonlinear interactions.

This section describes an approach to the generation of intense mode-locked pulses in the VUV spectral range for use as pump radiation in third and higher order nonlinear optical mixing processes. Since the VUV pulses are to be amplified in molecular laser amplifiers which have narrow amplifying bandwidth, typically $\Delta\lambda = 0.1$ Å, it is impossible to use only successive stages of harmonic generation to produce VUV pulses and expect them to overlap spectrally with available amplifier gain lines. Consequently, in combining two or more wavelengths to produce the VUV pulses, it is necessary that at least one of the sources be tunable with accuracy sufficient to insure overlap

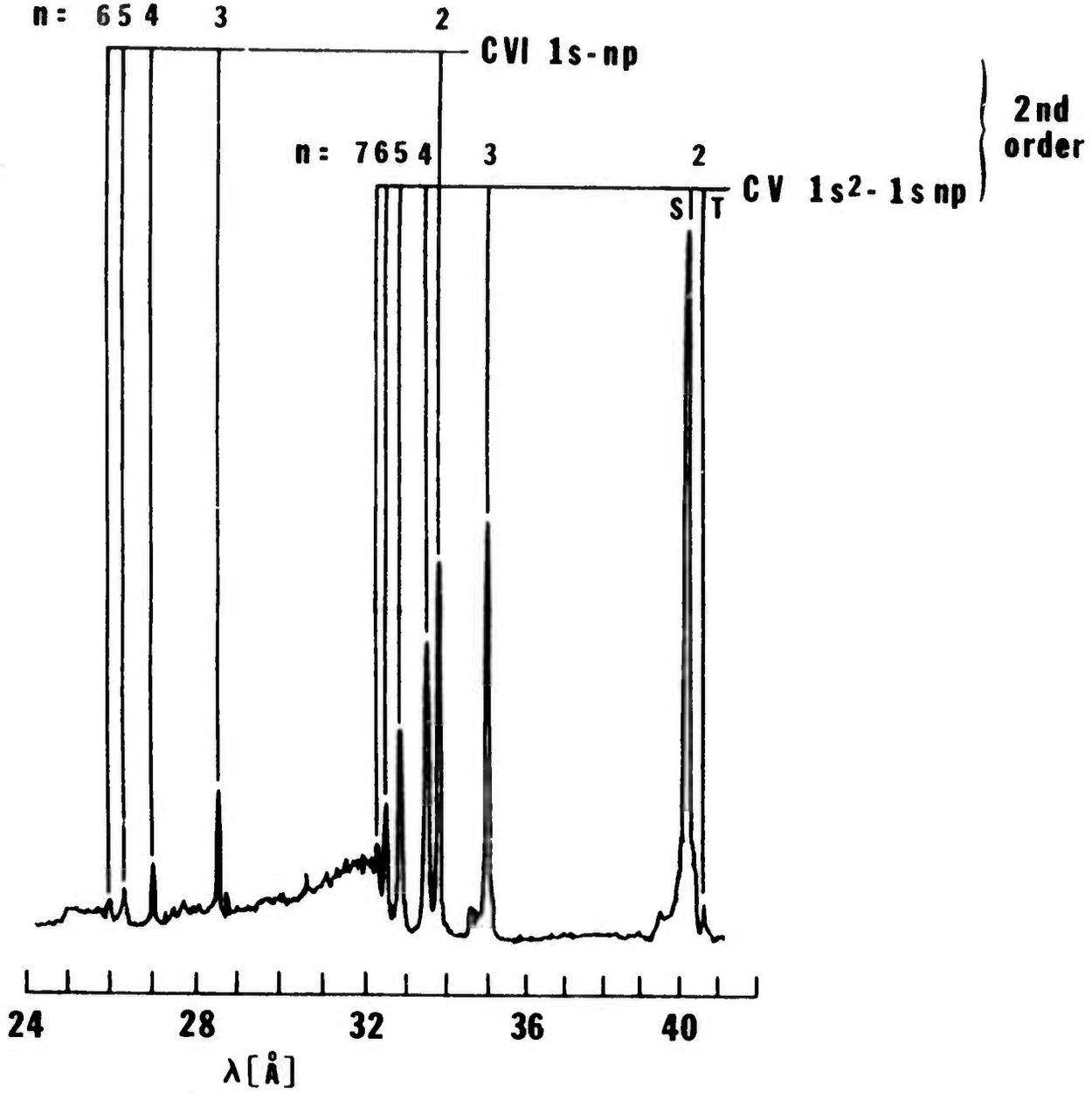

Fig. 26 — Typical spectra taken with the apparatus shown in Fig. 24. The spectra clearly shows that CV and CVI series in second order

between the generated radiation and the gain distribution of the laser amplifier.

IV. B. NONLINEAR MIXING

In the last report an experimental approach to this problem was described which involves generating tunable picosecond pulses in the visible which are combined in a nonlinear medium to generate VUV pulses suitable for amplification. The technique is again presented for sake of completeness in Fig. 27. Light from a Nd laser at 1.06 μm is converted into ultraviolet radiation at either the third or fourth harmonic in each of two parallel arms. The ultraviolet radiation in each arm is used to pump a mode-locked tunable laser with an output wavelength in the range of 4800 Å. The outputs of the two tunable sources are combined as shown, and mixed in a vapor cell to give a mode-locked pulse at a frequency $\omega_3 = 2\omega_1 + \omega_2$. By using two tunable sources, ω_1 can be tuned into coincidence with a two photon resonance in the mixing vapor, enhancing the efficiency of the mixing process. Then by tuning ω_2 the frequency of the generated light, ω_3, can be made to coincide with the desired gain line of the VUV amplifier. The power to be expected at various stages of this system are summarized in Table III.

TABLE III - PARAMETERS OF THE NL MIXING SYSTEM

STAGE	PULSE ENERGY	PULSE DURATION	η	P(W)
INPUT	180 mj	30 psec		6×10^9
1st SH CRYSTAL	90 mj	30 psec	50%	3×10^9
2nd HARMONIC (Mixing) CRYSTAL	9 mj	30 psec	5%	3×10^8
TUNABLE LASER OUTPUT	0.09 mj	10 psec (EST.)	0.05% (EST.)	9×10^6
OUTPUT OF NONLINEAR MIXING CELL	0.03 mj	10 psec	0.018% (EST.)	3×10^6
OUTPUT OF H_2 AMPLIFIER (30 TORR)	1 mj	10 psec		10^8
OUTPUT OF H_2 AMPLIFIER (760 TORR)	25 mj	10 psec		2×10^9

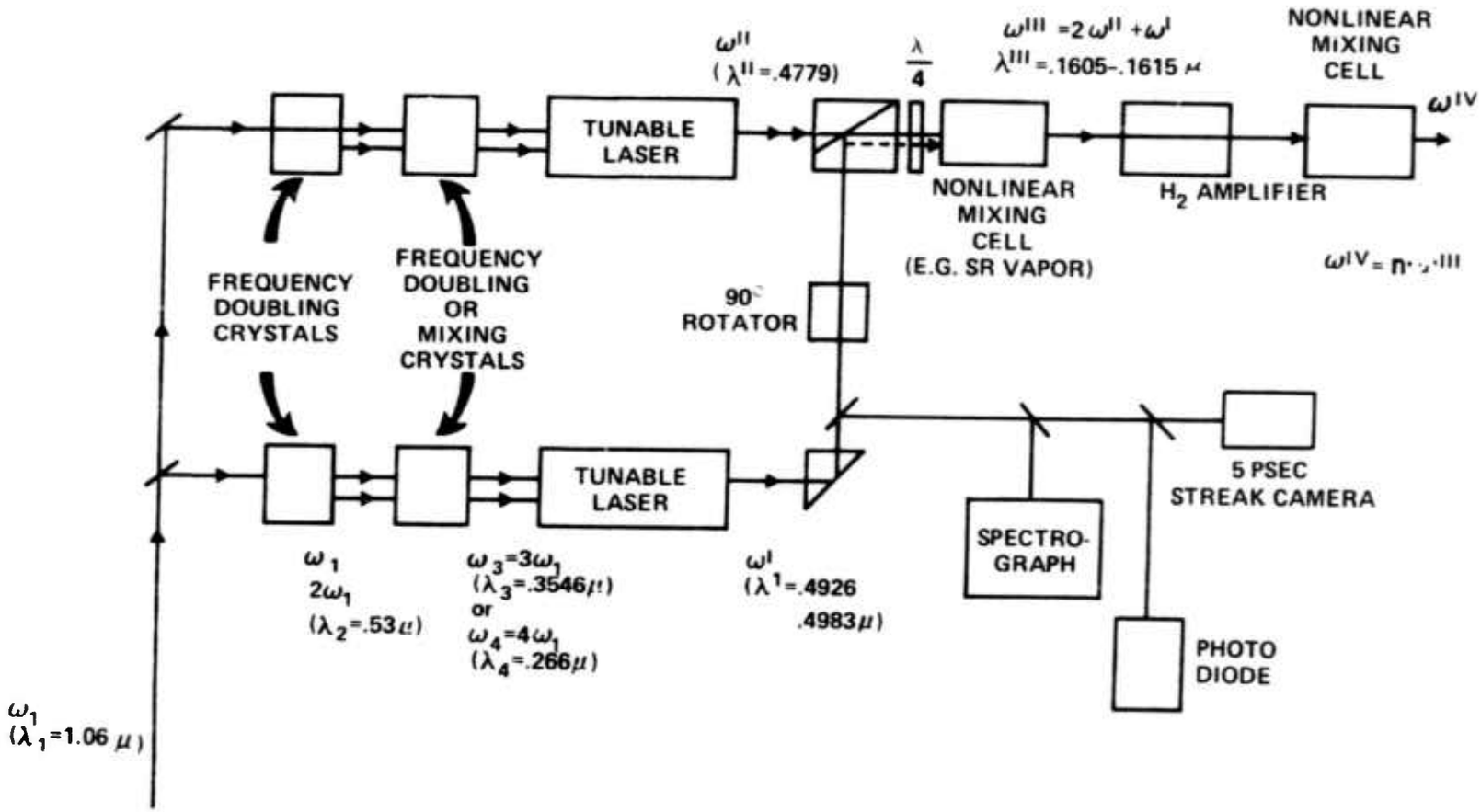

Fig. 27 — Schematic diagram for production and amplification of intense picosecond pulses in the VUV from fundamental radiation at 1.06μ

Experimental progress in this period has consisted mainly of obtaining the necessary crystals and components for generating the tunable visible radiation. Our preliminary experiments in harmonic generation showed that second harmonic conversion efficiencies in excess of 50% were achievable with the current mode-locked laser system. Similar efficiencies in conversion from the second to the fourth harmonic in 1" long ADP crystals which were phase matched by angle tuning were inferred from measurements of pump depletion at 0.52 μm. However, actual available power at 2660 Å was lower than expected, presumably because of the low quality ADP crystals being used. Furthermore, no visible radiation could be detected in attempts at single pass parametric conversion from 2660 Å to 5000 Å using a 1" long ADP crystal which was angle phase matched at room temperature. These results indicated that temperature stabilized 90° phase matching is needed for both harmonic conversion and parametric down conversion in ADP to extend the coherence length and that only the highest grade material can be used to minimize UV losses from absorption and scattering. A complete set of harmonic crystals and temperature controlling ovens have now been obtained and conversion experiments are being set up. The range of wavelengths available with this system is shown by the tuning curve of ADP in Fig. 28. In addition, fixed frequencies at 2660 Å, 5300 Å, and 1.06 μm are also available from the laser fundamental and its harmonics.

The nonlinear mixing process to be used in the generation of VUV pulses from the visible and soft x-rays from the VUV is indicated schematically in Fig. 29. Figure 29a shows a 3rd harmonic process in a suitable nonlinear medium, Fig. 29b shows a sum frequency generation process of the form $\omega_3 = 2\omega_1 + \omega_2$ and Fig. 29c shows an n photon process. In each case one of the frequencies (ω_1) is tuned to an even multiphoton resonance with an upper level to provide resonant enhancement of the process. Additional resonant enhancement can be obtained by tuning ω_3 to lie near a single photon transition to the ground state. The actual wavelengths involved depend on the available pumping radiation and the medium used. Successful conversion has been reported from the visible to the VUV in Sr vapor[1].

A survey of possible interactions that can be used to generate radiation shorter than 1000 Å has begun. The most accessible of these involve the lowest order nonlinear porcesses and Table IV lists some possible choices. In this table, the pumping wavelength listed in the second column, is obtained from the combination of visible and UV wavelength listed in the third. The next two columns list the detuning for the even photon resonances respectively and the last column indicates whether a H_2 laser is capable of providing additional power at the pump wavelength.

The first two examples listed generate 3rd harmonics of wavelengths that are not accessible to a H_2 laser. They can therefore be studied

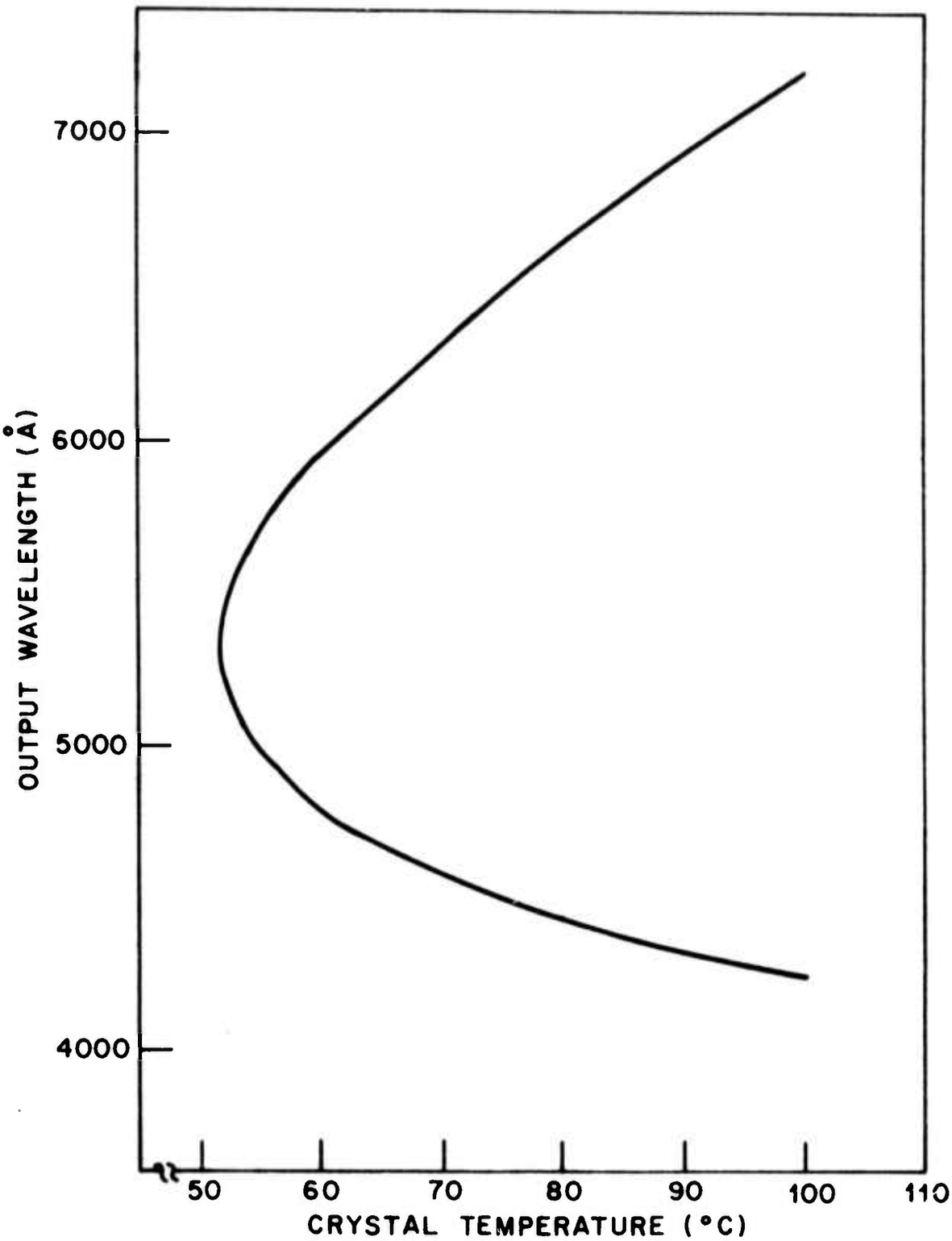

Fig. 28 — Temperature tuned phase matching curve for parametric down conversion in ADP for pump radiation at λ = 2660 Å

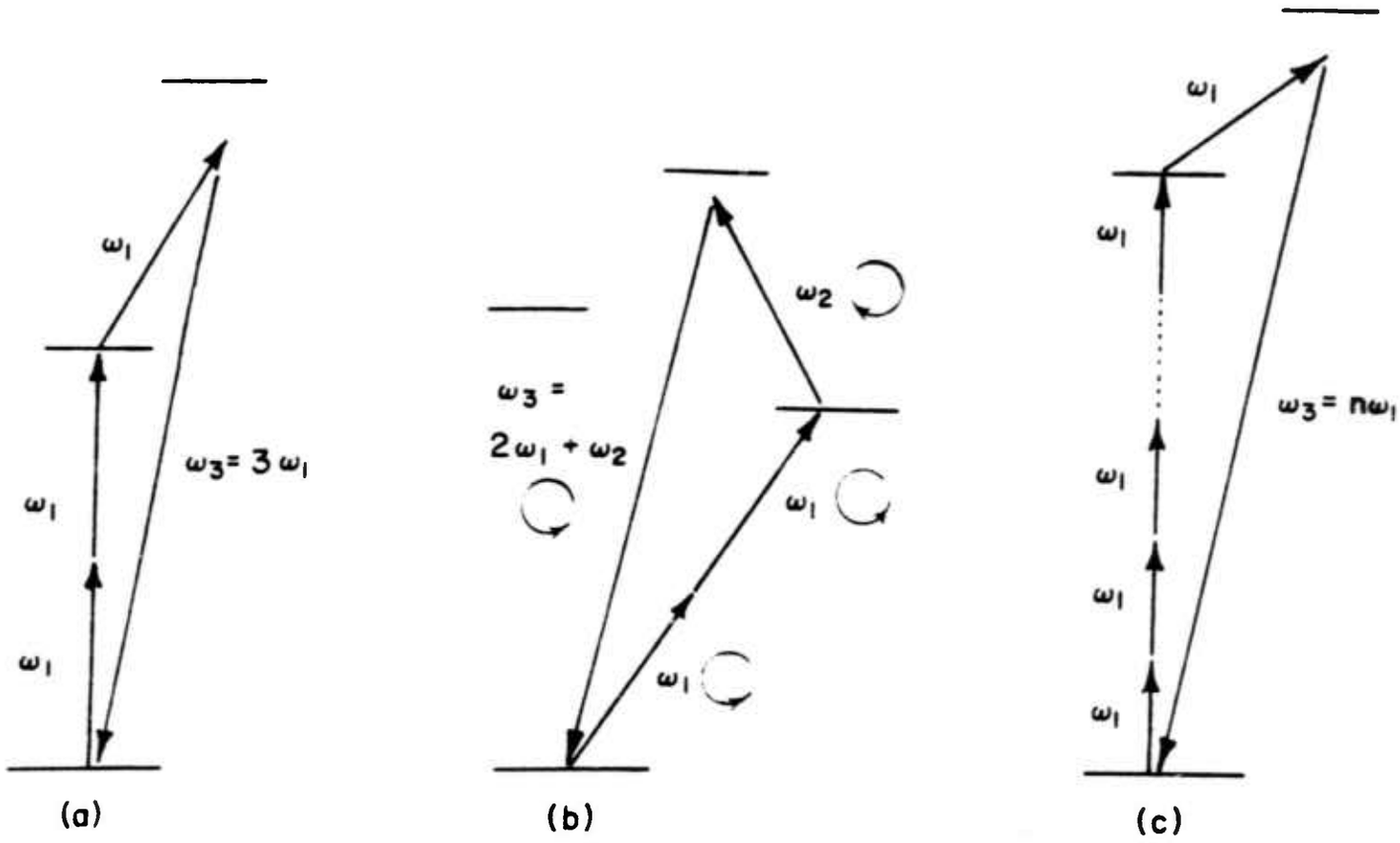

Fig. 29 — Schematic illustration of level diagrams involved in resonantly enhanced nonlinear mixing processes. (a) Third harmonic generation, $\omega_3 = 3\omega_1$; (b) sum frequency generation, $\omega_3 = 2\omega_1 + \omega_2$; (c) nth order harmonic generation, $\omega_3 = n\omega_1$.

TABLE IV

INITIAL EXPERIMENTS INVOLVING GENERATION OF SHORT WAVE RADIATION THROUGH NONLINEAR MIXING

ACTIVE MEDIUM	PROCESS	GENERATION OF VUV	λ_{out} Å	$\Delta_{2\pi}$ cm^{-1}	$\Delta_{3\pi}$	UV AMPLIFIER
He	3 x 1512 Å	3 x 4536 Å	504	34,000	c	NO
He	3 x 1202 Å	2 x 4385 Å + 2660 Å	400	0	c	NO
He	3 x 1610 Å	2 x 4779 Å + 4935 Å	537	42,000	16.7	YES
He	3 x 1230 Å	2 x 4575 Å + 2660 Å	410	3,700	c	YES
Li^+	9 x 1608.4 Å	2 x 4779 Å + 4920 Å	178.7	7,309	2,186	YES
Li^+	7 x 1230	2 x 4575 Å + 2660 Å	175	2,270	7,400	YES

while the H_2 amplifier is being developed. The first example generates the shortest wavelength that can be propagated in neutral Helium. Although the two photon resonance between the $1S^2\ ^1S$ and the $1s2s\ ^1S$ levels is not particularly close, it does represent an enhancement of about 6 times over the antiresonant term. Additional single photon resonances can be expected from ω_3 which lie near the continium. Linear absorption of ω_3 is expected to be small because the largest part of the oscillator strength is used in lower lying transitions. The next two examples, again third harmonic generation in He vapor, make use of gain from a H_2 amplifier. Here the resonances are not as close because of the wavelength restrictions imposed by the narrow width of the H_2 gain lines.

The wavelengths generated in these examples are all comparable to one another since they all represent 3rd harmonics of radiation between 1200 and 1600 Å. Shorter wavelengths can be generated as higher order harmonics in other materials, as is indicated in the last two examples. In the first of these, an 8-photon resonance of light at 1608.4 Å is utilized in singly ionized Li between the $1S^2\ ^1S$ and $1s2s\ ^1S$ levels to generate the 9th harmonic of the pump radiation. The second generates the 7th harmonic of a pump at 1230 Å utilizing a 6-photon resonance between the same two levels. Since in these latter two cases, the generated power depends on the 9th and 7th power of the pump radiation, it is anticipated that the loss in efficiency due to slight mistuning from exact resonance will be offset by increased pump power from the H_2 amplifier. Of course use of broader band amplifiers (e.g., molecular Xe) would provide even higher efficiences. Calculations are being performed to estimate conversion efficiencies of these processes with our available pump power.

REFERENCES

1. R. T. Hodgson, P. P. Sorokin and J. J. Wynne, Phys Rev. Lett. 32, 343 (1974).

2. It was demonstrated in reference 1 that a considerable amount of resonant enhancement with low absorption was possible in Sr vapor even when the final state lies in the ionizing continuum.

IV. C. HYDROGEN AMPLIFIER

Progress with the hydrogen amplifier has been in two areas: (1) the construction of an experiment to demonstrate atmospheric pressure operation using photopreionization and (2) design and fabrication of a laser triggered spark gap as the essential part of the synchronization scheme.

The photoionization experiment is designed to establish whether CO can be used as a source of electrons in the atmospheric pressure

H_2 device. The first strong absorption band in CO starts at around 1500 Å; hence it will pass 1600 Å hydrogen radiation. Two step photoionization is possible in CO using weakly allowed molecular states at 2000 Å, 1780 Å, and 1580 Å which lie about half way to the ionization limit of 14 eV. Radiation in this region can be produced using high pressure Xe flashlamps with special Supersil envelopes for maximum UV transmission ($\lambda > 1600$ Å). An experiment has been designed and constructed to measure the electron distribution produced in a mixture of CO and H_2 by a Xe flashlamp. The experimental apparatus is similar to that used for CO_2 and tri-n-propylamine[1] and it is illustrated in Fig. 30. This experiment has an added problem in the UV region. The photons from the flashlamp being used are sufficiently energetic to produce photoelectrons in the Faraday cup independent of any photoionization taking place. An example of this effect is shown in Fig. 31. The lower trace represents the flashlamp current pulse and the upper trace is the Faraday cup response. Figure 31(a) is for one atmosphere of N_2, 31(b) is the same except a glass slide is place in front of the Faraday cup to filter the hard UV photons. Attempts to remedy this problem by coating the grid in front of the Faraday cup with an UV absorbing insulator are underway.

Several modifications are necessary in order to convert the traveling-wave discharge system from operation as an emission source to operation as an amplifier of tunable picosecond pulses. These modifications are: (1) the addition of a laser triggered switch to allow the amplifier to be fired by an optical pulse from the long wavelength (1.06 μm) laser, and (2) the use of oil for immersing the laser to prevent breakdown while awaiting the arrival of the pulse which is to be amplified.

The laser triggered switch has been fabricated and is shown in Fig. 32. It was designed to add as little inductance as possible to the Blumhein circuit. When filled with high pressure gas it should hold off the 70 - 80 kV d.c. charge until triggered by the advance laser pulse. At present only one laser switch has been built and it has been positioned to produce the first approximation to a traveling wave. Several switches can be added if necessary. In addition, the plate is already equipped with one long switching channel which can be used if sufficient laser power is available. Since several alternatives are available synchronization of the amplifier gain with the tunable picosecond pulse should not be exceedingly difficult.

Transformer oil in which to immerse the laser is readily available at NRL as are the methods to handle and purify it. It remains to be seen however, if all of the structure for supporting the laser plates will withstand the d.c. charge. Modifications in supporting blocks and in vacuum and electrical lines may be needed. The extent of these modifications as well as the operation of the laser triggered switch will be assessed in the near future.

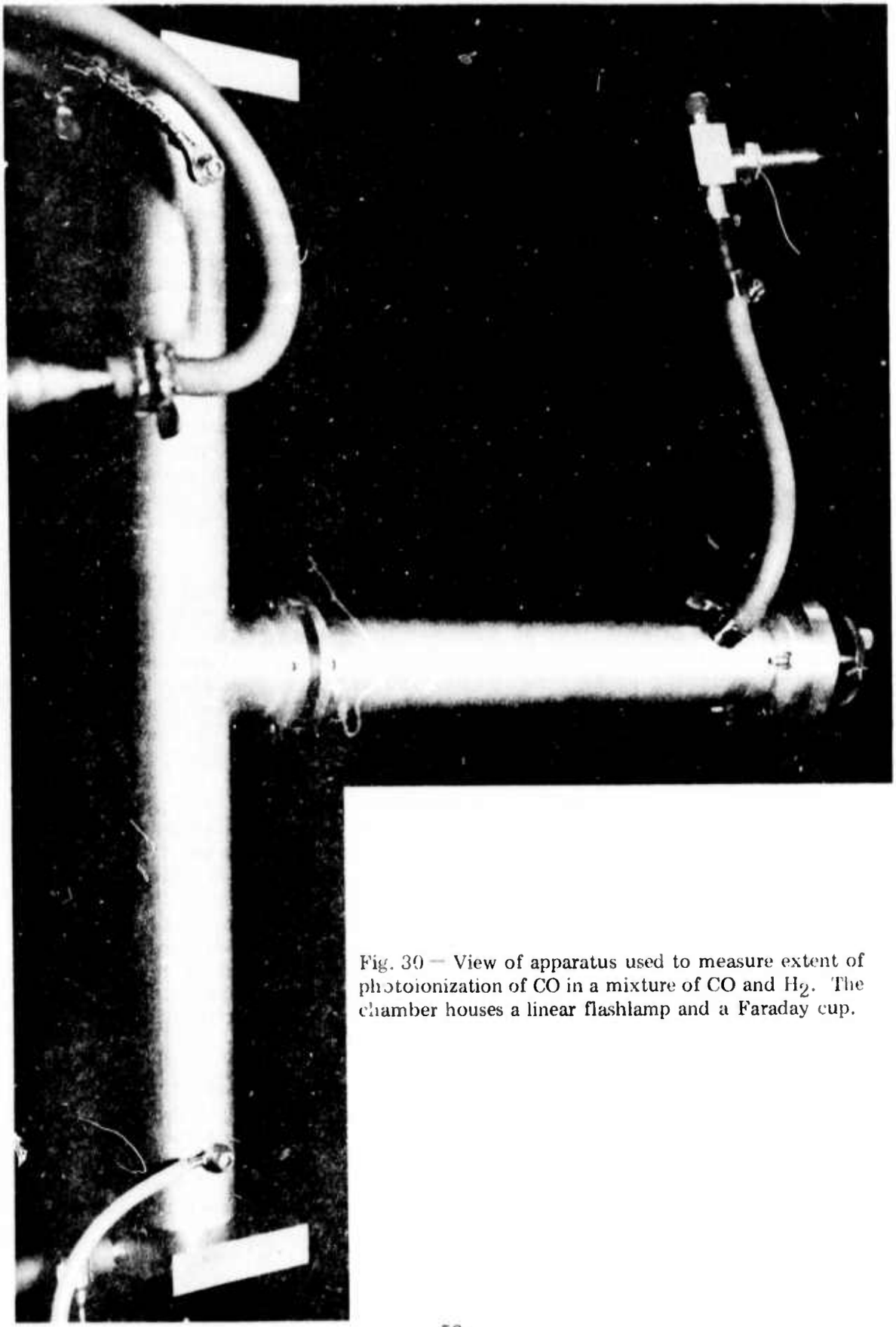

Fig. 30 — View of apparatus used to measure extent of photoionization of CO in a mixture of CO and H_2. The chamber houses a linear flashlamp and a Faraday cup.

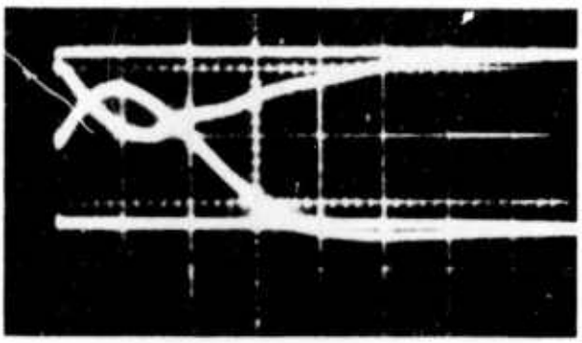

(a)

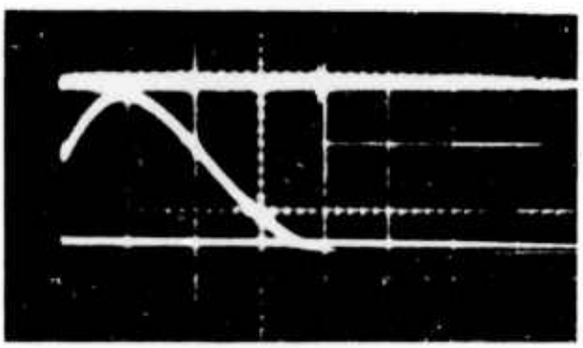

(b)

Fig. 31 — Typical measurements using the apparatus shown in Fig. 30. In each case the upper trace in the Faraday cup response and the lower trace is the flashlamp current pulse. (a) 1 atm. of N_2; (b) same as (a) except a glass slide in front of the Faraday cup.

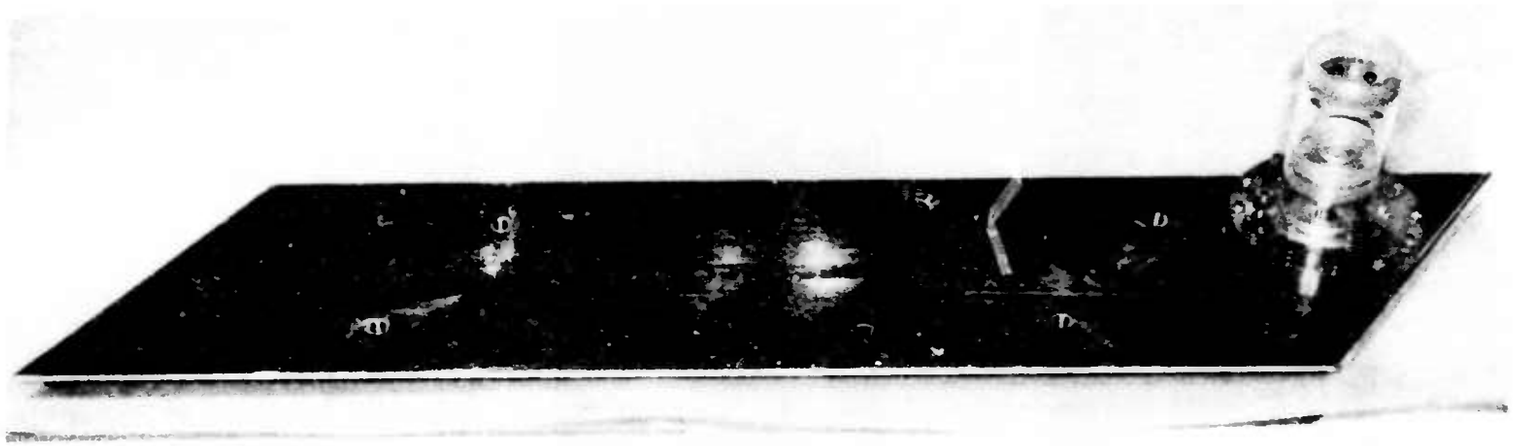

Fig. 32 — Illustration of the newly designed laser triggered spark gap for the H_2 laser device

REFERENCE

1. J. S. Levine and A. Javan, Appl. Phys. Letters 24, 258 (1974).

IV. D. TWO PHOTON RESONANTLY ENHANCED SELF-DEFOCUSING IN Cs VAPOR AT 1.06 μm

As a part of the effort to understand nonlinear optical processes in vapors and to explore the possibilities for 1) generation of tunable radiation around 1600 Å, and 2) mixing processes that work from 1600 Å to the soft x-ray region, a fortuitous situation was found to exist. This consists of a near exact coincidence between the 1.079 μm line of the Nd:YAG laser and the two photon 6s → 7s transition in Cs vapor. The previous report briefly described a preliminary experiment to investigate this effect.

The observation of self defocusing of mode locked at 1.06 μ pulses in Cs vapor was reported in a recent publication[1]. The negative nonlinear refractive index responsible for this effect has been measured ($n_2 = 1.5 \times 10^{-30} N$), and the first observation of its use in compensating the self focusing that occurs in other transparent materials has been made. Since the useful output power from large Nd laser systems is limited by self focusing due to the laser glass ($n_2 \approx 1.6 \times 10^{-13}$ esu), these experiments suggest the possibility of increasing this power by using Cs vapor for compensation; e.g., one could insert Cs cells at various stages of the glass amplifier chain.

At 1.06μ, the nonlinear susceptibility of Cs vapor is determined almost entirely by interaction between the $|6s\rangle \equiv |0\rangle$ ground state and the $|6p\rangle \equiv |1\rangle$ and $|7s\rangle \equiv |2\rangle$ levels. It has been shown that in the case of linearly polarized light, the nonlinear susceptibility can be analyzed into two distinct contributions[1]. The predominant one arises from the polarization $\rho_{02}(t)$ due to the two photon resonance between $|6s\rangle$ and $|7s\rangle$. The other term, which is also negative at 1.06 μm, arises from induced population changes between the $|6s\rangle$ and $|6p\rangle$ levels, and is analogous to the nonlinear refractive effects observed by Grischkowsky and Armstrong[2].

In this experiment, where the pulses are much shorter than the inverse linewidth of $|6p\rangle$, the nonlinear contribution to the refractive index becomes

$$\delta n^{NL} = n_2 \langle E^2(t) \rangle, \qquad (1)$$

where

$$n_2 = -\frac{2\pi}{h^3}\left[\frac{\mu_{01}^2\,\mu_{12}^2}{(\nu_{10}-\nu)^2(2\nu-\nu_{20})} + \frac{\mu_{01}^4}{(\nu_{10}-\nu)^3}\right] N, \qquad (2)$$

E(t) is the optical field of frequency $\nu=c/\lambda$, N is the atomic number density, μ_{ij} the dipole matrix element between levels $|i\rangle$ and $|j\rangle$, and ν_{ij} the corresponding frequency splitting. Nonresonant contributions have been ignored in (2), since at 1.064 μm, ν/c = 9398 cm^{-1}, while $(\nu_{10}-\nu)/c$ = 2149 cm^{-1} and $(2\nu-\nu_{20})/c$ - 260 cm^{-1}. For circularly polarized radiation, the $|0\rangle \rightarrow |1\rangle \rightarrow |2\rangle$ transition is not allowed, and only the second term of (2) remains nonvanishing. With longer pulses, one would obtain additional contributions to δn^{NL} proportional to the integrated intensity[1].

In order to measure n_2 vs. N the self-defocusing of mode locked Nd:YAG pulses in a 100 cm long Cs vapor cell at several densities between n = .080 X 10^{17} and .32 X 10^{17} cm^{-3} was studied. The input beam was a single 35 psec pulse of 1.1 mm 1/e diameter and 50-60 MW peak power. The output beam profile was recorded by imaging the exit window of the cell onto a silicon photodiode array. In analyzing the data, the constant shape approximation[3] was used, and the instantaneous profile over the pulse duration was numerically integrated. The value of n_2 that gave the best theoretical fit to the measured profile was then chosen. The results for linear and circular polarization are shown in Fig. 33, and the corresponding values of n_2/N are compared with theory in Table V. The second column is obtained from Eq. (2), the third includes the nonresonant contributions to n_2, and the fourth is the value calculated by Miles and Harris[4]. The theory is in good agreement with these measurements, with the discrepancy in the circularly polarized case due mainly to the integral terms mentioned above.

In the compensation experiment, a 2 cm long cell of CS_2 was inserted 45 cm from the entrance window of the Cs cell, and the beam profile was measured at the exit window. With 1 mJ pulses and no Cs in the cell, the (FWHM) width was 0.96 mm. With a Cs density of .13 X 10^{17} cm^{-3} and similar pulses, this width increased to 1.07 mm, which is close to the 1.12 mm width measured in the absence of both Cs and the CS_2. The Cs vapor thus appears to effectively compensate for the CS_2: however, no attempt was made to optimize this. Further experiments are currently in progress, and conditions required for the practical application of Cs vapor compensation are being investigated.

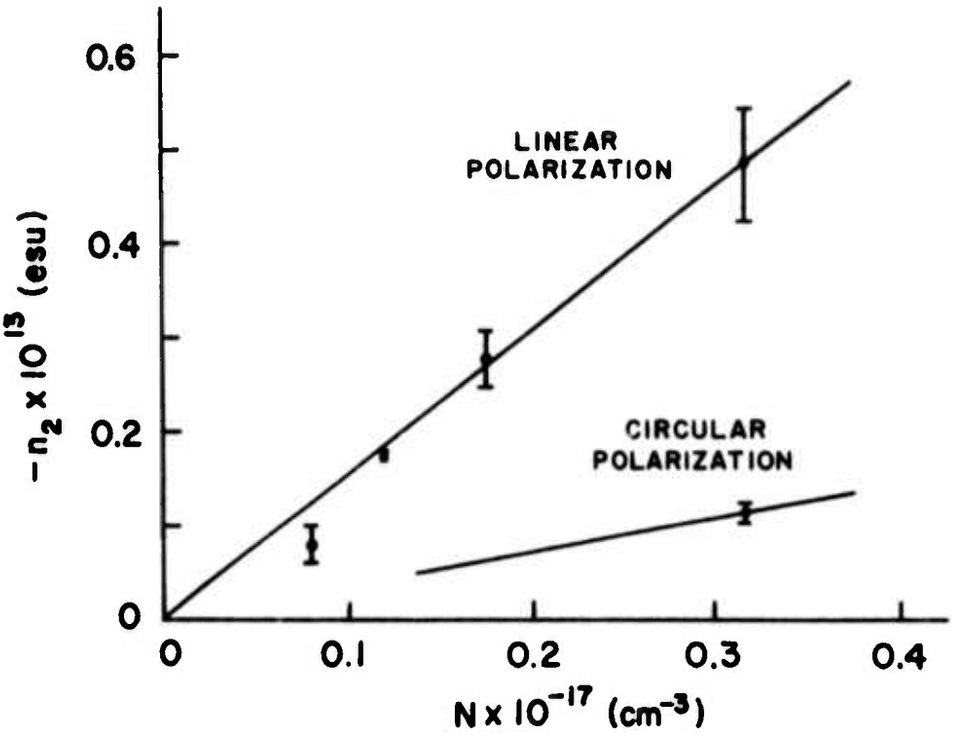

Fig. 33 — Results of the self-defocusing experiments and comparison with theory for circular and linear input polarizations. The value of n_2 is plotted as a function of Cs vapor density.

TABLE V

COMPARISON OF MEASURED AND THEORETICAL NONLINEAR REFRACTIVE INDICES

$$\frac{n_2}{N} \times 10^{30} \text{ (esu)}$$

	EXPERIMENTAL	THREE LEVEL MODEL RESONANT	THREE LEVEL MODEL EXACT	MILES & HARRIS JQE 9, 470 (1973)
↑	-1.5 ± 0.2	-1.84	-1.93	-0.66
↻	-0.35 ± 0.04	-0.29	-0.28	

REFERENCES

1. R. H. Lehmberg, J. Reintjes and R. C. Eckardt, Appl. Phys. Lett. 25, 374 (1974); NRL Memorandum Report 2932 (reproduced in an Appendix of this report).

2. D. Grischkowsky and J. A. Armstrong, Phys. Rev. A 6, 1566 (1972).

3. S. A. Akhmanov, R. V. Khokhlov and A. P. Sukhorukov, Laser Handbook, Vol. 2, edited by F. T. Arecchi and E. O. Schulz-Dubois (North Holland Publishing Company, Amsterdam, 1972).

4. R. B. Miles and S. E. Harris, IEEE J. Quant. Electron. QE-9, 470 (1973).

V. TRAVELING-WAVE PUMPED UV AND VUV LASERS

The importance of traveling-wave excitation for the production of long gain path lengths in the face of short excited state lifetimes has been discussed previously. It was pointed out in the previous report that the production of long gain paths with conventional coaxial electron beam machines was difficult and that the operation of such devices for traveling-wave excitation was not possible. Because traveling-wave pumping is desirable for both laser sources and amplifiers in the spectral region below 1000 Å, this program to develop a traveling-wave electron beam system has been pursued. The system under development provides a gain path of 1.6 meters and will operate with or without mirrors at pressures in the

1 - 10 atmosphere region. The initial design parameters were given in the first report.

Even though NRL was thoroughly experienced in the general design of flat plate Blumlein lasers there was a desire to incorporate several improvements in this laser system. These improvements are: (1) a removable diode and laser gas chamber section which can be modified or replaced without rebuilding the entire system, (2) the ability to charge the bottom plate so that the difficulty of gas discharges when making vacuum connections to the laser were not present (previously the charged plate had to be connected to detectors or spectrographs and it was not possible to operate without a gas discharge resulting and obscuring the data) and (3) operation with purified water on either side of the polyethylene dielectric in the Blumlein plates. All of these requirements were desirable. Their implimentations led to compromises in the plans for energy storage, and necessitated modifications in the device in order to reach successful operation.

The modifications made to the laser were: (1) the addition of O-rings in the energy storage plates to exclude water and to improve the energy transfer from an existing capacitor storage system, (2) the additional of vacuum systems to both the top and bottom plates to assist in excluding water from the plates, (3) the expansion of the vacuum system conductance to lower the pressure in the diodes and reduce extraneous discharges and, (4) addition of contact plates to insure smooth current conduction at the junction of the storage plates and laser diode assembly.

Many changes also have been made in the diodes themselves. Several foils have been tried: 25 μ thick titanium and 25 μ aluminum. Several methods of reinforcing the foils have also been tried. The best method appears to be the sandwiching of the foils between two thin reinforcing plates equipped with small o-rings. In a test fixture this has held well, but it has not been incorporated into the device yet. Several cathode materials have been tried: razor blades, closely spaced needle points, and 125 μ thick graphite. The most successful diode appears to be a combination of 125 μ graphite cathode and 12.5 μ thick titanium foil window. The entire device is shown in Fig. 34. This picture is a double exposure to illustrate the overall features plus the relatively uniform discharge. The device presently has been operated with 180-200 kV across the diode and with some modification could reach 250-300 kV. The failure rate due to breakdown of the polyethylene Blumlein dielectric has been rather small ($\sim$ 1 breakdown per 75-100 shots) but this would certainly go up at the higher voltages.

Operation of the excitation system is verified by the typical time integrated photograph shown in Fig. 34. This photo shows the emission of the excited gas in the laser chamber and it appears reasonably uniform. Numerous diagnostics are either in use or are being

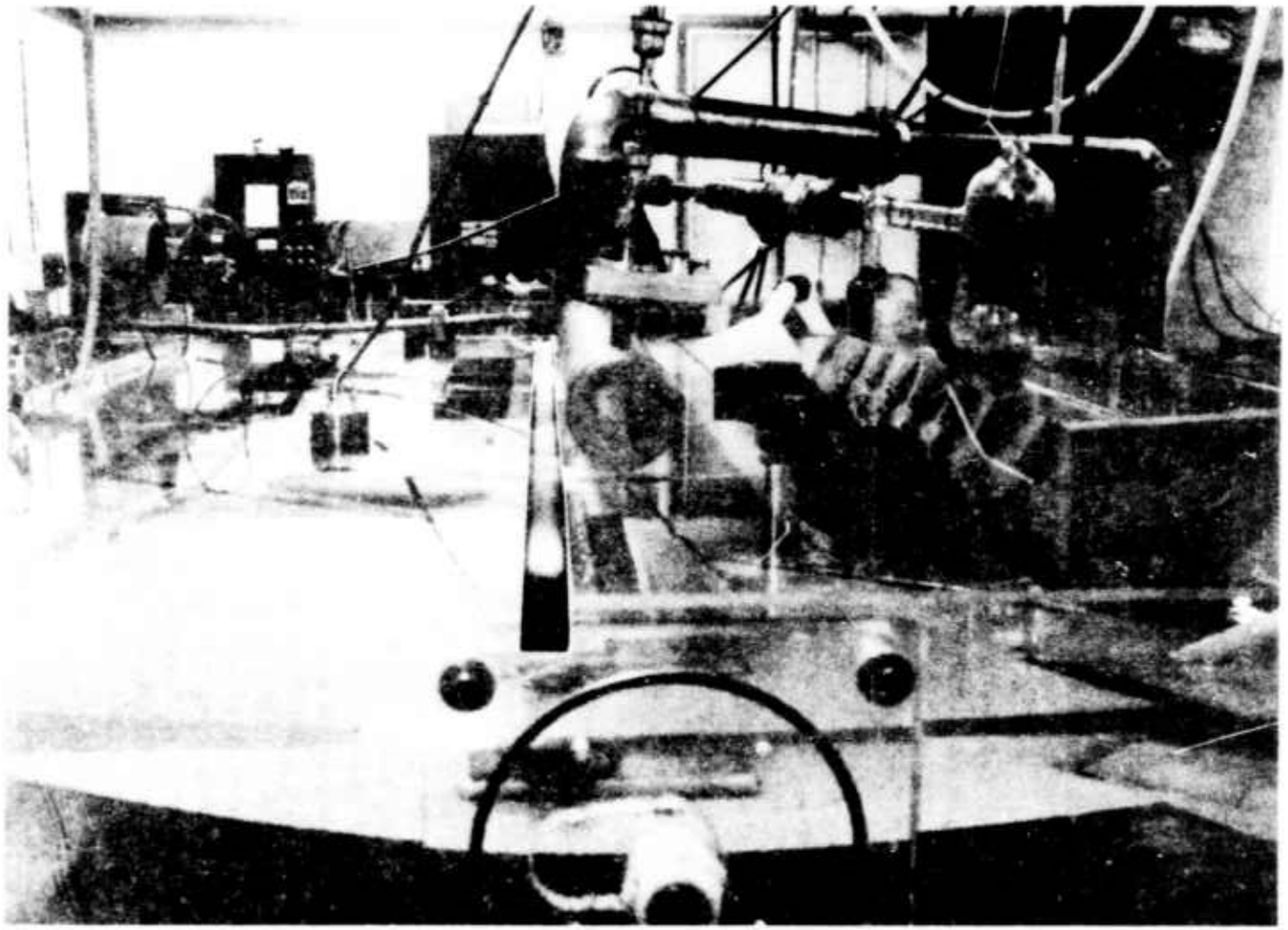

Fig. 34 — The TW e-beam device. This picture is a double exposure to illustrate the overall features plus the relatively uniform discharge

readied for use in determining the temporal and spatial characteristics of the excitation. These diagnostics are: (1) capacitive voltmeters for determining voltage on the storage plates, (2) resistive voltage dividers for checking storage plate and coupling capacitor voltages, (3) current loops to determine plate current waveforms, (4) photomultipliers and filters to measure the time history of the emission, (5) a high speed image converter camera to determine the velocity of excitation, (6) lucite, cellophane, and radiochromic "wittness plates" which are exposed or damaged by the beam in proportion to the spatial intensity of the beam and (7) a vacuum monochromator capable of monitoring emission in the 300 Å - 6000 Å region.

Preliminary results have been obtained from several of the diagnostics. Both the resistive voltage dividers and capacitive voltmeters give similar results showing that the plate voltage is in the 90 - 100 kV range, and that the dielectric switches fire at or near the peak of the resonant voltage waveform. Lucite and blue cellophane witness plates give preliminary indications of a narrow electron beam (< 0.5 cm), but care must be taken since the response of these materials as a function of intensity is not well known. The image converter camera has not yet given photographs with sufficient intensity at the sweep rate necessary to measure excitation velocity. Work on this diagnostic is continuing. The measurement is simple to make since all that is necessary is to streak the laser channel at approximately a nanosecond per mm writing speed and measure the wedge angle that results. Several observations have been made with the vacuum monochromator when the system was filled with 1 - 2 atmosphere of N_2. These observations are discussed below.

As outlined in the first report it seems possible that the rare gas molecules will make relatively efficient lasers in the 600 - 900 Å region of the spectrum. In this spectral region the use of resonant cavities is difficult because no mirror substrate transmits radiation. The traveling-wave approach should enable long gain paths and unidirectional A.S.E. type operation without a resonant cavity. This approach may be useful above 1000 Å when high intracavity laser intensities damage the resonant reflector surfaces. When successfully operated these lasers will serve as useful amplifiers for the tunable pulses generated by nonlinear mixing as described in section IV above.

Experiments using the rare gases have not been actively pursued during the recent modifications to the electron-beam device because of the high cost of research grade rare gases. In order to purity these gases and to reclaim them from the laser chamber a vacuum system and liquid nitrogen trap have been assembled which will permit the rare gases to be frozen out, pruified, and reused later. This system has been tested with Xe and at least 95% of the gas was reclaimed.

As pointed out in the first report there is speculation that molecular hydrogen could be made into a much more efficient laser by

operating it on transitions which terminate above the dissociation limit of the ground state of the molecule. The traveling-wave electron beam should be a good excitation source for this laser. This system would operate at high pressures on the parahydrogen component of the molecules. One source of parahydrogen molecules is from the boil-off of liquid hydrogen. So far no access to liquid hydrogen has been located near NRL, but it is possible that small amounts of liquid hydrogen can be made at NRL. Since 25% of the molecules of ordinary bottled hydrogen are parahydrogen molecules, the experiment can be done even if no enrichment can be performed.

The previous report also mentioned some preliminary data that may have come from recombination in the nitrogen atom. In the experiments nitrogen, at pressures in the 1 - 2 atmosphere range, was placed in the laser gas chamber. Excitation from the travel-wave electron beam produced a strong 3650 Å line. This experiment has been repeated with the improved system operation and the emission again has been observed. Recent experimentation has been aimed at insuring that the emission is not from an impurity. It was suggested that nitrogen may contain sufficient oxygen to produce NO which could radiate in this spectral region, but addition of large amounts of NO did not increase the intensity of the line. Other impurities such as Ar, O, Kr, Al, Xe, and Ti could account for this radiation as they are present in the atmosphere or in the construction of the device. By a systematic procedure of adding or eliminating gases it should be possible to find the source of the emission. If nitrogen is the source, the method of excitation must be determined. Since this is an easy and convenient experiment to do, it will likely continue to receive the most attention until the traveling-wave electron beam has been diagnosed completely.

Near term future work will center on the diagnosis of the electron beam. Temporal diagnosis will incorporate photomultipliers and an image converter camera with faster film. Fast scintillators may be used to directly observe the temporal characteristics of the beam. Better current measurements are expected from the current loops being constructed. Spatial diagnostics include a calibrated radiachromic film sensitive to the electron beam as well as miniature Faraday cups which will be suspended at numerous locations in the beam. A carbon calorimeter will also be built to determine energy flow into the gas. Once these diagnostics have been completed it will be appropriate to consider the more difficult high pressure, short wavelength experiments.

The traveling-wave discharge system for excitation of short wavelength lasers was developed at NRL and has produced numerous new laser lines in the 1000-2000 Å region. The nitrogen molecule has a recently discovered electronic state, $b^1\Pi_\mu$, which as a high probability of making transitions to the upper vibrational levels of the ground state, $X^1\Sigma_g^+$. These transitons have wavelengths in the 900-980 Å region where no lasers have been built. For the 1.6 meter

system an inversion density of about 2×10^{12} cm^{-3} would be required to reach threshold for a mirrorless system. Lifetime of the excited state is on the order of one nanosecond so fast pumping risetimes are required. Since the 1 meter discharge system produced lasing in H_2 at 1161 Å, it is hoped that the longer system now available will be able to produce gain at still shorter wavelengths.

REFERENCES

1. I. N. Knyazev, V. S. Letokhov, and V. G. Movschev, "On the Collisional Four-Level H_2 VUV Laser", Opt. Comm., Vol. 6, pp. 424-426, December 1972.

VI. THEORY AND ANALYSIS

VI. A. 3p → 3s QUASI-CW INVERSION

As described in the last semiannual report, it has been shown by rather simple calculations[1] that it appears possible to achieve sufficient gain on 3p→3s transitions in plasma ions to extend successful visible and near-UV cw ion laser transitions into the vacuum-UV region, where reflecting cavities are not available. These population inversions become quasi-cw, limited by the time during which a high electron temperature can be maintained.

To better ascertain the proper operating conditions for an experiment to test this scheme, an existing hot-spot plasma code[2] was adapted[3]. The initial results were reported in the previous semiannual report. The calculated gain coefficient α for the O^{2+} (O III) carbon-like ion is summarized in Fig. 35 for three values of electron density. This gain dependence can be understood (and extrapolated) quite simply as follows, assuming the upper laser state density $N_u = N_2(N_e X_{23}/A_{33})$, where X_{23} is the collisional excitation rate coefficient from level 2 (the ground state) to 3 (the upper lasing level) and A_{33} is the spontaneous decay rate for the laser transition. At low N_e ($< 10^{15}$ cm^{-3} for O^{2+}) and fixed length,

$$\alpha \propto N_2 \left(\frac{N_e X_{23}}{A_{33}} \right) A_{33} \propto N_e^2 X_{23} , \qquad (1)$$

giving the N_e^2 dependence shown in Fig. 35. For moderate densities ($\sim 10^{16}$-10^{17} cm^{-3}), where collisionally-induced decay from the upper to the lower laser level exceeds A_{33},

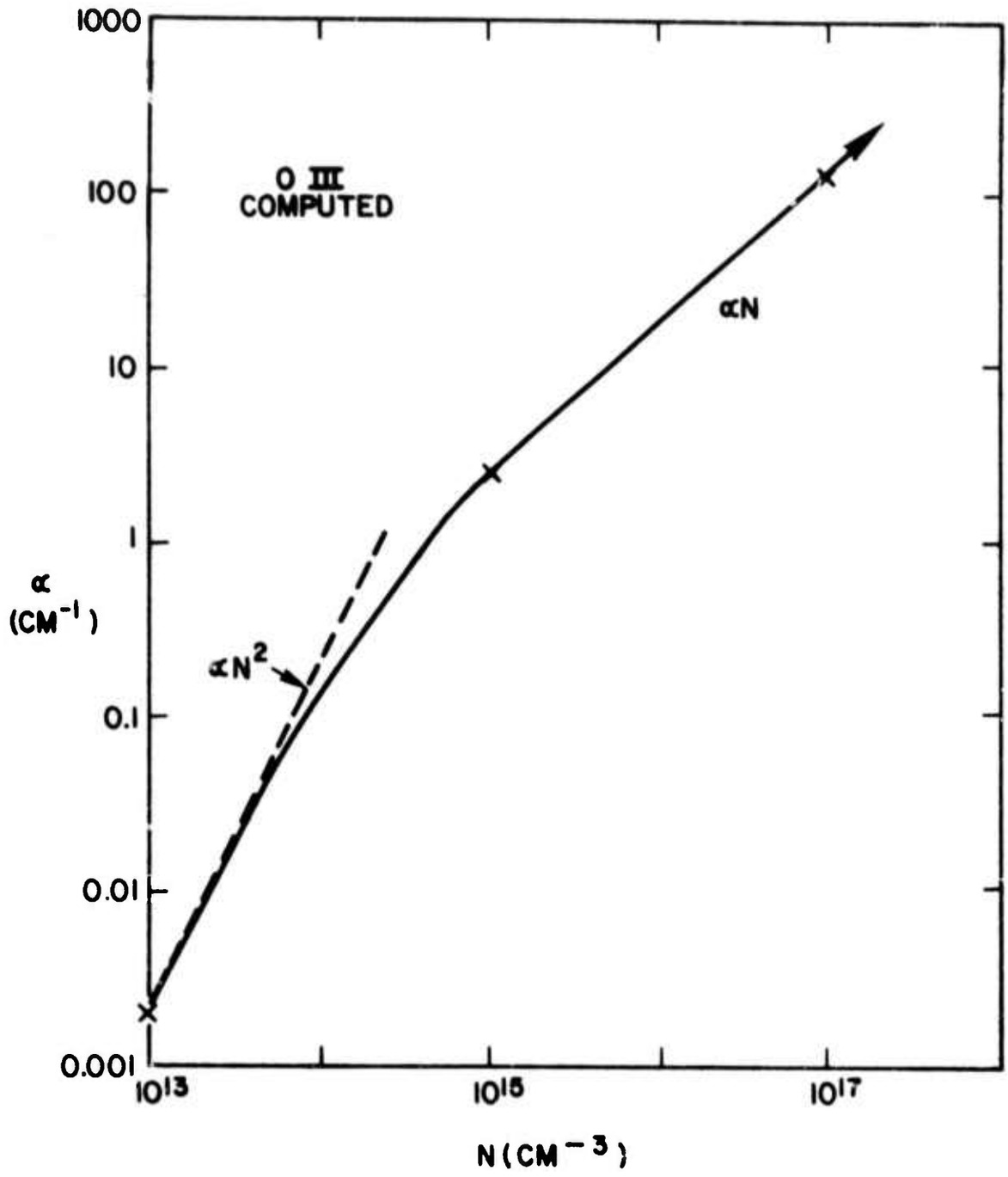

Fig. 35 — Gain coefficient α versus ion density computed by the previously adapted Hot Spot code at three values, for $3p \rightarrow 3s$ transitions in the carbon-like O^{2+} (OIII) ion. The varying dependence of α is understood by increased collisional mixing at higher densities, as discussed in text.

$$\alpha \propto N_2\left(\frac{N_e X_{23}}{N_e D_{33}}\right) A_{33} \propto N_e A_{33}, \qquad (2)$$

and the density dependence becomes linear. Here D_{33} is the collisional deexcitation rate coefficient. High densities are pertinent to the particular case of axial laser heating of a preformed plasma. At densities $\sim 10^{18}$ cm^{-3}, the axial pumping classical absorption length L_{abs} becomes comparable to the laser-medium length and scales as N_e^{-2} according to

$$L_{abs} \propto T_e^{3/2}/N_e^2\lambda^2, \qquad (3)$$

for a fixed ion charge[3]. The gain product αL then becomes

$$\alpha L_{abs} \propto N_e^{-1}\left[A_{33}\left(\frac{X_{23}}{D_{33}}\right)\left(\frac{T_e^{3/2}}{\lambda^2 z}\right)\right] \qquad (4)$$

and decreases as N_e^{-1}. Finally, at extremely high densities ($> 10^{18}$ cm^{-3}) $N_e D_{32}$ becomes comparable to A_{32} (the lower laser depopulation spontaneous decay rate), collisions dominate, and equilibrium distributions evolve with no inversion.

The numerical model has been extended to these higher density limits as described below. An important concern is the true degree of advantage achieved in such a quasi-cw mode over a self-terminating scheme, where population inversion is limited to a time of A_{33}^{-1}. The hot-spot code predicted inversion times of approximately 100 ns and 1 ns at densities of 10^{15} and 10^{17} cm^{-3}, respectively, as shown in the previous semiannual report. For the O^{2+} ion, A_{33}^{-1} = 10 ns so that the scheme appears roughly comparable to self-termination at a density of 10^{16} cm^{-3} with a gain coefficient (Fig. 35) of about 20-30 cm^{-1}. In the Hot-Spot model, the gain is limited by a rapid drop in electron temperature due to thermal conduction losses to a cold surrounding medium. This may indeed not be realistic for laser-produced plasmas and there have been a number of suggestions recently that self-generated magnetic field isolation may reduce such conduction. Therefore, more complete modeling is required to resolve this matter, and of course data from the experiment described in Section II will be used for a real-world comparison.

For this and other reasons, a new and more versatile program XRL-1 has been assembled specifically for modeling the x-ray laser

schemes. Initially it will compare results with the Hot-Spot modeling already completed for the O^{2+} ion, after which it will be used for extrapolation to other ions and shorter laser wavelengths. The new XRL-1 code is similar to the Hot-Spot code in that it solves a set of coupled differential rate equations with the atomic level populations and the electron and ion temperatures as dependent variables. The input and output routines for this code have been written to facilitate its use for any atomic level systems expected to produce lasing and to allow easy addition and removal of extra atomic levels and physical processes. This code has now been debugged and tested for atomic schemes consisting of up to six energy levels and three stages of ionization.

Most of the XRL-1 runs thus far have been made for O^{2+} ions using a three-level system. Several other assumptions and simplifications were used in most of these initial runs as follows. Only the ground level and upper and lower laser levels of the O^{2+} ion were considered, i.e., ionization and recombination were ignored. Electron collisional excitation and deexcitation and radiative decay were considered to affect the level populations. Also, the plasma was considered optically thin and was assumed to maintain a constant ion density, which is reasonable for the short time scales considered. Energy losses by thermal conduction (see above) and by radiation were neglected. The electron temperature was turned on instantaneously and was usually chosen to be 10-100 times the ion temperature. Equilibration between these two temperatures was computed by the code. In all cases this relaxation time was much longer than time scales of interest for lasing. The rates for atomic processes considered were computed from formulas published by Elton[4].

In Fig. 36 are plotted curves of the peak gain coefficient, α, (in cm^{-1}) attained as a function of ion density for several initial electron temperatures and for an ion temperature of 1 eV. For these runs, the assumptions listed in the proceeding paragraph apply. These curves agree with the analytical predicitions above in that they show the low density regime around $N_i = 10^{14}$ where α varies as N_e^2, the moderate density region around $N_i = 10^{16}$-10^{17} where α is proportional to N_e (e.g., for $T_e = 100$ eV and $N_e = 5 \times 10^{16}$ cm^{-3} $N_e D_{33} = 10 A_{33}$), and the rapid decline in α at densities large enough for collisional equilibrium to dominate. The output from the computer runs which produced these curves also shows good agreement ($\sim$ 20%) for predicted excited state population densities compared to those predicted by the Hot-Spot code at $N_i = 10^{15}$ cm^{-3}. The latter code also produced results at $N_i = 10^{17}$ cm^{-3} but here population densities predicted by the new code were about a factor of 5 higher than Hot-Spot predictions. They may be due to the fact that ionization and recombination are not included in the present output from the new XRL-1 code.

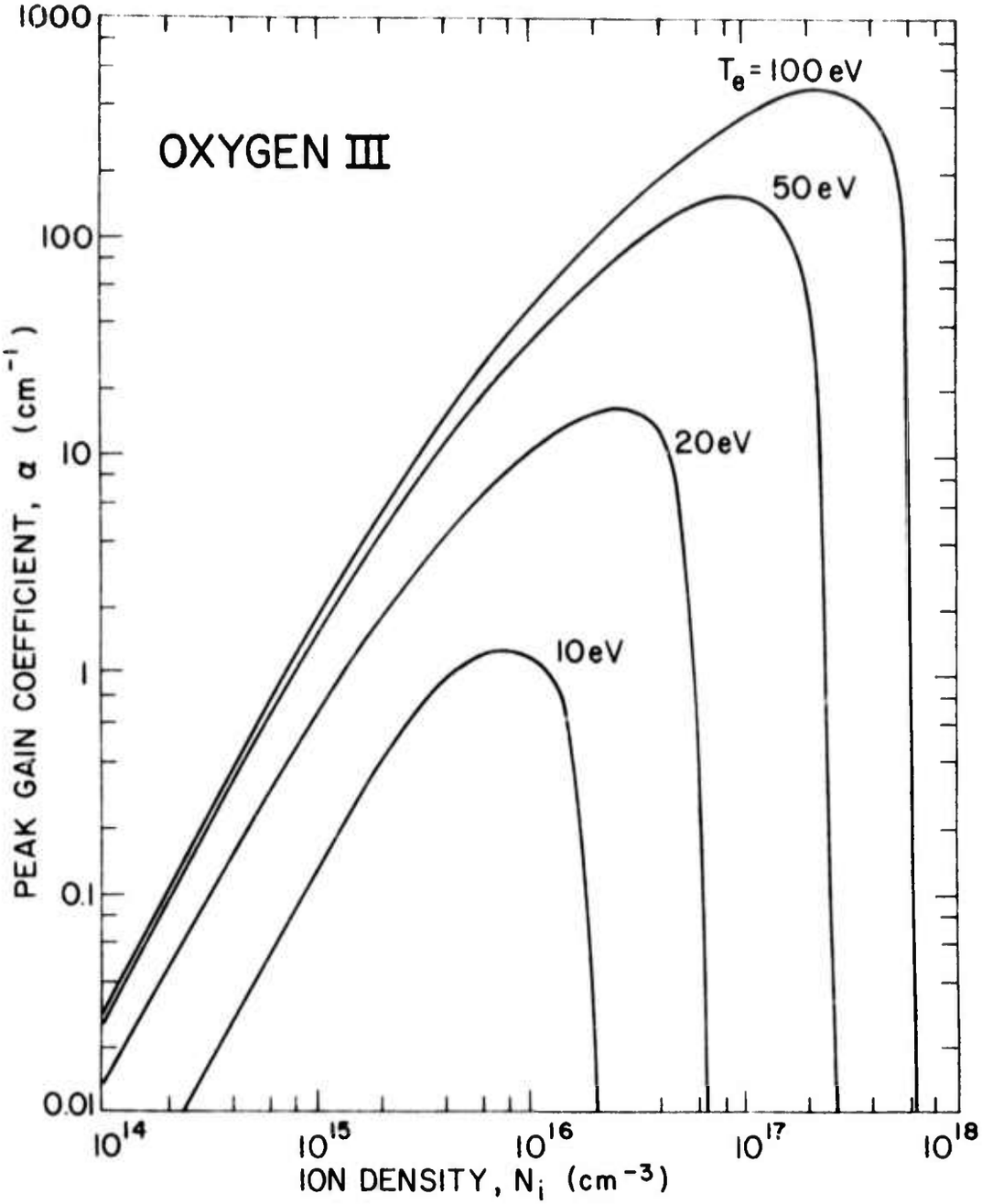

Fig. 36 — Newly computed 3p — 3s peak gain coefficient versus O^{2+} ion density for various temperatures

Plans for the continuation of this study over the next several months include adding more physical complexity in the form of more energy levels, more ionization stages, and more energy exchange mechanisms to the scheme being modeled and to study their effects, with an eye toward predicting the lasing duration as well as specific atomic species and plasma conditions which would be most favorable for producing lasing experimentally. More specifically, near term plans include addition of one more O^{2+} level and the ground terms of the O^{1+} and O^{3+}, ions. Also, since shorter wavelength lasing is of ultimate conern, the code will be used to model more highly-ionized species which are isoelectronic with O^{2+} going next to Ne^{4+}, beyond which input atomic rates will be extrapolated.

REFERENCES

1. R. C. Elton, "Extension of 3p→3s Ion Lasers into the Vacuum-UV Region", NRL Memorandum Report 2799, May 1974; also Appl. Optics, 14, 97, 1975.

2. K. G. Whitney and J. Davis, J. Appl. Phys. 45, 5294 (1974); also K. Whitney, J. Davis and E. Oran, NRL Memorandum Report 2644, June 1973.

3. R. C. Elton, T. N. Lee, J. Davis, J. F. Reintjes, R. H. Dixon, R. C. Eckardt, K. Whitney, J. L. DeRosa, L. J. Palumbo and R. A. Andrews, Physica Fennica 9, Suppl. S1 (1974).

4. R. C. Elton, "Atomic Processes" in Methods of Experimental Physics Vol. 9 Plasma Physics Part A, H. R. Griem and R. H. Lovberg (Eds.), New York: Academic Press (1970), Chapter 4.

VI. B. ELECTRON-COLLISIONAL PUMPING

Electron-collisional pumping of potential laser ions using the approach described earlier, i.e., picosecond laser heating of an preexisting cold plasma, can be divided into five problem areas: (1) the generation of a cold plasma with a large fractional population of the laser ion species; (2) synchronization of the electron heating laser pulse with the plasma generation; (3) obtaining optimum electron heating; (4) identifying potential ion laser configurations; and (5) establishing tests and criteria for observation of net gain. Areas (2), (3), and (4) have been looked at in some detail and the results of this work are described in full in the Appendix.

Briefly, the synchronization problem has been solved and is the technique described in Section II both in this report and the previous report. On a picosecond time scale and for moderate plasma densities it can show that inverse brehmstrahlung is the primary heating mechanisms and that stimulated Compton scattering is also a possibility in special cases. Electron temperature up to but not exceeding about

1 keV are possible and this limits the applicability of this technique to the soft x-ray region. Two new candidates for pulsed (self-terminating) lasers are identified: K-like and Si-like ions. K-like ions for ScIII and higher Z have an electron configuration unique to ions, i.e., a single 3d electron ground state. The laser transition in this series is $4p \rightarrow 4s$. Si-like ions have a $(3s)^2(2p)^2$ ground configuration. The first allowed excited states are the $(3s)(2p)^3$ states. The potential laser transitions are $^3S^o$, $^3P^o$, or $^3D^o$ $(3s2p^3) \rightarrow {}^1S$ or ^1D $(3s^22p^2)$. This is an intercombination line but spectroscopic data shows that in the cases of interest it is fairly strong and can lead to useful gain. (See Appendix)

VII. SUMMARY

This reporting period has seen substantial progress in all areas of the program. This progress has varied from important technological improvements in experimental facilities to new insights based on continuing analysis and numerical modeling. The charge transfer experiment and the nonlinear mixing approach to shorter wavelengths were initiated during the last period and have made substantial progress in this period.

The most significant results obtained during this period for each of the program areas are as follows:

E-COLLISIONAL PUMPING -

1. The short pulse laser facility has seen substantial technological improvements. The Q-switched oscillator part of the system has been improved to limit longitudinal mode structure, reduce the jitter in buildup time, and improve reproducibility. The jitter in synchronization of the two pulses has been reduced to $\sim$ 0.2 nsec by improved pulse and spark gap techniques. The nanosecond amplifier have also been brought on-line during this period.

2. A series of laser-plasma interaction experiments has been completed. This series studied the effect of prepulses on x-ray yield and electron temperature using two 25 psec. pulses.

RESONANT CHARGE TRANSFER -

3. The experiment has been designed, fabricated, assembled, and initial checkout and calibration is underway. The experiment consists of a 2 meter grazing incidence spectrograph, target chamber with multiple target capacity, and a gas manifold for "puffing" gas into the target area in synchronism with the firing of the laser.

4. Further analysis on this experiment has reinforced our confidence in this approach and identified several new laser possibilities involving the use of gases other than helium.

NONLINEAR MIXING APPROACH -

5. The nonlinear mixing components including NL crystals, ovens, and mounts have been procured and being evaluated on an individual basis.

6. A laser triggered spark gap has been designed and constructed for the hydrogen amplifier. This spark gap is an essential part of the scheme to synchronize this amplifier with the laser oscillator at the beginning of the chain.

7. A experiment to test the feasibility of building an atmospheric pressure photo-preionized hydrogen amplifier has been designed and constructed. The experiment will measure the electron density that can be produced in a mixture of hydrogen and CO when pumped with a hard UV emitting flashlamp. This experiment is undergoing checkout at this time.

TW PUMPING -

8. The TW e-beam device has undergone a number of technological improvements during this period. Among other things the optimum diode design has been determined and new diagnostics have been designed and investigated.

9. Laser emission at 3650 Å has been observed with the TW discharge device. This radiation is believed to be from N_2 but other possibilities are being explored.

THEORY, ANALYSIS, AND MODELING -

10. Modeling of the quasi-cw $3p \rightarrow 3s$ laser scheme has continued. A new, more versatile code has been developed and applied to the O III ion along with others. The results are in good agreement with trends predicted using previous theoretical analysis.

11. The self-terminating pulsed e-collisional laser has also been analyzed. The electron heating mechanism has been looked into and two new ion laser isoelectronic sequences have been identified.

In addition to the above the negative n_2 work which was mentioned

in the last report was continued with partial support from this program during this period. A more definitive experiment was completed with the results in complete agreement with theory. These results may lead to faster more intense lasers for pumping sources in the x-ray laser work.

In brief this period has seen a good amount of progress, both in experiments and analysis and in technological improvements. This sort of mix will probably continue during the next period. However, the e-collisional and charge transfer experiments are at a point where important and definitive measurements will be made in the next reporting period.

Finally, reprints of the important publications and talk abstracts are including as an appendix to this report. These represent work performed during this period and are included to provide details on various parts of the program.

Appendix

PUBLICATIONS* AND PRESENTATIONS FOR THE REPORTING PERIOD

*In the case of NRL Reports the cover page only is reproduced. These documents are available on request.

IV. INTERNATIONAL CONFERENCE ON VACUUM-ULTRAVIOLET RADIATION PHYSICS

VUV IV

HAMBURG

Congress Centrum Hamburg CCH

July 22–26 1974

EXTENDED ABSTRACTS

6 ION LASERS FOR THE VACUUM-UV REGION

R. C. ELTON

Naval Research Laboratory
Washington, D. C., U.S.A.

ABSTRACT

A simplified three-state analysis of ions in the carbon isoelectric sequence indicates the feasibility of obtaining significant amplification by stimulated emission in the hundreds-of-Ångstrom region on 3p→3s transitions in a single-pass system. The minimum gain length is density-limited due to collisional depopulation; however lengths ≤1 cm are predicted. Such lengths are compatible with laser-produced plasmas. Reasonable pumping power densities are also predicted. Future plans and needs are discussed.

INTRODUCTION

Lasers in the vacuum-UV region below 1000 Å will likely be limited to superfluorescent devices of high brightness and collimation but with limited spatial coherence, due to a lack of efficient resonant cavities. However, a high degree of coherence can conceivably be achieved by progressive non-linear mixing techniques which have been applied successfully[1] so far for reaching 887 Å. The decreasing efficiencies of such up-conversion steps can then be compensated-for with VUV amplifiers, maintaining the original coherence.

In developing such VUV amplifiers, large pumping fluxes are inevitably required because of a strong wavelength dependence of the gain coefficient. Thus, the production of a plasma laser medium will invariably occur. It is therefore natural to consider plasma ions as the amplifying vehicle, in a linear geometry such as created from a solid surface by a line-focused laser. The length of plasma that can presently be heated sufficiently to achieve multiple ionization is in the centimeter range. Thus, the question becomes whether such a medium can be used at a sufficiently high density to generate significant net gain while at the same time avoiding excessive collisional quenching of the inversion.

There exists a host of literature on near-UV and visible lasing from multiply-ionized atoms in plasmas, and it is reasonable to begin investigating some of these transitions for shorter wavelengths, using isoelectronic ions.

An initial inspection of the collisional mechanisms involved shows that transitions between n=3 levels are most promising, based upon a general model of electron collisional n=2→3 pumping through a non-dipole, slow-decaying transition and lasing into another n=3 level, which undergoes rapid 3→2 spontaneous dipole decay. Pumping into higher quantum states (n=4, 5, etc.) could produce shorter wavelength laser emission; however these levels are much more susceptible to rapid collisional ionization and collisional mixing with dipole-decaying states. Helium-like ions with possible 3→2 lasing transitions require excessive $1s^2$-$1s3\ell$ pump energy. Therefore, transitions between 3p and 3s states in, for example, carbon-like ions seem to offer a reasonable initial compromise, and hold promise of achieving amplification in the 300 Å region with molybdenum ions.

ANALYSIS

A simple analysis[2] can be carried out assuming that 2p→3p monopole pumping by electron collisions proceeds at a rate comparable to 2p→3d dipole excitation, as evidenced by experimental and theoretical studies. For such $\Delta\ell=0$ transitions, the effective Guant factor approximate formula may be conveniently used to obtain the pumping rate[3]. The n=3 excited state densities are then estimated as $N_3/N_2=N_eX/A_3$, where N_3 and N_2 are the excited and ground state population densities, respectively, N_e is the electron density, X is the excitation rate coefficient, and A_3 is the dominant decay mode of each n=3 state. With $A_u \ll A_\ell$, where the subscripts refer respectively to the n=3 upper and lower laser states, a population inversion is achieved, at least until some further equilibrium state is reached.

At high densities, collisional mixing will couple the upper laser state with other n=3 states which decay rapidly to n=2. By limiting this collisional mixing rate to a value of the laser transition probability for spontaneous decay, we can arrive at a maximum tolerable density. The collisional mixing rates for $\Delta\ell=0$ transitions can be estimated, assuming the rates are double the calculated line widths[4]. Numerical results for the carbon-like sequence indicate a slight advantage over other sequences in which lasing has been observed. For the elements and estimated temperatures listed in Table 1, the collisional mixing by electrons exceeds that by ions sufficiently to ignore the latter. Equating the electron collisional mixing rate N_eX_{33} for the laser transition to A_{33}, the corresponding spontaneous decay rate, gives

the maximum electron density $(N_e)_{max}$ tabulated.

The minimum length over which gain factors of $\alpha L=1$ (threshold) and 5 [in the relation $I/I_o=\exp(\alpha L)$] are achieved at the maximum permitted density are calculated from the gain formula[5] for Doppler broadened lines. The results are included in Table 1 for the particular case where the electron temperature T_e exceeds the ion temperature T_i by a factor-of-10. This condition is achieved by rapid electron heating with, for example, an auxiliary axial laser beam and in a time period shorter than the electron-ion energy equipartition time. The results indicate that lengths on the order of a centimeter are feasible for achieving gains greater than threshold.

TABLE 1

Parameter \ Ion	Ne^{4+}	Al^{7+}	Ca^{14+}	Cu^{23+}	Mo^{36+}
λ (Å)	2269	1148	756	473	306
$kT_i = kT_e/10$ (eV)	24	50	200	480	1100
$\tau_u(ns)=A_{33}^{-1}/2$	2	1	0.6	0.4	0.3
$10^{-17}(N_e)_{max}(cm^{-3})$:	0.02	0.2	3.5	16	72
$L_{min}(cm)$:					
$\alpha L=1$	0.86	0.45	0.33	0.39	0.52
$\alpha L=5$	4.2	2.2	1.7	2.0	2.7
$10^{-12}P/a$ (W/cm^2) (for inv. brem. abs. length $\hat{L}$):					
$\alpha L=1,5$	2	2	2	2	2

The pump power density P/a (required to overcome radiative decay) in the auxiliary laser beam is estimated for $\alpha L=5$ from $N_u A_{33} \hat{L} E_{23}$, where E_{23} is the excitation energy interval. This result is included in Table 1 and is encouraging when compared to state-of-the-art picosecond lasers that produce 10^{14} W/cm^2, even if an $\sim$1% total pumping efficiency is assumed.

The laser action will be self-terminating in an equilibrium relaxation time to be determined by a detailed numerical analysis. In any case, it is not expected to be shorter than $\tau_u=A_{33}^{-1}/2$, the upper laser state lifetime, tabulated in Table 1 and seen to be sufficiently long for present 10-25 ps pumping lasers.

DISCUSSION

The present analysis is of preliminary nature and intended to serve as impetus for sophisticated numerical modeling of the atomic and plasma physics, and for experiments in laser-plasma production and heating with short pulses. For the modeling, it is clear that data are in short supply on almost all relevant atomic processes, radiative and collisional, for high-Z ions; here both theoretical calculations and experiments are needed. For experiments, higher power lasers are always desirable for increased pumping. Also, fast (ps) vacuum-UV detectors are needed for time-resolved diagnostics. An efficient resonant cavity for the vacuum-UV would be most desirable in the sense that it would reduce the severe requirements on pumping and media density through multiple-pass operation, although again it is not essential for achieving amplification.

In conclusion, the presently described simple analysis offers encouraging prospects for extending proven ion laser schemes into the vacuum-UV region for amplification of coherent radiation. More detailed numerical analysis and experiments are required and are presently underway[6].

REFERENCES

1. S. E. Harris, A. H. Kung and J. F. Young, J. Opt. Soc. Am. 64, 556 (1974).
2. R. C. Elton, Naval Research Laboratory Memorandum Report No. 2799, May 1974.
3. R. C. Elton, "Atomic Processes", (in) Methods of Experimental Physics - Plasma Physics, Vol. 9A, eds. H. R. Griem and R. H. Lovberg, (Academic Press, New York, 1970).
4. H. R. Griem, "Broadening of Spectral Lines by Charged Particles in Plasmas" (Academic Press, New York, 1974).
5. R. C. Elton, R. W. Waynant, R. A. Andrews and M. H. Reilly, "X-Ray and Vacuum-UV Lasers: Current Status and Prognosis," NRL Report 7412, May 2, 1972.
6. T. N. Lee, J. Davis, J. F. Reintjes, R. H. Dixon, R. C. Eckardt, K. Whitney, J. L. DeRosa, R. A. Andrews and R. C. Elton, Bull. Am. Phys. Soc. 19, 558 (1974); Proc. VIII IEEE International Quantum Electronics Conf. (1974).

PROCEEDINGS

OF THE

INTERNATIONAL CONFERENCE

ON

X-RAY PROCESSES IN MATTER

HELSINKI UNIVERSITY OF TECHNOLOGY

OTANIEMI, FINLAND, JULY 28 - AUGUST 1, 1974

PUBLISHED IN

PHYSICA FENNICA

VOL. 9, SUPPLEMENT S1, JULY 1974

OTANIEMI, 1974

QUASI-STATIONARY POPULATION INVERSION ON Kα TRANSITIONS

R.C. Elton

U.S. Naval Research Laboratory, Washington, D.C., 20375, USA

For lasing in the x-ray spectral region, 2p→1s, Kα-type transitions are most desirable because of the high photon energy. The pumping flux necessary to sustain a population inversion against spontaneous decay is, however, formidable[1], due to the large x-ray and Auger transition probabilities. The femtosecond risetimes required for pre-aquilibrium operation in a self-terminating mode[2] are an additional severe problem[1]. Stripping of outer electrons so that hydrogenic or helium-like ions are utilized would eliminate both the Auger contribution to the decay and the attenuation of the beam due to photoionization. In any case, however, such short-lived inversions could only be useful as amplifiers, since the coherence length is ≤ 1 μm, prohibiting cavity use without extremely well-synchronized repetitive operation or a traveling wave pumping.

If, however, an inverted density can be maintained in a quasi-stationary mode[3] for nanoseconds, operation with Bragg-reflecting resonators may be feasible. Stankevich[4] suggested such a possibility, providing that the <u>total</u> rate for transfer of L-vacancies (lower laser state) to the M-shell exceeds the <u>total</u> K-vacancy (upper laser state) decay rate. His analysis, based upon early data, indicated that sustained inversions on the $K\alpha_1$ and $K\alpha_2$ transitions was possible for elements with $Z \leq 36$ and 47, respectively. Using a similar approach with more recent data[5], we find [3] that the necessary conditions may

possibly be met for only the $K\alpha_2$ transition and for $25 \leq Z \leq 45$. Also, the degree of inversion and the resultant gain are limited by a maximum excess L- over K- vacancy depletion rate of ~30%.

However, the creation of double LL- or LM_1 vacancy states following K-Auger transitions can produce a sufficient energy shift to avoid resonant absorption of the amplified K x-ray emission. In this refined model, it is only necessary for the total L-decay rate to exceed the K x-ray rate; significant rate excesses and net gain then become possible for both $K\alpha_1$ and $K\alpha_2$ transitions and for $13 \leq Z \leq 50$. This line shift model is based upon a delicate balance between (a) rapid Auger cascading to higher M-vacancy states with multiple ionization, associated decay rate decreases, and insufficient line shift; and (b) recombination which must proceed at a comparably high rate to prevent excessive depletion of amplifying atoms through ionization. This latter condition places an upper limit on the temperature permitted ($kT \approx 30$-100 eV according to Stankevich[4]) and, in a continuously pumped medium, on the inversion period; hence the quasi-stationary nature of the inversion. The achievement of the proper balance will be found both by a full numerical model and from careful experimental diagnostics.

Based upon this line-shift model, respective calculations[3] for Si, Ca, and Cu at wavelengths of 7.1, 3.4, and 1.5 Å indicate first that only concentrated x-ray photon beams can provide the required pumping energy density. For the same elements, x-ray photon densities (in the K-absorption bands) of (2, 4, and 20)10^{20} cm^{-3} are required to overcome photoionization losses. This is equivalent to (5, 20, and 200)10^{15} W/cm^2 and results in gain coefficients αL of 70, 30 and 15, for a

laser-medium length L of 300 μm and diameter 30 μm. With a 10% conversion efficiency, this could be provided by IR lasers of 4, 9, and 200 TW, powers within present means and expectations.

It is interesting to note that, for the same elements, the pump power requirements are equivalent to 1% of the total blackbody radiation at achievable temperatures of kT = 0.5, 0.7 and 1.2 keV with peak emissions at convenient wavelengths of 5, 4, and 2 Å, respectively. It is suggested that some experimental efforts be directed towards developing a "tuned" pump source approaching blackbody conditions in a desired spectral band, e.g., with a pseudo-continuum of saturated L-line emission from heavy elements; some VUV efforts on uranium plasma emission already exist.

References

1. M.A. Duguay and R.M. Rentzepis, Appl. Phys. Letters 10, 350 (1967).

2. R.C. Elton, R.W. Waynant, R.A. Andrews, and M.H. Reilly, Naval Research Laboratory Report 7412 (May 1972).

3. R.C. Elton, Naval Research Laboratory Memorandum Report (to be published, 1974).

4. Yu.L. Stankevich, Sov. Phys.-Doklady 15, 356 (1970).

5. E.J. McGuire, Phys. Rev. 185, 1 (1969); Phys. Rev. A 3, 587 (1971); 5, 1052 (1973). Also D.L. Walters and C.P. Bhalla, Phys. Rev. A 3, 1919 (1971); Atomic Data 3, 301 (1971). Also J.H. Scofield, Phys. Rev. 179, 9 (1969); Phys. Rev. A 9, 1041 (1974).

400

TOWARDS X-RAY LASERS WITH VUV AMPLIFICATION ON 3p→3s TRANSITIONS

R.C. Elton, T.N. Lee, J. Davis, J.F. Reintjes, R.H. Dixon,

R.C. Eckardt, K. Whitney*, J.L. DeRosa, L.J. Palumbo, and R.A. Andrews

U.S. Naval Research Laboratory, Washington, D. C. 20375, USA

Proposed devices for obtaining amplified spontaneous emission (ASE) in the x-ray spectral region appear to have very limited spatial and temporal coherence, and attempts to improve this by addition of an x-ray resonator appear unrealistic at present. High quality, coherent x-ray laser beams may ultimately be achieved by short wavelength amplification of collimated, coherent laser radiation obtained by frequency up-conversion using non-linear optical techniques. Wavelengths as short as 887 Å have so far been obtained, starting with 1.06-μm laser radiation[1]. With limited conversion efficiencies, VUV amplification becomes necessary, where superfluorescent ASE devices suffice. In developing such amplifiers, it is reasonable to consider extending present near-UV ion laser transitions into the VUV region[2]. For example, UV lasing at wavelengths as short as 2700 Å has been demonstrated using 3p→3s transitions in a number of multiply-ionized low-Z elements in plasmas[3]. Excitation 2p→3p is by electron collisions and 3s→2p electric dipole depopulation is rapid. With fairly efficient cavities, sufficient gain is achieved without

---

*Science Applications, Inc., Arlington, Virginia, U.S.A.

collisional mixing problems at low-to-moderate particle densities. In the VUV region, where resonators become nonexistent, multiple ionization at the high densities required for superfluorescent gain requires large pumping energy densities and small volumes for existing power sources, e.g., focused laser beams.

With the gain factor achievable limited by the density at which collisions compete with stimulated emission, a simple 3-level analysis[4] for carbon-like ions indicates that the minimum laser-medium length required scales with the electron (T_e) and ion (T_i) temperatures as $(T_i/T_e)^{\frac{1}{2}} \exp(\Delta E_{23}/kT_e)$, where ΔE_{23} is the 2p-3p energy difference. Hence, a high electron temperature is important and a low ion temperature is desirable for short laser-medium lengths. Including the other important variables such as laser wavelength λ_L, transition probability, and density, the analysis indicates a reasonable length on the order of 1 cm for Z extending to 42 (Mo, $\lambda_L \approx 300$, where a hydrogenic-ion spectrum has already been observed in a laboratory discharge[5]. An extended analysis with a more sophisticated numerical model, which includes interactions with other levels and ionic species, is underway. This analysis is based on a "hot-spot" plasma model which includes impulse heating and radiative and conductive cooling. Preliminary results indicate $T_e/T_i \approx 10$ for initial time periods of ~50 ps, which is shorter than the upper laser state lifetime and longer than the 25 ps pumping laser pulse. An additional result expected from the numerical analysis is the relaxation time of the inverted population, which could conceivably exceed the 3p level lifetime [4, 6].

Experiments are underway[7] in which a line plasma laser-medium is created by focusing an IR laser on an appropriate target material to produce the desired ion species and density in expansion. An existing 4GW, 25 ps Nd:YAG laser pulse is to be directed axially into this plasma and provide the preferential electron heating for collisional population inversion. Initial experiments on characterizing the plasma have been performed with a point focus from the short-pulse laser and using x-ray diagnostics on plasmas of Na, Mg, Al, and Si. Resonance lines from helium-like species are observed in all cases and from hydrogenic ions for the first three. The observed species and relative intensities are in agreement with predictions of the numerical model. The diagnostics are presently being extended into the more "cluttered" VUV region, as the two-laser system is made operational.

References

1. S.E. Harris, A.H. Kung and J.F. Young, Abstract, UV and X-Ray Laser Symposium, Optical Society of America Meeting Washington, D. C. 25 April 1974; J. Opt. Soc. Am. (to be published).

2. M.A. Duguay, Laser Focus 9, 45 (Nov. 1973); R. A. Andrews, Naval Research Laboratory Memorandum Report No. 2677 (Oct. 1973).

3. Y. Hashino, Y. Katsuyama and K. Fukuda, Japan J. Appl. Phys. 11, 907 (1972); 12, 470 (1973).

4. R.C. Elton, Naval Research Lab. Memorandum Report 2799 (May 1974).

5. J.J. Turechek and H.-J. Kunze, to be published.

6. R.C. Elton, R.W. Waynant, R.A. Andrews, and M.H. Reilly, Naval Research Laboratory Report 7412 (May 1972).

7. T.N. Lee, J. Davis, J.F. Reintjes, R.H. Dixon, R.C. Eckardt, K. Whitney, J. L. DeRosa, R.A. Andrews and R.C. Elton, Bull. Am. Phys. Soc. 19, 558 (1974).

Reprinted from APPLIED OPTICS, Vol. 14, page 97, January 1975

Extension of $3p \rightarrow 3s$ Ion Lasers into the Vacuum Ultraviolet Region

R. C. Elton

The feasibility of extending existing near-ultraviolet ion lasers into the vacuum ultraviolet spectral region is analyzed with a simplified three-state model. Single-pass amplification in a laser-produced plasma of reasonable length, pump power, and rise-time requirements is predicted, especially for high electron temperatures. The results are intended to serve as a basis and incentive for detailed numerical modeling and for experiments.

I. Introduction

Lasing in multiply ionized atoms has been demonstrated in the visible and near-ultraviolet spectral regions with gas discharges in resonant cavities.[1] It would be of great interest and importance to translate these results to shorter wavelengths isoelectronically.[2] At vacuum ultraviolet (vuv) wavelengths shorter than 2000 Å, conventional cavities become inefficient, and impractical below 1600 Å. However, for amplification of, for example, a frequency upconverted coherent vacuum-uv beam,[3] a resonant cavity is not required, provided significant gain can be achieved in a single photon pass through an inverted medium of reasonable length. Higher inverted state densities are required for single-pass amplification and for short wavelengths, with an upper density limit set by rapid depletion due to charged particle collisions. Population inversions are often self-terminating in time as equilibrium population distributions are approached, and the required rise time of the pumping source usually decreases with decreasing wavelength according to increasing transition probabilities for spontaneous decay. Also, the higher excitation energy in the heavier elements required for short wavelengths (isoelectric extrapolation) requires increased particle energies and densities for collisional pumping.

With these general guidelines we have attempted to analyze the scalability to shorter wavelengths. The highest degrees of ionization in heavy elements are obtained in high density plasmas, in short bursts, and in small volumes with a limited amount of available energy. A conceivably practical device, compatible with present technology, would be a linear plasma of about 1 cm in length, with the necessary ions and particle densities produced from a solid target by a line-focused laser beam. Longer plasmas may eventually be generated to produce increased overall gain, or perhaps decreased density for improved efficiency, as more powerful lasers are developed. Longer lengths may also become a possibility with axial heating of gaseous media by long wavelength lasers, a concept similar to that proposed for fusion plasma heating.[4] However, absorption and heating is a function of the plasma temperature and density, and uniform heating with narrow channeling[5] must first be proved. For short wavelengths and high Z materials, solid targets are generally more readily available than gases. It therefore seems reasonable to model the present analysis around a transverse irradiated and vaporized solid target plasma medium.

After expansion the initial plasma would be pumped axially with a separate short-pulse laser; this would preferentially heat the electrons, which in turn would produce the inversion by electron-ion collisions. A high electron temperature T_e is often very beneficial in producing a high inversion when, as here, the electron density is limited; also a low ion temperature reduces the (Doppler) line width and increases the possible gain (see Eq. (1) below). Thus, an electron-ion temperature differential is desirable and this may be achieved by allowing the ions to expand and cool (faster than recombination takes place) and by heating the electrons in times shorter than the electron-ion energy equipartition time.

Considering resonance-line absorption and stimulated emission, the gain in a homogeneous medium of length L is given by $I/I_0 = \exp(\alpha L)$, where α is the gain coefficient[6]:

The author is with the U.S. Naval Research Laboratory, Washington, D.C. 20375.
Received 17 June 1974.

$$\alpha = [\lambda^2(\pi \ln 2)^{1/2}/4\pi^2\Delta\nu]A[N_u - (g_u/g_l)N_l]. \quad (1)$$

Here, λ is the laser wavelength, A the transition probability, $\Delta\nu$ the Doppler line width in frequency units, and g_u, g_l, N_u, N_l the statistical weights and population densities for the upper and lower laser levels, respectively. Photoionization losses are omitted here, since only (K and) L shell electrons are present, and the photon energy of the short wavelength laser lines is insufficient to remove L electrons; likewise competition from Auger decay does not exist. Loss of laser photons through scattering has also been neglected here. A selection of a particular αL product (unity for threshold, $\gtrsim 5$ desirable) determines the minimum length of the medium, since the other parameters (e.g., density) are fixed or limited in the medium. Thus, we intend to show that a practical length of the order of 1 cm is reasonable for a particular transition.

Laser transitions between two states, both with $n = 3$ principal quantum number, were chosen for detailed analysis. Electron pumping is assumed to proceed directly from a $n = 2$ ground state of a particular ion through a nondipole transition (slowly decaying) by electron collisions to a $n = 3$ state, followed by lasing through a dipole transition to a lower $n = 3$ state, after which the electron decays more rapidly to the $n = 2$ ground state. (It is not necessary to invoke a seemingly less probable combined ionization-excitation single-step collisional process in the analysis.) Laser transitions from a $n = 4$ upper state (pumped from $n = 2$) to a $n = 3$ lower state would produce shorter wavelength lines. However, the proximity of other $n = 4$ dipole-decaying states limits the maximum electron (and ion) density to too low a value to give reasonable laser lengths. Also, $n = 3$ to $n = 2$ transitions in helium like ions, pumped from the $1s^2$ ground state, were considered; however, the large $1s \rightarrow 3s$ energy gap severely limits the collisional excitation rates (see Eq. (5)) and therefore the available inversion density and the minimum laser length obtainable. (Note that this $3 \rightarrow 2$ laser scheme may prove practical when pumped from above by rapid downward cascading following electron capture.)

Pumping into a $n = 3$ upper laser state that is not dipole-coupled to $n = 2$ levels is one necessary condition for maintaining a large population density, since spontaneous depopulation of this state is limited to the $\Delta n = 0$ laser transition with a relatively low rate. Conversely, the lower laser state population is kept low by a high $n = 3 \rightarrow 2$ dipole depopulation rate. The collisional transition for populating the upper laser state can be monopole; e.g., $2p \rightarrow 3p$ ($2p \rightarrow 3s$ is not followed by $3 \rightarrow 3$ dipole decay). Quadrupole $2s \rightarrow 3d$ excitation is also conceivable. However, in the two instances where this might be particularly important, namely, the lithiumlike and berylliumlike (singlet) ground state ions, an inverted population will not be obtained, since the pumped $3d$ upper laser state has a shorter lifetime than the lower laser state due to a low-lying $2p$ state.

Lasing following monopole $2p \rightarrow 3p$ excitation has been observed in ions belonging to the beryllium (triplet system) through the fluorine isoelectronic sequences.[1] For a particular element (such as oxygen for which data are available), the trend is towards shorter wavelengths (and correspondingly lower gains) for the more highly ionized species (Be-like). Also, pumping by collisional excitation becomes more difficult for the larger $2 \rightarrow 3$ energy gap in the highly stripped ions. It is also desirable to have a large energy separation between the upper lasing state and any nearby states that are dipole-coupled to the ground state, in order to reduce collisional-radiative depopulation; here, the boron- and carbonlike ions are slightly favored.

II. Analysis

While observations of lasing in multiply ionized atoms have been reported,[1] no similar attempt towards analysis of the mechanisms and limitations has been found in the literature. The present three-state analysis for carbon-like ions is intended to serve as a guide and stimulus for a more sophisticated and complete time-dependent numerical analysis (presently underway). Pumping is assumed to take place in a $2p^2\ ^3P \rightarrow 2p3p\ ^3D$ monopole ($\Delta l = 0$) transition, followed by lasing in a $2p3p\ ^3D \rightarrow 2p3s\ ^3P$ dipole transition, with the final state rapidly decaying by a dipole transition to the $2p^2\ ^3P$ ground state. Lasing from a $2p3p\ ^3S$ upper term is also possible. Two-electron radiative-Auger decay to a $2s2p^3$ configuration is expected to have a negligible effect.[7] Along the isoelectronic sequence, data are generally available up to neon.[7-11] Beyond that, wavelengths are scaled[12] as z^{-1}, where z is the charge seen by the active electron ($z - 1$ = ion charge). The oscillator strength for the laser transition is extrapolated according to a $Z^{-1.5}$ empirical best fit (Z is the nuclear charge of the ion), and the associated laser transition probability is deduced[9] from $A \propto f/\lambda^2$. The equilibrium kinetic temperature of the plasma in which the ions are produced is taken as $kT \approx 0.25\chi_{z-2}$, where χ_{z-2} is the ionization potential of the next lower ion state. For estimating the excitation rate, and consequently the inversion density, it is assumed that the monopole excitation rate is approximately equal to a corresponding dipole rate. This assumption is supported by experimental and theoretical results[13] on plasma ions and is further discussed below for the high electron temperature situation. For this, the $2p^2\ ^3P \rightarrow 2p3d\ ^3D$ allowed transition was used and the oscillator strength was extrapolated empirically to unity with higher Z. This oscillator strength, as well as the $n = 2$–3 energy difference ΔE_{23}, are required in the approximation used for calculating the excitation rate in Eq. (5) for $\Delta n \neq 0$ transitions. The energy difference ΔE_{23} was estimated through extrapolation by keeping the ratio $\Delta E/\chi$ constant along the isoelectronic sequence.

In evaluating the collisional mixing rate between the upper laser state and a nearby state that has a short lifetime for dipole decay to the ground state,

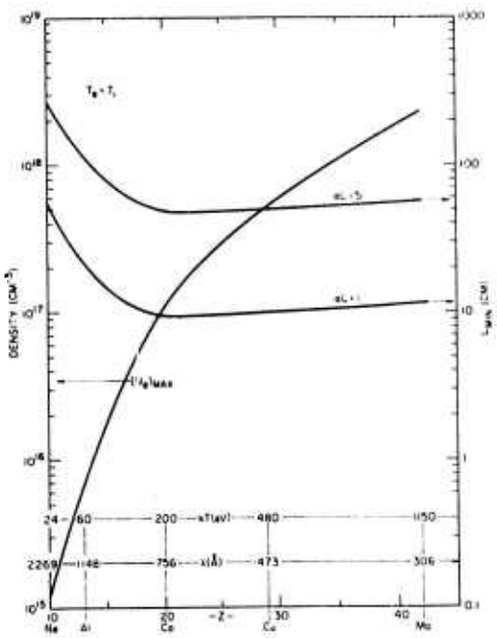

Fig. 1. Minimum length L_{min} for amplification in carbonlike ions with gain $\exp(\alpha L)$ vs atomic number Z, wavelength λ, and temperature, where the electron (kT_e) and ion (kT_i) temperatures are assumed equal. Maximum electron density $(N_e)_{max}$ is also shown.

the lower laser state was chosen, since—for the carbon sequence at least—it was close and thereby had a typical overlap. (In carbonlike ions there are six clustered $n = 3$ states that should be properly considered in a more sophisticated collisional analysis.) The electron collisional mixing rate C_e at an electron temperature T_e and density N_e is best estimated for $\Delta n = 0, l = 1 \rightarrow l = 0$ transitions from twice the line width given by the portion of Eq. (526) of Ref. 14, which pertains to $l \rightarrow l - 1$ transitions:

$$C_e = 6\pi N_e (2\pi/\pi k T_e)^{1/2} (\hbar/mz)^2 n^2 (n^2 - l^2)[l/(2l+1)] \times \ln\{5 - (4.5/z) + \xi^{-1}[(1 + kT_e n^2/\chi_H z(z-1)]^{-1}\}, \quad (2)$$

where $n = 3$, $l = 1$, and where $\xi = (z - 1)\, e^2\, \omega/m v_e^3$ from Eq. (515) of the same reference. Here, χ_H is the ionization potential of hydrogen and ω is the laser angular frequency. The ratio C_e/N_e has been tabulated[15] for $T_e = T_i$.

The ion collisional mixing rate C_i has also been evaluated by Eqs. (517) and (518) of Ref. 14 (with the former multiplied by the square of the ion charge $(z - 1)^2$ for ions heavier than protons):

$$C_i = [4\pi^2/(2l+1)]\,\frac{3}{5}(\hbar n/mz)^2[N_e/(z-1)](z-1)^2 \times (M/kT_i)\left[l(n^2 - l^2)v_e \times \exp\left(-\frac{5}{6}Mv^2/kT_i\right)\right], \quad (3)$$

where

$$v = [6\pi(z-1)e^2\omega kT_i/M^2]^{1/5}. \quad (4)$$

Here, M is the ion mass, T_i the ion temperature, and $N_e/(z - 1)$ is used for the ion density. The parameter C_i/N_e has also been tabulated[15] and is found to range from about five to two orders of magnitude less than C_e/N_e for the neon to molybdenum ions, respectively.

The maximum electron density is determined by setting the collisional mixing rate equal to the spontaneous emission probability A_{33} for the laser transition. Then, $(N_e)_{max} = A_{33}/(C_e N_e)$, for $C_i \ll C_e$. This density upper limit has been tabulated[15] and is plotted in Figs. 1 and 2. The maximum electron densities shown are quite consistent with those available in an expanding and cooling laser-produced plasma.

If the upper and lower laser terms are assumed to be populated by electron collisions from the $n = 2$ ground state (density = N_g) only (see Introduction), final coronal equilibrium values, given in a first approximation by $N_g(C_{23}/A_{32})$, are reached in a characteristic e-folding time of $\sim A_{32}^{-1}$. This time is much shorter for the lower laser level than for the upper, and the lower level reaches a much lower equilibrium concentration more rapidly. The collisional excitation rate C_{23} is calculated with the effective Gaunt factor approximation in the convenient form[16]:

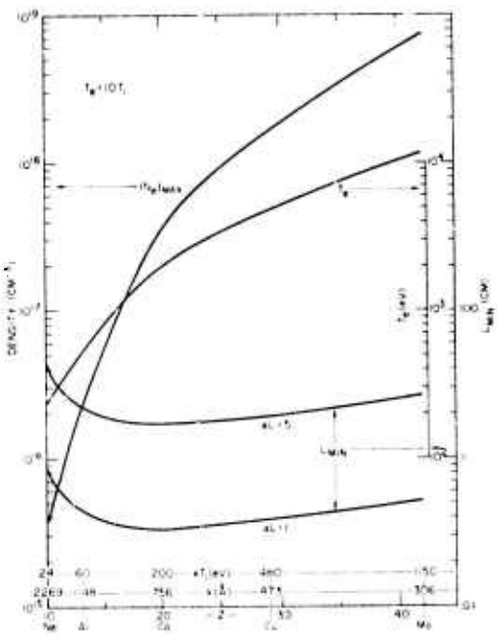

Fig. 2. Minimum length L_{min} for amplification in carbonlike ions with gain $\exp(\alpha L)$ vs atomic number Z, wavelength λ, and ion kinetic temperature kT_i. The electronic kinetic temperature kT_e is assumed equal to $10\,kT_i$ and is plotted. Maximum electron density $(N_e)_{max}$ is also shown.

$$C_{23} = [1.6 \times 10^{-5} f_{23} \bar{g} \exp(-\Delta E_{23}/kT_e)/\Delta E_{23}(kT_e)^{1/2}] \times N_e \text{ sec}^{-1}, \quad (5)$$

for ΔE_{23} and kT_e in eV and where $\bar{g}$ is the average Gaunt factor ($\approx$0.2). By setting $N_g \approx N_e/(z-1)$, the upper laser state density may be calculated and is found[15] to be $\approx 10^{-3} N_g$.

A question remains as to how long an inversion is maintained; i.e., what equilibrium population distribution is reached and in what time interval? At first glance it appears possible that inversion can be sustained for an indefinite period. Clearly, a detailed time-dependent numerical rate equation analysis is needed, including as many effects from other levels (such as cascading) as possible. This refinement is now underway.

III. Results

It is now possible to estimate the minimum length necessary to achieve a particular gain product αL. For Doppler line broadening (Stark broadening is estimated from $0.5C_{ei}$ and found to be negligible), this length is given for large inversion by[6]

$$L = (8\pi\alpha\lambda_{23}^3 A_{23} N_g \lambda_{33}^3)(2\pi kT_i/M)^{1/2}. \quad (6)$$

This is plotted as $L_{\min}$ vs element, temperature, and wavelength in Fig. 1 for $\alpha L = 1$ and 5, and for $T_e = T_i$. The analysis is carried up to molybdenum ($Z = 42$), which is the heaviest element for which high stages of ionization have been reported.[17] It is seen that the parameters involved scale with Z such that $L_{\min}$ is approximately constant for elements heavier than $Z \approx 17$ and never becomes less than 10 cm, which is somewhat long for laser-produced plasmas. However, for neon, the length is consistent with 1-m cavity discharge experiments, since $\alpha I \approx 1.5\%$ is sufficient.

Since it is hoped that the ions may cool in expansion and that subsequently the electrons may be heated preferentially, it is of great interest to observe the effect here. Neglecting the logarithmic term in Eq. (2), C_e/N_e scales as $T_e^{-1/2}$ so that $(N_e)_{\max}$ increases as $T_e^{1/2}$. Also, from Eq. (5), C_{23}/N scales as $(\bar{g}/T_e^{1/2})\exp(-\Delta E_{23}/kT_e)$, as does N_u/N_e. Therefore, $N_u \propto N_e T_e \exp(-\Delta E_{23}/kT_e)$, and $L \propto (T_i/T_e)^{1/2} \exp(\Delta E_{23}/kT_e)$. The advantage in allowing the ions to cool (while N_e decreases to the maximum value allowed) is indicated here, although the dependence upon T_i is much weaker than on T_e, particularly for $kT_e < \Delta E_{23}$. In Fig. 2, the ion temperature is maintained at the equilibrium value assumed above (i.e., $0.25\chi_{z-1}$) and T_e is taken as $10T_i$. The effect is to reduce $L_{\min}$ below unity for threshold gain and as low as 1.7 cm for $\alpha L = 5$. This indicates the dramatic effect of increased pumping at higher electron temperatures. The $L_{\min}$ curves in Fig. 2 are to be shifted downward according to $\propto T_i$ for significant cooling with frozen-in ions. Just which ions will be most useful (i.e., the carbonlike sequence analyzed here or another sequence) will probably be determined by experiments (presently underway[18]).

There are two concerns that warrant further consideration for high electron temperatures. One is the depopulation of the laser states by electron collisions, the net result being a possible increase in gain length over that estimated above. An estimate[16] for ionization from the $n=3$ states indicates that in all cases the rate is much less than the dominant collisional mixing rate C_e used above. A second concern at high electron temperatures involves the assumption, made above, that the nondipole-transition collisional pumping rate is approximately equal to that of a corresponding dipole transition; i.e., for atoms, at least, the cross section for the former decreases more rapidly at high electron energy (high T_e) than does the cross section for dipole transitions. For the present $T_e = T_i$ analysis, $kT_e/\Delta E_{23} < 1$, and for the $T_e/T_i = 10$ analysis, $kT/\Delta E_{23}$ increases from approximately 3 for neon to 5 for molybdenum. From existing experimental and theoretical data[18,19] for multiply-ionized atoms, there is no evidence that the $n=2 \rightarrow 3$ nondipole rates will be significantly less than the corresponding dipole rates for $kT_e/\Delta E_{23}$ up to 5. Furthermore, data exist[20] for $n=3 \rightarrow 3$ transitions with $kT_e/\Delta E_{33}$ varying from 1 to 15, which also shows no significant deterioration in the relative nondipole rates (although the absolute value of the cross section is reduced below that for dipole transitions in this case). Data on relative nondipole excitation rates at high electron temperatures are important, not only to the present analysis, but to other short wavelength ion laser approaches[21] that depend directly on a *weak* monopole excitation rate for the lower laser level at anomalously high electron energies in plasmas.

The required internal pump power density can be found from $N_g C_{23} \Delta E_{23}$, assuming $N_g = N_e/(z-1)$. With a volume determined by the product of the cross-sectional area a and the length L, and assuming a fractional absorption of L/L_{abs} along with a total energy conversion efficiency of η, the axial pumping laser irradiance P/a that is required is given by

$$P/a = N_e C_{23} \Delta E_{23} L_{\text{abs}} \eta/(z-1). \quad (7)$$

Here, L_{abs} is the classical inverse-bremsstrahlung absorption length, given by[4]

$$L_{\text{abs}} = 5 \times 10^{17} T_e^{3/2} N_e \lambda (z-1) \text{ cm} \quad (8)$$

for densities much less than the critical value ($\approx 10^{21}$ cm^{-3} for $\lambda = 1.06$ μm radiation) at the plasma frequency. Here, T_e is in eV, λ is in cm, and N_e is in cm^{-3}. Then,

$$P/a = (2 \times 10^{11})[T_e f \exp(-\Delta E_{23}/kT_e)/(z-1)^2\eta] \text{ W cm}^{-2}, \quad (9)$$

with Eq. (5). Within the present approximations, P/a is therefore independent of density and medium length.

Numerical results indicate, for an estimated total conversion efficiency of 1%, a required irradiance up to approximately 10^{14} W/cm^2 for the ions indicated in the figures, and for $T_e = 10T_i$. This may be obtained with a 0.1-J, 10-psec laser focused to a 100-μm diam. The 1% efficiency estimate is arrived at by assuming 10% for laser heating and 10% for excitation of the particular upper configuration, in competition both with other excitation modes and with ionization (ionization from the $n = 2$ orbit proceeds at a rate[16] comparable to that for excitation to $n = 3$ levels for the enhanced electron temperature case).

IV. Discussion

The experimental scheme proposed above involves the transverse generation and subsequent expansion of a cylindrical plasma and the additional heating and pumping by an axial laser beam. A Maxwellian electron distribution has implicitly been assumed in the analysis. The electron equilibration time scales as $N_e^{-1}T_e^{3/2}$ and reaches the nanosecond range for the high electron temperature cases, which is comparable both to the upper laser state lifetimes and the collisional excitation times. Electron-ion equipartition times are, however, still much longer, so that high T_e/T_i ratios may be maintained. A more sophisticated analysis will either have to account for this relatively slow electron equilibration or depend upon electron heating at higher densities with an associated risk of excessive cooling during the ensuing expansion phase. The latter approach would not require additional pump irradiance, according to the present analysis; however, a complicated dynamic numerical plasma model would be required for analysis. Experiments will undoubtedly be done with various heating times.

V. Summary

The present three-state analysis indicates that it is promising to extrapolate successful near-ultraviolet ion laser transitions into the vacuum-uv region for amplification, by using expanding laser-produced cylindrical plasma as an initial medium that is subsequently pulse-heated axially with available lasers to increase the electron temperature for efficient pumping. The particular ion species that are generated and maintained in a frozen-in state will be identified in experiments. The added effects of other levels, as well as the true time dependence of the gain, will hopefully evolve from a numerical model presently under development. Such modeling of increasing sophistication will require more refined extrapolation methods and more basic data, particularly as it proceeds to higher Z elements.

The author is grateful to H. R. Griem for helpful suggestions towards evaluating the collisional rates involved here. Valuable discussions with his colleague R. A. Andrews are also recalled with appreciation.

References

1. R. S. Pressley, Ed. *Handbook of Lasers*, (Chemical Rubber Co., 1972) p. 242; C. K. Rhodes, IEEE J. Quantum Electron. **QE-10**, 153 (1974); Y. Hashino, Y. Katsuyama, and K. Fukuda, Japan J. Appl. Phys. **11**, 907 (1972); **12**, 470 (1973), for recent low Z ion lasing in a z-pinch discharge.
2. M. Dugnay, Laser Focus 9, 45 (1973); R. A. Andrews, NRL Memo. Rept. 2677 (1973).
3. S. E. Harris, A. H. Kung, and J. F. Young, J. Opt. Soc. Am. **64**, 556 (1974).
4. J. M. Dawson, A. Hertzberg, R. E. Kidder, G. C. Vlases, H. G. Ahlstrom, and L. C. Steinhauer, *IAEA Symposium on Plasma Physics and Controlled Fusion Research, Madison* (IAEA, Vienna, 1971), p. 673.
5. L. C. Steinhauer and H. G. Ahlstrom, Phys. Fluids **14**, 1109 (1971).
6. R. C. Elton, R. W. Waynant, R. A. Andrews, and M. H. Reilly, "X-Ray and Vacuum-UV Lasers: Current Status and Progress," NRL Rept. 7412, (May 2, 1972).
7. R. L. Kelly with L. J. Palumbo, "Atomic and Ionic Emission Lines Below 2000 Å," NRL Rept. 7599 (1973).
8. C. E. Moore, "Atomic Energy Levels" NSRDS-NBS 35 (Dec. 1971); NSRDS-NBS 3 (1965–1971); NBS Circular 488.
9. W. L. Wiese, M. W. Smith, and B. M. Glennon, "Atomic Transition Probabilities, Vol. I Hydrogen through Neon" NSRDS-NBS-4 (May 1966); W. L. Wiese, M. W. Smith and B. M. Miles, "Vol. II, Sodium through Calcium" NSRDS-NBS 22 (October 1969).
10. W. L. Wiese, Appl. Opt. **7**, 2361 (1958).
11. M. W. Smith and W. L. Wiese, Astrophys. J. **23**, 103 (1971).
12. B. Edlen, in *Handbuch der Physik* (Springer Verlag, Berlin, 1964), Vol. 27, p. 80.
13. H.-J. Kunze, Space Sci. Rev. **13**, 565 (1972).
14. H. R. Griem, *Broadening of Spectral Lines by Charged Particles in Plasmas* (Academic Press, New York, 1974).
15. R. C. Elton, NRL Memo. Rept. 2799 (May 1974); Proceedings IV Int. Conf. on Vacuum-Ultraviolet Radiation Physics, Hamburg, 1974.
16. R. C. Elton, in *Methods of Experimental Physics-Plasma Physics*, H. R. Griem and R. H. Lovberg, Eds. (Academic Press, New York, 1970), Vol. 9A.
17. J. J. Turechek and H.-J. Kunze (to be published).
18. T. N. Lee, J. Davis, J. F. Reintjes, R. H. Dixon, R. C. Eckardt, K. Whitney, J. L. DeRosa, R. A. Andrews, and R. C. Elton, Bull. Am. Phys. Soc. **19**, 558 (1974); Proc. VIII IEEE International Quantum Electronics Conf. (1974).
19. H.-J. Kunze and W. D. Johnson, III, Phys. Rev. A **3**, 1384 (1971); W. D. Johnson III and H.-J. Kunze, Phys. Rev. A **4**, 962 (1971).
20. R. U. Datla, H.-J. Kunze, and D. Petrini, Phys. Rev. A **6**, 38 (1972).
21. T. C. Bristow, M. J. Lubin, J. M. Forsyth, E. B. Goldman, and J. M. Sources, Opt. Commun. **5**, 315 (1972).

Two-photon resonantly enhanced self-defocusing in Cs vapor at 1.06 μ *

R. H. Lehmberg, J. Reintjes, and R. C. Eckardt

Naval Research Laboratory, Washington, D. C. 20375
(Received 5 July 1974)

The electronic nonlinear refractive index in Cs vapor at 1.06 μ is shown to be negative and to consist of two distinct contributions. One of these contributions arises from a two-photon resonance in the susceptibility and can be made comparable in magnitude to the positive n_2 in laser glass. The other term arises from population redistributions between the ground and first excited state. We present measurements of self-defocusing of a single pulse from a Nd : YAG mode-locked laser that are in agreement with the theoretical predictions.

The useful output power which can be generated in many pulsed solid state lasers is limited by the occurrence of self-focusing and self-phase-modulation due to the positive nonlinear refractive index n_2 of the amplifying material. It would appear to be possible to raise the useful output power from such lasers by compensating for the self-action effects of the laser amplifier with complementary self-action effects in a material with a negative nonlinear refractive index. Such compensation is anticipated to be effective under conditions where the spatial and temporal distortions of the beam due to the positive n_2 are small.

The negative nonlinear refractive indices which have been observed previously have arisen either from two-level resonance effects which occur in restricted wavelength ranges attainable only by the use of tunable lasers,[1] or from thermal effects[2] which are too slow to be of use in compensating for the self-focusing of pulses in the nanosecond range or shorter. It has recently been noted that Cs vapor should exhibit a negative value of n_2 at the Nd : YAG wavelength.[3] Using Cs, one should therefore be able to investigate compensation of the self-focusing and self-phase-modulation in high-power glass lasers.

In this letter, we study in more detail the negative nonlinear refractive index of Cs at 1.06 μ. We show that it arises from two distinct contributions; i.e., one from a two-photon resonance and the other from population redistributions. Under easily attainable experimental conditions, the magnitude of n_2 can be made comparable to that of laser glass. Because of its resonance behavior, the two-photon term can make the largest contribution to the nonlinearity, making compensation for self-focusing of short pulses feasible. We present measurements of self-defocusing of a single pulse from a Nd : YAG mode-locked laser, and show that the results are in good qualitative and fair quantitative agreement with the theory.

The energy level diagram of Cs is shown in Fig. 1. The nonlinear susceptibility at 1.06 μ is determined primarily by interactions between the $|6s\rangle$ ($\equiv|0\rangle$) and the $|6p\rangle$ ($\equiv|1\rangle$) and $|7s\rangle$ ($\equiv|2\rangle$) levels because of nearby one- and two-photon resonances, respectively. In the slowly varying envelope approximation, it can be shown that the nonlinear refractive index has two distinct contributions:

$$\delta n^{NL} = n - n_0 = \delta n_A + \delta n_B, \tag{1}$$

where n_0 is the linear refractive index.

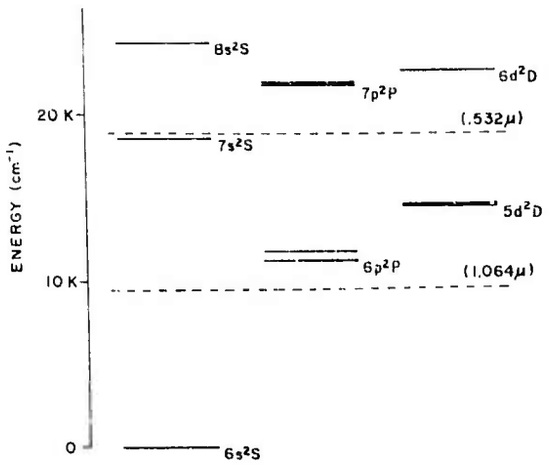

FIG. 1. Energy level diagram of Cs. With reference to the text the $6S$ level is referred to as level $|0\rangle$, the $6P$ levels as $|1\rangle$, and the $7S$ level as $|2\rangle$. The dotted lines show the position of the laser fundamental at 1.06 μ and its two-photon level at 0.532 μ.

The first term is given by

$$\delta n_A \equiv n_2^{02}\langle E^2(t)\rangle = \frac{\pi N \mu_{01}^2 \mu_{12}^2}{\hbar^3(\omega_{20}-2\omega)(\omega_{10}-\omega)}\left(\frac{1}{\omega_{10}-\omega}+\frac{1}{\omega-\omega_{21}}\right)\langle E^2(t)\rangle, \tag{2}$$

where $E(t)$ is the optical field of frequency $\omega = 2\pi c/\lambda$, N is the atomic density, μ_{ij} are the atomic dipole matrix elements between levels $|i\rangle$ and $|j\rangle$, and ω_{ij} is the atomic frequency splitting between $|i\rangle$ and $|j\rangle$. The $\langle\rangle$ denotes an average over an optical cycle. In the case of 1.06-μ radiation in Cs, $\omega_{10}-\omega$, $|\omega_{20}-2\omega| \ll \omega$, and we are justified in ignoring antiresonant contributions to the above expression. In deriving this result, we have also assumed that the atomic and laser linewidths are small compared to the detuning frequencies $\omega_{10}-\omega$ and $|\omega_{20}-2\omega|$.

Expression (2) arises from a two-photon interaction between the $|6s\rangle$ and $|7s\rangle$ levels. In solids such terms are usually positive and are generally accepted as being responsible for the self-focusing observed in materials sueh as laser glass.[4] For 1.06-μ radiation in Cs vapor, however, $\omega_{20}-2\omega<0$, while both $\omega_{10}-\omega$ and $\omega-\omega_{21}>0$; hence, $n_2^{02}<0$, and one obtains self-defocusing and negative frequency chirping for laser pulses. The effect is resonantly enhanced by the two-photon denominator ($\omega_{20}-2\omega \approx -260$ cm^{-1}), and n_2^{02} can be comparabte in magnitude to the n_2 of laser glass at modest vapor densities ($N\sim 10^{17}$ cm^{-3}).

The second contribution to δn^{NL} arises from intensity-dependent population redistribuitions between the $|6s\rangle$ and $|6p\rangle$ levels, and is given by

$$\delta n_B = -\frac{\pi N}{\hbar}\left(\frac{2\mu_{01}^2}{\omega_{10}-\omega}+\frac{\mu_{12}^2}{\omega-\omega_{21}}\right)\frac{\mu_{01}^2}{2\hbar^2}\times\left[\int_{-\infty}^{t}\exp\left(\frac{-(t-t')}{T_1}\right)\mathcal{E}^*(t')\times\int_{-\infty}^{t'}dt''\exp[i(\omega_{10}-\omega+i/\tau)(t'-t'')]\mathcal{E}(t'')+\text{c.c.}\right], \tag{3}$$

where $\mathcal{E}$ is the complex amplitude of the optical field defined by $E(t)=\frac{1}{2}\mathcal{E}(t)\exp(i\omega t)+\text{c.c.}$, T_1 is the lifetime of the $|6p\rangle$ level, and τ is the atomic dephasing time. The actual form of δn_B depends on the magnitude of the laser pulse duration t_p relative to τ and T_1. For short pulse durations $t_p \ll \tau,\ T_1$,

$$\delta n_B = n_2^{01}\langle E^2(t)\rangle = -\frac{\pi N}{\hbar^3(\omega_{10}-\omega)^2}\left(\frac{2\mu_{01}^4}{\omega_{10}-\omega}+\frac{\mu_{01}^2\mu_{12}^2}{\omega-\omega_{21}}\right)\langle E^2(t)\rangle, \tag{4}$$

This term is analogous to the expression derived by Grischowsky in the adiabatic following approximation of the two-level system.[1] It has the same form of intensity dependence as δn_A, and is also negative, since $\omega_{10}-\omega$, $\omega-\omega_{21}>0$.

When $\tau \ll t_p \ll T_1$, Eq. (3) reduces to

$$\delta n_B = 2\tau^{-1} n_2^{01}\int_{-\infty}^{t} dt'\,\langle E^2(t')\rangle, \tag{5}$$

where n_2^{01} is defined in Eq. (4). The term leads to a form of thermal self-defocusing.

In order to verify these results, we studied the self-defocusing of radiation from a mode-locked Nd:YAG laser in a cell of Cs vapor. The input beam consisted of a single pulse with a duration of 30 psec and an energy which was varied between 0.2 and 8 mJ. The beam had a spatial profile in the form of a collimated Airy disk with a diameter $D_0 = 3.5$ mm between minima. The Cs cell was 1 m long with an atomic density of 0.5×10^{17} cm^{-3}. The temperature of the Cs reservoir was maintained at 330 °C while the temperature of the cell was held at 600 °C in order to reduce linear absorption from Cs dimers. The output beam profile was measured by imaging the beam emerging from the vapor cell onto an image converter camera with a minimum resolution of 6 lp/mm. The change in beam size was observed as the input energy was varied over a factor of 40.

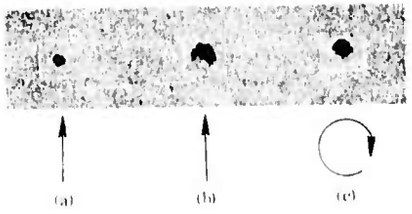

FIG. 2. Photographs of the output beam profile after propagating through a 1-m cell of Cs vapor. (a) Input beam linearly polarized at 0.2 mJ (2.8×10^8 W/cm^2). (b) input beam linearly polarized at 8 mJ (1.1×10^{10} W/cm^2). (c) input beam nearly circularly polarized at 8 mJ (1.1×10^{10} W/cm^2).

Figure 2 shows typical results from three different measurements. In part (a), the output beam is shown for a low-power (0.2-mJ) linearly polarized input beam, with the cell filled with Cs. The beam diameter here is essentially the same as that which was observed without Cs in the cell. Part (b) shows the results of the same measurement when the input beam power is increased by a factor of 40 to about 8 mJ ($I_{in} = 1.1 \times 10^{10}$ W/cm^2). The beam diameter has increased by a factor of about 5 over that observed in part (a). Measurements at intermediate intensities showed that the output beam diameter increased monotonically with increasing input power, indicating that the change in beam size is actually due to self-defocusing, rather than self-focusing. Part (c) shows the result obtained when nearly circularly polarized light was used instead of linearly polarized light. With the same input energy of 8 mJ, the increase in beam diameter is only a factor of 3.7.

We can estimate the expected change in beam size using the paraxial ray approximation[2] and the expressions for n_2 given earlier. If we approximate the Airy profile of the input beam by a Gaussian profile with a 1/e diameter of the intensity distribution equal to d_0 $= \frac{1}{2}D_0$, the ratio of output to input beam diameters is given by

$$\frac{D_{out}}{D_0} \approx \frac{d_{out}}{d_0} = \left[1 + \frac{P_0}{P_c}\left(\frac{4l}{kd_0^2}\right)^2\right]^{1/2}, \tag{6}$$

where P_0 is the input power, l is the cell length, $k = 2\pi/\lambda$, and $P_c = \lambda^2 c/32\pi^2 n_2$.

For the experiments described above, the high-level input power is 270 MW. For a Cs density of 0.5×10^{17} cm^{-3}, we find that $n_2^{(2)} = -0.9 \times 10^{-13}$ esu from Eq. (2) and $n_2^{(1)} = -0.25 \times 10^{-14}$ esu from Eq. (4). Under these experimental conditions, the atomic dephasing time is 40 psec, so Eq. (4) is not precisely valid for calculating $n_2^{(1)}$; however, it can be used to give a lower estimate of its magnitude. The nonlinear index then results mainly from the two-photon resonance term, and its response is expected to be instantaneous on the time scale of the laser pulse. We expect the largest effect for linearly polarized light, since both the δn_A and δn_B terms contribute to the nonlinear index, and both are negative. In this case, the expected increase in beam size given by Eq. (6) is a factor of 4.4, in fair agreement with the observed increase of a factor of 5.

If circular polarization is used, the defocusing is expected to be smaller, since in this case the two-photon resonance term does not contribute. The theory predicts an increase in beam size by a factor of 2. The increase in beam size in Fig. 2(c) is observed to be smaller than that in Fig. 2(b) in qualitative agreement with the theory, although the observed difference is not as large as predicted. The discrepancy could be due to the use of Eq. (4) in predicting the value of δn_B, rather than the more exact expression in Eq. (3). It could also result from a deviation of the input beam from true circular polarization, possibly caused by birefringence in the sapphire cell windows. The observations are, however, in qualitative agreement with the theory.

We have shown that the electronic nonlinear refractive index in Cs vapor has two distinct contributions. One contribution arises from a two-photon resonance and the other from population changes between the ground and first excited state. For radiation at 1.06 μ, both terms are negative and can be made comparable in magnitude to the n_2 of laser glass at modest vapor densities. We have observed self-defocusing in Cs vapor of a single pulse from a Nd:YAG mode-locked laser under conditions in which the two-photon resonance term makes the major contribution to the nonlinear index. The increase in beam size for linear polarization is in reasonable agreement with the theory. The increase in size of a nearly circularly polarized beam is in good qualitative agreement and fair quantitative agreement. A more complete study of the interaction of these two effects will be published elsewhere.

The authors would like to acknowledge many useful discussions with O. Barr, J. McMahon, and P. Rey, as well as the technical assistance of J. DeRosa.

[1]This work was supported jointly by the Defense Advanced Research Projects Agency (DARPA Order No. 2694) and the U.S. Atomic Energy Commission [Contract No. AT(04-3)-878].

[2]D. Grischkowsky and J. A. Armstrong, Phys. Rev. A **6**, 1566 (1972).

[3]S. A. Akhmanov, R. V. Khokhlov, and A. P. Sukhorukov, in *Laser Handbook*, *Vol.* 2, edited by F. T. Arecchi and E. O. Schulz-Dubois (North-Holland, Amsterdam, 1972).

[4]R. B. Miles and S. E. Harris, IEEE J. Quantum Electron. **QE-9**, 470 (1973).

[5]J. T. Fournier and E. Snitzer, IEEE J. Quantum Electron. **QE-10**, 473 (1974).

REPRINTED FROM 1974 "IEDM TECHNICAL DIGEST"

A MULTIPLE PULSE LASER SYSTEM WITH SYNCHRONIZED MODE-LOCKED AND Q-SWITCHED OUTPUTS

J. Reintjes, R. C. Eckardt, and J. L. DeRosa

Naval Research Laboratory

Washington, D.C. 20375

ABSTRACT

The development of a pulsed laser system which generates multiple synchronized output pulses on both a picosecond and nanosecond time scales is described. The system consists of a mode-locked Nd:YAG oscillator-amplifier syatem and a Q-switched Nd:YAG and Nd:Glass system synchronized by a versatile switching technique. The unique features of this laser include the synchronization of two 200 mJ 30 psec pulses with separation variable between 0 and 10 nsec with a shuttered portion of a Q-switched pulse variable in lergth from .5 to 30 nsec and with energy in the range of 1 to 10 J.

We describe a laser system which has been developed to meet the needs of some experiments in plasma generation and x-ray spectroscopy being carried out at NRL. This laser system produces multiple synchronized output pulses on both a nanosecond and picosecond time scale simultaneously. Although it waa designed primarily for the performance of laser-plasma interaction studies involving controlled prepulsing of laser produced plasmas, it is a versatile research tool which can find use in other types of nonlinear optical experiments where pulses on vastly different time scales are needed.

A schematic of the laser aystem is shown in Fig. 1. The picosecond pulaes are generated in a mode-locked Nd:YAG laser that produces two 200 mJ pulsea of 30 psec duration with a time delay between them variable between 0 and 10 nsec. The nanosecond pulse ia generated in a Q-switched laser and is variable in duration between about 0.5 nsec and 30 nsec. with energy in the 1 to 10 J range. The two lasers are synchronized with a versatile switching technique which overcomes the jitter inherent in the generation of either of the pulses separately and can provide jitter times in the aubnanosecond range.

The mode-locked laaer consists of a Nd:YAG oscillator, a Pockel's cell shutter, five Nd:YAG amplifiers, beam expansion optics, beam-splitter, and an optical delay track. The Pockels cell shutter transmits a aingle pulse from the train of mode-locked pulses generated in the oscillator. The pulse is amplified in the first three amplifiers and then split into two components. Each of the two resulting pulses paases through its own fourth amplifier. One pulse transverses a variable optical delay track. Beam expansion optics are required so the pulses will just fill each of the two final two amplifiers of ½ inch diameter.

Performance of the mode locked system at various stages is summarized in Table I. The oscillator is mode locked by a flowing dye cell contacted with the output mirror. It produces a train of about 15 pulses with a peak energy of .25 mJ. An aperture is used for transverse mode control and the spatial profile was measured to follow a Gaussian profile out to the 10% intensity points.

Considerable care was exercised in design of the amplifier chain to the advantage of the full cross section of the final stages while avoiding distortion due to self focusing and self-phase modulation. The amplifiers are pumped with four linear xenon lamps in a clover leaf reflector which provide a uniform gain profile across the whole rod. Beam processing optics are used between the first and second amplifier to convert the beam profile to an elliptical Airy disc which matches the projection of the Brewster angle rods.

The third amplifier is used to aperture the Airy Fraunhofer pattern at the first minima so no self focusing due to edge diffraction occurs. At the output levels recorded in Table 1, 40% of the energy stored in the ½" rods is extracted and the beam shows no evidence of small scale self focusing. At higher output energies, however, gross beam self focusing begins to appear. The output pulses were analyzed temporally with a 5 psec streak camera, (Fig. 2) and spatially by measuring the far field pattern (Fig. 3). The streak camera recording shows a pulse of approximately 30 psec duration with no temporal substructure, indicating the absence of severe self phase modulation. The spatial profile shows that the beam can be focused to nearly its diffraction limited spot size. Using a 30 cm f/30 lena, the beam at the target is about 30 X 60μ in diameter with an intensity of 5×10^{14} W/cm^2.

The O-switched laser consists of a Nd:YAG oscillator followed by a Pockels cell shutter and three Nd:Glass amplifiers. The oscillator is formed by a 10 m radius 100% mirror and a 3-sapphire-flat resonant reflector coupler. It is O-switched with a Pockels cell and produces a single longitudinal mode pulse 30 nsec in duration with an energy of 20 mJ. The Pockels cell shutter gates out a variable duration section of this pulse for amplification to a level between 1 and 10 J, depending on the duration of the gated pulse. Transverse mode control is obtained with an intracavity aperture. Nd:YAG is used in the oscillator to improve the longitudinal mode structure, while Nd:glass is necessary in the amplifiers to provide the required energy for the amplified pulse.

The synchronization of the two lasers is accomplished according to the scheme shown in Fig. 4. The major problems in synchronizing two independent lasers is the jitter in buildup of the pulses in each laser cavity. The technique used here overcomes this problem by timing each step in the switching sequence from the appearance of an optical signal, rather than an electrical one. Spark gaps are used for switching because of their fast risetimes, short delays and low jitter.

The operating characteristics of each of the lasers were adjusted to make them compatible with the synchronizing process. The mode locked pulse train has about 8 pulses between the 50% and 100% points of the train. This duration is sufficient to insure overlap on every shot with the Q-switched pulse which has a build up time of 125 $\pm$ 25 nsec. The Q-switched pulse has a duration of about 30 ns, which insures that a mode locked pulse can be reliably selected near its peak, allowing for the jitter of 6-7 ns in the mode locked pulse selector.

The synchronization process starts with the appearance of the mode-locked pulse train with a jitter of about $\pm$ 10 nsec relative to the flash lamp pulse. A PIN silicon photodiode is used to detect the pulse train and trigger an electronically switched spark gap that removes the voltage from the Pockels cell Q-switch in the second laser. The Pockels cell is switched on an early pulse in the mode-locked pulse train to allow for the 35 nsec delay of the spark gap and build up time of the Q-switched oscillation. The peak of the Q-switched pulse is synchronized to the peak of the mode-locked train with a jitter of $\pm$ 25 nsec (Fig. 5). A laser triggered spark gap is then switched on the leading edge of the Q-switched pulse and a voltage pulse is applied to another Pockels cell which switches out a single pulse from the mode-locked train (Fig. 6). The jitter in timing of the selected pulse is limited by the 6-7 nsec pulse spacing in the train. The selected mode-locked pulse is then used to shutter out a portion of the Q-switched pulse near its peak (Fig. 7). This last switching event can be accomplished by using a greatly overdriven spark gap, which can provide ultimate synchronization accuracy in the subnanosecond range.

TABLE 1

MEASURED PARAMETERS OF PICOSECOND LASER SYSTEM

STAGE	PULSE ENERGY (mJ)	PULSE DURATION (PSEC)	POWER (W)	BEAM PROFILE	INTENSITY (W/CM^2)	AMPLIFIER GAIN
OSCILLATOR	.20	25	8×10^6	1 mm (Circular Gausaian)	10^9	
AMPLIFIER 1st STAGE	4.8	25	1.9×10^8	2 mm	6×10^9	30 (30)
2nd STAGE	13.2	25	5×10^8	.6 X .3 CM (ELLIPTICAL AIRY DISC)	3.5×10^9	10.6 (12)
3rd STAGE	114.0	30	4×10^9	5 X .9 CM	1.1×10^{10}	9.4 (12)
4th STAGE	210	30	7×10^9	.5 X 1.2 CM	1.25×10^{10}	4.1 (7)
TARGET	190	30	6.3×10^9	30 μ X 60 μ	5×10^{14}	

NOTE: The parameters of the picosecond laser system are tabulated at various stages. Large signal gain under actual operating conditions is given in the last column with small signal gain in parentheses. Total gain is reduced from the product of individual gains by power loss at the apertures and reflections.

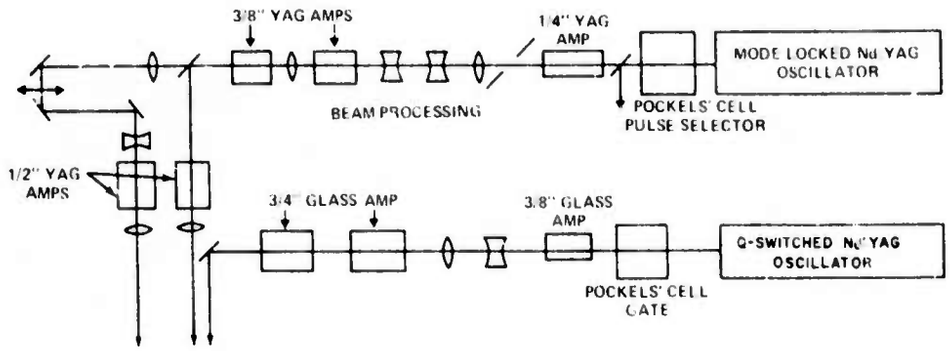

Fig. 1. Schematic diagram of coupled mode-locked and Q-switched laser system.

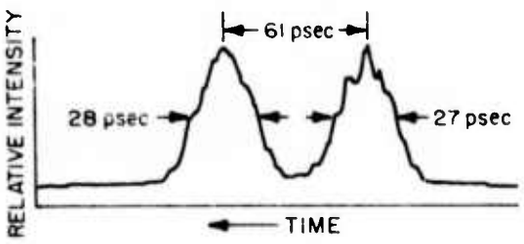

Fig. 2. Densitometer trace of fast streak camera record of two reflections of the same amplified mode-locked pulse.

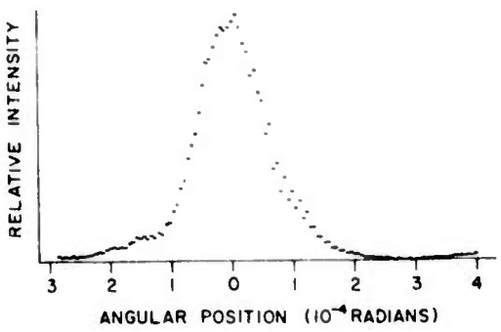

Fig. 3. Spatial intensity profile of a single amplified mode-locked pulse recorded at the focus of a 4 m, $f/400$ lens.

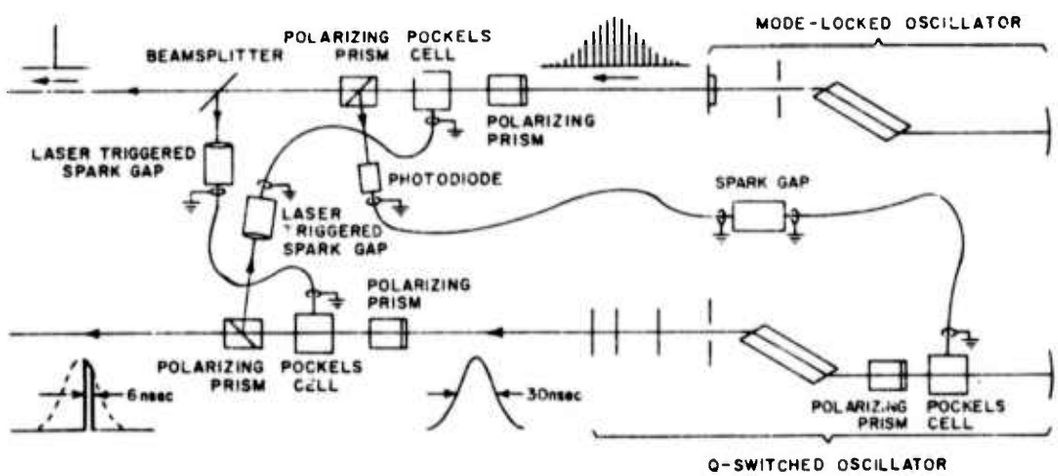

Fig. 4. Synchronization scheme of pulsed laser oscillators.

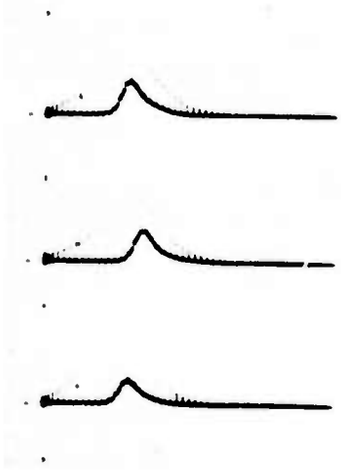

Fig. 5. Oscillograms displaying both synchronized mode-locked pulse train and Q-switched laaer pulse. Both laser beams were incident on the aame photodiode. Sweep duration is 300 nsec. Three successive oscillograms indicate reproducability.

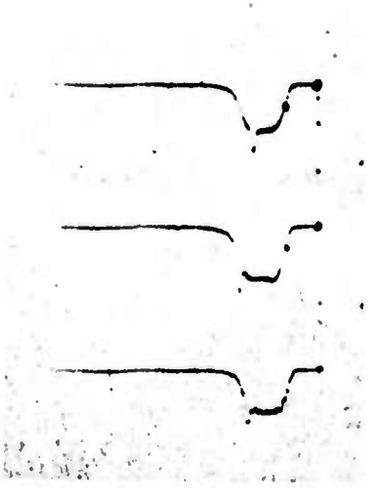

Fig. 7. Oscillograms of synchronized switched out mode-locked pulse and 6 nsec shuttered portion of Q-switched pulse. Both pulsea were incident on the same photodiode. Sweep durstion is 30 nsec. Successive oscillograms are shown.

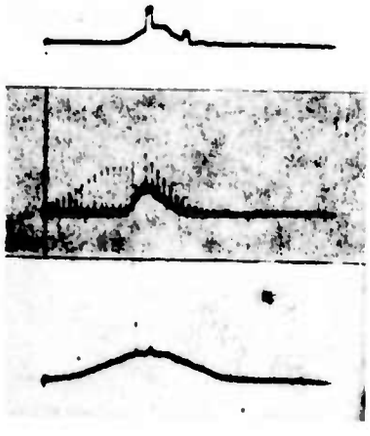

Fig. 6. Oscillograms showing synchronization of aelected mode-locked pulse and Q-switched pulse. (a) Q-switched pulse snd electrical pulse from laser triggered spark gap. Some cable reflection is present in the combined signals. (b) Q-switched pulse and rejected pulae train. (c) Q-switched laser pulse and selected mode-locked pulse. Sweep durations are 300 nsec for (a) and (b) and 120 nsec for (c).

THREE QUASI-CW APPROACHES TO SHORT WAVELENGTH LASERS*†

by

R. C. Elton
Naval Research Laboratory
Washington, D. C. 20375

ABSTRACT

Three approaches towards achieving extended-period quasi-cw amplification by stimulated emission in the vacuum-UV and x-ray spectral regions are discussed, in a somewhat logical progression towards shorter wavelengths, increased complexity, and demands. Extrapolation of visible and near-UV tuned-cavity cw lasers using higher density plasma media is first discussed for the near-to-mid VUV region. Further extension to the soft x-ray region is described, using preferential resonance charge transfer pumping. This and related intense incoherent x-ray source development could ultimately lead to successful quasi-cw Kα inversions, as is discussed. Experiments underway to test the first two schemes are described.

I. INTRODUCTION

The basic problems that hamper a rapid extension of lasers into the vacuum ultraviolet (VUV) and x-ray spectral regions can be summarized with a few simple relations. Since high reflectance cavities do not appear to be realistic for wavelengths shorter than $\sim$ 1000 Å, significant gain must be achieved in a single pass; this immediately implies an increase by orders-of-magnitude in the inverted state density required for a given net gain at a particular wavelength. Hence, at truly short wavelengths we are usually speaking of amplified spontaneous emission (ASE) devices, which alone represent more of an amplifier than a tuned oscillator producing highly coherent radiation. In fact, the devices developed will probably prove most useful, at least for the near term, as amplifiers for coherent VUV radiation produced by frequency multiplication from the IR and visible regions.

---

*Presented at Orbis Scientiae II, Center for Theoretical Studies, University of Miami, January 20, 1975 (Proceedings to be published).

†Supported in part by the Defense Advanced Research Projects Agency, DARPA Order 2694.

For an amplifying medium of length L, the ASE gain is given by $I/I_o = \exp(\alpha L)$, where α is the gain coefficient. The product αL is often written as[1]

$$\alpha L = \frac{\lambda^2 A_{u\ell}}{4\pi^2 \Delta\nu} L \left(N_u - \frac{g_u}{g_\ell} N_\ell \right) , \qquad (1)$$

where g_u, g_ℓ and N_u, N_ℓ refer to the statistical weights and population densities of the upper and lower laser states, respectively, $\Delta\nu$ refers to the line width in frequency units, and λ refers to the wavelength of the laser transition. With the transition probability $A_{u\ell}$ for spontaneous emission scaling as $f\lambda^{-2}$, and for larger inversion (i.e., $N_u \gg N_\ell$), Eq. (1) can be written as a proportionality:

$$\alpha L \propto f N_u L/\Delta\nu, \qquad (2)$$

with the oscillator strength f fairly constant along an isoelectronic sequence. This demonstrates the need for narrow lines and a large product $N_u L$. In plasma media where short wavelengths occur in ionized species, $\Delta\nu$ is often dominated by Dopper or collision broadening[2] (see Fig. 1). The lack of a wavelength-dependent factor in Eq. (2) is somewhat deceiving, since a large N_u is difficult to achieve against radiative depopulation rates scaling as λ^{-2}.

Trade-offs are possible in raising $N_u L$. For example, with electron collisional pumping in a plasma N_u scales as electron density N_e squared, so that a high density plasma of necessarily short length (for pumping) is appropriate for the shortest wavelengths. For increased density, N_u scales more as N_e due to increased collisional effects, and longer lengths can be more appropriate. At very high densities, a longitudinal-pump absorption length can decrease rapidly and $N_u L$ may actually decrease with increasing density, unless transverse pumping is employed. (These scaling laws are expanded for the $3p \rightarrow 3s$ scheme below.) This illustrates the obvious need for careful modeling for any particular scheme, since many parameters enter. Before proceeding to the pump power requirements, it is worth noting that the presence of outer electrons, e.g., in innershell laser transition schemes, decreases the net gain α_T through photoionization losses (α_{pi}) to the main beam, i.e., $\alpha_T \approx \alpha - \alpha_{pi}$. This is discussed further below for the Kα innershell scheme.

A second general concern is the pump power per unti area P/a required. This can be expressed as:

$$P/a = N_u L h\nu(\Gamma + A) \propto \alpha L \nu^4 \left(1 + \frac{\Gamma}{A}\right)\left(\frac{\Delta\nu}{\nu}\right), \qquad (3)$$

using Eq. (1). Here ν is the laser frequency and Γ is the Auger rate, which enters for innershell transitions. For low Z and for metastable laser transitions, Γ can be much greater than A which increases the pump requirements. Since the presence of excess outer electrons also decreases the net gain as discussed above, there are clear advantages to using transitions that avoid these problems when possible, e.g., with hydrogenic and helium-like ions (as well as alkalis for certain longer-λ transitions). Since the same $N_u L$ product occurs in Eq. (3), similar scaling examples to that above for αL may be applied. It is worth noting from Eq. (3) that the ratio $(P/a)/\alpha L$, i.e., pump power density per gain product, scales as ν^4 ($\Delta\nu/\nu \doteq \Delta\lambda/\lambda$ being approximately constant -- see Fig. 1); thus an advance from 1 μm to 10 Å in wavelength translates to a factor of 10^{12} in pump power density at a particular gain product. With limited power, the need for a small pump area a is obvious.

The third general problem that must be considered is the lifetime of the inversion. Any transition can be inverted for a pre-equilibrium interval limited approximately by A^{-1}, at which time lasing is "self-terminating". This time is in the nanosecond (10^{-9} sec) range for wavelengths in the 1000 Å region, but becomes femtoseconds (10^{-15} sec) for typical 1-2 Å dipole transitions. Longer-lived metastable states with lower f-values and transition probabilities require higher $N_u L$ products for equivalent gain and comparable pumping flux, according to Eqs. (2) and (3); the higher densities can then lead to rapid collisional destruction of inverted metastable-state populations so that the advantage is lost. A sustained (cw or quasi-cw) inversion* is the most desireable mode of operation at short wavelengths and is achieved in principle when the final laser level is depleted at a more rapid rate than it is filled; this is particularly difficult for resonance transitions. Three possible quasi-cw approaches will be considered in the following.

II. SELECTED QUASI-CW APPROACHES

A. 3p → 3s

Numerous visible and near-UV lines from 3p → 3s transitions have been reported to lase, including some in plasmas of moderate density

---

*The cw-mode or stationary-inversion terminologies designate a sustained population inversion, in contrast to the self-terminating mode. Quasi-cw or quasi-stationary inversion implies that the inversion is limited in time by the environment or by the pumping pulse available, not by the basic atomic rates. The degree of inversion is distinct from its mere existence and a high value may have an additional transient dependence associated, e.g., with high initial electron temperatures in electron collisional pumping as discussed herein.

(using cavities).[3-5] While the appropriate mechanisms for producing inversion are the subject of continuing discussions, we have used a single-ion excitation model shown schematically in Fig. 2 for carbon-like ions. Electron collisional pumping $2p \rightarrow 3p$ is followed by $3p \rightarrow 3s$ lasing, with the final 3s level more rapidly depopulated by radiative dipole decay to the 2p ground state, thereby maintaining the inversion. At the densities anticipated, collisional mixing and depopulation of $n = 3$ states must be included. An initial analysis for carbon-like ions extrapolated to Z as high as 42 has been published[6] and the resulting gain lengths are consistent with near-UV O^{2+} observations. Results of this initial analysis indicated a significant advantage for ASE in having a high electron temperature T_e for collisional pumping and a low ion temperature T_i for narrow lines. The resulting minimum lengths for αL products of 1 (threshold) and 5 (desired) and for $T_e = 10\ T_i$ are shown in Fig. 3 versus nuclear charge Z for the carbon-like isoelectronic sequence. Also indicated are the electron densities $(N_e)_{max}$ at which collisional depopulation becomes equal to radiative decay for the $3p \rightarrow 3s$ laser transition; at higher N_e the gain dependence becomes weaker as discussed below.

More recently, a "hot-spot" atmospheric plasma model[7] has been applied to this problem.[8] In this numerical model, energy is deposited in a short burst and the electrons are assumed to be heated (by inverse bremsstrahlung only) in times much shorter than the electron-ion energy equipartition time. Peak T_e/T_i ratios of 60 are predicted and, with the necessary atomic physics included, higher gains are found for OIII (O^{2+}) as plotted in Fig. 4 for the three densities chosen so far. The practical and desirable duration of such an enhanced electron temperature and associated gain depends both upon the rate of depletion of lasing ions through ionization as well as the rate of electron cooling through collisions. The gain is also affected by any rapid plasma expansion. A refined program to properly include these effects for the particular experiment underway is now being assembled. It is of importance to emphasize such modeling at this stage to ascertain whether the high gains predicted so far (Figs. 3 and 4) and associated with the enhanced electron temperature are indeed sustained for times significantly longer than A^{-1}, i.e., with a definite advantage of quasi-cw operation over self-terminating laser transitions.

The gain dependence (shown in Fig. 4) can be understood and extrapolated quite simply as follows, assuming $N_u = N_3 = N_2(N_e X_{23}/A_{33})$, where X_{23} is the collisional excitation rate coefficient from level 2 to 3. At low N_e ($< 10^{15}$ cm^{-3} for O^{2+}) and fixed length,

$$\alpha \propto N_2 \left(\frac{N_e X_{23}}{A_{33}} \right) A_{33} \propto N_e^2 X_{23} , \qquad (4)$$

giving the N_e^2 dependence shown. For moderate densities ($\sim 10^{16}$ cm^{-3}),

$$\alpha \propto N_2\left(\frac{N_e X_{23}}{N_e D_{33}}\right) A_{33} \propto N_e A_{33} \ , \tag{5}$$

and the density dependence becomes linear. Here D_{33} is the collisional deexcitation rate coefficient. For high densities, consider the particular case of axial laser heating of a preformed plasma. At densities $\gtrsim 10^{18}$ cm^{-3}, the axial pumping classical absorption length L_{abs} becomes comparable to the laser-medium length and scales as N_e^{-2} according to

$$L_{abs} \propto T_e^{3/2}/N_e^2\lambda^2 \ , \tag{6}$$

for a fixed ion charge. The gain product αL then becomes

$$\alpha L_{abs} \propto N_e^{-1}\left[A_{33}\left(\frac{X_{23}}{D_{33}}\right)\left(\frac{T_e^{3/2}}{\lambda^2 z}\right)\right] \tag{7}$$

and decreases as N_e^{-1}. Finally, at extremely high densities ($\sim 10^{21}$ cm^{-3}) $N_e D_{32}$ becomes comparable to A_{32} (the lower laser depopulation spontaneous decay rate), collisions dominate, and equilibrium distributions evolve with no inversion. This is all done for O^{2+} at present, and is being extended to other ions.

In any case, the outlook is most encouraging for reaching the mid-vacuum-UV region by extrapolation of known laser transitions. Except at the very highest densities, $L < L_{abs}$ and the pump power required scales independently of L or N_e, with about $2X10^{14}$ W/cm^2 a reasonable requirement.[6] Experiments are presently underway at NRL using short pulsed (25 ps) lasers of high quality to deliver a large P/a pumping flux axially to a preformed linear plasma as indicated in Fig. 5 and discussed elsewhere in these proceedings by R. A. Andrews. The first goal of these experiments (following initial plasma characterization) will be to verify the existence of population inversion by relative line intensity measurements; and then to proceed with orthogonal measurements to demonstrate net axial gain.

B. Resonance Charge Transfer Pumping

Detailed extrapolations analogous to the 3p → 3s scheme described above have not been carried out for transitions of higher energy, such as 4→3 or 3→2. A preliminary analysis has indicated that for the former, collisional mixing of the n = 4 terms will deplete the inversion at too low a density to be practical for significant amplification. The second possibility requires helium-like or hydrogenic ions without n = 2 electrons.

With collisional excitation from the low-lying 1s level, the large 1s-3s energy gap makes pumping by free electron collisions in a plasma prohibitively difficult, according to the model employed above. What is required is a less demanding (energy-wise) mechanism for preferential population of n = 3 levels, and particularly the 3s level which could cw-lase into 2p, in turn more rapidly depopulating to 1s. Cascading from higher levels following capture of a free electron in a recombination transition is one possibility considered. However, electron capture by low-energy resonance charge transfer has by far the largest cross section, providing the proper combination of ion and atom can be found. The scheme is illustrated schematically in Fig. 6 for certain transitions to be described below. Vinogradov and Sobelman[10] originally suggested this mechanism for populating higher states of highly ionized neon in collisions with helium atoms, and pointed out that the peak cross section is approximated by $\pi a_o^2 z^2$, where z is again the charge of the ion. When this $\sim 10^{-16} z^2$ is compared to a total radiative recombination cross section[11] of about $10^{-20} z$; the advantage of the resonance effect is obvious.

The resonance referred to here is at very low energies (measured in eV instead of 10's of keV for the higher energy resonance) and is described conveniently by the Landau-Zener formulism[12], worked out for s-s transitions. This theory requires a classical potential energy curve crossing between the initial and final states of the system, and therefore requires exothermic reactions, with an energy defect ΔE. In Fig. 6 are plotted the resonance charge transfer cross sections[12] versus relative particle energy for various values of ΔE in eV, with smaller but finite defects obviously favored. In the present analysis, we have chosen H, He, and Ne as the atomic species, with the intention that they provide a gaseous atomic environment into which plasma ions can rapidly expand, from a laser produced plasma for example. Hydrogen and helium provide low-lying 1s electrons, for which the theory is intended; neon provides six 2p electrons which would be a useful test for p-p or p-s exchange transitions. The velocity required in utilizing Fig. 7 (and indicated there) is assumed thermal, with kT taken as one-fourth the ionization energy required to produce the ion desired. For initial ions, both completely stripped and hydrogenic ions are considered, since no n = 2 electrons are permitted for the 3-2 laser transition. The data for n+ ion stages of both classes is sufficiently independent of element to be combined for present purposes.

By inverting the data in Fig. 7 for each species, we obtain the cross section as a function of ΔE shown in Fig. 8. A survey of possible transitions between the indicated ions and atoms shows the quantum states into which charge transfer is likely to occur at a high rate. For the 3s-2p transition, hydrogenic initial ions are most promising, since the resulting 3s helium-like ion level will not be as strongly coupled to 3p by collisions. Here B^{4+} + H and C^{5} + He are both promising; for the former, hydrogen atoms do not have to be produced from gaseous molecules, as the cross section is of similar magnitude for both the atomic and molecular states.

Further parameters for some of the possible transitions are included in Table 1, where transitions to the ground state are intentionally omitted since inversion of such seem most unlikely possibilities, at least at present.[10] In this table are given the laser wavelengths, the "maximum" electron densities above which collisional depopulation seriously competes with radiative decay, the maximum background-atom pressure P_A permitted for transmission of the radiation over a 3 cm length. (P_A could be increased up to about 100 Torr before laser breakdown effects become troublesome, should significant photoionization of the background gas occur; for hydrogen the protons produced by photoionization do not absorb). Also shown are the spontaneous lifetimes t_u of the upper laser level, of use for self-terminating transitions (not for the 3s → 2p scheme). Finally the gain coefficient is given as derived from Eq. (1) assuming N_u given by $N_A N_i \sigma_{rct} v_i / A_{u\ell}$.

Table 1. Resonance Charge Transfer Laser Pumping

	Δ_n	λ (Å)	$10^{-18} N_e$ (cm^{-3})	P_A (Torr)	$10^{12} t_u$ (sec)	α (cm^{-1})
$(Be, B)^{4+}$ + H	3-2	400	1	0.7	75	20
$(B, C)^{5+}$ + (He, Ne)	3-2	250	6	1	60	30
$(C, N)^{6+}$ + H	4-3	520	2	0.3	80	50
	4-2	130	2	20	90	40
$(N, O)^{7+}$ + (He, Ne)	4-3	380	6	0.3	45	30
	4-2	95	6	20	50	30

An experiment intended to test this method of pumping has been designed[9] and is shown schematically in Fig. 9. A high power glass laser beam will be focused in a line image onto various target materials placed on a rotatable disc in front of the entrance slit of a grazing incidence vacuum spectrograph. The plasma formed will expand into a background gas in an upward direction, parallel to the slit, and in a confined slab configuration by the use of a solenoidal magnetic field (not shown). Rotation of the focusing lens will permit both axial and transverse observations for indications of amplification. Spatial resolution along the direction of expansion will be provided by a slot placed between the entrance slit and the grating as indicated. Experiments to verify anomalous populations under optically-thin conditions will be carried out at lower densities further from the target by a simple

displacement of the target and lens assembly.

C. Kα Quasi-Stationary Inversion

As mentioned above, inversion with the ground state by the above scheme of resonance charge transfer pumping seems at the present unlikely, both because of the short times involved in the self-terminating transitions and of the pump power required.[10] However, as pointed out by Vinogradov and Sobelman,[10] this could be a source of intense spontaneous radiation in a single line or perhaps a series of closely spaced lines. If successfully extended to the x-ray region, this could be a connection to a third scheme which has received serious consideration for amplification in the x-ray region, i.e., quasi-cw inversion of K-α innershell transitions. In a concept originally proposed by Stankevich[13], amplification would occur by the depletion of K-shell vacancies resulting in the creation of L-shell vacancies (using x-ray terminology). Self-termination in femtosecond times would be avoided by Auger depletion of the L-vacancies to higher shells at a rate higher than that for K-vacancy decay (see sketch in Fig. 10). The relative rates R_L/R_K (reconstructed from the brief description given by Stankevich) which relate to the population inversion $N_u/N_\ell \doteq N_2/N_3$ achievable are shown in Fig. 9. Also shown are the results of a more recent reanalysis[2] using recent data.

What appears now to be only a marginal gain possibility in Stankevich's original concept, becomes more promising if the further sophistication of shifts in potentially absorbing lines accompanying K-shell Auger-ionization transitions is introduced, as indicated in Fig. 11 (note that recombination must continue at a "balanced" rate). The results of this additional effect are shown in Fig. 12. In the final analysis the details of which will not be repeated here except in Table 2, sufficient pumping must be accomplished to overcome photoionization losses to the main laser beam in the medium, since there are by necessity many outer-shell electrons present. This pumping must also be selective for removal of the K-shell electron without disturbing the outershell structure significantly. It can be shown[2] that the magnitude and selectivity required can only be achieved by photoionization with the "tuned" photon flux density of magnitude N_ν, and power density F which are indicated in Table 2, along with the resulting gain αL for a length of 300 μm. It is suggested[2] that blackbody sources of appropriate temperatures kT_{BB} with peak wavelengths given by $(\lambda_m)_{BB}$ be employed, for example, with bands of intense lines in the correct wavelength region. What is needed in this approach is a very intense x-ray pump source limited to a rather narrow specific wavelength band concentrated onto a small area, probably in a traveling wave pumping mode to avoid minimum disturbance of the medium prior to inversion. In addition to the charge transfer source mentioned above, the further development of heavy element (e.g., uranium) condensed spark pseudo-continuum sources to the x-ray region has been suggested[2] for pump source development; further concentration of the x-ray flux is a separate problem.

Table 2. $K\alpha_2$ Pumping Requirements

ELEMENT	λ (Å)	$10^{-20} N_v$ (cm^{-3})	$10^{-3} F$ (TW/cm^2)	αL	kT_{BB} (keV)	$(\lambda_m)_{BB}$ (Å)
^{14}Si	7.1	2	4.8	70	0.5	5
^{20}Ca	3.4	4	21	30	0.7	4
^{29}Cu	1.5	20	230	15	1.2	2

III. SUMMARY

Present modeling has demonstrated that the extension of laser action can be actively pursued into the vacuum-uv and eventually x-ray spectral regions without high reflectance cavities, for the initial purpose of feasibility demonstration and for amplification of coherent frequency multiplied beams. Extension of proven visible and near-uv laser transitions into the mid vacuum-UV region with plasmas of increased density and decreased size seems to be a most reasonable starting point. Extension to shorter wavelengths into the soft x-ray region could be achieved by selective population in, e.g., helium-like ions, where the Auger and photoionization effects of outer electrons are absent; here resonance charge transfer appears to be the most promising candidate, providing that a sufficient density of ion-atom interactions can be achieved. Experiments are well underway at NRL towards testing these two schemes. Success here or with other intense x-ray sources could finally lead to sufficient amplification on $K\alpha$ innershell transitions to overcome the losses associated with the multiple outer electrons required for quasi-cw and eventually possible resonant cavity operation.

IV. ACKNOWLEDGMENT

The cooperation of Drs. K. G. Whitney and J. Davis in computing the $3p \rightarrow 3s$ gain with their hot-spot program, leading to the data in Fig. 4, is greatly appreciated. Many illuminating discussions with Dr. R. A. Andrews and Prof H. R. Griem are also recalled with appreciation.

V. REFERENCES

1. R. C. Elton, R. W. Waynant, R. A. Andrews and M. H. Reilly, "X-Ray and Vacuum-UV Lasers, Current Status and Prognosis" NRL Report 7412, May 1972.

2. R. C. Elton, "Quasistationary Inversion on K-α Innershell Transitions", NRL Memorandum Report 2906, October 1974; submitted for publication.

3. P. K. Cheo and H. G. Cooper, J. Appl. Phys. 36, 1862 (1965).

4. Y. Hashino, Y. Katsuyama and K. Fukuda, Japan J. Appl. Phys. 11, 907 (1972).

5. C. K. Rhodes, IEEE J. Quant. Elect. QE-10, 153 (1974), Table of UV-Laser transitions p. 170.

6. R. C. Elton, "Extension of 3p→3s Ion Lasers into the Vacuum-UV Region", NRL Memorandum Report 2799, May 1974; also Appl. Optics, 14, 97, 1975.

7. K. G. Whitney and J. Davis, J. Appl. Phys. 45, 5294 (1974); also K. Whitney, J. Davis and E. Oran, NRL Memorandum Report 2644, June 1973.

8. R. C. Elton, T. N. Lee, J. Davis, J. F. Reintjes, R. H. Dixon, R. C. Eckardt, K. Whitney, J. L. DeRosa, L. J. Palumbo and R. A. Andrews, Physica Fennica 9, Suppl. S1 (1974).

9. Staff Report: ARPA/NRL X-Ray Laser Program, NRL Memorandum Report 2910, October 1974.

10. A. V. Vinogradov and I. I. Sobel'man, Sov. Phys. JETP, 36, 115 (1973).

11. R. C. Elton, "Atomic Processes", (in) Methods of Experimental Physics-Plasma Physics, Vol. 9A, eds. H. R. Griem and R. H. Lovberg, (Academic Press, New York, 1970).

12. H. J. Zwally and D. W. Koopman, Phys. Rev. A 2, 1851 (1970).

13. Yu. L. Stankevich, Sov. Phys. Doklady 15, 356 (1970).

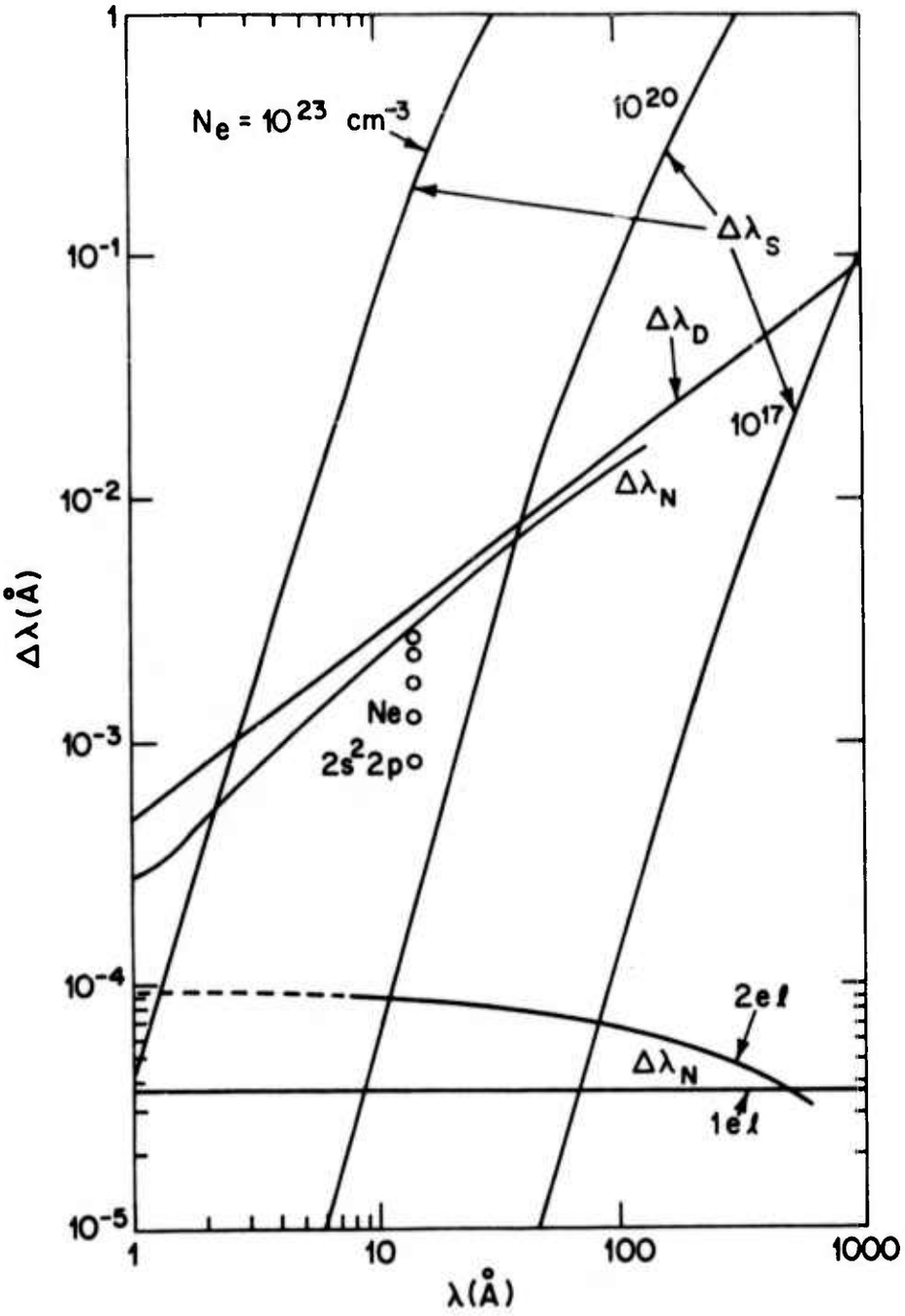

Fig. 1 — Estimates of line widths for Kα type transitions versus wavelength λ, with natural ($\Delta\lambda_N$), Doppler ($\Delta\lambda_D$) and Stark ($\Delta\lambda_S$) effects included. The decrease in natural broadening with ionization is indicated by circles for neon; and hydrogenic and helium-like ionic species are included. (See Ref. 2).

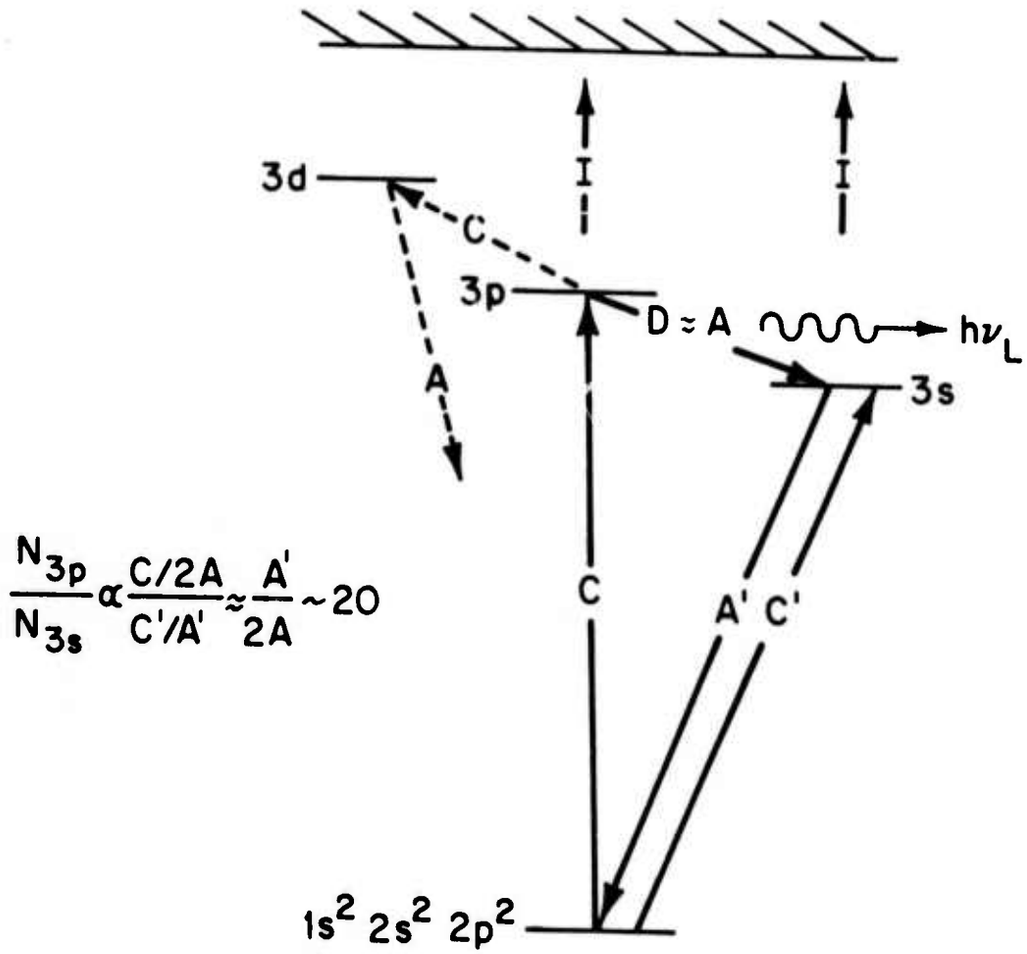

Fig. 2 — Schematic energy level diagram for carbon-like ion species. Collisional excitation is designated by C and C′, radiative decay by A and A′, ionization by I, and collisional depopulation by D. The relative 3p to 3s population densities are estimated from a modified corona model, where excitation is balanced by radiative decay and collisional de-excitation. Competing collisional depopulation to the 3d level is also indicated.

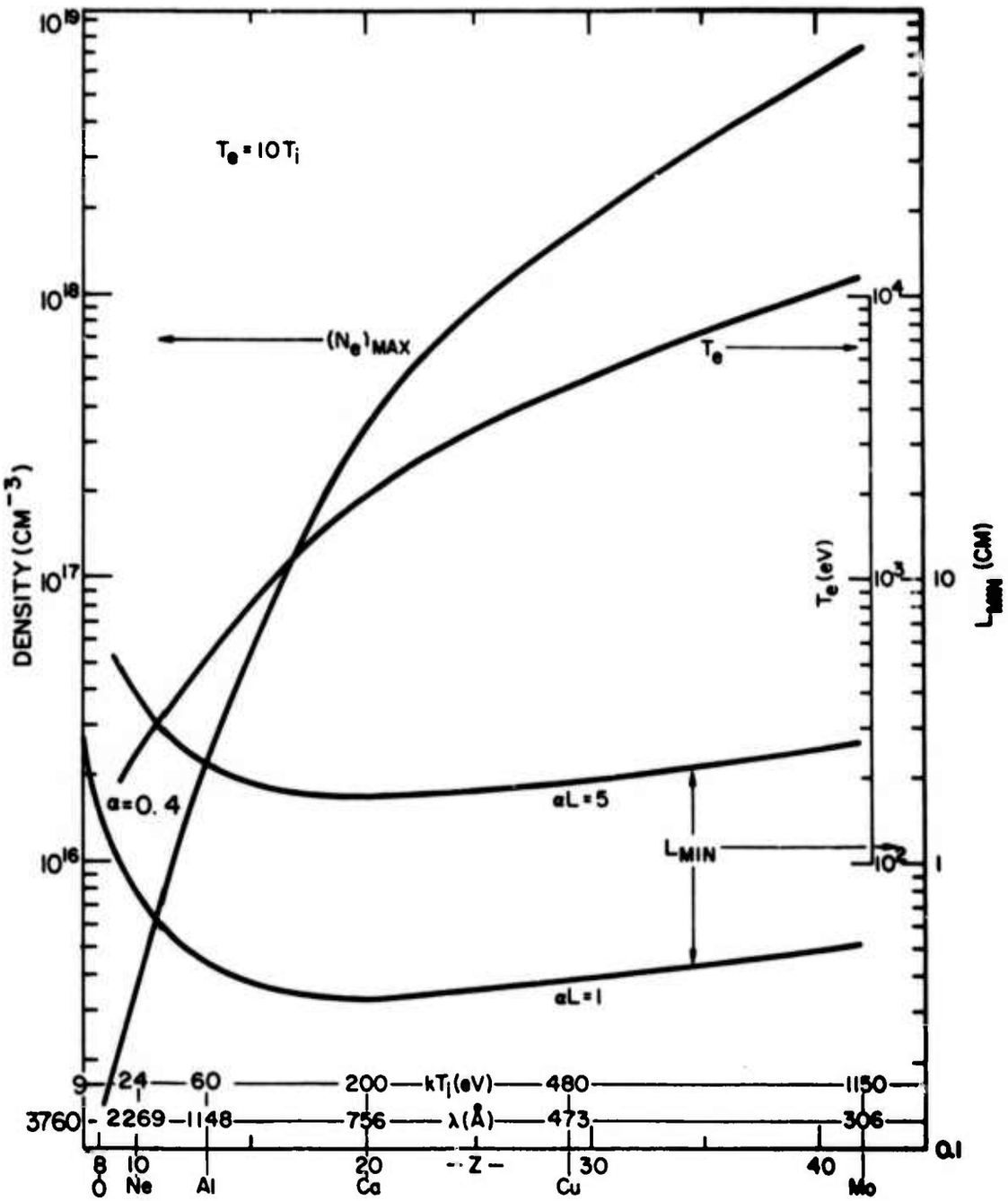

Fig. 3 — Minimum length L_{min} for amplification in carbon-like ions with a gain of exp (αL) versus atomic number Z, wavelength λ, kinetic temperature kT_i. The electron temperature T_e is assumed equal to 10 T_i and is plotted. The electron density $(N_e)_{max}$ at which collisional mixing becomes important is also plotted. Data extrapolated to O^{2+} (OIII) comparison with Fig. 4 (See also Ref. 6).

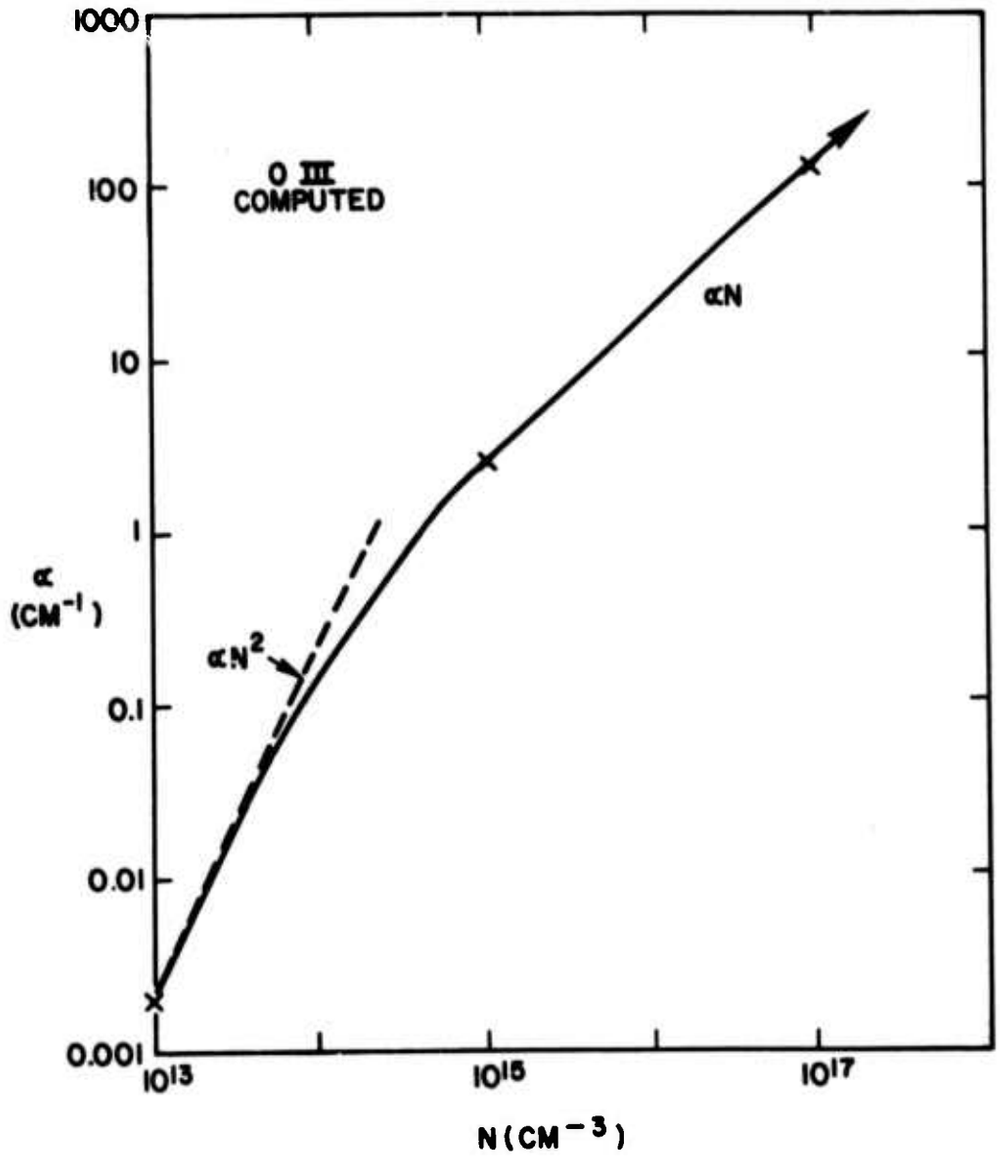

Fig. 4 — Gain coefficient α versus ion density computed at three values for $3p \rightarrow 3s$ transitions in the carbon-like O^{2+} (OIII) ion. The varying dependence of α is understood by increased collisional mixing at higher densities, as discussed in text.

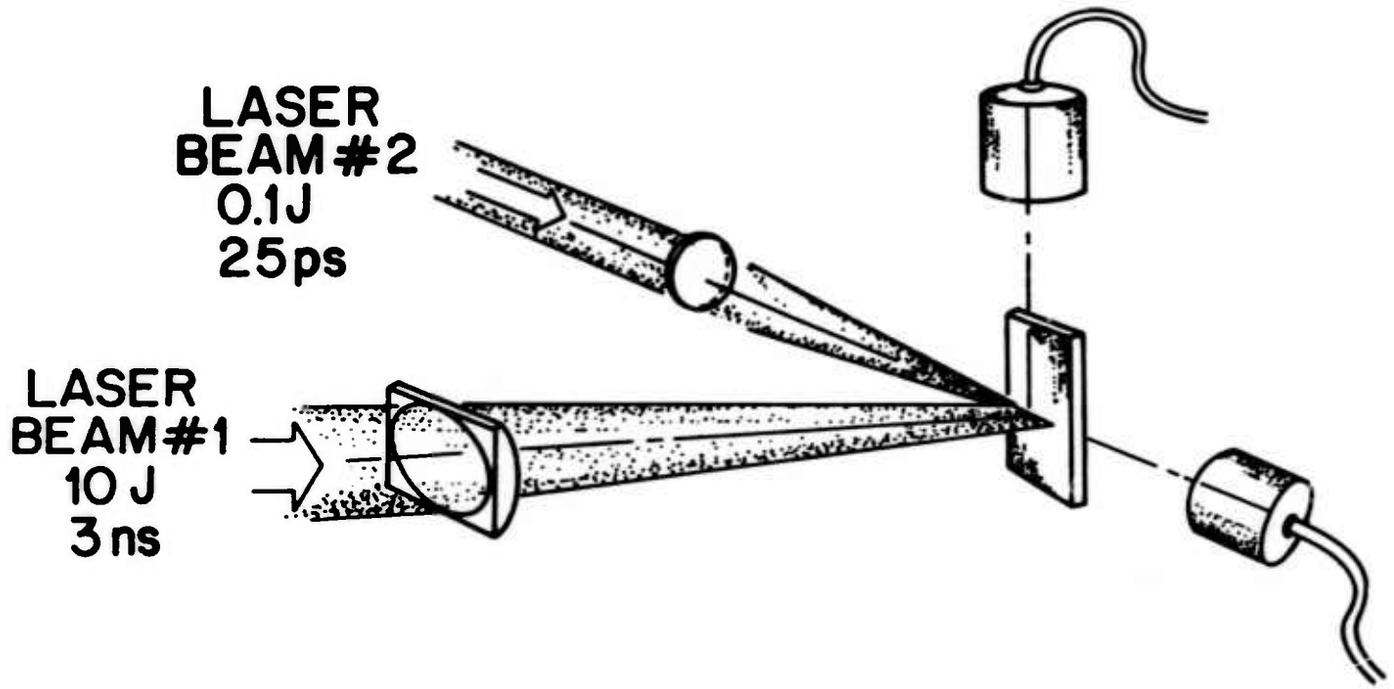

Fig. 5 — Schematic of experiment designed to verify gain on 3p → 3s transitions pumped by electron collisions in a plasma.

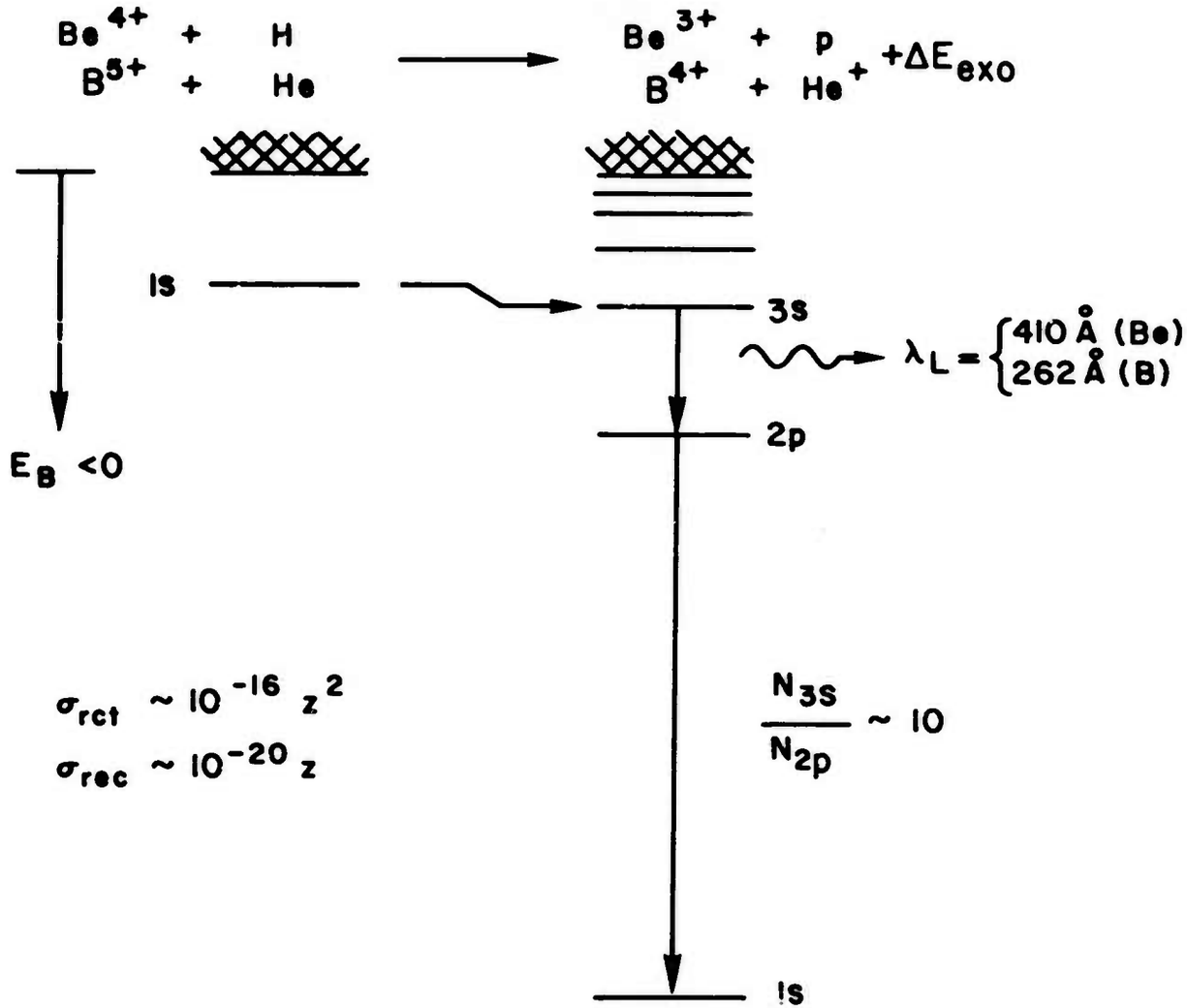

Fig. 6 — Schematic diagram of exothermic s-s resonance charge transfer reaction leading to a quasi-stationary population inversion between 3s and 2p levels in certain helium-like or hydrogenic ions. Refer to Fig. 8 for other possible ion/atom combinations. E_B is the binding energy; σ_{rct} and σ_{rec} show the cross section scalings for resonance charge transfer and radiative recombination, respectively.

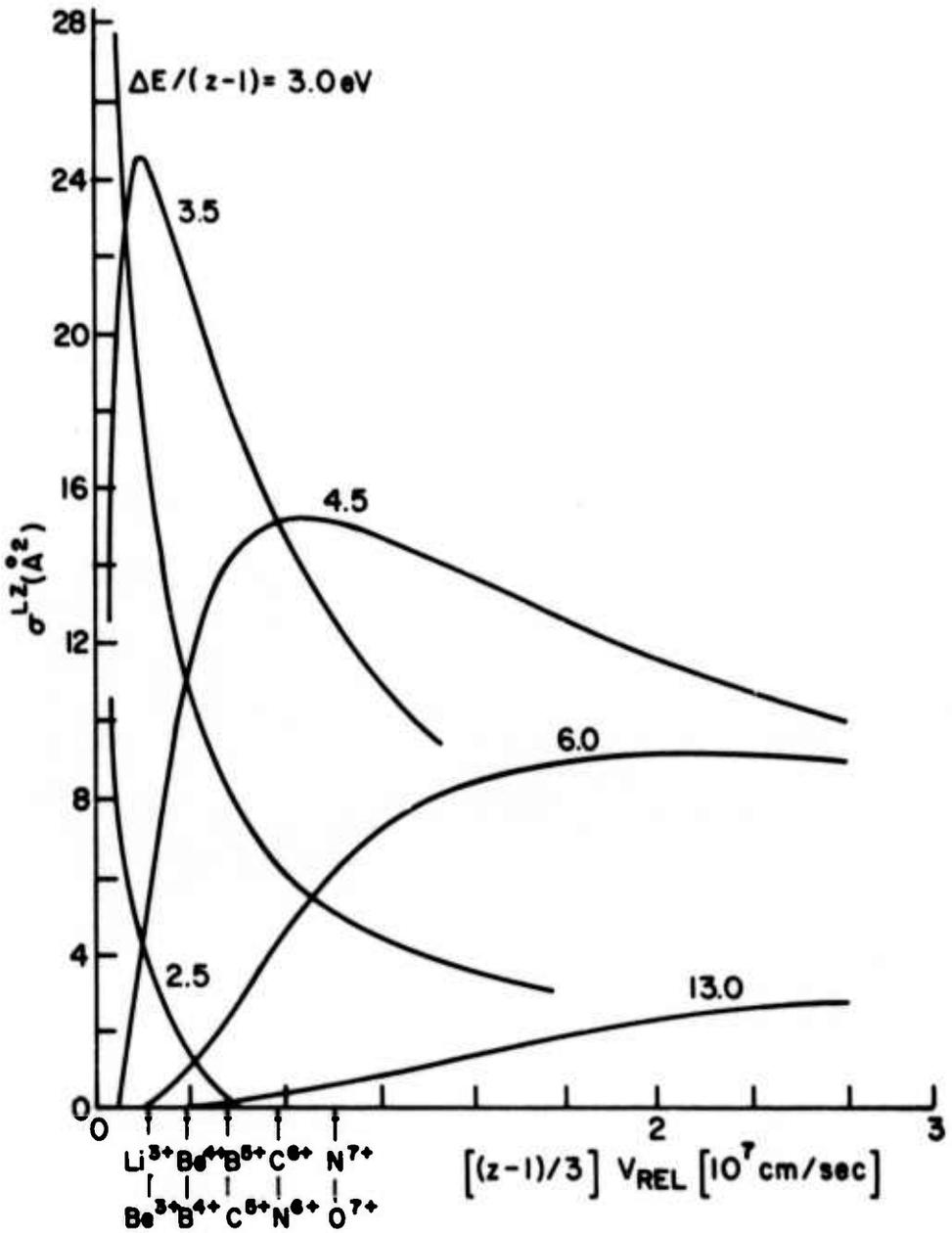

Fig. 7 — Resonance charge transfer cross section from s-s Landau-Zener theory versus scaled relative velocity for the atom-ion combination. (Data adapted from Ref. 12). ΔE represents the energy defect in eV for the exothermic reaction, z the effective charge of the ion. Velocities for ions designated are assumed thermal, with the kinetic temperature chosen as I.P./4 for creating the ion.

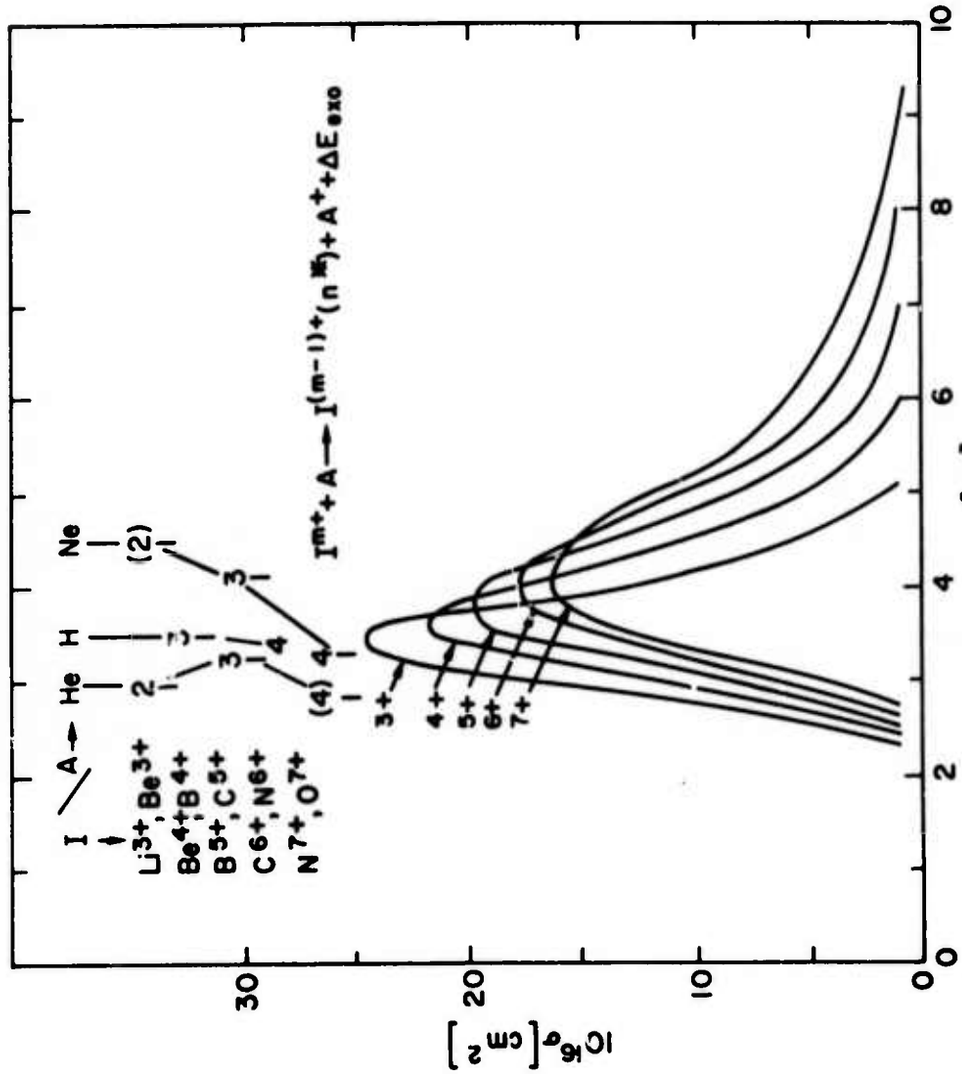

Fig. 8 — Resonance charge transfer cross section obtained by inversion of Fig. 7 data. Final quantum states of high capture probability for each ion I^{m+} and atom A combination are indicated by numerals, with parentheses to indicate less probable transitions. ΔE is the exothermic energy defect and z the effective ion charge.

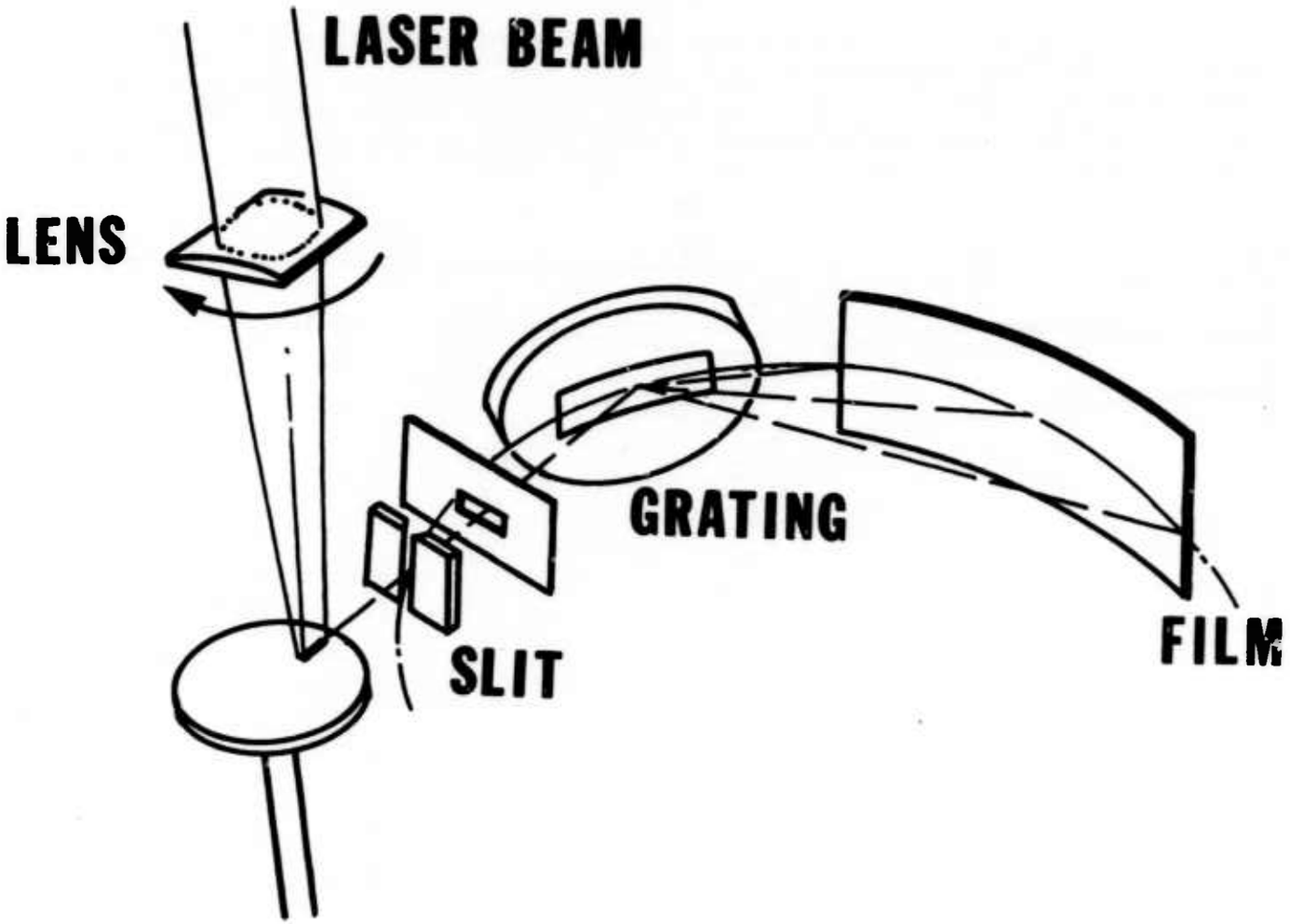

Fig. 9 — Schematic diagram of the NRL resonance charge transfer experiment, including the grazing incidence vacuum spectrograph. The horizontal slot provides spatial resolution along the direction of plasma expansion from the target surface. Rotation of the lens permits both axial and radial viewing. The background (atomic) gas is not indicated, nor is a planned guiding magnetic field.

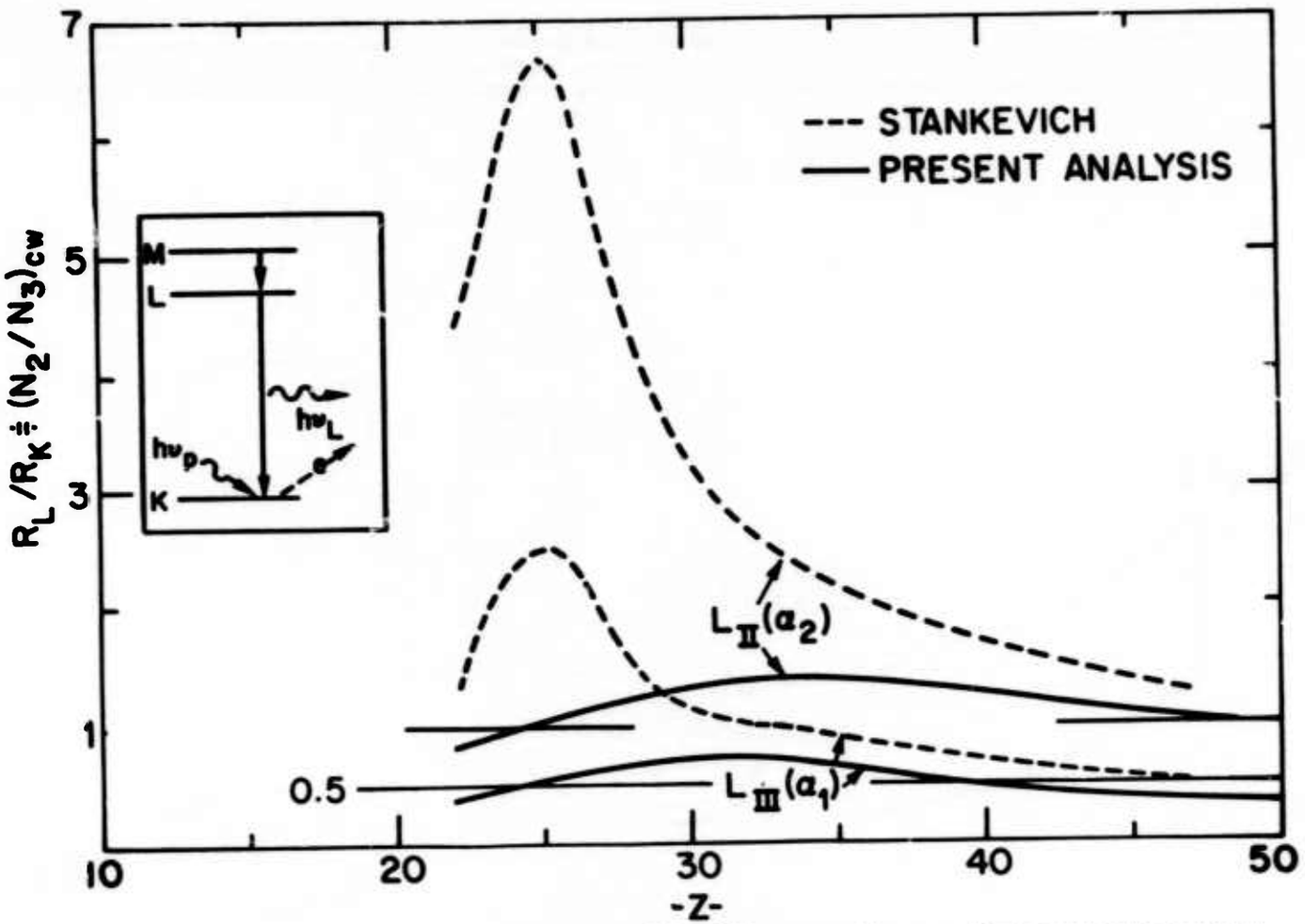

Fig. 10 — Ratio of rates R_L/R_K for total transitions out of L and K vacancy states, respectively, versus atomic number Z. This ratio is equivalent to N_u/N_ℓ (or N_2/N_3 in Ref. 1) for equilibrium conditions reached after long times in cw operation. Values exceeding unity and one-half indicate gain for the $K\alpha_2$ and $K\alpha_1$ transitions, respectively. The model here assumes *all* K-vacancy decay transitions produce potential absorbers for laser radiation. Present analysis is based on recent data; an attempt to reproduce the results of Stankevich[13] is shown dashed. Both $K \rightarrow L_{II}$ and $K \rightarrow L_{III}$, α_2 and α_1 respective transitions are shown. The electron scheme is diagrammed as inset. (See also Ref. 2).

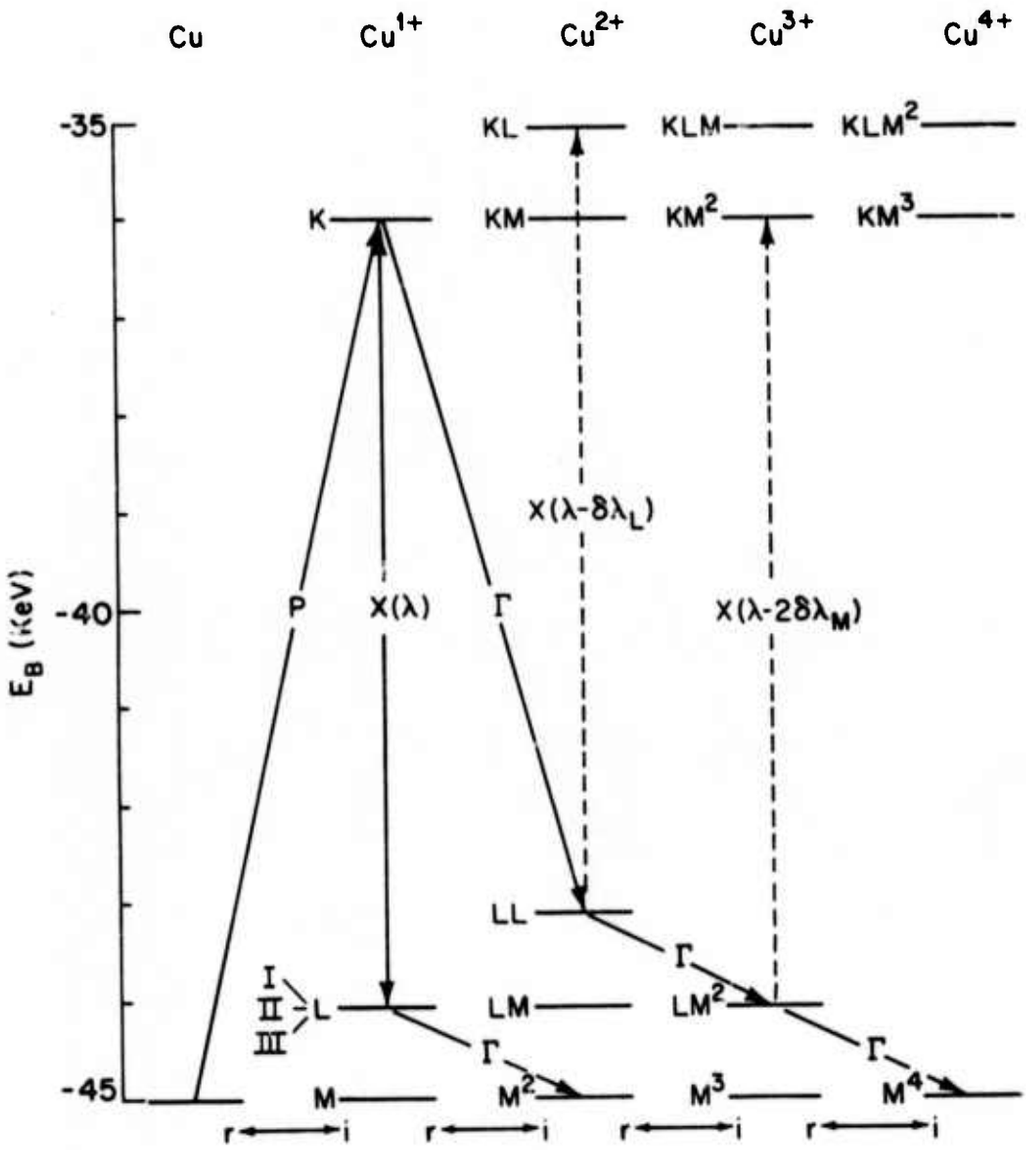

Fig. 11 — Vacancy diagram according to binding energies E_B for copper. K, L and M designate shell-vacancies. P, X, and Γ are the rates for pumping, x-ray [emission or absorption (dashed)] and Auger transitions, respectively; r, i indicate recombination and ionization, respectively. Auger line shifts δλ are shown. (See also Ref. 2).

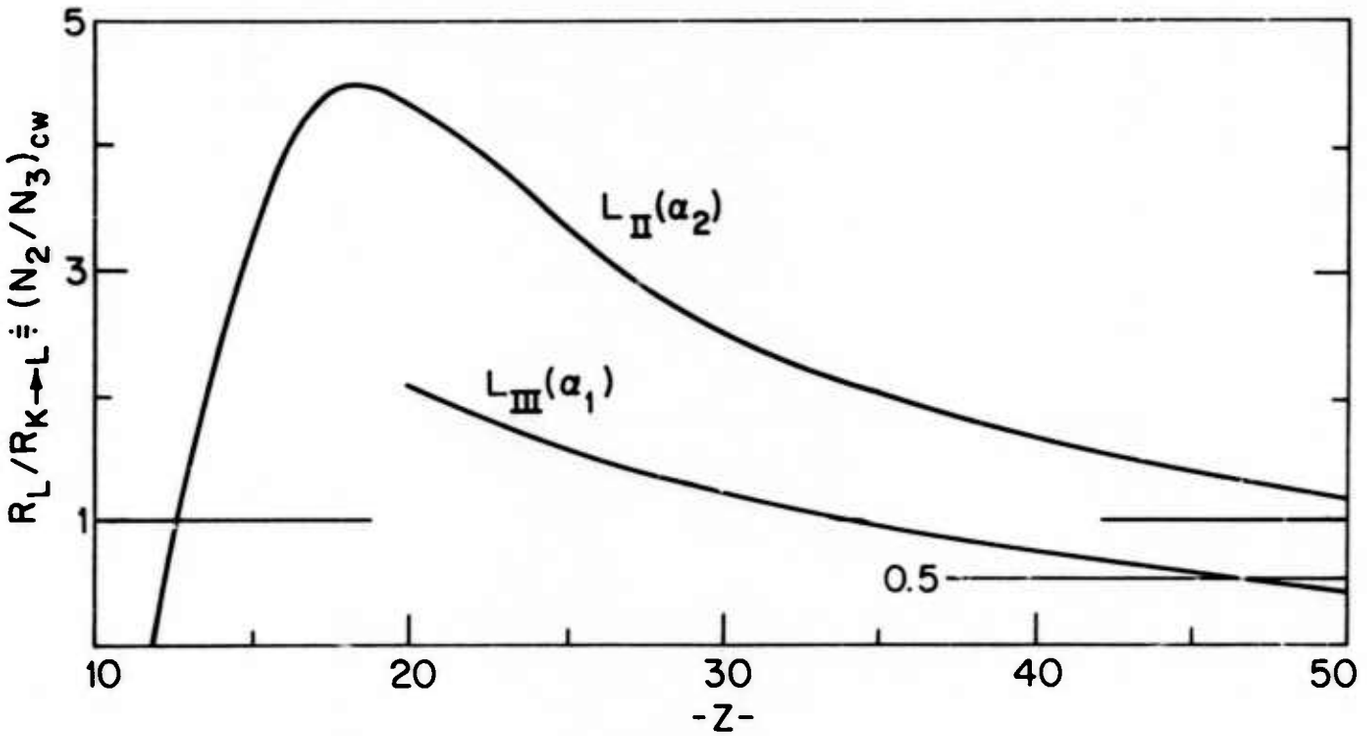

Fig. 12 — Ratio of rates $R_L/R_{K\rightarrow L}$ for total transitions out of a L vacancy state and radiative decay out of a K vacancy state versus atomic number Z. This ratio is equivalent to N_u/N_ℓ (or N_2/N_3 in Ref. 1) for equilibrium conditions reached after long times in cw operation. Values exceeding unity and one-half indicate gain for the $K\alpha_2$ and $K\alpha_1$ transitions, respectively. The model used assumes only radiative transitions produce absorbers, with Auger transitions generating shifted ion lines. Both $K\rightarrow L_{II}$ and $K\rightarrow L_{III}$, α_2 and α_1 respective transitions are shown.

SOFT X-RAY LASERS VIA ELECTRON-COLLISIONAL PUMPING*

R. A. ANDREWS

Naval Research Laboratory
Washington, D. C. 20375

I. INTRODUCTION

One possible technique for obtaining gain in the soft x-ray region of the spectrum is to use electron-collisional pumping of an appropriate ion species. This can be done in a manner analogous to known ion lasers which operate in the visible portion of the spectrum. The differences being 1) more highly ionized ions are used to obtain shorter wavelength transitions, 2) the pumping electrons are at a higher temperature to populate the more energetic transitions, and 3) the lifetimes are shorter which implies higher pump intensity per unit area ($P/a \propto \nu^4$). In the case of shorter wavelength transitions one can project known laser transitions isoelectrionically to higher Z ions and hence shorter wavelengths or investigate unique ionic electron configurations that are not observed in neutral or weakly ionized species. This technique works well for electronic configurations with relatively few electrons. With many electrons systems level crossings and other anomalous effects with increasing Z limit the range over which a group of levels which are a viable laser scheme can be isoelectronically projected to higher Z. A further problem with short wavelength lasers is that the techniques available for generating significant

---

* This work was partially supported by the Defense Advanced Research Projects Agency, ARPA Order 2671.

amounts of energy with very short risetimes are limited. Discharges are limited to about 10^{-7} sec. Mode-locked lasers, however, can be used down to the 10^{-11} sec range with significant amounts of energy. Short wavelength requirements lead to many other problems for the attainment of an inversion and net positive gain. Several of these are discussed in this paper along with a particular approach to the short wavelenth laser problem.

A particularly promising concept for an electron-collisional pumped laser is the use of a picosecond laser pulse to heat the electrons in a cold plasma which has a large fractional population of the laser ion species.[1,2] The initial plasma can be created by a variety of techniques. However, if one is seriously considering highly ionized species then a laser produced plasma offers distinct advantages since large amounts of energy can be deposited in small volumes in short times. This initial plasma would typically be generated with a line focus laser to create a plasma/laser media with a large aspect ratio and hence maximum gain length. This plasma must be allowed to expand, cool, and develop a maximum fractional population of a particular laser ion species. Cooling is important since the laser line is Doppler broadened and Boltzmann population of low lying levels may ruin a possible inversion. Also expansion must be limited since laser heating of the electrons will not be effective if the density is too low. Once the initial plasma has evolved, a short laser pulse propagating along the plasma axis heats the electrons as shown schematically in Fig. 1. If the pulse width and hence the heating time is much less than the electron-ion equilibration time for the particular plasma conditions (temperature, density) then in principle it is possible to obtain conditions where the electron temperature is much higher than the ion temperature. Depending on the laser

scheme and the energy of the upper laser levels, there will be an optimum electron temperature. Finally, once there is sufficient inversion of the laser levels there will be superfluorescent emission or traveling wave (TW) amplification of a synchronized input pulse. Due to the general lack of efficient reflectors for short wavelengths and the very high power densities in short wavelength lasers, an oscillator analogous to visible lasers does not seem possible. Further, the short characteristic times associated with short wavelength transitions prevents gain from being maintained for long enough times to allow several round trip resonator transits. In fact, long gain lengths at very short wavelengths can only be obtained by TW pumping. This is shown in Fig. 1. The laser pulse and the gain pulse travel through the plasma at approximately the speed of light. The width of the gain pulse is determined by the lifetime of the laser transition for the case of self-terminating laser action. The heating pulse may be shorter than this.

A discussion of this approach can be divided into five problem areas: 1) the generation of a cold plasma with a large fractional population of the laser ion species; 2) synchronization of the electron heating laser pulse with the plasma generation; 3) obtaining optimum electron heating; 4) identifying potential ion laser configurations; and 5) establishing tests and criteria for observation of net gain. The following sections of this paper will concentrate on areas (3), (4), and (2) along with comments on recent experimental work at NRL.

II. SHORT PULSE ELECTRON HEATING

Ultrashort laser pulses with peak intensity, $I > 10^{13}$ W/cm^2 can be used very effectively to preferentially heat the electrons in a plasma. These intensities are most easily generated by modelocked lasers generating pulses

on the picosecond time scale. These short pulses are very important for self-terminating pulsed lasers. In fact, they limit the wavelength where lasing can be expected since the pulse width, $\tau \sim A^{-1}$ where A is the transition probability of the laser transition ($A \propto \lambda^{-2}$). The short pulse width simplifies the analysis of the electron heating since plasma hydrodynamics and collective plasma oscillations can be neglected.

In high intensity fields the plasma electrons oscillate with the frequency of the incident laser radiation. This energy of this oscillation is like "internal" energy independent of the thermal or translational energy. If the electron does not undergo a collision while the intense field is present then the oscillation energy goes back into the laser field and nothing is changed i.e., the electron temperature is not increased and the laser pulse is transmitted through the plasma. However, if the oscillating electron suffers a collision then the oscillation energy is converted to translational or thermal energy at the expense of the high intensity laser field. The oscillation energy is given by

$$E_{osc} = \frac{e^2\mathcal{E}^2}{4m\omega^2} = \frac{2\pi e^2 I}{mc\,\omega^2}$$

where e is the electronic charge, m the electron mass, c the velocity of light, and ω the angular frequency of the incident laser radiation of intensity I. At 1.06 μm

$$E_{osc}\ [eV] = 1.02 \times 10^{-13}\ I\ [W/cm^2].$$

Hence, $E_{osc} \gtrsim E_e$ (electron thermal energy) $\sim 3/2\ kT_e$ (electron temperature) for intensities $I > 10^{13}$ W/cm^2 and relatively cold plasmas ($T_e \sim 1$ eV).

The electron's energy is the sum of the thermal and oscillation energies. If E_{osc} is high enough, a single collision can excite an energetic ionic level. Alternatively with many collision the electron temperature can be increased to higher values. This large thermal energy can then excite more energetic ion levels in inelastic collisions. The potentially important heating mechanisms are inverse bremsstrahlung and stimulated Compton scattering. Potential cooling mechanisms are inverse Compton scattering, expansion, ion collisions, and bremsstrahlung. Each of these cooling mechanisms can be shown to be negligible on the picosecond timescale for plasma parameters of interest here.

The inverse bremsstrahlung heating rate is given by

$$\left(\frac{dE}{dt}\right)_B = E_{osc} \nu_{eff}$$

where ν_{eff} is the effective electron collision rate and is given by

$$\nu_{eff} \sim 2\sqrt{3\pi/m}\ Z^3 e^4 n_e \ell n \Lambda/(E_e + E_{osc})^{3/2}$$

where Z is the net ionic charge, n_e is the electron density, and $\ell n \Lambda$ is the Coulomb logarithm. The heating rate for stimulated Compton scattering[3-5] is given by

$$\left(\frac{dE}{dt}\right)_{sc} = 3\pi\sigma_o \Omega I^2/4m\omega^2\Delta\omega$$

where $\sigma_o = 8\pi e^2/3mc^2$ is the Thompson cross section, Ω is the solid angle of the focused laser radiation, and $\Delta\omega$ is the width of the heating laser line. $\Delta\omega/\omega$ is about 10^{-4} for Nd:YAG lasers and about 10^{-3} for Nd:glass lasers. For

a given laser ($\Delta\omega/\omega$) and focusing optics (Ω) only those electrons which satisfy the condition,

$$\frac{\Delta\omega}{\omega} > 1/2\sqrt{\frac{\Omega T_e}{mc^2}} \quad ,$$

will be heated by stimulated Compton scattering. In typical situations stimulated Compton scattering is important for Nd:glass lasers and of minor importance for Nd:YAG lasers. In the latter case after T_e reaches some relatively low value inverse bremsstrahlung is the dominant heating mechanisms. As T_e increases ν_{eff} decreases. Hence for a given pulse width, τ, the number of collisions $\nu_{eff}\,\tau$ decreases. For very high intensities there are insufficient collisions to obtain high T_e. Figure 2 shows $E_e(\tau)$ for a number of ion densities as a function of intensity, I. Note that there is a maximum E_e for a given n_i and this occurs at an intensity where $\nu_{eff}\,\tau$ is on the order of unity. At higher intensities there is not enough time for effective heating ($\nu_{eff}\,\tau < 1$). Also under typical conditions for this problem the maximum temperature attained via inverse bremsstrahlung heating is on the order of 1 keV. Under conditions where stimulated Compton scattering is important (using Nd:glass lasers) this maximum can potentially be increased but only with extremely high intensities. Hence, using state-of-the-art laser technology one can produce $T_e \sim 1$ keV conditions in a plasma without increasing T_i. This is sufficient to pump x-ray lasers with $h\nu$ in the range of 100 eV depending on the particular laser scheme.

Electron-collisional excitation probabilities for atoms and ions can be calculated.[6] There are considerable experimental data for atoms and very little for ions. What data exist for ions are for simple ions with low

degrees of ionization. The graph in Fig. 3 qualitatively indicates the results of theoretical analysis of this problem. For large values of E_e/E_{exc}, cross sections (σ) can be calculated using the Born-Coulomb approximation. Theory shows that for allowed transitions σ falls off as $\ell n E_e/E_e$ and for unallowed transitions it falls off as E_e^{-1}. For atoms the cross section is maximum for $E_e \sim (2\text{-}3)\, E_{exc}$ and depending on the situation σ (allowed) can be comparable to σ (unallowed). In the case of ions σ has a finite value at $E_e = E_{exc}$ due to the Coulomb field and hence the maximum cross section is at lower values of E_e/E_{exc}. Also σ for ions scales as Z^{-4} which is an important consideration for short wavelength (higher Z) electron-collisional laser schemes. In brief, the general considerations for collisional pumping are the following: (1) to preferentially populate an allowed transition over unallowed dipole transitions use $E_e > 3E_{exc}$, and (2) to obtain maximum population of multipole transitions use $E_e \sim E_{exc}$.

III. ION LASER CONFIGURATIONS

When predicting potential short wavelength laser transitions one usually starts with known transitions and projects along an isoelectronic sequence to higher Z. $\Delta n = 0$ (n = principal quantum number) transitions scale as $\lambda \propto Z^{-1}$ and $\Delta n = 1$ transitions scale as $\lambda \propto Z^{-2}$. Hence $\Delta n = 1$ transitions are required for really short wavelengths using reasonable states of ionization. The laser scheme can be either "quasi-cw" where an inversion is maintained in near equilibrium conditions or "pulsed, self-terminating" where an inversion is developed in transient, extreme nonequilibrium conditions. The quasi-cw scheme has recently been discussed by Elton both in the literature[7] and in an earlier paper in this symposium. Since the ion populations must finally be

in equilibrium for "quasi-cw" operation (i.e. the gain is limited only by the duration of the pumping) this implies T_e approaches $T_i \sim 1/4\ \chi_{Z-1}$ (χ_{Z-1} = Ionization potential of Z-1 ion) and an initial advantage of a large T_e/T_i ratio disappears in a limited time $\sim$ (1-10) A^{-1}. Therefore, a true quasi-cw condition requires long lengths of hot low density plasma to achieve reasonable gain. In the case of the pulsed, self-terminating laser scheme, collisional mixing is not a problem in a first approximation, since gain only exists for times on the order of the lifetime of the states involved. Further, pumping times are much less than the electron-ion equilibrium time and hence $T_i \ll T_e$. This scheme can lead to very high gain; however, as the wavelengths become shorter the period of time over which gain can be maintained decreases.

The self-terminating electron-collisional laser scheme has several requirements.[8] First the laser transition should preferably be one with $\Delta n = 1$. Second, the upper laser level (U) should be connected to the ground level (G) by a resonance line in order to make use of resonance trapping, and not connected by an electronic-dipole transition to any lower level except the lower laser level (L). The density of the plasma must be sufficient to insure resonance trapping of the spontaneous emission from the upper laser level. This also implies that if the ground level is split, that the splitting be small enough to maintain uniform ground state population and therefore reabsorption of the resonance radiation. The resonance trapping insures efficient collisional pumping since there are effectively no radiation losses. Third, the lower laser level should <u>not</u> be connected to the ground state by an electric dipole transition and it should be sufficiently above the ground level so that it is not populated

by the Boltzmann distribution at T_i, the relatively cold ion temperature. The radiative transition probabilty of the laser line, A_{UL}, should be less than that of the resonance line and the length of the pump pulse, τ_p, should be shorter than A_{UL}^{-1}. This will insure that an adequate inversion can be achieved for high gain. On the other hand, A_{UL} should not be too small since this will increase the gain length to unreasonable values. Thus,

$$10^{-4} A_{UG} \lesssim A_{UL} \lesssim 10^{-1} A_{UG},$$

and

$$\tau_p < A_{UL}^{-1}.$$

Ions isoelectronic with potassium and ions isoelectronic with silicon represent two possible electron-collisional self-terminating laser schemes. Figure 4 illustrates the K-like isoelectronic sequence. KI and CaII have one 4s electron in the ground state. However, the ions ScIII and above have a single 3d electron in the ground state. This configuration is not found in neutral species and hence is a unique ionic configuration. The ground state is $3d(^2D)$. The first allowed excited state is $4p(^2P)$ which is also connected by an allowed transition to the lower lying $4s(^2S)$ state. These three levels make up a possible self-terminating laser which meets the criteria discussed above: the resonance line is $3d \rightarrow 4p$ and the laser line is $4p \rightarrow 4s$ as shown. This lower laser level is connected to the ground state by an electric quadrapole transition. This scheme suffers the disadvantage that the laser transition is $\Delta n = 0$ and hence it will not scale to very short wavelengths. The levels in Fig. 4 are plotted through NIX using actual spectroscopic data[9]. The pump energy scales as Z^{-2} and for very moderate values of Z is much larger than the

laser photon energy. It is seen that for NiX the laser transition is at a wavelength slightly less than 1000 Å while the pump energy is close to 100 eV. This isoelectronic extrapolation breaks down above NiX for another reason also. The manifold of levels corresponding to the $(3d)^2$ excited state start to fall below the (4p) and (4s) excited states and the conditions discussed above are no longer satisfied.

The Si-like isoelectronic sequence has a $(3s)^2(3p)^2(^3P)$ ground state as shown in Fig. 5. For ions SIII and above the first excited states are all of the configuration $(3s)(3p)^3$. This is split into $^3S^o$, $^3P^o$, and $^3D^o$ levels. Ions in this sequence have particularly strong intercombination lines connecting these excited states to the singlet ground levels $(3s)^2(3p)^2(^1S)$ and (^1D). Hence these levels fit the collisional self-terminating laser requirements discussed above. Laser transitions can be any of the following: $^3S^o \rightarrow {}^1S$, $^3S^o \rightarrow {}^1D$, $^3P^o \rightarrow {}^1S$, $^3P^o \rightarrow {}^1D$, $^3D^o \rightarrow {}^1S$, $^3D^o \rightarrow {}^1D$. This scheme also has $\Delta n = 0$ for the laser transition and hence the laser wavelength scales as Z^{-1}. For TiIX the $^3S \rightarrow {}^1S$ transition is close to 400 Å, and for ZnXVII it extrapolates to around 240 Å. The ^1S state is the preferred lower laser level over the ^1D state since it is higher above the ground state and does not limit T_i to too low of a temperature. The curves in Fig. 5 were drawn from spectroscopic data.[9] Reference 9 lists several observed intercombination lines for this isoelectronic sequence. These are listed in Table I. The branching ratio shows the ratio of observed line intensities of the listed line and the corresponding line to the ground (^3P) state. This ratio approximates the ratio of the A values for these two transitions.

A general schematic of the collisional laser using the short pulse laser

heating approach is shown in Fig. 6. The axial length of the gain region, L, is determined by the confocal parameter of the focused short pulse radiation. The focusing optics also determine the diameter of the gain region. For a 10^{10} Watt, 1.06 μm laser, the desired peak intensity for optimum electron heating determines the dimensions of the gain region as shown.

As an example of this type of laser consider ScVIII with the $^3S \rightarrow {}^1S$ laser line at ~ 450 Å. Using a 10^{10} Watt, 1.06μ laser focused to 10^{14} W/cm^2 and a pulse width of 10^{-11} sec; then from Fig. 2 an electron energy of about 150 eV can be obtained with a density of $n_i \sim 5 \times 10^{17}$ cm^{-3}. This energy is $\sim 4.5E_{exc}$ for the upper laser level and should insure optimum pumping. Also, this density is sufficient to guarantee an optically thick pumping line since optical thickness, τ, is given by

$$\tau = 5.5 \times 10^{-17} \lambda \, n_i \, d \, \sqrt{M/T_i}$$

where M is the atomic mass number.[10] For $\tau = 10$ this requires $n_i > 6 \times 10^{15}$ cm^{-3} for this example. This is adequate assuming the condition $T_i \sim 1$ eV can be maintained. The electron-ion equilibration time is

$$\tau_{e,i} = 3.2 \times 10^7 \, M T_e^{3/2} / n_e$$

and for this example $\tau_{e,i} = 6 \times 10^{-8}$ sec. Hence, $\tau_p \ll \tau_{e,i}$ and the conditions for obtaining $T_e \gg T_i$ are satisfied. Also $\tau_p \ll A_{UL}^{-1} = 5 \times 10^{-9}$ sec [11] which satisfies the requirement for obtaining maximum gain. Gain can be estimated using the expression for a doppler broadened line

$$\alpha = 1.6 \times 10^{-32} \, n_u \, \lambda^3 \, A_{UL} \, \sqrt{M/T_i}$$

Using the values given above, an estimated $n_u \sim 5 \times 10^{15}$ cm^{-3}, and a gain length $L \sim 1.5$ cm (based on a 10^{10} W, 1.06 μm laser focused to 10^{14} W/cm^2) then

$$\alpha L \sim 14.$$

If plasmas of higher density and the same temperature can be achieved then this number should increase accordingly.

IV. SYNCHRONIZATION OF ELECTRON HEATING PULSE.

This approach to a soft x-ray laser requires two laser pulses, one to produce the plasma and the second to preferentially heat the plasma electrons. Energy is a primary consideration in the first pulse which must ionize neutral target atoms to produce the desired stage of ionization. Hence, typically this pulse can be a nanosecond pulse assuming that extremely high values of Z are not required. The heating pulse must be a picosecond pulse to achieve the desired heating. These two laser pulses must be synchronized with a jitter time short compared to d/v where d is the diameter of the gain medium and v is a typical plasma velocity. Hence, the jitter must be $< 10^{-9}$ sec. This problem has recently been solved at NRL. Figure 7 shows a schematic diagram of the NRL dual laser system. The picosecond laser consists of a modelocked Nd:YAG oscillator and four Nd:YAG amplifiers: one 1/4", two 3/8", and one ½". The performance of this laser is indicated in Table II. The laser produces 30 psec pulses at a intensity $> 10^{10}$ Watts. The second laser consists of a Q-switched Nd:YAG oscillator followed by three Nd:glass amplifiers. It produces 3 nsec pulses at an intensity of 10^9 Watts. Its characteristics are indicated in Table III. The synchronization technique is shown schematically in Fig. 8. The sequence of events is as follows: (1) the flashlamps for both oscillators

are fired, (2) the modelocked pulse train begins to appear, (3) an early pulse in the modelocked train triggers the pockels cell of the Q-switched oscillator (at this point jitter ~ 10-20 nsec), (4) the Q-switched pulse appears and triggers the pulse selecting pockels cell in the modelocked train (at this point jitter = interpulse spacing in modelocked train ~ 6-7 nsec) and, (5) the selected modelocked pulse triggers the gate which passes a 3 nsec portion of the Q-switched pulse. At this final point the jitter has been measured to be < 1 nsec. This short jitter time is achieved by overdriving the final laser triggered spark gap with the single selected modelocked pulse. Figure 9 shows the two laser pulses at various stages of the syncrhonization process. Of course, once these pulses are generated and amplified the delay between them can be varied by changing their respective optical path lengths to the target.

V. EXPERIMENTAL STUDIES

Experiments are underway at NRL to investigate the possibility of demonstrating gain in the soft x-ray region using collisional pumping in a picosecond laser pulse heated plasma. The early experiments have been aimed at (1) demonstrating the attainability of $T_e \gg T_i$ conditions and (2) investigating the effect of laser prepulses on the x-ray yield from a laser produced plasma.

The 30 psec, 10^{10} Watt laser has been used to generate laser produced plasmas. These plasmas have been diagnosed with soft x-ray spectrometers for a variety of medium Z targets. A typical x-ray spectrum for aluminum is shown in Fig. 10 which shows He-like and H-like aluminum lines. This series of experiments has been modeled using the NRL "Hot Spot" code which has been described elsewhere.[12] The result of this modeling is shown in Fig. 11 where the integrated intensities of the aluminum lines shown previously are compared with theory.

The experimental data has been normalized to the AlXII ($1s^2$ - 1s5p) line. It is seen that the agreement is quite good. The low experimental value for the ($1S^2$ - 1s2p) line is due to film saturation and the low experimental value for the (1s - 2p) line is due to an optically thick plasma. This same code has been used to predict the time history of the evolution of the various Al ions. These results are shown in Fig. 12. Projections of this type along with experimental data will be required to determine the optimum time for pumping a particular laser ion species in the development of a laser produced plasma. Based on the experimental data this code has also been used to trace the time development of T_i and T_e. These results are shown in Fig. 13. The results indicate quite clearly the attainability of $T_e > T_i$ conditions.

A second series of experiments investigated the effect of a prepulse on the x-ray yield from the plasma. The prepulse was incident along the same path as the main pulse. It preceeded the main pulse by ~ 6 nsec and was 1/3 the intensity of the main pulse. Both pulses were 30 psec in duration. The results of these experiments are shown in Fig. 14. Both with and without a prepulse there seems to be two temperatures, one ~ 1 kev and one < 0.5 kev. With the prepulse the total x-ray flux is increased by almost an order of magnitude. These results evidence how effectively picosecond pulses can couple into a preexisting plasma.

VI. SUMMARY

Electron collisional pumping of ions in a plasma heated by picosecond laser pulses is potentially a means of generating gain in the soft x-ray region. The approach uses isoelectronic projections of known laser transitions to higher Z and shorter wavelengths or in some cases electronic configurations

unique to ionic species such as K-like ions with a (3d) ground state. The advantages of this approach are that there are no photoionization losses in the laser medium; no Auger effects; and for the case of self-terminating lasers, collisional effects are not limiting in a first approximation. In the self-terminating case very high gains can be achieved.

The disadvantages are that the electron heating is probably limited to ~ 1 KeV and hence the laser transitions to ~ 100 eV. Isoelectronic projections are difficult over large ranges of Z due to level crossing and anamolous effects. This approach tends to be inefficient at longer wavelengths since the densities are low and the laser absorption low. Finally, it is very difficult to obtain high densities of a single "cold" ion species which is the optimum media for this approach.

ACKNOWLEDGEMENT

This paper describes work done as part of the NRL/ARPA x-ray laser program which is a combined effort of many individuals besides the author. These include Drs. R. Elton, J. Reintjes, and T. Lee and Mr. R. Eckardt who were involved with the work described in this paper. The NRL "Hot Spot" code was developed by Drs. J. Davis and K. Whitney of the NRL Plasma Physics Division.

REFERENCES

1. I. N. Knyazev and V. S. Letokhov, Optics Comm. 3, 332 (1971).
2. T. P. Donaldson, R. J. Hutcheon, M. H. Key, and C. Lewis, VII Intn'l Quantum Electronics Conf. Montreal, paper C.9, (1972).
3. P. I. Peyraud, J. de Phys. 29, 88 (1968).
4. P. I. Peyraud, J. de Phys. 29, 306 (1968).
5. P. I. Peyraud, J. de Phys. 29, 872 (1968).
6. J. B. Hasted, "Physics of Atomic Collisions" (American Elsevier, New York, 1972).
7. R. C. Elton, NRL Memo Report No. 2799, (1974); Appl. Optics (in press).
8. W. T. Walter, N. Solimene, M. Piltch, and G. Gould, IEEE J. Quantum Electronics QE-2, 474 (1966).
9. R. L. Kelly and L. J. Palumbo, NRL Report No. 7599 (1973).
10. R. C. Elton in "Methods of Experimental Physics - Plasma Physics", Ch 4, Vol 9A, eds. H. R. Griem and R. H. Lovberg, (Academic Press, New York, 1970).
11. W. L. Wiese, M. W. Smith, and B. M. Miles, Nat. Bur. Stand. Report NSRDS-NBS 22 (1969).
12. K. G. Whitney, J. Davis, J. Appl. Phys., 45, 5294 (1974).

FIGURE CAPTIONS

Fig. 1: Schematic diagram of the electron-collisional laser using the picosecond pulse heating of a plasma approach. The heating pulse propagates down the axis of the plasma to provide TW pumping. The width of the gain pulse is determined by the lifetime of the upper laser level.

Fig. 2: Plot of final electron energy $E_e(\tau)$ after heating via inverse bremsstrahlung with an intense pulse of duration 10^{-11} sec. for various ion densities. $\nu_{eff}\tau$ is the number of collisions during the pulse.

Fig. 3: Characteristic curves of electron-collisional excitation cross sections for atoms and ions as a function of [electron energy (E_e)]/[excitation energy for a particular level (E_{exc})].

Fig. 4: Energy level diagram for the K-like isoelectronic sequence showing the 3d, 4s, 4p, and $(3d)^2$ levels. For a laser scheme with 3d ground state, 4p upper state, and 4s lower state the pump energy and laser photon energies are plotted on the right hand ordinate. The data for these curves was taken from R. Kelly and L. Palumbo, NRL Report 7599 (1973).

Fig. 5: Energy level diagram for the Si-like isoelectronic sequence showing the $3s^23p^2$ levels and the $3s3p^3$ levels. For a laser scheme using the $^3S^o$, state as an upper level and the ^1S level as a lower level the laser photon energy is plotted on the right ordinate. The data for these curves was taken from R. Kelly and L. Palumbo, NRL Report 7599 (1973).

Fig. 6: Schematic of the picosecond laser heated plasma approach with laser parameters for a 10^{10} Watt, 1.06μ laser.

Fig. 7: Schematic diagram of the NRL dual synchronized laser system which generates a 30 psec, 10^{10} W pulse synchronized with jitter < 1 nsec to a 3 nsec 10^{9} W pulse.

Fig. 8: Schematic diagram of the synchronization technique used for obtaining two pulseswith jitter < 1 nsec. See text for details of the sequence of events.

Fig. 9: Laser pulses at various stages of synchronization. (a) Q-switched pulse with mode locked train, (b) selected single mode locked pulse with Q-switched pulse, (c) selected mode locked pulse with shuttered Q-switched pulse.

Fig. 10: A typical x-ray spectrum of a laser produced plasma generated using a 30 psec, 0.1 Joule pulse. This spectrum shows H-like and He-like Aluminum lines.

Fig. 11: Comparison of theoretical model with integrated experimental data for Aℓ. The data was normalized to the He-like 5p line. The 2p line was saturated on the film which accounts for the low value for this line. The plasma was optically thick for the H-like 1s-2p line accounting for the low experimental value of this line.

Fig. 12: Theoretical predictions made with the "Hot Spot" code of the time history of the various Al ion populations.

Fig. 13: Theoretical predictions made with the "Hot Spot" code of the time history of T_i and T_e.

Fig. 14: Experimental data showing the effect of a prepulse on the total x-ray output of the laser produced plasma. Both pulses are 30 psec in duration; the prepulse is 1/3 of the main pulse which follows the prepulse by ~6 nsec.

TABLE I

OBSERVED INTERCOMBINATION LINES

IN Ci-LIKE IONS

ION	TRANSITION	WAVELENGTH	BRANCHING RATIO
P II	$^3D^o - {}^1D$	1772 Å	1:100
	$^3P^o - {}^1D$	1473	1:170
S III	$^3S^o - {}^1D$	789	2:3
Ci IV	$^3S^o - {}^1S$	756	1:11
	$^3S^o - {}^1D$	662	3:11
Ar V	$^3S^o - {}^1S$	651	1:70
	$^3S^o - {}^1D$	571	8:70
K VI	$^3S^o - {}^1S$	572	1:25
	$^3S^o - {}^1D$	502	1:25
Ca VII	$^3S^o - {}^1D$	448	2:45

TABLE II

MEASURED PARAMETERS OF PICOSECOND LASER SYSTEM

STAGE	PULSE ENERGY (mJ)	PULSE DURATION (PSEC)	POWER (W)	BEAM PROFILE	INTENSITY (W/CM^2)	AMPLIFIER GAIN
OSCILLATOR	.20	25	8×10^6	1 mm (Circular Gaussian)	10^9	
AMPLIFIER						
1st STAGE	4.6	25	1.9×10^8	2 mm	6×10^9	30 (30)
2nd STAGE	13.2	25	5×10^8	.6 X .3 CM (ELLIPTICAL AIRY DISC)	3.5×10^9	10.6 (12)
3rd STAGE	114.0	30	4×10^9	.5 X .9 CM	1.1×10^{10}	9.4 (12)
4th STAGE	210	30	7×10^9	.5 X 1.2 CM	1.25×10^{10}	4.1 (7)
TARGET	190	30	6.3×10^9	30 μ X 60 μ	5×10^{14}	

NOTE: The parameters of the picosecond laser system are tabulated at various stages. Large signal gain under actual operating conditions is given in the last column with small signal gain in parentheses. Total gain is reduced from the product of individual gains by power loss at the apertures and reflections.

TABLE III

PICOSECOND LASER SYSTEM PARAMETERS
Q-SWITCHED LASER (SYNCHRONIZED)

STAGE	PULSE ENERGY (J)	PULSE DURATION (ns)	POWER (W)	BEAM PROFILE	INTENSITY (W/cm^2)
DESIGN GOALS					
OSCILLATOR OUTPUT	0.05	50	1×10^6 (PEAK)	2 mm (CIRCULAR GAUSSIAN)	
OUTPUT FROM GATED SHUTTER	0.003	3	1×10^6	2 mm	
AMPLIFIER OUTPUT (3 STAGE)	3.0	3	1×10^9	2 cm	
TARGET	3.0	3	1×10^9	50μ X 50μ (CIRCULAR FOCUS)	5×10^{13}
				50 μ X 2 mm (LINE FOCUS)	1.25×10^{12}
SYNCHRONIZATION ACCURACY		$\leq$ 1 ns			
MEASURED OUTPUT					
OSCILLATOR	.02	30	$.67 \times 10^6$	2 mm	

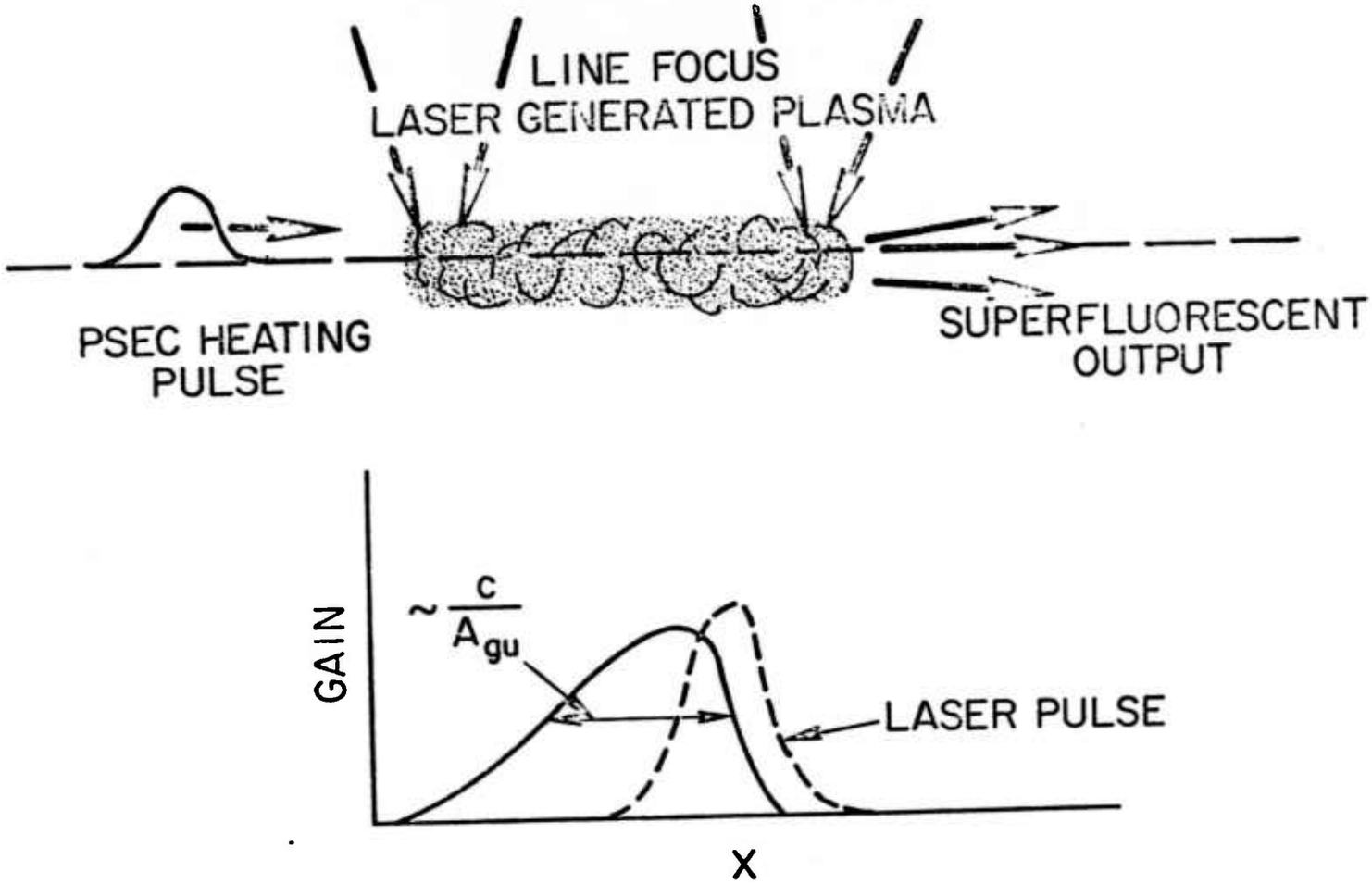
LINE FOCUS
LASER GENERATED PLASMA
PSEC HEATING PULSE
SUPERFLUORESCENT OUTPUT
GAIN
~ C / A_gu
LASER PULSE
X

FIGURE 1

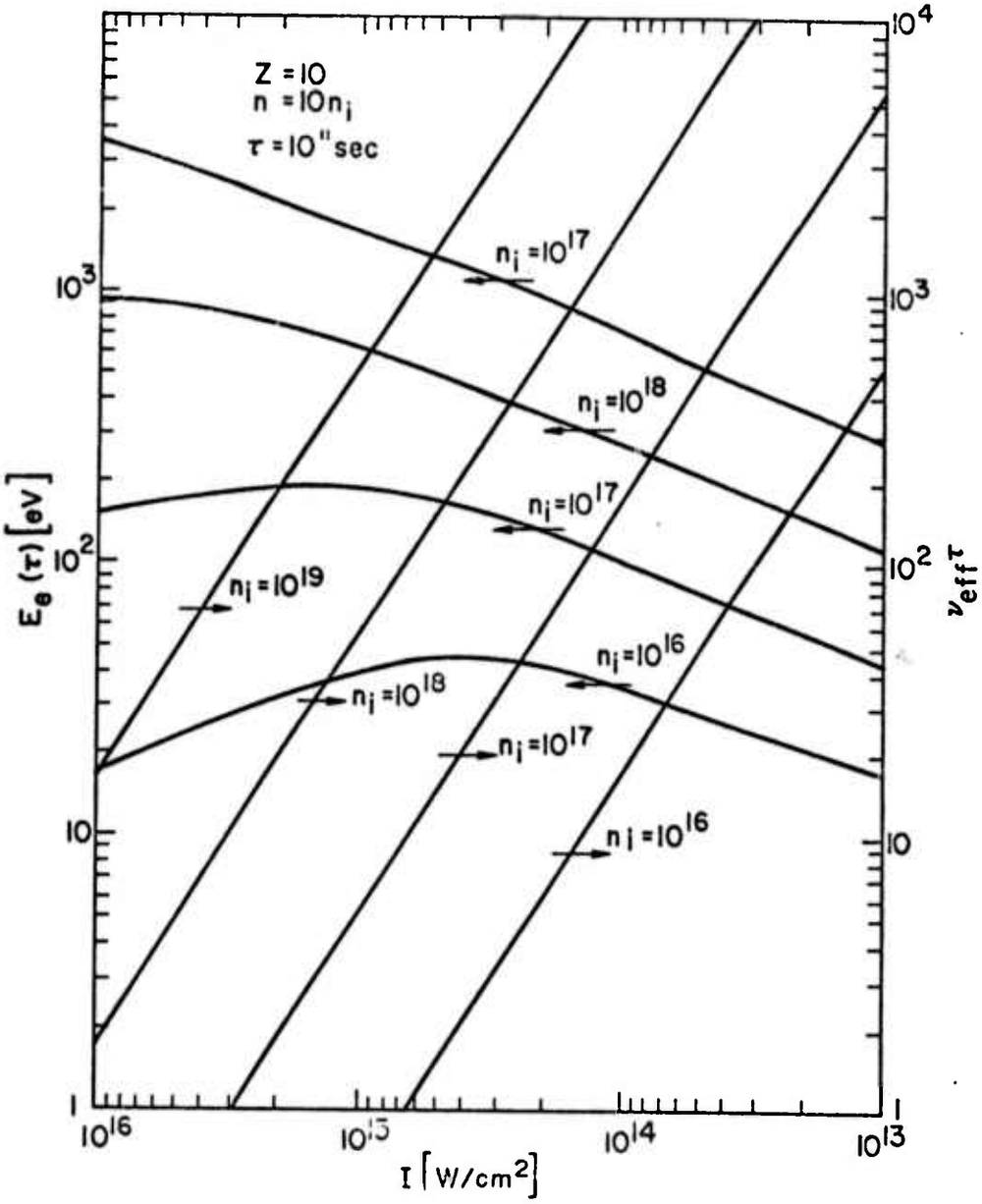
Z = 10
n = 10n_i
τ = 10" sec
n_i = 10^17
n_i = 10^18
n_i = 10^17
n_i = 10^19
n_i = 10^16
n_i = 10^18
n_i = 10^17
n_i = 10^16
E_e (τ) [eV]
ν_eff τ
I [W/cm^2]
10^16
10^15
10^14
10^13
1
10
10^2
10^3
10^4

FIGURE 2

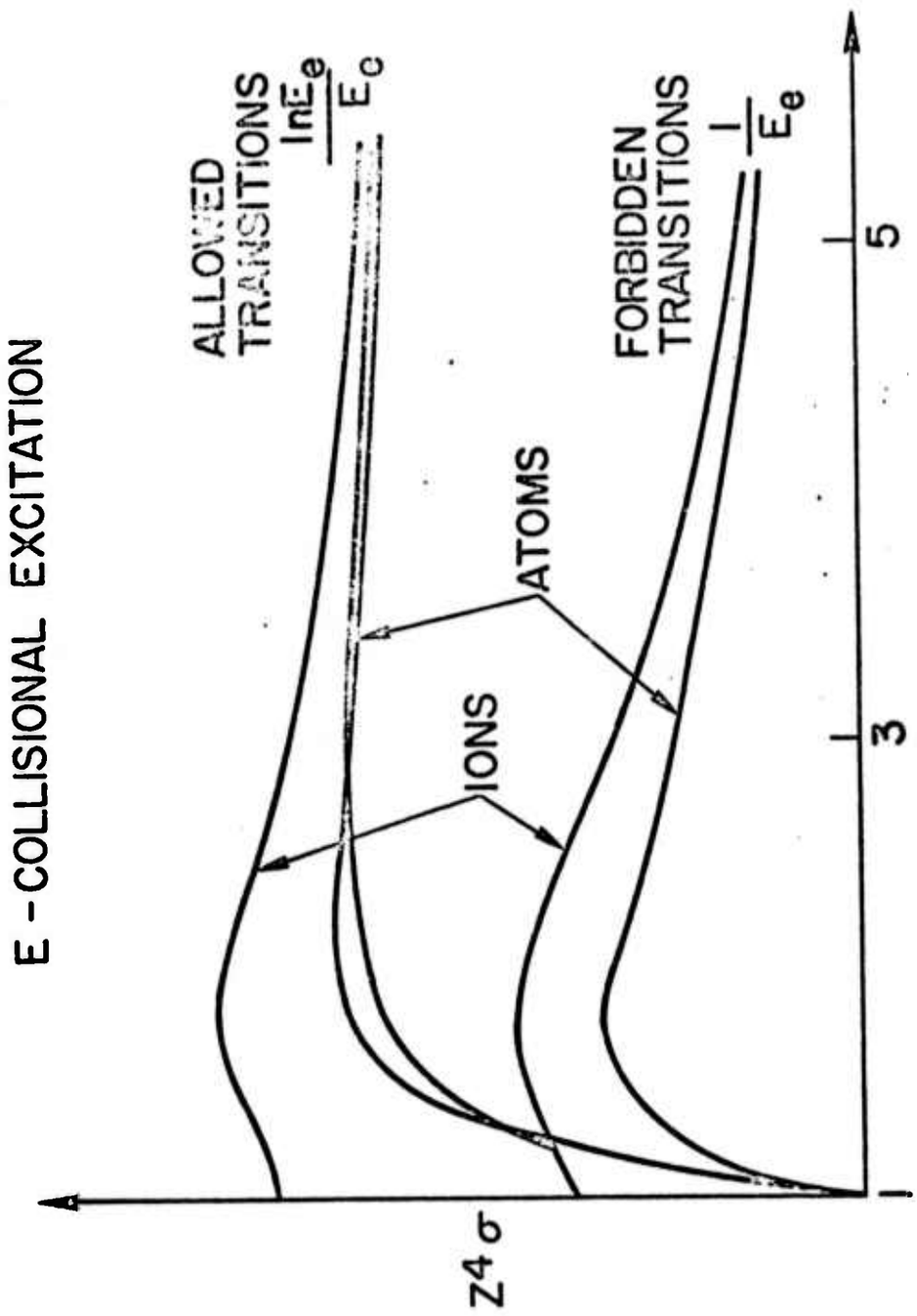
E - COLLISIONAL EXCITATION
ALLOWED TRANSITIONS
$\frac{\ln E_e}{E_c}$
FORBIDDEN TRANSITIONS
$\frac{1}{E_e}$
ATOMS
IONS
$Z^4\sigma$
1
3
5
E_e / E_{exc}

FIGURE 3

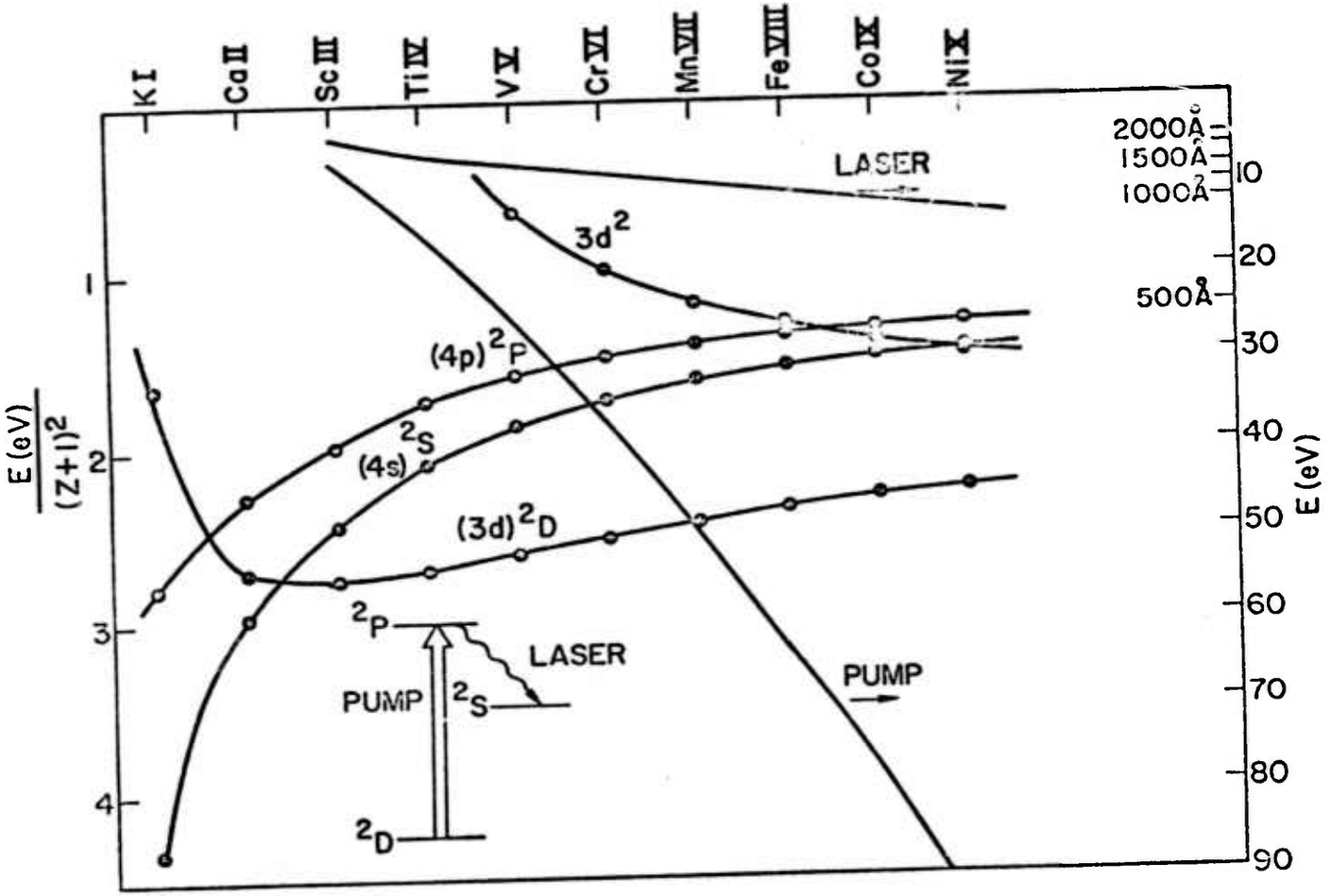
K I
Ca II
Sc III
Ti IV
V V
Cr VI
Mn VII
Fe VIII
Co IX
Ni X
LASER
$3d^2$
$(4p)^2P$
^2S
$(4s)$
$(3d)^2D$
^2P
LASER
PUMP
^2S
^2D
PUMP
2000Å
1500Å
1000Å
500Å
$\frac{E(eV)}{(Z+1)^2}$
E (eV)

FIGURE 4

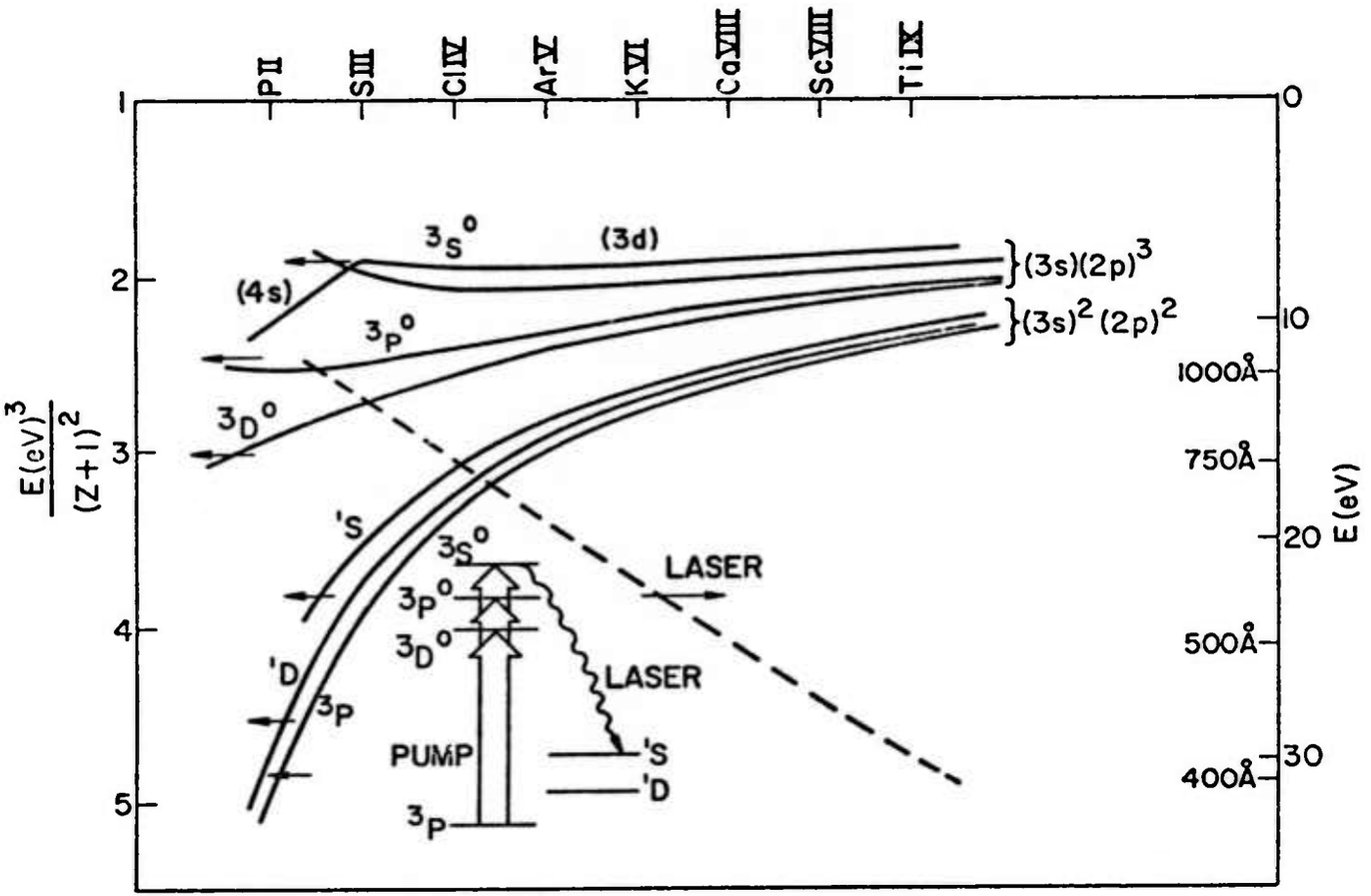
PII
SIII
ClIV
ArV
KVI
CaVII
ScVIII
TiIX
1
2
3
4
5
0
10
20
30
E(eV)
1000Å
750Å
500Å
400Å
$\frac{E(eV)^3}{(Z+1)^2}$
$^3S^0$
(3d)
(4s)
$^3P^0$
$^3D^0$
^1S
^1D
^3P
(3s)(2p)^3
(3s)^2(2p)^2
LASER
PUMP
LASER

FIGURE 5

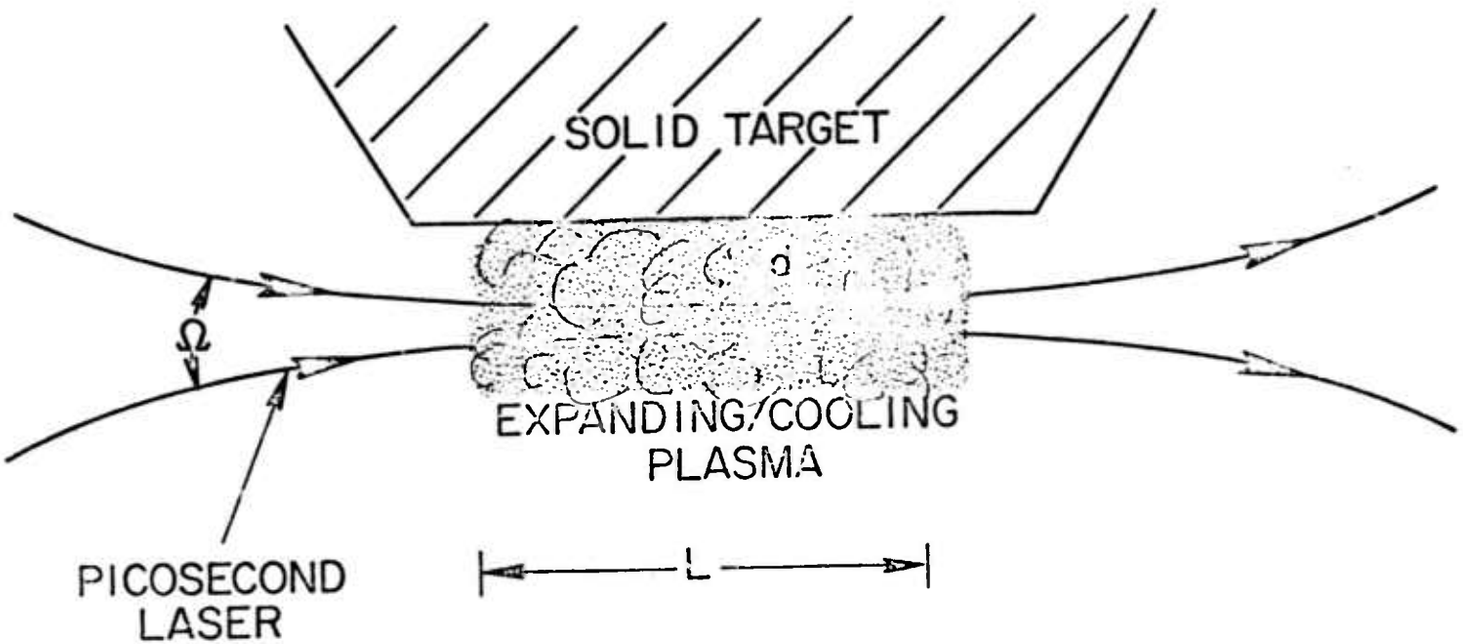

FOR 10^{10}W, 1.06μm LASER:

I[W/cm^2]	d[μm]	L[μm]	Ω[STER.]
10^{14}	100	15000	3.5×10^{-4}
10^{15}	30	1300	4×10^{-3}

FIGURE 6

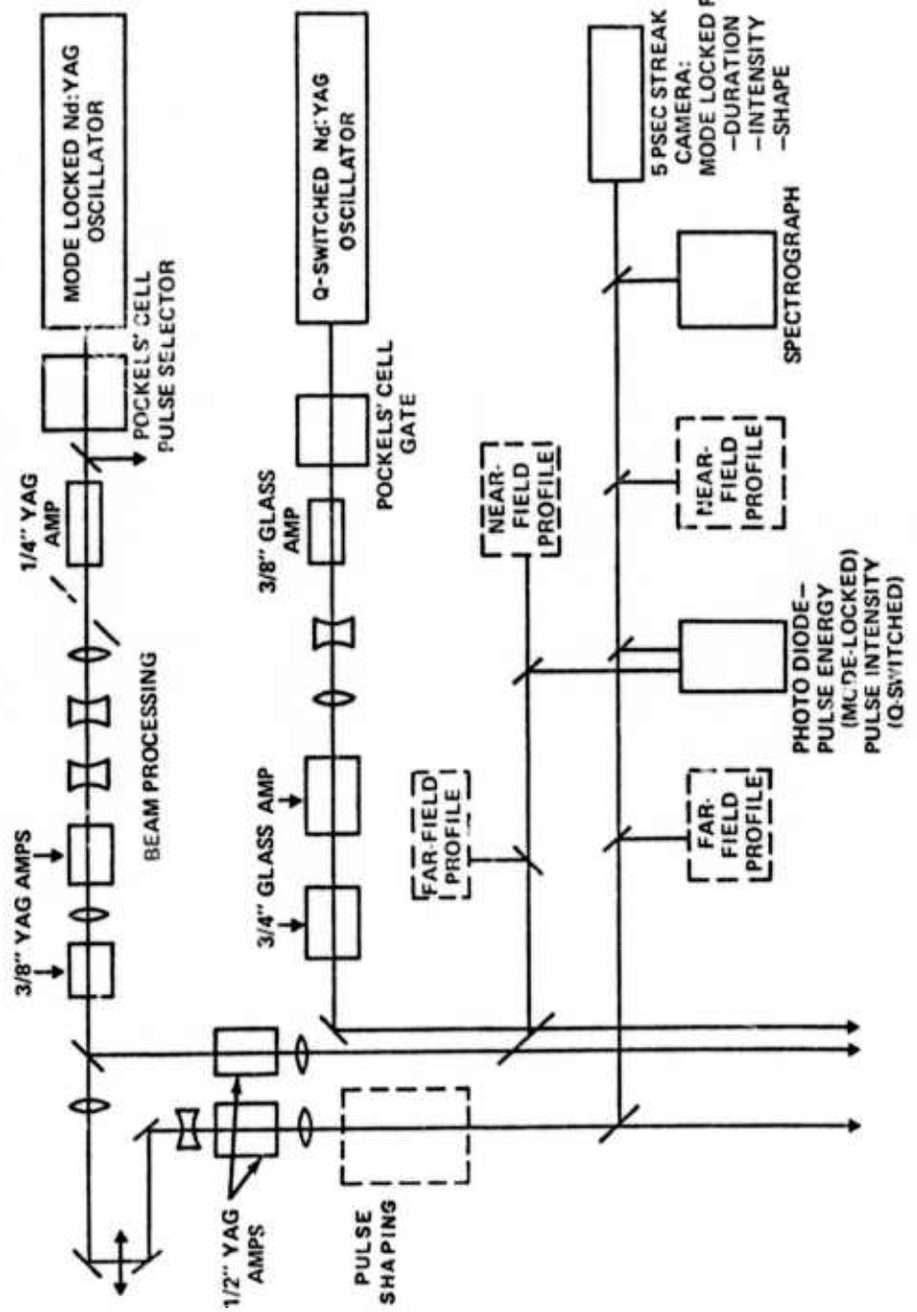
MODE LOCKED Nd:YAG OSCILLATOR
POCKELS' CELL PULSE SELECTOR
1/4" YAG AMP
3/8" YAG AMPS
BEAM PROCESSING
3/8" GLASS AMP
3/4" GLASS AMP
Q-SWITCHED Nd:YAG OSCILLATOR
POCKELS' CELL GATE
FAR-FIELD PROFILE
NEAR-FIELD PROFILE
5 PSEC STREAK CAMERA: MODE LOCKED PULSE -DURATION -INTENSITY -SHAPE
SPECTROGRAPH
NEAR-FIELD PROFILE
PHOTO DIODE- PULSE ENERGY (MODE-LOCKED) PULSE INTENSITY (Q-SWITCHED)
FAR-FIELD PROFILE
1/2" YAG AMPS
PULSE SHAPING

FIGURE 7

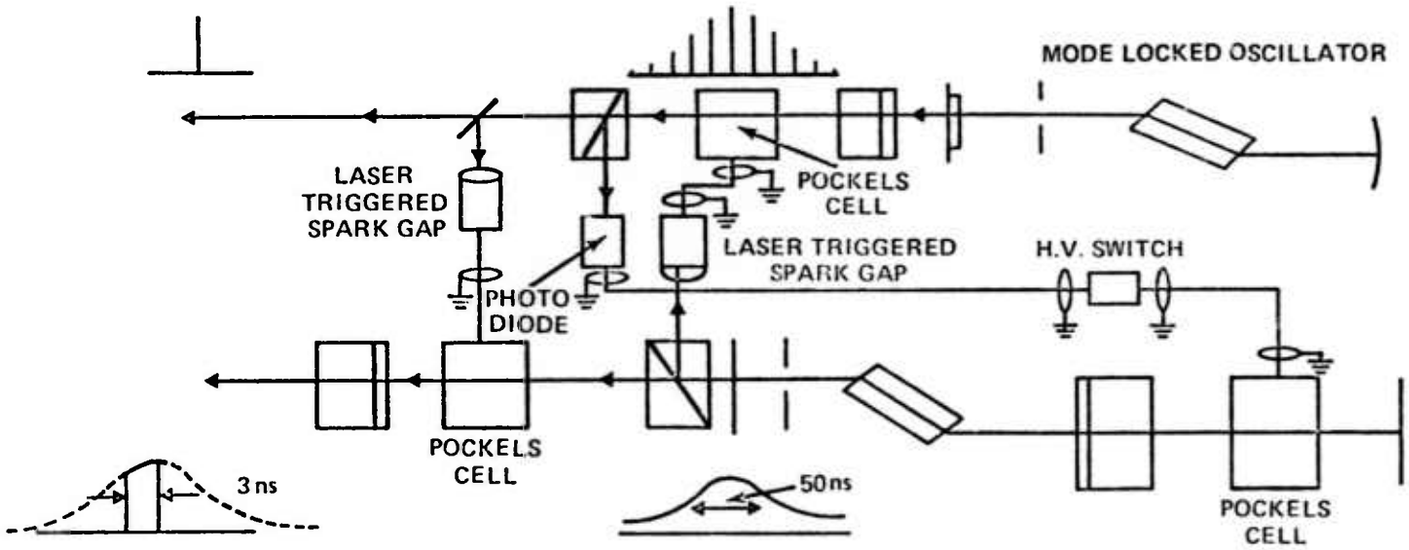

SEQUENCE OF EVENTS:

1. START OF MODE LOCKED LASER PULSE TRAIN
2. Q-SWITCHED LASER TRIGGERED ON EARLY PULSE FROM MODE LOCKED TRAIN
   ($\Delta t \sim$ 10-20ns
3. MODE LOCKED PULSE SELECTED AFTER START OF Q-SWITCHED PULSE
   ($\Delta t \sim$ 6-7ns
4. SECTION OF Q-SWITCHED PULSE GATED OUT BY SELECTED MODE LOCKED PULSE
   ($\Delta t < 1$ns

FIGURE 8

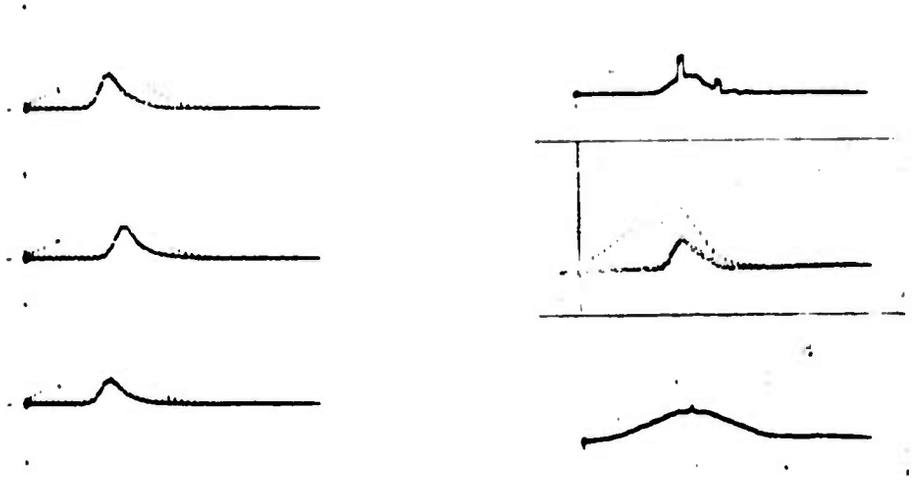

(a)

(b)

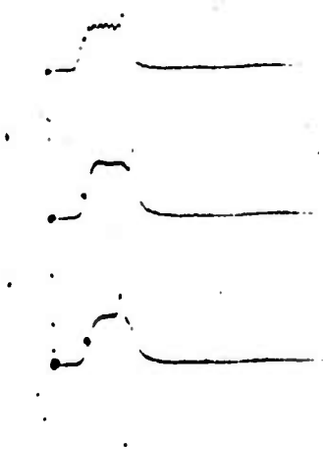

(c)

FIGURE 9

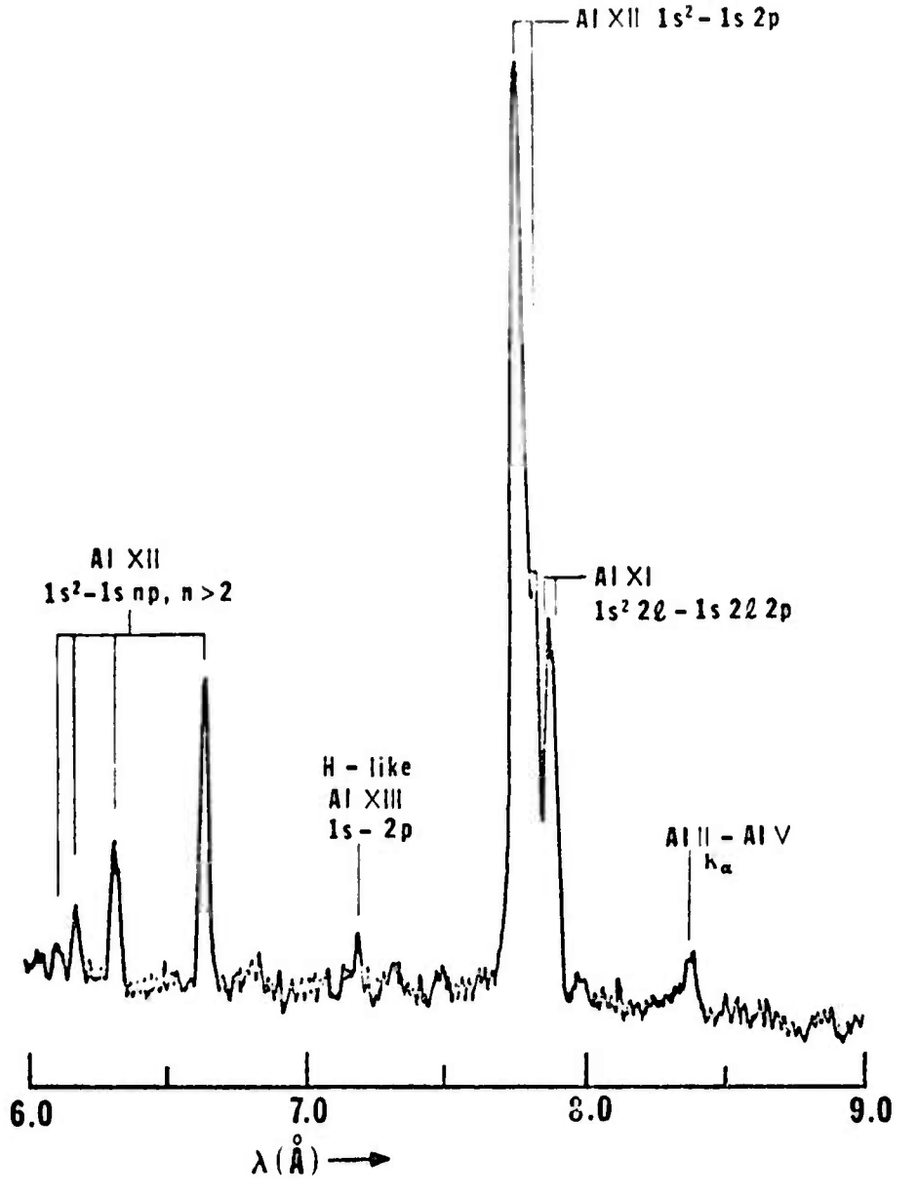
Al XII 1s² – 1s 2p
Al XII
1s² – 1s np, n > 2
Al XI
1s² 2ℓ – 1s 2ℓ 2p
H – like
Al XIII
1s – 2p
Al II – Al V
Kα
6.0
7.0
8.0
9.0
λ (Å) ⟶

FIGURE 10

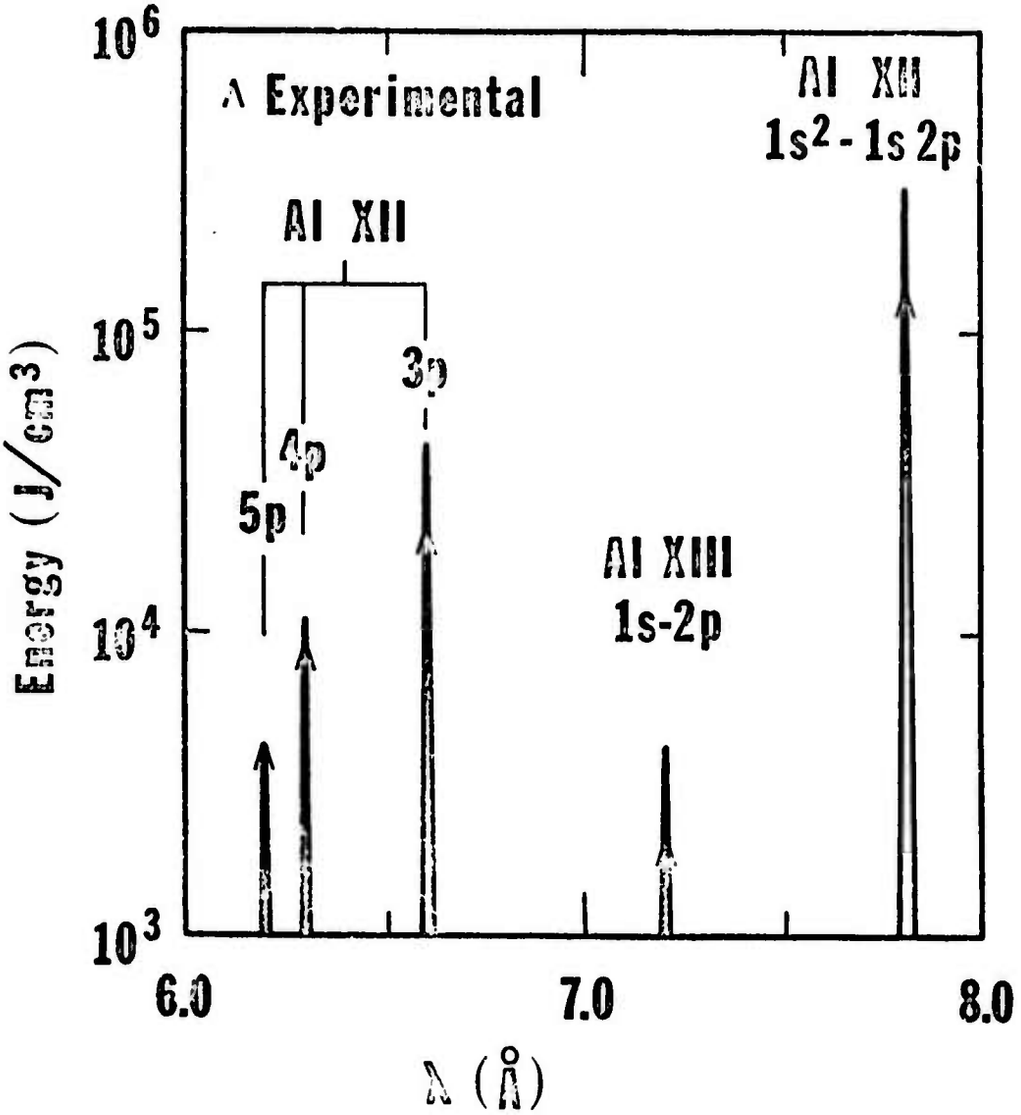
Experimental
Al XII
1s2 - 1s 2p
Al XII
3p
4p
5p
Al XIII
1s-2p
Energy (J/cm3)
10^6
10^5
10^4
10^3
6.0
7.0
8.0
λ (Å)

FIGURE 11

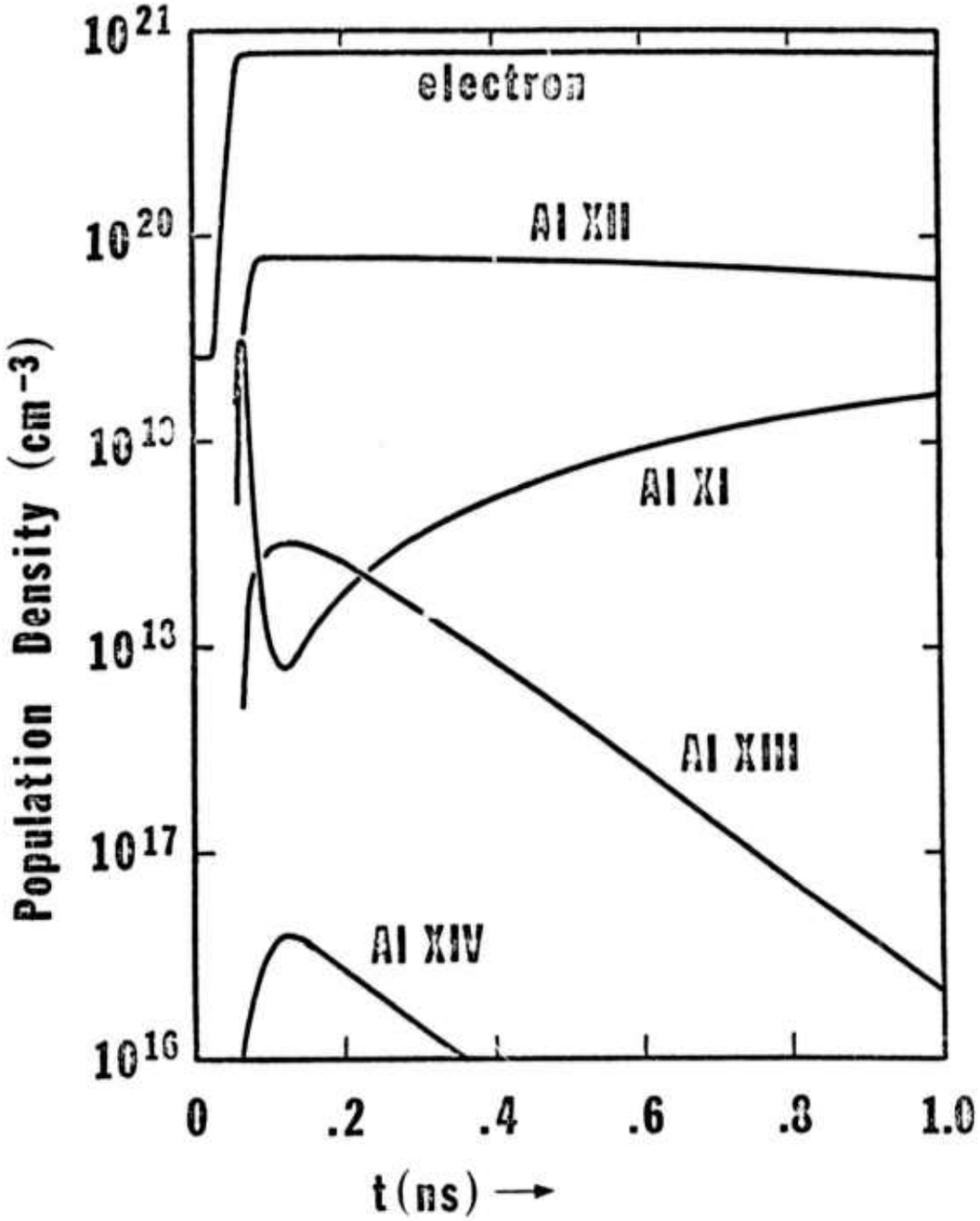
electron
Al XII
Al XI
Al XIII
Al XIV
Population Density (cm-3)
10^21
10^20
10^19
10^13
10^17
10^16
0
.2
.4
.6
.8
1.0
t(ns) →

FIG. 12

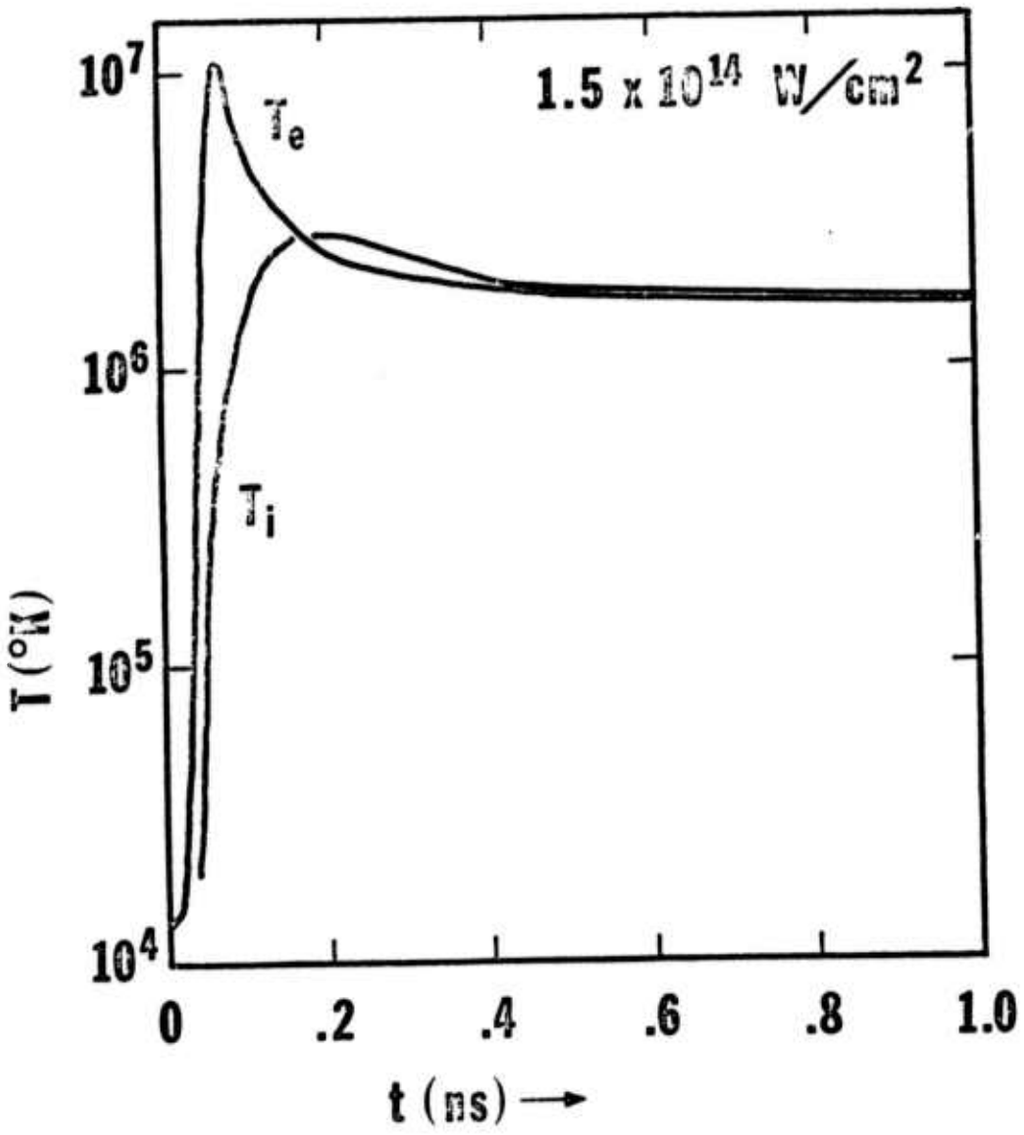

FIGURE 13

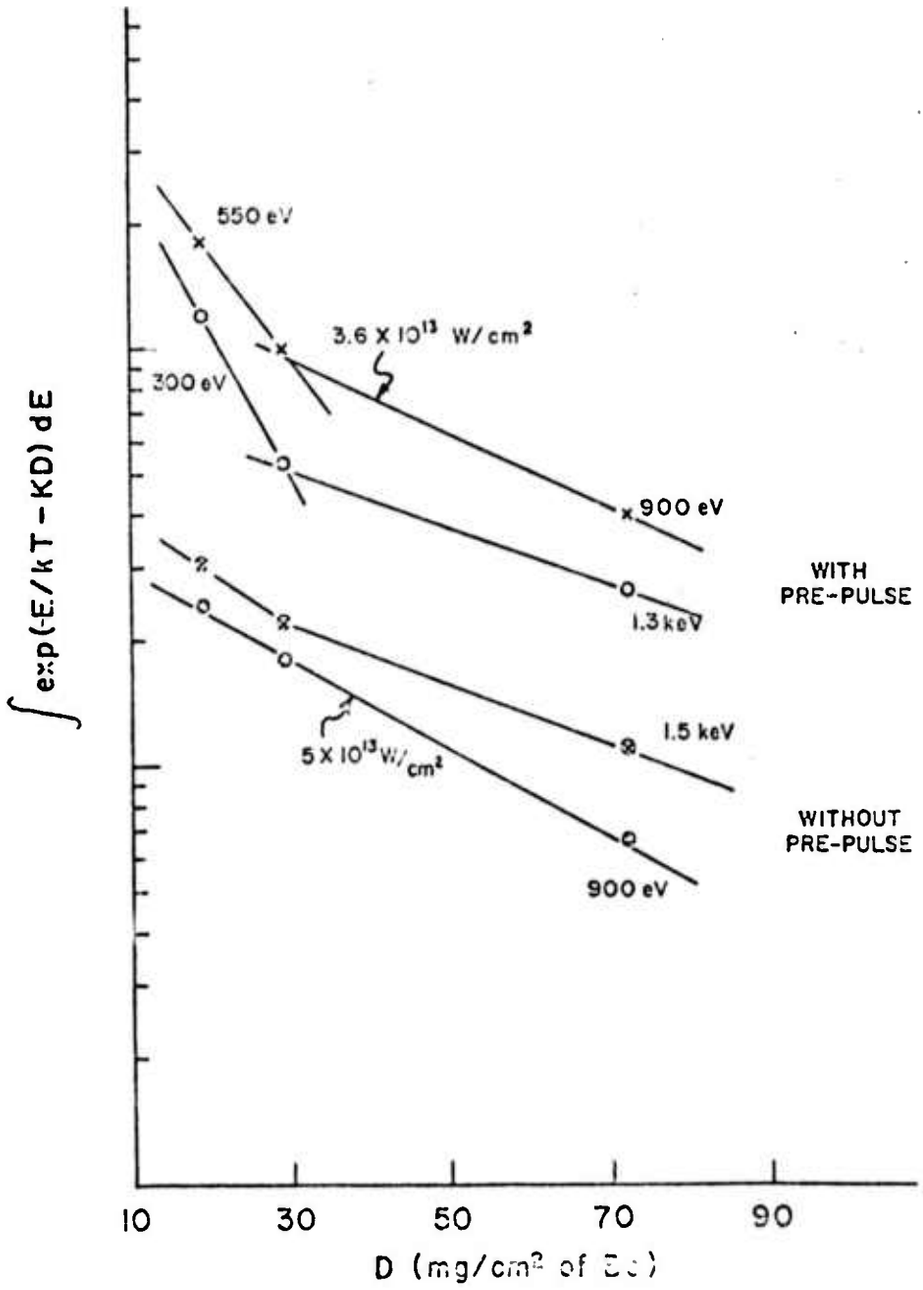
550 eV
3.6 X 10^13 W/cm^2
300 eV
900 eV
1.3 keV
WITH PRE-PULSE
1.5 keV
5 X 10^13 W/cm^2
WITHOUT PRE-PULSE
900 eV
∫ exp(-E/kT - KD) dE
10
30
50
70
90
D (mg/cm^2 of Be)

FIGURE 14

PREPRINT

To be Publish in the Journal of Applied Optics

May 1975

Quasistationary Population Inversion on K$_\alpha$ Transitions

R. C. Elton

U. S. Naval Research Laboratory, Washington, D. C. 20375

In a search for an x-ray laser scheme capable of operating in a quasi-cw mode, a suggested K$_\alpha$-innershell scheme is examined using recently calculated rates. This scheme involves the decay of a K-shell vacancy followed by a more rapid (for certain elements) L-vacancy decay, which maintains the inversion. The present analysis indicates that the scheme is only marginally feasible unless a depletion of resonant absorbers is accomplished through line shifts associated with multiple ionization following K-vacancy production. The pumping requirements for overcoming photoionization losses in the beam and the associated gain conditions are estimated for three elements, namely silicon, calcium and copper, and it is concluded that photoionization pumping in a selective energy band is required, with emission approaching the blackbody level. A multiline heavy-ion plasma source is suggested.

I. INTRODUCTION AND BACKGROUND

For x-ray lasing, K$_\alpha$-type transitions would seem to be a first choice, both because of the inherent short wavelengths, and the large transition probabilities (which imply increased gain). However, with the rapid K-vacancy decay

rate is associated a short (femtosecond[1] for penetrating x-rays) equilibration period τ, during which lasing is completed for a simple self-terminating transient inversion scheme[2]. With coherence lengths $c\tau \sim 10^{-5}$cm, conventional cavity operation becomes impractical (even if cavities could be constructed to withstand x-ray laser intensities), and traveling-wave operation would be tedious. Sufficient pumping for significant single-pass lasing (amplified spontaneous emission) is also a formidable task during such a short lasing period.

An alternative to the short-pulse self-terminating laser approach is to somehow create a stationary (or at least quasi-stationary) population inversion by eliminating final laser states, which are potential absorbers, more rapidly than they are created. For Kα-innershell transitions, this translates to depleting the density of atoms (or ions) with a particular L-shell vacancy more rapidly than they are created by lasing transitions from K-vacancy atoms. (It is not necessary that the L-shell be filled, since isolate spectral lines are produced for each of the series of possible L-vacancy configurations as discussed below.) A particular L-vacancy state may be depleted by either adding or removing an electron to the L-shell, but again it must take place at a very rapid rate and preferably without external stimulus. Stankevich[3] in 1970 first suggested that this be accomplished by electron cascading from outer shells through rapid Auger as well as radiative transitions, and suggested that this combined specific rate exceeds that for K-vacancy depletion. This particular scheme depends strongly on a sufficient density of outer-shell electrons, i.e., is classified as an innershell[4] transition scheme. Although the description of the model Stankevich used is sketchy, it is possible to approximately reconstruct[5] his results, which were based upon K-vacancy depletion rates from experimentally obtained K-level widths[b], propor-

tioned[7] as 2:1 for $K\alpha_1$ and $K\alpha_2$ lines; and L-vacancy depletion rates estimated from the difference between the K-level widths and measured K-line widths[6]. Some of these numerical data are included in Table 1, and the ratio R_L/R_K of L- and K-vacancy depletion rates is plotted in Fig. 1 versus atomic number Z. In equilibrium, $N_2R_K=N_3R_L$, where N_2 and N_3 are, respectively, the upper and lower laser state densities[2], populated originally by pumping from state 1. Therefore the ordinate in Fig. 1 corresponds to the population density ratio, and inversion is achieved when $N_2/N_3 > g_2/g_3$ where the statistical weight ratio g_2/g_3 is 1 for the $K\alpha_2(KL_{II})$ line and 0.5 for the $K\alpha_1(KL_{III})$ line. (Stankevich apparently assumed $g_2/g_3=1$ for both lines.) Thus, for the data available to Stankevich, net quasistationary inversion appears possible for the Z = 20-45 range.

II. PRESENT ANALYSES

A. Total Rate Model with Recent Data

When a similar analysis is carried out[5] with the more recent calculations of Auger and radiative rates shown also in Table 1, the prospect for quasi-stationary inversion appears considerably more marginal. K-shell rates have been calculated by McGuire[8], Walter and Bhalla[9], and Scofield[10,11] (radiative only) in the 1970-1972 period and are in close mutual agreement for present purposes. McGuire[12] in 1971 also calculated L-shell radiative, Auger, and Coster-Kronig rates, from which are obtained total effective L sub-shell vacancy depletion rates by increasing the L_{II} rate and decreasing the L_{III} rate according to the tabulated Coster-Kronig rates. It is interesting to note (Table 1) that the total line widths obtained from these calculated rates agrees reasonably well at

high Z with the widths published by Blokhin and Sachenko[6] and used by Stankevich; however the relative rates are different, and L-depletion is not as rapid as originally supposed[3]. A $K\alpha_1/K\alpha_2$ transition rate ratio of 2:1 is again assumed. The result is a maximum population density inversion of about 30 percent in the Z=30-35 region, as shown also in Fig. 1. Thus, even with the most recent data, quasistationary inversion using total decay rates remains a possibility, but with a more limited degree of inversion.

B. Partial Rate Model with Line Shifting

It may only be necessary for the L-hole depletion rate to exceed the radiative x-ray rate for K-vacancy decay[13, 14], which for low-Z elements is much less than the total rate used above. To better understand this model, a total binding-energy level[15] diagram for copper is shown in Fig. 2, with various single and multiple shell-vacancies designated by capital letters (e.g., K, L, M, KL, LL, etc.), and vacancy transitions by K→L, etc. As indicated, the scheme evolves from creating K-vacancies by pumping (P) in neutral copper, but is equally relevant beginning with a particular ion species (providing an excessive decrease in the $L\rightarrow M^2$ Auger rate does not occur with depletion of M-electrons). Also the diagram is relevant to other materials with some attention to the relative importance of x-ray (X) and Auger (Γ) rates. The L state and some of the LM^2 states shown are potential reabsorbers of the K→L laser radiation. The newer idea here is that laser absorption by multiple-L-vacancy states (e.g., LL) and certain LM^2 states may take place at a shifted wavelength (indicated by $\lambda-\delta$) in Fig. 2), and therefore may not contribute to resonance-absorption losses in the laser beam. Indeed it has been recently shown both theoretically[16] and experimentally[17] that K-line shifts due to multiple-L-vacancies exceed the line widths.

If we then limit laser resonance absorption to L-states and only consider x-ray decay of the K-vacancy, a high degree of inversion is reached for both $K\alpha_1$ and $K\alpha_2$ transitions and for Z as low as 13, as shown in Fig. 3. In this figure, the low-Z cutoffs are due for α_2 to a lack of M-electrons and for α_1 to a lack of 3d M-shell electrons to fill $2p_{3/2}$ (L_{III}) holes (data for $M_1 \rightarrow L_{III}$, ℓ-transitions, are not available). The high degree of inversion in the Z=20 range makes this model particularly attractive as far as pumping requirements are concerned. It should be noted that this line shift modification will not appreciably extend the high-Z, short-wavelength limit; however, it could make measurements at longer wavelengths (low-Z) considerably easier.

There are some potential problems associated with the shifted-line model. Double L-vacancies will cascade to M^4 states as indicated in Fig. 2 at a rapid rate, just as do single L-vacancies, leading to decreased line shifts. The (sparse) data[16] available on line shifts with multiple M-vacancies indicate that an emission-absorption line overlap fortunately is not expected if only natural (x-ray plus Auger) broadening is important and if M_I and M_{II} vacancies are present; an overlap for higher M-shell vacancies appears to be unavoidable. For light elements up through Z=20, only M_I and M_{II}-shell electrons exist (Auger loss of N-electrons has a low probability[12]). For Z larger than 20, further cascading may transfer M_I, M_{II}-vacancies to M_{III}, M_{IV}, M_V states (by radiative and Coster-Kronig transitions), where the line shift is negligible. Rate data are available[18] for including this effect, but the complexity is beyond this analysis.

A further complication in the line-shift scheme is electron-ion recombination (r in Fig. 2). As Stankevich points out[3], recombination must proceed at a

sufficient rate to inhibit over-depletion of amplifying atoms. This implicitly places an upper limit on the plasma temperature. However, a recombination rate exceeding the K- and L-vacancy depletion rates will also produce LL→L recombination transitions following K→ LL Auger transitions and again provide absorbers; we are then back to the less promising conditions in Fig. 1. For true cw-operation, such a high recombination rate is required. However, as we show below, inversions of ~1% are required to achieve net gain. Thus, perhaps a lower recombination rate is possible, permitting a gradual depletion of atom density through ionization (with an accompanying increase in pump-power requirements) in order to achieve some degree of stationary inversion for a limited time (hence "quasistationary" inversion), hopefully long enough to have multiple transverses in a resonant cavity or to permit reasonable pump-pulse risetimes. This will perhaps be a delicate balance to achieve, and clearly requires a rather sophisticated numerical model for further analysis. For example, electron collisional ionization, as well as photoionization, of outer electrons should be included (i in Fig. 2). Also, the adverse effect on gain due to line shifts associated with multiple vacancy production accompanying radiative decay (radiative-Auger effect) should be included[11,19]. The basic information for such an analysis is generally available and the payoff, i.e., quasistationary population inversion, is potentially high. Further advantages of the line shift model will be indicated in the pump requirement estimations which follow, particulary for low-Z elements.

III. PUMPING REQUIREMENTS

A. General Requirements

Of next concern is the pumping energy required to achieve significant net gain, since photoionization of outer electrons by the laser beam will add to the normal line-absorption losses. Also, Auger decay (dominant for light elements) tends to deplete at a rapid rate the K-vacancy upper-laser-states created. Both processes imply large pumping powers to maintain inversion. These are problems common to all innershell x-ray laser schemes (except alkalis without Auger losses for n=2 vacancies) and also result in low system efficiency; on the other hand one is not overly concerned at present about efficiency if a quasi-cw mode is achievable with available pumping powers. (It should be remembered that, were it not for the potential of quasistationary inversion, Kα-innershell pumping would not be a serious candidate for x-ray lasing because of these losses.)

The restrictions set by the requirement that net stimulated emission exceed photoionization losses in the medium are derived from ~ 2X the minimum threshold condition, i.e.,

$$\frac{\lambda^2 A}{4\pi^2 \Delta\nu} \left[\tau N_1 \left(\frac{N_2}{N_1} \right) \right] \geq \frac{2\mu\rho}{10^{23}} N_1, \qquad (1)$$

where the left side is the net gain factor due to stimulated emission[2] and the right side represents photoionization losses on the original states of density N_1, with subscripts as defined above. The transition probability A is different from the x-ray rate X which is averaged over all terms. The parameter λ is the laser wavelength, $\Delta\nu$ is the line width in frequency units, μ is the solid absorption coefficient[20] and ρ is the density of (solid) absorber. The factor $\mu\rho/10^{23}$ is the Kα photoionization cross section. The

bracketed factor is the inversion density

$$\Delta N \equiv N_2 - (g_2/g_3)N_3$$
$$= N_1 \left(\frac{N_2}{N_1}\right)\left[1 - \frac{g_2 N_3}{g_3 N_2}\right] \equiv T\, N_1 \left(\frac{N_2}{N_1}\right) , \qquad (2)$$

where T indicates the degree of inversion and is evaluated in steady state by assuming N_3/N_2 to be given by the ratio of K- to L-vacancy depletion rates shown in Figs. 1 and 3. In a more complete time dependent model, T represents the stationary inversion achieved following the transient approach to equilibrium.[2]

For a first-evaluation of Eq. (1), the product $\lambda^2 A$ may be approximated by 0.2 (c.g.s.) and $2\pi\Delta\nu$ by the Auger rate, which does not vary rapidly with Z and is about 200 atu^{-1} or 8 X 10^{14} sec^{-1}. Thus, a first-cut yields a ratio N_2/N_1 which is required to be greater than 10^{-1} to 10^{-3} depending on the absorption cross section $\varkappa$ and the degree of inversion (T) achieved. If the line width exceeds the "natural" width assumed (see below), even more inversion will be required.

Some relaxation of this requirement on inversion density could be achieved with multiple ionization, i.e., removal of some absorbing valance electrons. This could be an added advantage in the line shift model above if these valence electrons are in M_{III} shells or higher. However, ionization of electrons from lower shells will decrease the L-vacancy depletion rate and affect the degree of inversion achieved. A proper balance could come from a detailed numerical analysis.

A desired ratio $N_2/N_1 \approx 1\%$ may be considered to be achieved by electron-collisions in a plasma, particle (electron) beam bombardment of a target, or by photon bombardment of a target. Only the latter appears at all feasible[5], since excessive plasma densities ($\gtrsim 10^{25}$ cm^{-3}) are required for either ionization[21] or dielectronic capture[22] electron-collisional pumping schemes; and a required electron beam current of $\sim 10^{14}$ A/cm^2 is greatly in excess ($\sim 10^8$X) of that currently available in unfocused beams. Also, in both of these cases the rate for ionization from outer-shells exceeds that for the K-innershell by orders of magnitude, so that efficient collisional innershell pumping seems most-unpromising.

B. Photon Beams

For photon pumping, preferential innershell ionization can be achieved with a source "tuned" to emit predominantly in the K-absorption region, so that outershell photoionization is reduced.[1] The pumping rate P is given by $N_\nu \sigma^K_{pi} c$, where N_ν is the x-ray photon density and σ^K_{pi} is the K-shell photoionization cross section. In this particular case, it is possible to obtain this threshold value independent of absolute cross section, since photoionization losses are balanced against photoionization pumping. In equilibrium, $N_2/N_1 = P/(\Gamma + X)$ and Eq. (1) becomes

$$\frac{\lambda^2 A}{2\pi} \tau N_1 \left[\frac{N_\nu \sigma^K_{pi} c}{(\Gamma+X)^2}\right] \geq 2 \sigma^L_{pi} N_1, \qquad (3)$$

where $2\pi\Delta\nu = \Gamma + X$ is assumed for natural line broadening (see below for validation of this assumption). With $\lambda^2 A \approx 0.2$ again and $\sigma^K_{pi}/\sigma^L_{pi} \approx 8$ near the K-absorption edge[20], the required photon density is $N_\nu \geq 5\pi (\Gamma + X)^2/2Tc$ cm^{-3}.

Calculations are carried out for three cases, namely silicon, calcium and copper, using published values[8-12] in Eq. (3) for the total decay rate $\Gamma + X$ (since $K\alpha_1$ and $K\alpha_2$ transitions must be pumped), values for T from Eq. (2) and the results plotted in Fig. 3, i.e., assuming the line shift mode of operation is possible. The results are listed in Table 2, where for copper the results without the line shift advantage are also included in parentheses by calculating T from the data in Fig. 2. The photon densities N_ν derived are converted to pump source radiances F by multiplying by $c(3hc/\lambda)$, where the latter factor represents the approximate pumping photon energy. Up to this point, the density of the laser medium has not entered.

The gain αL achievable with a chosen length L may be found from using the gain coefficient α given by the right side of Eq. (3), i.e.,

$$\alpha L = 2N_1\sigma^K_{pi}(\sigma^L_{pi}/\sigma^K_{pi})\ L \div N_1\sigma^K_{pi}L/4. \qquad (4)$$

With σ^K_{pi} (see Table 2) calculated from Ref. 23 at a pumping photon energy of 1.25 times the $K\alpha$ photon energy, and assuming $N_1 = 10^{23}$ cm^{-3}, the gain is calculated for a length of 300 μm, which is 10X a reasonable 30 μm focal width (w). The results for the three cases are listed in Table 2. For all three cases, the mean free path of a pumping x-ray photon, given by $(N_1\sigma^K_{pi})^{-1}$, is much less than the length, so that transverse (or oblique traveling wave) pumping is required, and the area is given by $Lw = 9 \times 10^{-5}$ cm^2. With this area, and providing for a 10% efficiency of power conversion from the original pumping source to x-rays of the proper energy, the pump power P required is

derived and listed. Also indicated is the corresponding pump energy E required for a 10 ps wide pulse, e.g., for a laser heated target x-ray source.

From Table II we may conclude that, with the advantage gained from line shifting, high net gain (≈70) is available in silicon with a reasonable pump, e.g., 40 J in a 10 ps pulse. Since it is unlikely that the vapor density can be maintained at 10^{23} cm^{-3} (solid), the high gain is a safety factor, i.e., with a medium density as low as 7×10^{21} cm^{-3}, a gain of $\sigma L=5$ is still possible. For shorter wavelengths the pumping energy increases to, e.g., 2 kJ for copper, which is still within the realm of reality.

The assumed conversion (from pumping source to x-ray photons) efficiency of 10 percent is probably high, since the pump source must be converted into a somewhat narrow band of x-ray photons towards the high energy side of the K-absorption edge; at lower photon energies excessive outer-shell ionization will occur. If indeed the conversion could take place in the medium itself or in the immediate area, and/or if a properly "tuned" pumping source is available, this efficiency might be realistic. An initially attractive possibility is radiation resulting from radiative recombination of electrons into 1s orbitals of hydrogenic and/or helium-like ions of the lasing element in a surrounding "blanket" of high density plasma. As the inverse process of photoionization, the recombination spectral energy distribution complements the absorption process; i.e., there is preferential recombination emission at energies above the k-absorption edge. Taking the silicon example[5], the recombination emission for a 1 cm thick blanket can be calculated[24], and it is found that a charged particle density of approximately 10^{23} cm^{-3} is required, which is technically difficult to achieve. Broadband bremsstrahlung emission

is hundreds of times lower[21].

This difficulty with insufficient recombination radiation at reasonable plasma densities is associated with low emissivity. Blackbody radiation at a sufficiently high temperature is often considered as a limiting case (as for sodium in the VUV, for example[25]). Included in Table 1 are the blackbody temperatures kT_{BB} in keV required to produce the required x-radiance with 1% utilization of the total blackbody emission. Also listed are the peak wavelengths (from Wien's law) for these temperatures. The results are very reasonable as regards both plasma temperature and the matching of the peak of the emission with the absorption band. The problem is how to create such a blackbody source, since continuum emission is down by several orders of magnitude at reasonable densities. A possibility is a multiline source created in a heavy element, where the individual broadened lines have blended emissions approaching the continuous blackbody "limit". This "saturation" is not unusual for intense VUV lines and, with a careful selection of material, some tuning should be possible. For example, uranium has L and M atom and ion emission lines near 1 and 4 Å, respectively, and some work has already been performed on uranium discharges for intense pseudo-continuum sources in the vacuum-UV region.

IV. Line Broadening

Whenever a plasma is created in the laser medium, either intentionally to achieve a high density for pumping purposes or unavoidably due to intense ionization pumping with Auger processes contributing to the free electron production, the effect on the line width must be considered, since the gain

varies inversely with line width[2]. Enhanced broadening (over the natural broadening assumed above) may exist due to random Doppler shifts and to charged particle interactions (Stark broadening). Both are considered here for radiation in the Kα spectral regions for various elements. The results are not only relevant to Kα innershell lines but to resonance lines of helium-like and hydrogenic ions; in fact, Stark broadening rates are taken for Ly-α lines for convenience and availability.

An estimate of the Doppler width $\Delta\lambda_D$ is obtained from[21]:

$$\Delta\lambda_D/\lambda \approx \Delta\nu_D/\nu = 7.7 \times 10^{-5} (kT_i/\mu)^{\frac{1}{2}}, \qquad (5)$$

where kT_i, the ion kinetic temperature, is in eV and μ is the atomic mass number of the element. Assuming as an approximation that $kT_i = h\nu/4$ (ν the Kα-laser frequency) in an "equilibrium" plasma and $\lambda = \lambda$(Lyman-α), $\Delta\lambda_D$ can be evaluated as a function of laser wavelength λ. The result is plotted in Fig. 4.

Stark widths for Kα transitions may be estimated[26,27] with sufficient accuracy for present purposes, from the lesser[26] of the widths given by formulas for the quasi-static linear Stark effect (Holtsmark theory) and for the electron impact broadening. The former is given approximately for Lyman-α transitions by

$$\Delta\lambda_{II} \approx \frac{2n^2\lambda^2}{\pi c} \frac{h}{m} \frac{\bar{Z}_p}{Z_i} N_p^{2/3}, \qquad (6)$$

where Z_i is the ion charge and $\bar{Z}_p$ the average perturber charge of density N_p. For a single-ion plasma where $Z_p = Z_i$ this becomes

$$\Delta\lambda_H \approx \frac{2n^2\lambda^2}{\pi c}\left(\frac{h}{m}\right) N_e^{2/3} \qquad (7)$$

for the (lesser) electron-perturber limit. The electron impact broadening[27] is found from

$$\Delta\lambda_e \approx \frac{3n^4\lambda^2}{c}\left(\frac{h}{mZ_i}\right) \frac{N_e}{v_e} \quad , \qquad (8)$$

where the factor $n^2(n^2-3)\ln(\epsilon_{max}/\epsilon_{min})$ has been approximated numerically by n^4 for Lyman-α transitions. Also, v_e may be replaced by the mean thermal velocity for the electrons at the plasma kinetic temperature derived above, i.e., $h\nu/4$. The resulting Lyman-α (n=2) Stark widths $\Delta\lambda_S$ are plotted in Fig. 4 as a function of wavelength for three electron density values. The magnitudes of these two Stark broadening processes are approximately the same for present conditions. There is, for some schemes, an advantage in increasing the electron temperature preferentially over the ion temperature for increased electron collisional pumping without additional Doppler broadening. This will have the effect of decreasing the (Lorentz) width through v_e in Eq. (8).

From Fig. 4 a comparison is now possible between plasma line widths (Doppler and Stark) for Kα transitions and natural widths $\Delta\lambda$ ($\lambda^2\Delta\omega/2\pi c$) determined from $\Delta\omega = \Gamma + X$; Γ being the Auger rate and X the x-ray decay rate. The Auger data used here are mostly for single K-vacancies in neutral atoms; for one case, namely neon (λ=14.6 Å), the reduction in natural width with multiple ionization is indicated[28]. Also shown for general interest are the natural widths $\Delta\lambda_N$ ($\Delta\omega$=A, the transition probability) for helium-like and hydrogenic species, where the latter is a straight line since Ly-α wavelengths

were used, i.e., $A \propto \lambda^{-2}$ and $\Delta\lambda_N \propto \lambda^2 A$.

From Fig. 4 it is clear that Doppler broadening is not significantly larger than innershell natural broadening at a low degree of ionization. Also, Lyman-α type (n=2) Stark broadening even at solid densities ($\sim 10^{23}$ cm^{-3}) is not dominant for wavelengths shorter than 4 Å. Therefore, line broadening alone does not preclude a unified plasma approach to x-ray lasing on Kα transitions. The significant reduction in line width shown and the avoidance of photoionization losses offered by hydrogenic and helium-like ions could only be realized in a relatively tenuous, expanded, low temperature plasma with "frozen-in" ions of these types; where quasi-cw operation according to the present scheme is not possible.

V. Summary

Quasistationary population inversion appears to be possible, even with the most recent calculations of Auger rates, for elements with Z less than 40. It appears that the line shift with multiple ionization will help in maintaining inversion; however the need for a more complete numerical rate equation analysis is clearly indicated. Assuming quasi-cw operation is feasible, the pump power requirements necessary to overcome photoionization losses and at the same time achieve useful gain do not appear to be completely unreasonable, particularly when blackbody x-ray emission is considered as a pumping source. It is suggested that partial blackbody radiation in the selected wavelength band required for innershell photoionization pumping be acquired with intense multiline radiation from heavy atoms and ions.

REFERENCES

1. M. A. Duguay and R. M. Rentzepis, Appl. Phys. Letters, 10, 350 (1967).
2. R. C. Elton, R. W. Waynant, R. A. Andrews and M. H. Reilly, Naval Research Laboratory Report 7412, May 1972.
3. Yu. L. Stankevich, Sov. Phys. Doklady 15, 356 (1970).
4. As used here, "innershell" implies that at least one additional electron exists in a shell of larger principle quantum number than for that shell in which the initial vacancy is produced.
5. R. C. Elton, Naval Research Laboratory Memorandum Report No. 2906, 1974; also Physica Fennica 9, Suppl. S1, p. 397 (1974).
6. M. A. Blokhin and V. P. Sachenko, Izv. Akad. Nauk. USSR, 21, 1333 (1957).
7. M. A. Blokhin, "The Physics of X-Rays" (translated), USAEC Report AEC-tr-4502, 1961.
8. E. J. McGuire, Phys. Rev. 185, 1 (1969); Phys. Rev. A, 2, 273 (1970).
9. D. L. Walters and C. P. Bhalla, Phys. Rev. A 3, 1919 (1971); Atomic Data 3, 301 (1971).
10. J. H. Scofield, Phys. Rev. 179, 9, (1969); also LLL Report No. UCRL-51231, June 1, 1972.
11. J. H. Scofield, Phys. Rev. A 9, 1041 (1974).
12. E. J. McGuire, Phys. Rev. A 3, 587 (1971).
13. P. J. Mallozzi, private communication, 1973; M. A. Duguay, private communication to R. A. Andrews, 1974.
14. F. T. Arecchi, G. P. Banfi and A. M. Malvezzi, Opt. Comm. 10, 214 (1974).

15. R. L. Kelly and D. E. Harrison, Jr., Atomic Data 3, 177 (1971).

16. L. L. House, Astrophys. J. Suppl. 18, 21 (1969).

17. T. N. Lie and R. C. Elton, Phys. Rev. A 3, 865 (1971); earlier evidence of innershell ion transitions is reviewed here.

18. E. J. McGuire, Phys. Rev. A 5, 1052 (1973).

19. T. Åberg, Phys. Rev. A 4, 1735 (1971).

20. F. R. Gilmore, RAND Report No. RM-2367-AEC, April 10, 1959.

21. R. C. Elton, in "Plasma Physics, Vol. 9A, Methods of Experimental Physics", edited by H. R. Griem and R. H. Lovberg (Academic Press, N.Y., 1970).

22. S. M. R. Ansari, G. Elwert, and P. Mücklich, Z. Naturforsch. 25, 1781 (1970); A. H. Gabriel and T. M. Paget, J. Phys. B 5, 673 (1972).

23. W. D. Barfield, G. D. Koontz and W. F. Huebner, J. Quant. Spectrosc. Radiant. Transfer 12, 1409 (1972).

24. H. R. Griem, "Plasma Spectroscopy" (McGraw-Hill, N.Y., 1964).

25. W. W. Jones and A. W. Ali, NRL Memorandum Report No. 2807; P. Bey, NRL Memorandum Report No. 2847 (1974).

26. H. R. Griem, private communication, 1974.

27. H. R. Griem, "Broadening of Spectral Lines by Charged Particles in Plasmas" (Academic Press, N.Y., 1974).

28. C. P. Bhalla, N. O. Folland, and M. A. Hein, Phys. Rev. A 8, 649 (1973).

Table I. Selected Atomic Rates[a] Used (in 10^{-2} atu^{-1})[b].

	Z = 22	30	38	47
Stankevich[3]				
1. K-level width[6] (K-rate)[b]	3.10	5.80	11.7	26.0
2. K-line widths[6,b]				
$K\alpha_1$ ($K\text{-}L_{III}$)	5.71	10.1	18.6	35.6
$K\alpha_2$ ($K\text{-}L_{II}$)	7.90	12.0	19.0	36.0
3. L-level widths[6] (L-rate)[b,c]				
L_{III}	2.61	4.30	6.90	9.60
L_{II}	4.80	6.20	7.30	10.0
Present Analysis				
4. K-rate[8]				
X-ray	0.89	3.41	10.2	24.45
Auger	2.63	3.14	4.00	4.42
Total	2.64	6.54	14.2	28.87
5. L-rate[12,d]				
L_{III}	0.885	2.95	3.92	6.36
L_{II}	0.886	2.87	5.27	9.50
6. Total (K-line width)				
$K\alpha_1$ ($K\text{-}L_{III}$)	3.52	9.49	18.1	35.2
$K\alpha_2$ ($K\text{-}L_{II}$)	3.53	9.41	19.5	38.4

a 1 a.t.u = 2.42×10^{-17} sec.

b rate [$a.t.u.^{-1}$] $\approx$ (4.14×10^{-2})X width [eV]

c Row 2 less row 1

d Coster-Kronig added to L_{II}, subtracted from L_{III}; x-ray rate included

Table II. K_α Pumping Requirements

Atom	λ (Å)	$10^{-14}(\Gamma+A)$ (sec^{-1})	T	$10^{-20}N$ (cm^{-3})	$10^{-3}F$ (TW/cm^2)	$10^{20}K$ $(cm^2)pi$	SL	P(TW)[a] $10^{-1}E(J)$	kT_{bb}[b] (keV)	$(\lambda_m)_{bb}$ (Å)
$_{14}Si$	7.1	6.7	0.6	2	4.8	9	70	4	0.5	5
$_{20}Ca$	3.4	11	0.8	4	21	4	30	9	0.7	4
$_{29}Cu$	1.5	21	0.6	20	230	2	15	200	1.2	2
			(0.2)	(60)	(700)			(600)	(1.6)	(1.5)

( ) Refers to no line-shift case

[a] For 10% conversion efficiency

[b] Using 1% of total blackbody spectrum

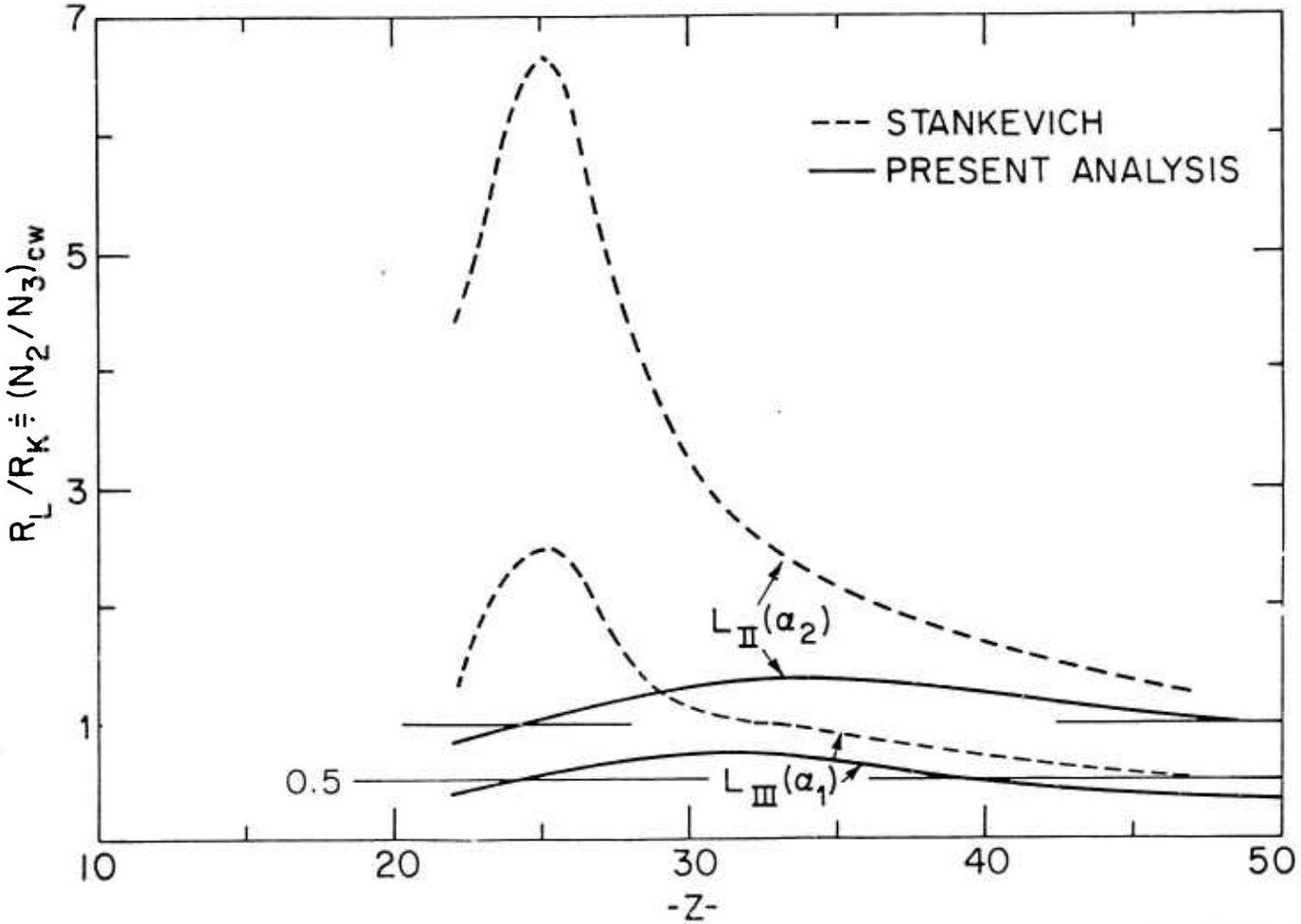

Fig. 1 Ratio of rates R_L/R_K for total transitions out of L and K vacancy states, respectively, versus atomic number Z. This ratio is equivalent to N_2/N_3 in Eq. (2) for equilibrium conditions reached after long times in cw operation. Values exceeding unity and one-half indicate gain for the $K\alpha_2$ and $K\alpha_1$ lines, respectively. The model here assumes all K-vacancy decay transitions produce potential absorbers for laser radiation. Present analysis is based on recent data[8-12]; an attempt to reproduce the results of Stankevich[3] is shown dashed. Both $K \rightarrow L_{II}$ and $K \rightarrow L_{III}$, α_2 and α_1 respective transitions are shown.

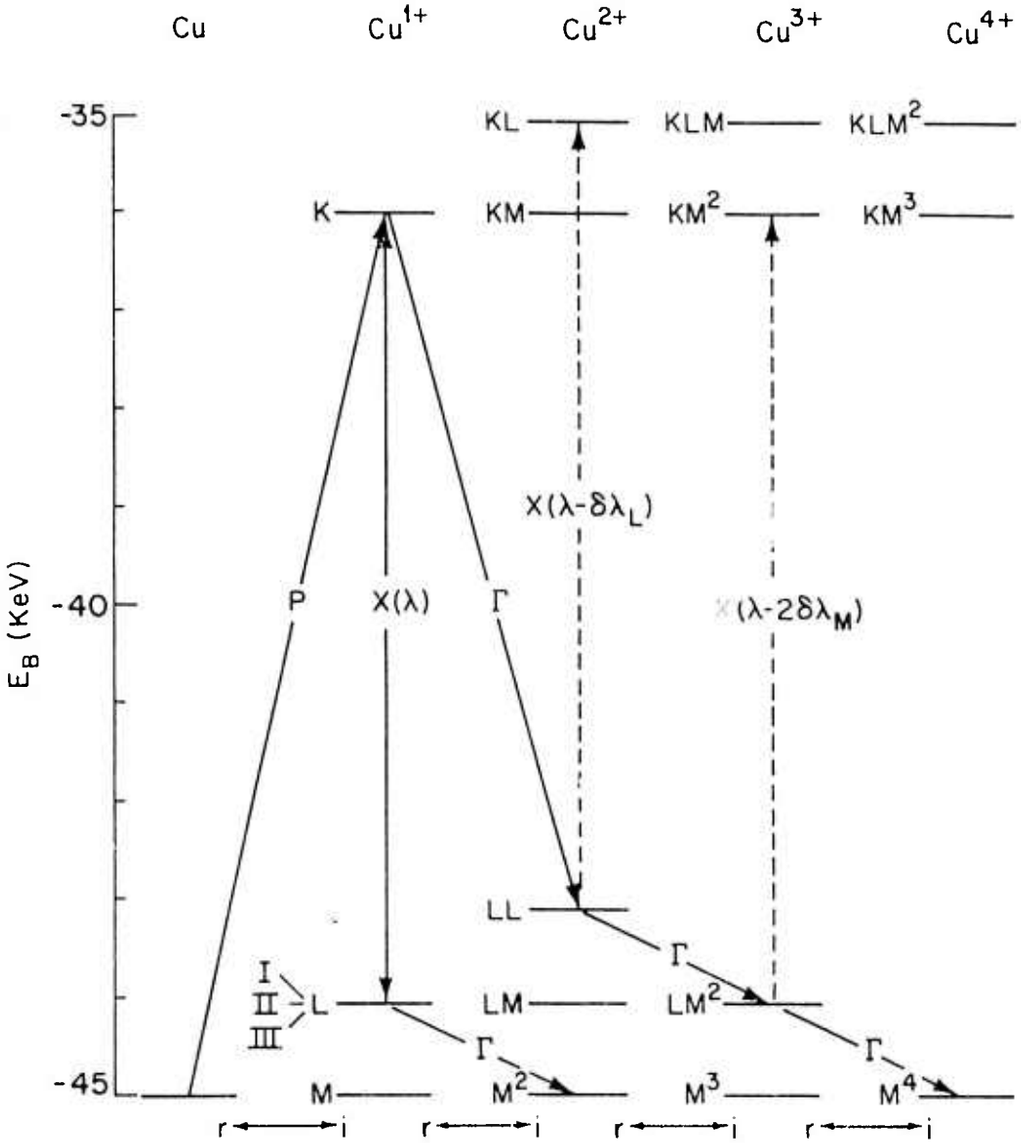

Fig. 2 Vacancy diagram according to binding energies E_B for copper. K, L and M designate shell-vacancies. P, X, and Γ are the rates for pumping, x-ray [emission or absorption (dashed)] and Auger transitions, respectively.

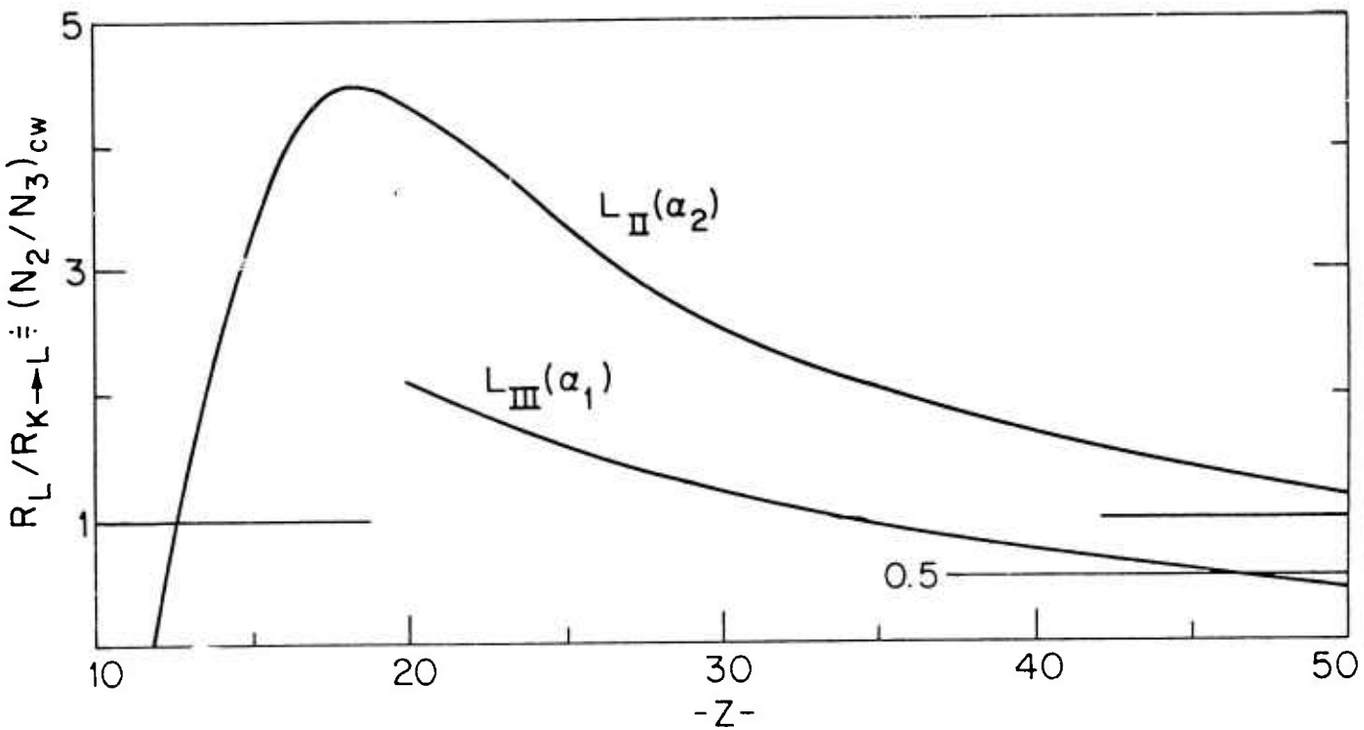

Fig. 3 Ratio of rates $R_L/R_{K\to L}$ for total transitions out of a L vacancy state and radiative decay out of a K vacancy state versus atomic number Z. This ratio is equivalent to N_2/N_3 in Eq. (2) for equilibrium conditions reached after long times in cq operation. Values exceeding unity and one-half indicate gain for the $K\alpha_2$ and $K\alpha_1$ lines, respectively. The model used assumes only radiative transitions produce absorbers, with Auger transitions generating shifted ion lines. Both $K\to L_{II}$ and $K\to L_{III}$ α_2 and α_1 respective transitions are shown.

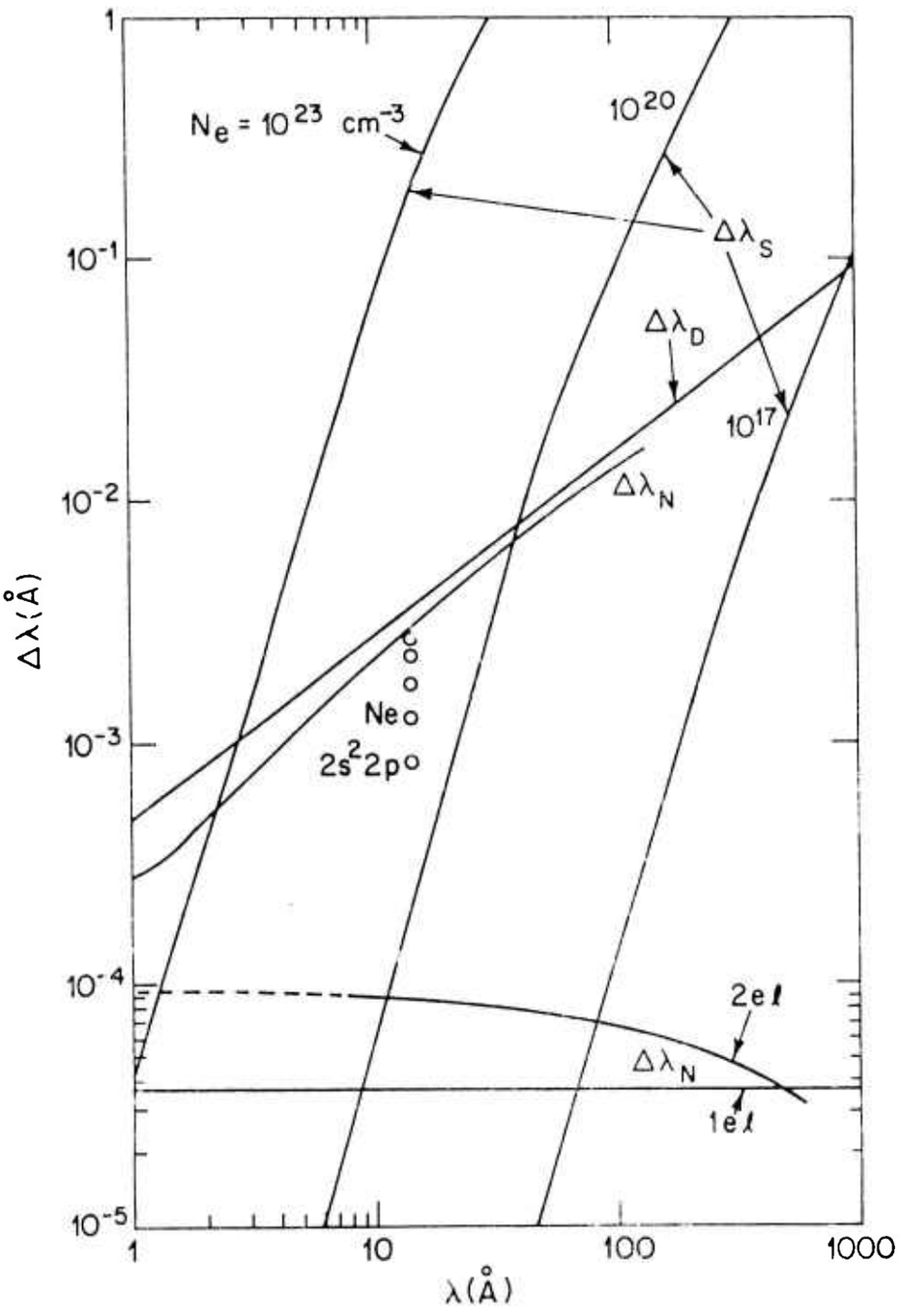

Fig. 4 Estimates of line widths for K type transitions versus wavelength λ [with natural ($\Delta\lambda_N$), Doppler ($\Delta\lambda_D$) and Stark ($\Delta\lambda_S$) effects included]. The decrease in natural broadening with ionization is indicated by circles for neon; and hydrogenic and helium-like ionic species are included.

NRL Memorandum Report 2906

Analyses of X-Ray Laser Approaches:
2. Quasistationary Inversion on K-Alpha Innershell Transitions

R. C. Elton

Interaction Physics Branch
Optical Sciences Division

October 1974

NAVAL RESEARCH LABORATORY
Washington, D.C.

NRL Memorandum Report 2932

Two Photon Resonantly Enhanced Self-Defocusing in Cs Vapor at 1.06 Micron

R. H. LEHMBERG, J. REINTJES, AND R. C. ECKARDT

Interaction Physics Branch
Optical Sciences Division

November 1974

NAVAL RESEARCH LABORATORY
Washington, D.C.

Abstract for an Invited Paper
for the Anaheim Meeting of the
American Physical Society

29 Jan - 2 Feb 1975

Atomic Physics In Laser Produced Plasmas. R. C. Elton, Naval Research Laboratory, Washington, D.C. (30 min.)

Atomic processes play a vital role in the efficient conversion of laser energy to charged particle energy in laser heated plasmas. Both classical and anomalous absorption processes must be thoroughly understood in order to exploit their optimum heating potential. Radiation losses, along with self-generated magnetic fields, threaten to reduce the amount of heating achieved in laser heated plasmas; thus their presence must be minimized. Laser radiation losses due to various scattering mechanisms are just beginning to be understood, as data become available at increasing laser flux densities. Atomic processes also continue to play an important role in plasma diagnostics. For the moderate particle densities encountered in gaseous target plasmas heated by long-wavelength lasers, established diagnostic techniques such as laser scattering, interferometry, and spectroscopy are proving satisfactory; and definitive measurements can be expected. For the supra-solid density plasmas expected from pellet fusion experiments and also desired for x-ray laser development, the plasma rapidly becomes opaque to visible radiation, and x-ray diagnostics are essential for interior measurements. Here the ionic physics connected with x-ray spectral analyses of solar observations becomes relevant, with the addition of some exotic excitation mechanisms unique to high-density plasmas. The state-of-the-art of x-ray diagnostics will be reviewed and problems of interpretation with existing atomic physics knowledge outlined. Also, possible spin-off contributions at atomic physics knowledge from well diagnosed plasmas will be made apparent. The close similarities between laser-fusion oriented experiments and x-ray laser research will be addressed, particularly since the development of the latter may be required for deep probing of extremely high density compressed pellet fusion plasmas.

Abstract Submitted
for the 16rh Division of Plasma Physics Meeting of the
American Physical Society
October 28-31, 1974

Physical Review
Analytic Subject Index
Number 35. Plasmas

Bulletin Subject Heading
in which Paper should be
placed Laser Produced Plasma

Session Title:
9. Laser Produced Plasma

Effect of Pre-pulse in 25 ps Laser Produced Plasma. J. F. REINTJES, T. N. LEE, R. C. ECKARDT, J. L. DeROSA, R. A. ANDREWS, and R. C. ELTON, Naval Research Lab.--X-ray emission spectra of low Z plasmas generated with a 25 ps laser pulse have been previously[1] described and compared with a numerical analysis. The study is extended to understand the plasma state which results when the laser pulse is preceded by a pre-heating pulse. A mode locked Nd:YAG laser providing beam energies up to 100 mJ in a 25 ps pulse is focused onto slab targets of C, Mg, and Al at a power density of about 10^{14} W/cm^2. The pre-pulse is obtained from the main laser beam using a beam splitter and is then focused collinearly onto the same spot as the main beam focus within $\pm$ 10 μm. The peak electron temperature is determined from a foil x-ray absorption measurement. A question of whether the plasma produced by the pre-pulse is largely transparent to or strongly absorbing to the main laser pulse will be discussed based on the experimental results.

[1] T. N. Lee, et al., Bull. Am. Phys. Soc. 19 558 (1974)

Submitted by

T. N. LEE
Signature of APS Member

T. N. Lee (Lie)
Code 5520
Naval Research Laboratory
Washington, D. C. 20375

Abstract Submitted
for the 16th Division of Plasma Physics Meeting of the
American Physical Society
October 28-31, 1974

Physical Review
Analytic Subject Index
Number 35. Plasmas

Bulletin Subject Heading
in which Paper should be
placed Plasma Focus

Session Title:
8. Plasma Focus

Diagnostics of a Vacuum-Spark Plasma. T. N. LEE and F. C. YOUNG, Naval Research Laboratory--Characteristics of neutron and x-ray emission from a laser-triggered linear-pinch discharge[1] (or vacuum spark) are investigated experimentally. To produce neutrons, $(CD_2)_n$ is imbedded into a 1-mm dia. hole in a metallic anode. Neutron measurements with both a moderated ^6Li-loaded glass activation detector and a large area time-of-flight detector indicate a total yield of 10^4 - 10^5 neutrons (~2.5 MeV) per discharge in time coincidence with the x-ray burst. This yield is consistent with that expected from a thermal plasma with the previously determined plasma parameters[1] of 50 μm dia., T_e = 8 keV and $N_i \sim 10^{19}/cm^3$. X-ray pinhole and streak photographs indicate that one or more minute plasmas (15-50 μm dia.) are produced initially as the result of highly localized pinches. These local constrictions tend to be produced at the vertex of the bullet-shaped anode plasma. These pinches are believed to be caused by the repetitive penetration of a strong azimuthal magnetic field through a cool poorly conductive anode plasma.

[1] T. N. Lee, Astrophys. J. 190, 467 (1974).

Submitted by

T. N. LEE
Signature of APS Member

T. N. Lee (Lie)
Code 5520
Naval Research Laboratory
Washington, D. C. 20375

Abstract Submitted
for the Washington, D.C. Meeting of the
American Physical Society
28 April - 1 May 1975

Physical Review
Analytic Subject Index
Number 71.65

Bulletin Subject Heading
in which Paper should be
placed Nonlinear Optics,
Lasers

Generalized Adiabatic Following Approximation.* R. H. LEHMBERG and J. REINTJES, Naval Research Lab.--The response of a two level atom to an intense near-resonant driving field $\mathcal{E}(t)$ can be described by the adiabatic following model[1] if the condition $1/\Omega(t) \ll \tau_p \ll T_1$, T_2 is satisfied throughout the pulse. Here, $\Omega(t) = (\Delta^2 + p^2\mathcal{E}^2/\hbar^2)^{\frac{1}{2}}$ is the precession frequency, $\Delta(t)$ the detuning, τ_p the pulsewidth, and T_1, T_2 the atomic level and phase relaxation times. From the Bloch equations, we have developed a generalized version of this approximation applicable to cases where T_1 and T_2 can be comparable to or less than τ_p; i.e., we require only $1/\Omega(t) \ll \tau_p$, T_1, T_2. In this model, the pseudospin remains oriented nearly parallel to the effective driving field $(\mathcal{E}(t), 0, \hbar\Delta(t)/\mu)$ in the rotating frame, but decays in length if T_2 is comparable to τ_p. The approximation bridges the gap between pure adiabatic following for $\tau_p \ll T_2$ and rate equation behavior for $\tau_p \gg T_2$, thereby allowing a more complete description of phenomena such as adiabatic inversion and resonantly enhanced self focusing and defocusing.[1]

*Work supported jointly by DARPA and USAEC.

[1] D. Grischkowsky and J. A. Armstrong, Phys. Rev. A6, 1566 (1972).

Abstract Submitted
for the Washington, D. C. Meeting of the
American Physical Society
28 April - 1 May 1975

Physical Review
Analytic Subject Index
Number 71.65

Bulletin Subject Heading
in which Paper should be
placed Nonlinear Optics,
Lasers

Negative Nonlinear Susceptibility of Cesium Vapor at 1.06μ.*
J. REINTJES, R. H. LEHMBERG, and R. C. ECKARDT, Naval Research Lab.--
We outline a theory of the nonlinear susceptibility of Cs at 1.06μ, and present the first measurement of the negative nonlinear refractive index n_2 responsible for the self defocusing recently observed[1]. The theoretical value of n_2 is $-1.95 \times 10^{-30} N$, in good agreement with our measured value of $-(1.5 \pm .2) \times 10^{-30} N$. The main portion of n_2 comes from a two-photon resonance between the 6s and 7s levels. An additional negative term arises from induced population changes between 6s and 6p. In our experiments, where the (35 psec) pulses are shorter than the 6s-6p inverse linewidth, the nonlinear susceptibility is proportional to the instantaneous intensity; however, with longer pulses, one obtains additional contributions proportional to time integrals over the intensity. Since the useful output power from large Nd laser systems is limited by self focusing due to the laser glass, our results suggest the possibility of increasing this power by using Cs vapor for compensation.

*Work supported jointly by DARPA and USAEC.

[1] R. H. Lehmberg, J. Reintjes, and R. C. Eckardt, Appl. Phys. Lett. 25, 374 (1974).

SELF DEFOCUSING OF MODE LOCKED Nd:YAG PULSES IN CESIUM VAPOR

R. H. Lehmberg, J. Reintjes, and R. C. Eckardt

Naval Research Laboratory
Washington, D. C. 20375
202-767-2730

ABSTRACT

We have measured the negative nonlinear refractive index of Cs vapor at 1.06μ. The result $n_2 = -(1.5 \pm .2) \times 10^{-30} N$ is in good agreement with theory. We report the first observation of its use in compensating self focusing from another material.

(Presented at the 1974 IEEE/OSA Conference on Laser Engineering and Application, Washington, D. C., May 1974.)